Universidad de La Laguna
Programa de Doctorado de Física e Informática

Tesis doctoral

Niveles y origen de gases reactivos y su relación con aerosoles en la proximidad a focos de emisión y en la troposfera libre de Tenerife

Levels and origin of reactive gases and their relationship with aerosols in the proximity of the emission sources and in the free troposphere at Tenerife

Yenny González Ramos

Directores:

Sergio Rodríguez González
Centro de Investigación Atmosférica de Izaña, AEMET

Juan Carlos Guerra García
Universidad de La Laguna

San Cristóbal de La Laguna, mayo 2012

D. Sergio Rodríguez González, doctor por la Universidad Politécnica de Cataluña, y D. Juan Carlos Guerra García, doctor por la Universidad de La Laguna,

HACEN CONSTAR,

que Dª. Yenny González Ramos, licenciada en Física por la Universidad de La Laguna, ha realizado bajo nuestra supervisión la presenta memoria titulada **Niveles y origen de gases reactivos y su relación con aerosoles en la proximidad a focos de emisión y en la troposfera libre de Tenerife**, para optar a el grado de Doctor en Ciencias Físicas.

Y para que así conste, autorizamos la presentación de la misma y firmamos la presente.

San Cristóbal de La Laguna, mayo de 2012

Fdo: S. Rodríguez González

Fdo: J.C. Guerra García

A los mios...

Acknowledgements

Ante todo quiero dar las gracias a mis directores de tesis, Sergio Rodríguez y Juan Carlos Guerra por su apoyo y dedicación, y por creer que algún día este trabajo llegaría a su fin. En especial a Sergio, por enseñarme y guiarme en los primeros pasos del investigador; por "aguantar" mis momentos de crisis, y por sus buenos consejos. También quiero darle las gracias a Emilio Cuevas por darme la oportunidad de entrar en el Observatorio de Izaña y vivir esta grata experiencia.

Esta tesis se la dedico a mis padres, Ruperto y Julieta, por vuestro amor y dedicación. A mis hermanos, Ely y Rober, por ser los mejores, por enseñarme a luchar, por vuestro apoyo y palabras y por ser inigualables. A mi tía Mary a mi dulce abuelita María por sus sabias palabras. Gracias familia, por vuestro cariño y apoyo incondicional.

Hay mil historias que contar en estos siete años que he compartido con mis niños del Observatorio. La pequeña gran familia, ¡qué hubiese sido de mi sin vosotros! Muchas gracias Ramón por tener la paciencia necesaria para enseñarme lo que sé hoy de instrumentación y por involucrarte. Cuántas horas de terapia laboral, verdad don César? Dar mil gracias a Matthias, por su paciencia; y a mis niñas, Yballa, Vane y Nayra, por vuestra amistad y cariño. A todos y cada uno, gracias por estar ahí y hacerme sonreír.

Este largo camino ha estado también lleno de risas y copas, gracias a mis amigos, Gladys, Sara y Aday, por hacerme siempre ver el lado positivo de este sacrificio. I would also like to say thank you to Chris, by supporting me in the last hard times and do not let that I never surrender. Gracias a todos por ser como sois.

No debo olvidar dar las gracias a la Consejería de Medioambiente del Gobierno de Canarias, y en especial a Víctor Gallo, Fernando Herrera y Alberto Blasco, que no han dudado ni un segundo en aportar toda la información necesaria para el desarrollo de los estudios de calidad del aire de la ciudad de Santa Cruz llevados a cabo en el marco de esta tesis doctoral.

Así mismo, agradecer a la Agencia Estatal de Meteorología (AEMET), al Barcelona Supercomputing Center-Centro Nacional de Supercomputación (BSC-CNS), y a la empresa Sieltec Canarias, S.L., por el apoyo técnico y económico para la realización de la presente tesis.

En cuanto a la presentación de este documento, quiero dar mi más sinceras gracias a mi amiga Ali, por su arte a la hora de diseñar la portada, y a José Manuel Rodríguez Sánchez por contar con su tiempo para el arreglo de muchas de las fotos que se presentan aquí.

During this work I've also met several great scientists in my short visit to Zugspitze and Hohenpeissenberg GAW stations. I would like to say a special thank you to Dr. Stephan Gilge and Dr. Wolfgang Fricke for their interest on helping me in all issues related to this work.

A todos, ¡muchas gracias! Thank you very much! Vielen Dank!

Resumen

Este estudio se centra en la identificación de las fuentes y procesos que contribuyen a la concentración de gases reactivos (NO_x, SO_2, CO y O_3) y partículas ultrafinas (PUFs), y su relación en el aire ambiente. La razón por la cual se está prestando una atención especial a las PUFs es debida al impacto que ejercen en la salud y en el clima. El estudio se basa en los datos de concentración de gases reactivos, PUFs (diámetro < 0.1 µm), black carbon, PM_{10} (diámetro < 10 µm) y $PM_{2.5}$ (diámetro < 2.5 µm) registrados en el aire ambiente, durante el periodo 2006 – 2010, en dos emplazamientos de la isla de Tenerife: i) el área metropolitana de Santa Cruz de Tenerife, donde se produce una emisión importante de contaminantes, y ii) la estación de vigilancia atmosférica global de Izaña, una estación de alta montaña localizada en la troposfera libre (~2.400 metros sobre el nivel del mar), por encima de la capa de estratocúmulos característica de las regiones oceánicas subtropicales.

En el área metropolitana de Santa Cruz de Tenerife, las principales fuentes de PUFs que se encontraron fueron: el tráfico rodado, los barcos y la refinería de crudo. Los resultados muestran que los niveles de fondo de PUFs en esta área están dominados por las emisiones del tráfico rodado, mientras que los episodios de alta concentración están inducidos por las emisiones de SO_2 de los barcos y de la refinería. La concentración de PUFs relacionadas con las emisiones del tráfico rodado tienen un máximo característico durante las horas punta de la mañana (07:00-09:00 UTC, 5,000 – 25,000 cm^{-3} = percentiles 25^{th} - 75^{th}), mientras que aquellas relacionadas con los barcos (15,000 – 45,000 cm^{-3}) y la refinería (25,000 – 95,000 cm^{-3}) presentan un máximo en el periodo de 10:00-17:00 UTC, debido a los efectos de la meteorología y la fotoquímica. En aquellos días en los que las concentraciones de PUFs (promedio 24-h) se mantuvieron en el rango de 2,000 – 20,000 cm^{-3} (percentiles 0.1^{th} - 70^{th}), el tráfico rodado fue la fuente predominante; siendo responsable del 85% de las PUFs observadas. Las concentraciones más altas (> 70^{th}, hasta 56,000 cm^{-3}, promedio de 24-h) fueron propiciadas por las emisiones de los barcos y refinería, durante el periodo de 10:00 a 17:00 UTC. En este periodo, las emisiones de los barcos contribuyeron en un 39% a las PUFs, mostrando concentraciones entre 19,500 – 46,700 cm^{-3} (percentiles 55^{th} – 90^{th}), mientras que la refinería contribuyó en un 60% a la concentración de PUFs, con valores comprendidos entre 46,700 – 99,100 cm^{-3} (percentiles de 95^{th} – 100^{th}). Por debajo de 19,500 cm^{-3} (percentil 55^{th}), el tráfico rodado fue el responsable del 91% de la concentración de PUFs registrada en esta zona urbana.

En el observatorio de montaña de Izaña, las concentraciones de gases reactivos están influenciadas principalmente por dos procesos: el transporte ascendente desde la capa de mezcla y el transporte de largo recorrido a escala sinóptica. Las concentraciones de gases reactivos muestran un marcado ciclo diario, inducido por el transporte ascendente de aire desde la capa de mezcla durante las horas de sol, y el transporte descendente de aire procedente de la troposfera libre durante la noche. Este flujo diurno está inducido por el desarrollo de corrientes de aire ascendente alrededor de Tenerife. Los ratios día-noche promedios fueron ~3 para NO_X, ~2 para SO_2, ~1 para CO y <1 para O_3. En promedio, el 75% de los NO_X, 50% del SO_2 y el 4% del CO registrado durante el periodo diurno se

atribuye al transporte ascendente de aire procedente de la capa de mezcla a Izaña. Esta contribución, es la responsable durante el día, de las concentraciones de NO_X, SO_2 y CO por encima del nivel de fondo nocturno de troposfera libre. Por el contrario, las concentraciones de O_3 son más bajas durante el día, debido al fuerte gradiente vertical de este gas traza en esta región.

Los procesos que contribuyen a las concentraciones de CO y O_3 en la troposfera libre de esta región fueron estudiados mediante el análisis de las concentraciones de dichos gases mostraron durante el periodo nocturno, herramientas meteorológicas y el uso de dos productos determinados a partir del análisis de retrotrayectorias (rutas de transporte y regiones fuente potenciales). El análisis de estos productos y la correlación que se observó entre el O_3 y el CO durante los cuatro años de estudio (2007 – 2010) ponen de manifiesto que la exportación hacia el este, de contaminantes procedentes de Norte América, modula la variabilidad de las concentraciones de O_3 y CO en la troposfera libre del Atlántico Norte. Bajo este escenario, el O_3 muestra concentraciones típicas en el rango de 34 - 76 ppb y ratios O_3 / CO entre 0.2 - 0.7. Los episodios de alta concentración de O_3 (47 – 87 ppb), ratios O_3 / CO altos (0.7 – 6.5) y baja correlación entre O_3 y CO ocurren al final de la primavera y el verano. Estos episodios, están asociados a transporte descendente de aire de la alta troposfera al este de las depresiones en el Atlántico Norte este. La influencia del transporte de largo recorrido en las concentraciones de NO_X y SO_2 registradas bajo las condiciones de troposfera libre no pudieron ser estudiadas debido a que las concentraciones de estos gases traza se mantuvieron bajo el límite de detección de los analizadores utilizados (60 ppt para SO_2 y 50 ppt para NO y NO_X en promedio de 5 min) durante el 37% y 92% del periodo nocturno por año, respectivamente.

En el observatorio de Izaña, las concentraciones de PUFs están fuertemente influenciadas por el desarrollo orográfico y diurno de corrientes de aire ascendentes. Estos flujos de aire ascendente, perturban la troposfera libre y resultan en un aumento en las concentraciones de vapor de agua, SO_2, NO_X y PUFs durante el día. El análisis de los datos muestra que los procesos de nucleación inducidos foto-químicamente (y probablemente de otros precursores gaseosos que no se midieron) juegan un papel fundamental en la formación de PUFs en estos flujos de aire ascendente. Debido a esto, las concentraciones de nanopartículas (3–10 nm) tienden a alcanzar valores altos durante el día. La formación de nuevas partículas se observó casi todos los días debido a las condiciones favorables asociadas a la entrada de aire de la capa de mezcla en la troposfera libre, incluso para concentraciones bajas de SO_2 (de decenas a centenas de ppt; es decir, de 1 a 3 órdenes de magnitud más bajas que en el área metropolitana de Santa Cruz). La reducida área superficial de las partículas pre-existentes, baja temperatura y alta intensidad de radiación solar, favorecieron la formación de PUFs y nanopartículas. Durante la noche, las concentraciones de PUFs eran similares a las registradas en otras estaciones emplazadas en la troposfera libre (~500 cm^{-3}). Estos resultados demuestran claramente que las altas montañas que alcanzan la troposfera libre, son regiones fuente activas de PUFs.

Estos resultados muestran importantes implicaciones que deberían de ser consideradas por los gestores de calidad del aire. En primer lugar, la mayoría de los estudios en PUFs y calidad del aire

urbano se han focalizado en las emisiones del tráfico rodado. De hecho, dicha fuente es la única sujeta a valores límites de PUFs. Los resultados de esta investigación demuestran claramente que las emisiones de SO_2 provocan altas concentraciones de PUFs (frecuentemente más altas que aquellas relacionadas a las emisiones del tráfico rodado). Debido a que estas altas emisiones de SO_2, las concentraciones de PUFs en el área metropolitana de Santa Cruz de Tenerife, muestran características (ej., evolución diaria, rangos de concentración típicos, cocientes PUFs – BC) que difieren de aquellas encontradas en otras ciudades donde las emisiones del tráfico rodado son la fuente principal de PUFs (ej., Londres, Milán, o Berna). La influencia de las emisiones de SO_2 en la concentración de PUFs, se observa incluso en lugares que distan de las fuentes de emisión de SO_2, como demuestran los datos recolectados en el observatorio de Izaña. En segundo lugar, en cuanto al debato abierto sobre si los actuales valores límite para el material particulado PM_{10} y $PM_{2.5}$ debería de ser complementado, este estudio concluye que la monitorización simultánea de PUFs, black carbon, PM_{10} y $PM_{2.5}$ es una estrategia adecuada para trazar los aerosoles contaminantes de diferente naturaleza (fresco frente a envejecidos) y para fuentes de emisión diferentes: 1) Las PUFs son un mejor trazador de las emisiones frescas de los vehículos, barcos y refinería, que el $PM_{2.5}$ y $PM_{2.5\text{-}10}$, 2) el $PM_{2.5}$ está influenciado de forma significativa por los aerosoles envejecidos, 3) se encontró que el black carbon es el mejor trazador de las partículas sólidas emitidas por el tráfico rodado. El incluir las medidas de PUFs en calidad de aire es de especial relevancia. Un estudio reciente basado en los datos producidos en este estudio, concluyó que existe una asociación entre las hospitalizaciones debido a fallos cardiacos y la exposición a PUFs en el aire ambiente de la ciudad de estudio.

Abstract

This study is focused on identifying the sources and processes that contribute to the concentrations of reactive gases (NO_X, SO_2, CO and O_3) and ultrafine particles (UFPs) and their relationship in ambient air. Because of their impact on human health and their influence on climate, particular attention is paid to ultrafine particles. The study is based on experimental data of reactive gases and ultrafine (diameter < 0.1 µm), black carbon, PM_{10} (diameter < 10 µm) and $PM_{2.5}$ (diameter < 2.5 µm) particles concentrations measured between 2006 and 2010 in the ambient air of two different environments of Tenerife Island: i) the Metropolitan Area of Santa Cruz de Tenerife, where important emissions of pollutants occur, and ii) the Izaña Global Atmospheric Watch (GAW) observatory, a remote mountain top site located in the low free troposphere (~2,400 meters above sea level), well above the stratocumulus layer characteristic of the subtropical oceanic regions.

In the Metropolitan Area of Santa Cruz de Tenerife, it was found that the main sources of UFPs are: vehicle exhausts, ships and a crude oil refinery. The results show that urban background concentration of UFPs is dominated by vehicle exhaust emissions, whereas UFPs events are induced by the emissions of SO_2 from ships and the refinery. The concentration of UFPs linked to vehicle exhaust emissions maximized in the morning (07:00-09:00 GMT, 5,000 – 25,000 cm^{-3} = 25th - 75th percentile), whereas those linked to ships (15,000 – 45,000 cm^{-3}) and refinery (25,000 – 95,000 cm^{-3}) emissions maximized in the 10:00-17:00 GMT period, due to the effects of meteorology and photochemistry. When UFPs (24-h mean) were present in concentrations within the range 2,000 – 20,000 cm^{-3} (0.1^{th} - 70^{th} percentile), vehicle exhausts were the predominant source, accounting for 85% of the observed UFPs. Higher concentrations (i.e., up to 56,000 cm^{-3}, >percentile 70^{th}, 24-h mean) were prompted by the contributions of ships and refinery emissions. The highest UFP concentrations were recorded in pollution events occurred from 10:00 to 17:00 GMT. In this period, ship emissions accounted for 39% of UFPs when their concentrations were within the range 19,500 – 46,700 cm^{-3} (percentile 55^{th} – 90^{th}), whereas the refinery accounted for 60% of UFPs when concentrations were within the range 46,700 – 99,100 cm^{-3} (percentile 95^{th} – 100^{th}). Below 19,500 cm^{-3} (percentile 55^{th}), vehicle exhausts accounted for 91% of UFPs.

At Izaña mountain observatory, the concentrations of reactive gases are influenced by two main processes: upward transport from the boundary layer and a synoptic scale long range transport. The concentrations of reactive gases show a strongly marked daily cycle, induced by the upward transport of air from boundary layer during daylight and downward transport of air from the free troposphere at night. This diurnal airflow is induced by the development of buoyant air flows around Tenerife. The mean daylight to night-time ratios were ~3 for NO_X, ~2 for SO_2, ~1 for CO and <1 for O_3. As average, the 75% of NO_X, 50% of SO_2 and 4% of the CO recorded during daylight are attributed to the upward transport from the boundary layer to Izaña. This contribution results in NO_X, SO_2 and CO concentrations above the free troposphere nocturnal-background during daylight. In contrast, the concentrations of O_3 are regularly lower during daylight than at night due to the strong vertical gradient of this trace gas in this region.

The processes that contribute to the concentrations of CO and O_3 in the free troposphere were studied by the analysis of the night-time concentrations of these gases with meteorological tools and products determined with back-trajectories (transport pathways and potential source regions). The analysis of these products and the correlation observed between O_3 and CO during the four study years (2007 – 2010) point that the eastward exportation of pollutants from North America modulates the variability in the concentrations of O_3 and CO in the North Atlantic free troposphere. In this scenario, O_3 typically shows concentrations within the range 34 - 76 ppb and O_3 / CO ratios within the range 0.2 - 0.7. In addition to these events, episodes of high O_3 concentrations (47 – 87 ppb), high O_3 / CO ratios (0.7 – 6.5) and low correlations between O_3 and CO occur in late spring and summer. These events are associated with downward transport of air from the upper troposphere in the eastern side of depressions developing in the Eastern North Atlantic. The influence of long range transport on NO_X and SO_2 concentrations recorded under free troposphere conditions could not be studied due to the concentrations of these trace gases were lower than the detection limit of the analysers used (60 ppt for SO_2 and 50 ppt for NO and NO_X for 5 min averages) during the 37% and 92% of night-time period/year, respectively.

At Izaña mountain observatory, the concentrations of UFPs are strongly influenced by the development of orographic buoyant upward flows during daylight. These ascending airflows perturbed the low free troposphere and resulted in an increase in the concentrations of water vapour, SO_2, NO_X and UFPs during daylight. The data analysis shows that photo-chemically induced nucleation of SO_2 (and probably other not measured gaseous precursors) plays a key role in the formation of UFPs in these ascending airflows. Because of this, the concentrations of nano-particles (3–10 nm) tend to reach high values during daylight. New particle formation was observed almost every day owing to the favourable conditions associated with the entry of boundary layer air in the low free troposphere, even if SO_2 concentrations are rather low (tens to hundreds of ppt; i.e. 1 to 3 orders of magnitude lower than in the Santa Cruz Metropolitan Area). The low surface area of pre-existing particles, low temperature and high radiation intensity clearly favoured the formation of ultrafine and nano particles. At night, the concentrations of UFPs are similar to those recorded in other free troposphere sites around the world (~ 500 cm^{-3}). These results clearly demonstrate that high mountains that enter in the free troposphere are active source regions of ultrafine particles.

These results have important implications that should be considered by air quality managers. First, most of studies on UFPs and urban air quality have focused on vehicle exhaust emissions. In fact, vehicle exhaust is the only source subject to limit values for emissions of UFPs. The results of this research clearly demonstrate that SO_2 emissions result in high concentrations of UFPs (frequently higher than those linked to vehicle exhaust emissions). Because of these high SO_2 emissions, UFPs in Santa Cruz Metropolitan Area exhibit features (e.g. daily evolution, typical concentrations ranges, UFP to black carbon ratio) different to those observed in cities where vehicle exhausts are the predominant UFPs source (e.g. London, Milan, Lugano or Bern). The influence of SO_2 emissions on UFPs concentrations is observed even at distant sites from the SO_2 emission sources, as demonstrated with the data collected at Izaña observatory. Second, about the open debate

on if the current limit values for PM_{10} and $PM_{2.5}$ should be complemented, this study concludes that the simultaneous monitoring of ultrafine, black carbon, PM_{10} and $PM_{2.5}$ particles is a suitable strategy of tracing aerosol pollutants of different nature (fresh vs. aged) and for difference sources: 1) UFPs are a better tracer of the fresh emissions of vehicle exhaust, ship and refinery, than $PM_{2.5}$ and $PM_{2.5-10}$, 2) $PM_{2.5}$ is significantly influenced by aged aerosols, 3) black carbon was found to be the better tracer of solid particles emitted by vehicle exhausts. To include UFPs measurements is of especial relevance. A recent research, based on the data set produced in this study, concluded that there is an association between hospitalizations due to heart failure and exposure to UFPs in the ambient air of the study city.

Contents

Chapter 1

Introduction

1.1 Air Pollution: from local to global scales

The 19th century industrial revolution resulted in a sharp increase in the emissions of air pollutants mostly due to combustion processes. The use of coal as fuel resulted in high concentrations of sulphur dioxide (SO_2), heavy metals (Hg, As, Cd, Ni, V, among other), carbonaceous particles and carbon monoxide (CO) in the ambient air of industrialized cities of Europe and North America (Markham, 1994). Human health impairment was the first identified adverse effect linked to these emissions (Lippman, 2000). Several events of high morbidity and mortality during 'fog – smoke' episodes occurred during the first half of the 20th century. The one occurred in London from 5th to 9th December 1952 is the most well known, when about 4,000 people died due to the exposure to high concentrations of SO_2 (up to 2,000 $\mu g \cdot m^{-3}$) and black smokes (up to 1,500 $\mu g \cdot m^{-3}$; UK Ministry of health, 1954).

The effects of air pollution on the environment have traditionally been studied in well differentiated scales: local, regional and global. The interest on the **local scale** has traditionally focused on the effects on human health. Since the 1950s, authorities of some European countries ordered the building of higher stacks, the segregation of the industrial from the residential areas, and prompted a better use of fuels, with the purpose of improving air quality. Since the 1960s to the 1980s, the emission rates of pollutants were individually managed by each country. Since the 1990s, the air quality management in most of Europe is subject to the standards set by the European Commission within the context of the European Union (EU). The EU Directive 2008/50/EC sets limit values for the concentrations of several air pollutants in the gaseous and particulate matter phases. In Table 1.1, the anthropogenic sources, features and impact of some key pollutants is summarized. The continuous monitoring of the ambient air concentrations of some of these key pollutants is nowadays one of the tools used for air quality management. In the EU context, this management is performed by each Member State.

The policies for air quality management during the 1970s and 1980s faced the problem by the principle 'the solution to pollution is dilution'. However, a set of phenomena, mostly observed during the last sixty years, have evidenced that some pollutants are effectively transport to distant regions, in such a way that they may present effects, on the environment and climate, in the **regional** and **global scales**. Some relevant findings:

→ The occurrence of regional acid rain events in North America and Europe became in a matter of concern during the 1970s due to the potential impact on terrestrial ecosystems (Likens and Bormann, 1974; Rodhe, 1976).

→ During the 1980s, high concentrations of tropospheric ozone in rural areas, downwind of cities, were much more frequent than expected (Logan, 1985). This type of pollution affects not only human health, but also crop productivity and forest health, resulting in significant impact on the potential economic growth (Logan et al., 1988).

→ Under the suspicion that fossil fuel burning could be increasing the concentrations of carbon dioxide (CO_2) in the troposphere, D.C. Keeling started to measure this greenhouse gas at the Mauna Loa mountain top (Hawaii; Keeling, 1960). The increase in CO_2 concentrations from 315 ppmv in 1958 to 385 ppmv in 2008 that has been observed at this site have been corroborated in the global scale.

→ In the mid 1980s, it was discovered that stratospheric ozone over the Antarctica experienced a sharp decrease in the austral spring (Farman et al., 1985). Because this could increase UV radiation at the Earth surface, with severe consequences on life, this depletion of stratospheric ozone layer rapidly turned into one of the first environmental world problem.

Because the public awareness, environmental issues started to be included in the international political agendas. Undertaken actions included international agreements for decreasing the emissions of some key pollutants (e.g. the Montreal Protocol for protecting the ozone layer at the end of 1980s, the United Nations Economic Commission for Europe Convention on Long-Range Transboundary Air Pollution Protocols included acid rain in the 1980s, and the Kyoto protocol for the reduction in the emissions of greenhouse gases in 1997) and the creation of global and regional monitoring and research networks for studying how human activities could be inducing changes in the composition of the atmosphere. One of these global networks was created by the World Meteorological Organization (WMO).

The WMO established the Global Atmospheric Watch (GAW) program in 1989. The objectives of the GAW program are to provide reliable long-term observations of the chemical composition of the atmosphere, and to organize assessments in support of formulating environmental policy (GAW, 2001a, 2005). The GAW monitoring program includes a coordinated global network of observing stations with supporting facilities and a network of regional stations. The GAW network is constituted by approximately 300 stations around the world. Only 27 of these are labelled as 'global' stations, representative of large geographical areas (Figure 1.1).

Table 1.1 Limit and target values and main features of the air pollutants regulated by EU Directive 2008/50/EC and measured in the GAW program. See more details in EU Directive 2008/50/EC and Seinfeld and Pandis, 1998

LIMIT / TARGET VALUES (average time and target values)**:**							
		O_3	**SO_2**	**NO_2**	**CO**	**PM_{10}**	**$PM_{2.5}$**
Human health		Max 8h mean/1d 120 $\mu g \cdot m^{-3}$ (<25 d/yr, 3 yr avrg)	350 $\mu g \cdot m^{-3}/h$ (< 24 times/yr) 125 $\mu \cdot g m^{-3}/d$ (< 3 times/yr)	200 $\mu g \cdot m^{-3}/h$ (<18 times/yr) 40 $\mu g \cdot m^{-3}/yr$	10 $mg \cdot m^{-3}$ daily max	50 $\mu g \cdot m^{-3}/d$ (< 35 times/yr) 40 $\mu g \cdot m^{-3}/yr$	25 $\mu g \cdot m^{-3}/yr$ (Target value entered into force 1.1.2010. Limit value enters into force 1.1.2015)
Vegetation		May - July, 18,000 $\mu g \cdot m^{-3}h$, 5 yr avrg.	20 $\mu g \cdot m^{-3}/yr$ and winter: Oct–March	30 $\mu g \cdot m^{-3}/yr$ (also NO_X)		25 $\mu g \cdot m^{-3}/yr$ (1/01/2015) 20 $\mu g \cdot m^{-3}/yr$ (1/01/2020)	-

IMPACTS:							
Human health		UV filter Lungs infection	respiratory ways constriction	alveoli irritation	O_2 transport in blood impairment	respiratory and cardio-vascular diseases	
Environ	*acid deposition*	√	√	√		-	
	visibility impairment		√	√	-	-	-
	eutrophication			√		-	

Figure 1.1 Global Atmospheric Watch stations
(http://www.wmo.int/pages/prog/arep/gaw/measurements.html)

The GAW program is divided in six subprograms:

1) Greenhouse Gases

2) Reactive Gases

3) Aerosols

4) Precipitation Chemistry

5) UV Radiation

6) Ozone

In addition, GAW has a specific program for urban areas: the Urban Research Meteorology and Environment (GURME) programme. Each of these programs has a Scientific Advisory Group (SAG) and GAW Central Facilities responsible for scientific guidance and technical details of the global network.

1.2 Atmospheric Aerosols and Ultrafine particles

1.2.1. Atmospheric Aerosols

Atmospheric aerosol, also so-called particulate matter (PM), referees to the solid and/or liquid particles suspended in the atmosphere. Aerosols are a matter of concern owing to their adverse effects on human health and on climate (Table 1.2).

Table 1.2 Influence of aerosols in processes affecting climate. BC: black carbon, OC: organic carbon. See more details in IPCC, 2007

Direct Effects: -0.5 ± 0.4 W m^{-2}	
Dispersion of sunlight	Sulphate, fossil fuel of OC, nitrate and mineral dust
Absorption of sunlight	BC and biomass burning
Indirect Effects: -0.7 [-1.8 to -0.3] W m^{-2}	
Cloud condensation nuclei (CCN)	Alteration microphysical and radiative properties of cloud: decrease size in cloud droplets, increase in life time of clouds and modification of regional rain patterns
Semi direct Effects: Some studies find a >0 effect; however, when absorbing aerosols are located above the cloud layer the semi-direct forcing can be negative (Johnson, 2003).	
May reduce cloud cover and liquid water content by heating the cloud and the environment within which the cloud forms	Highly absorbing aerosols such as BC

The original definition also includes the gas phase; however it is not commonly measured or studied (Hinds, 1982). Particles may be classified in different ways, according to their formation mechanism, origin, chemical composition or size, among other properties.

(1) **Formation Mechanisms.** Primary particles are those directly emitted in the aerosol phase. Secondary particles are formed in the atmosphere by gas o particle conversion processes: homogeneous nucleation (only involving gaseous precursors) or heterogeneous nucleation (i.e. reaction of gases with liquid or solid phases).

(2) **Chemical Composition**. The predominant chemical components of particulate matter (PM) are sulphate, nitrate, ammonium, sea salt, mineral dust (mostly clays, silicates, carbonates and iron oxide), organic matter, black carbon and elemental carbon (Table 1.3). Moreover, trace elements are also present (V, Ni, As, Cd among others).

(3) **Origin**. Aerosols can be classified as natural or anthropogenic. Natural tropospheric aerosols, include primary species, such as sea salt, mineral dust emitted by undisturbed soils due to the action of winds, volcanic ashes and biological debris, and secondary compounds, as sulphate formed by natural emissions of SO_2 (e.g. volcanoes or conversion of marine Dimethyl sulfide) or

secondary organic compounds (e.g. biogenic emissions of isoprene and monoterpenes). Anthropogenic primary particles include road dust (abrasion of brakes, tires and pavement), demolition dust and some carbonaceous compounds linked to combustion (elemental, black and organic), whereas anthropogenic secondary particles includes sulphate, nitrate, ammonium and carbonaceous compounds mostly linked to industrial, urban and agriculture-farming emissions of gaseous precursors (Querol et al., 2001).

Table 1.3 Summary of the features of the five main groups of PM components

Chemical Composition	**Composition**	**Source**
Mineral dust	Al, Ca, Si, Fe, Ti, K, Mg, Co, Rb, Ba, Sr Mineral composition: SiO_2, $CaCO_3$, $CaMg(CO_3)_2$, clays, feldspar, Fe_2O_3, $CaSO_4.2H_2O$ (Castillo, 2006)	Resuspension of arid soils and long range transport from arid regions
	NaCl (85%) + sulphates	
Sea salt	*Species* (Mészáros, 1999): Cl^-, Na^+, SO_4^{2-}, Br^-, HCO_3^-, Mg^{2+}, Ca^{2+}, K^+, $MgCl_2$, $MgSO_4$, Na_2SO_4, Al, Co, Cu, Fe, Mn, Pb, V, Zn	Generated by bubble processes on the ocean surface
Carbonaceous fraction	Elemental + black + organic carbon	Fuel combustion
Nitrogen compounds	NO_3^-, NH_4^+, NH_4NO_3	NH_3^- (aq) + NH_4^+ (g) → NH_4NO_3 (s) HNO_3 (g) + NH_3 (g) → NH_4NO_3 (s)
Sulphate aerosols	$(NH_4)_2SO_4$ (Hidy, 1994)	SO_2, DMS, COS: Erosion, soil resuspension, building materials, transport, industry, combustion

(4) **Size distribution**. The size of the particles may range from a few nanometres (nm) to tens of micrometers (μm; Figure 1.2). Whitby (1978) pointed out that the size distribution of atmospheric aerosols consists of modes (peaks in the distribution) which can be described by lognormal functions (normal distribution of a logarithmic variable). These distributions are classified in modes, and these modes have chemically distinct compositions due to their different sources (Hidy, 1994; Seinfeld and Pandis, 1998), and suffer variations with locations and time. The main features of the particles includes in these modes is summarised in Table 1.4 and Figure1.2:

a) *Nucleation mode*. Expands from 1 to 20 nm. These particles are formed by homogeneous nucleation gases. These particles have a relatively short lifetime. They tend to show high concentrations close to their sources or just after formation (Willeke and Baron, 1993). This gas to particle conversion may involve photochemical reactions, or homogeneous nucleation during the cooling of fresh combustion emissions (Rodríguez and Cuevas, 2007).

b) *Aitken mode*. Covers the range from 20 to 100 nm. Particles of this mode may originate from primary combustion emissions and from particle growth processes. The Aitken mode particles often make dominant contribution to the total particle number concentration in the size range >50 nm in continental areas (Tunved et al., 2003).

c) *Accumulation mode*. Ranges within 100 to 1000 nm. This mode is formed by gas-to-particle conversion through chemical reactions and condensation of secondary species (sulphate, nitrate, ammonium and organics) onto pre-existing particles, as well as coagulation.

d) *Coarse mode*. Referees to particles coarser than 1000 nm. Most of these particles are primary, such as sea salt, or formed by mechanical erosion processes. In the air quality context, the coarse mode is set to 2.5 μm.

In Figure 1.2A aerosol size distribution typical observed in Europe is shown. Figures 1.2B and 1.2C indicate the processes affecting particle concentrations in terms of *mass* and *number*. Residence time of aerosols (from hours to weeks) depends also on their size, thermodynamic properties and chemical composition. Two key issues should be considered (Table 1.4):

1) Ultrafine particles, i.e. the nucleation plus Aitken mode, accounts for most of the particle number concentration (typically 80-90%; Wehner and Wiedensohler, 2003; Rodríguez et al., 2007). However, they account for a very low fraction of the particle mass concentration. In contrast, most of the particle mass occurs in the accumulation and coarse modes, which accounts for 30-70% of the total mass each. These two modes accounts for a very low fraction of the particle number.

2) Ultrafine and coarse particles have a relative short residence time, hours and a few days, respectively. The former tend to be removed by evaporation, coagulation and deposition (diffusion controlled) on surfaces, whereas the latter tend to experience dry gravimetric deposition. In contrast, the accumulation mode particles are only removed by rainfall. Thus, these accumulation mode particles (0.1 – 1 μm) exhibits the longest residence time and are the most important contributor to aerosol background.

These differences in the size distribution in terms of number and mass concentration have implications that will be discussed in the next sections.

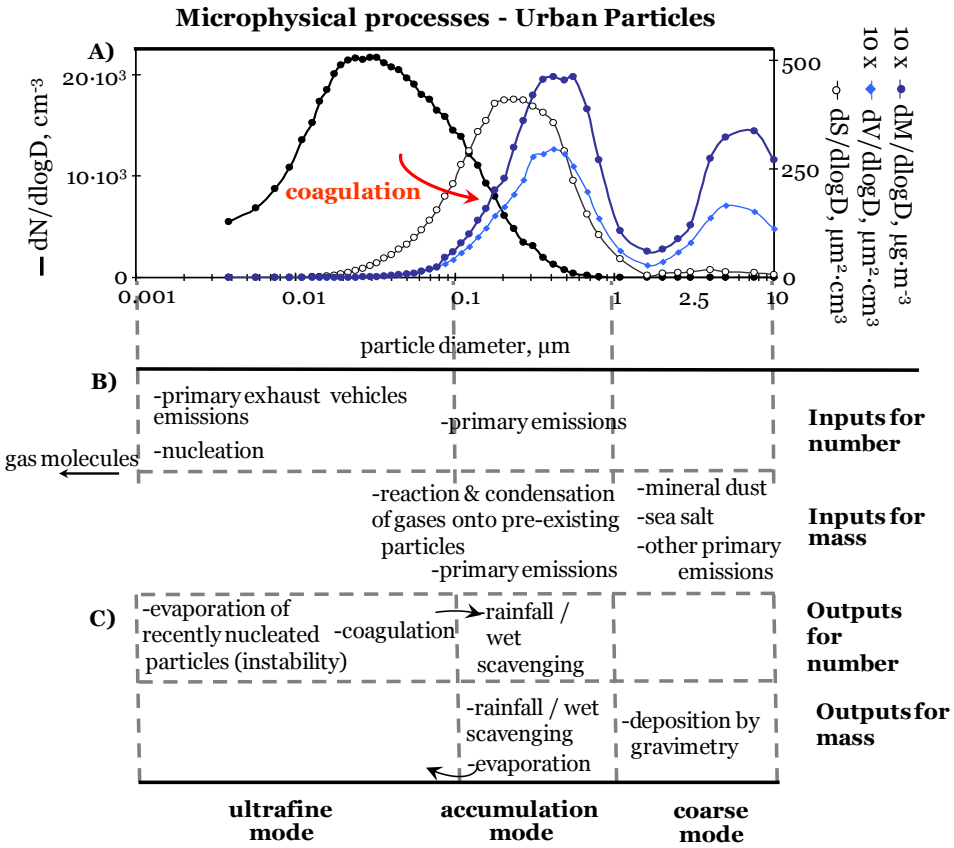

Figure 1.2 Particle size distributions (Rodríguez et al., 2006)

Table 1.4 Aerosol modes. N: particle number, PM: particle mass

	Ultrafine		**Accumulation**	**Coarse**
	Nucleation	***Aitken***		
Size range	< 0.02 μm Max. N	0.02 – 0.1 μm	0.1 - 1 μm	1 - 10 μm
Formation processes	*Binary nucleation*: e.g. H_2SO_4-H_2O (Kulmala et al., 1998) *Ternary nucleation*: e.g. H_2SO_4-H_2O-NH_3 (Korhonen et al., 1999) *Organics*	Primary soot emissions and particle growth (Wehner et al., 2002)	Condensation and adsorption of smaller particles	Mechanic erosion
PM contribution	80 - 90% of N < 10% of PM		10 - 15% of N 30 - 70% of PM	<<1% of N 30 - 70% of PM
Residence time	~ hours		~ 2 weeks	hours to some days
Composition	Organic compounds and sulphate (Zhang et al., 2004)	Urban soot and nucleation growth particles (Lingard et al., 2006)	Gas-to-particle conversion by *condensation in* and/or *reaction with* the pre-existing aerosol surface in ambient air	Primary emissions: sea salt, mineral dust, biological waste, resuspension caused by road traffic, public works
Sinks	Evaporation, growth and diffusion deposition	wet deposition (rainfall)		wet scavenging and dry deposition

1.2.2. Ultrafine particles in urban areas

The current European legislation for air quality set limit values for the ambient air concentration of airborne particles in terms of the mass concentrations of particles with an aerodynamic diameter < 10 μm and < 2.5 μm (Directive 2008/50/EC), PM_{10} and $PM_{2.5}$, respectively. The PM Working Group of the European Commission, the COST action 633, and an important fraction of the scientific community, have opened a debate on if these two metrics should be complement with other parameters, such as ultrafine particles and/or black carbon (Second Position Paper on PM, 2004; COST 633 Report, 2009).

Several studies have shown that exposure to ultrafine particles (UFPs, diameter < 100 nm) results in harmful effects on human health. Since the deposition in the respiratory system of inhaled UFPs is governed by diffusional processes, it is believed that UFP translocation within the human body is dependent on particle size. Thus, the smallest UFPs (e.g. <5 nm) mostly deposit in the nasopharyngeal region, whereas larger ones (≥ 20 nm) mostly reach the alveoli and enter the bloodstream (ICRP, 1994; Peters et al., 1997; Oberdörster et al., 2004). Translocation of inhaled UFPs from the lungs to the liver and accumulation in the liver has been documented as occurring in a matter of a few hours (Oberdörster et al., 2002). UFPs also produce an enhancement of atherosclerosis and cardiovascular ischemic events (Araujo et al., 2008; Araujo and Nel, 2009). Moreover, fresh soot particles are particularly surface - reactive and may also carry carcinogenic compounds (e.g. PAHs; Highwood and Kinnersley, 2006). These examples of toxicological studies tend to show that particles become more toxic per unit mass as their size decrease (Brown et al., 2000). Thus, attention is focused on particle number rather than mass fraction. Because of their very low mass, UFPs are typically measured in terms of number of particles per unit of air volume.

Studies, mainly carried out in Europe and the US, conclude that UFPs in urban air are mainly due to primary vehicle exhaust emissions. These particles tend to exhibit a size distribution with a "nucleation mode (<30 nm)" and a "soot mode (50–100 nm)" (Burtscher, 2005; Rose et al., 2006):

→ The *nucleation mode* is mainly attributed to binary H_2O–H_2SO_4 nucleation, nucleation of some organic compounds and subsequent particle growth (up to 30 nm) by condensation processes, during the dilution and cooling of vehicle exhaust (Harris and Maricq, 2001; Casati et al., 2007). Low ambient air temperature, low dilution conditions or high relative humidity increase the formation and growth rates of nucleation particles during the dilution and cooling of vehicle exhaust (Olivares et al., 2007; Casati et al., 2007).

→ The *soot mode* (50-100 nm) is mainly composed of elemental carbon, absorbed organic material and some other trace elements formed in the engine, and directly emitted in the aerosol phase (Burtscher, 2005; Harris and Maricq, 2001). These soot emissions have classically been higher in diesel than in gasoline vehicles.

During the last two decades the European Commission has progressively been reducing the particulate matter emission in the vehicle exhaust (Table 1.5). This decrease in the particulate matter has been performed in terms of particulate matter mass emission. EURO 5b that entered into force in September 2011, is the first legislation in establishing limit values for ultrafine particle emissions, based on total particle number. The fact that the EURO 1 - 6 had been established in terms of mass concentration led to a reduction in the emissions of particles >0.1 μm, i.e. the main contributors to $PM_{2.5}$ and PM_{10}. However, this may lead to an increase in the formation rates of new UFPs during the dilution and cooling of the vehicle exhaust (Figure 1.3).

Table 1.5 Evolution of the European regulations of PM and particle number (PN) on vehicles exhaust emissions

EURO	**Date**	**Directive**	**PM lim. ($g \cdot veh^{-1} \cdot Km^{-1}$)**		**PN lim. ($\# \cdot Km^{-1}$)**
			Diesel	**Petrol**	**Diesel**
EURO 1	Jul-1992	91/441/EEC-93/59/ECC	0.18	--	
EURO 2	Jan-1996	94/12/CE-96/69/CE	0.08	--	
EURO 3	Jan-2000	98/69/CE	0.05	--	
EURO 4	Jan-2005	98/69/CE-2002/80/CE	0.025	--	
EURO 5a	Sep-2009	Regulation 715/2007	0.005	0.005**	
EURO 5b	Sep-2011	Regulation 692/2008	0.005		$6.0 \cdot 10^{11}$
EURO 6	Sep-2014	Regulation 692/2008	0.005	0.005__	$6.0 \cdot 10^{11}$

** Applied only to vehicles with direct injection engines

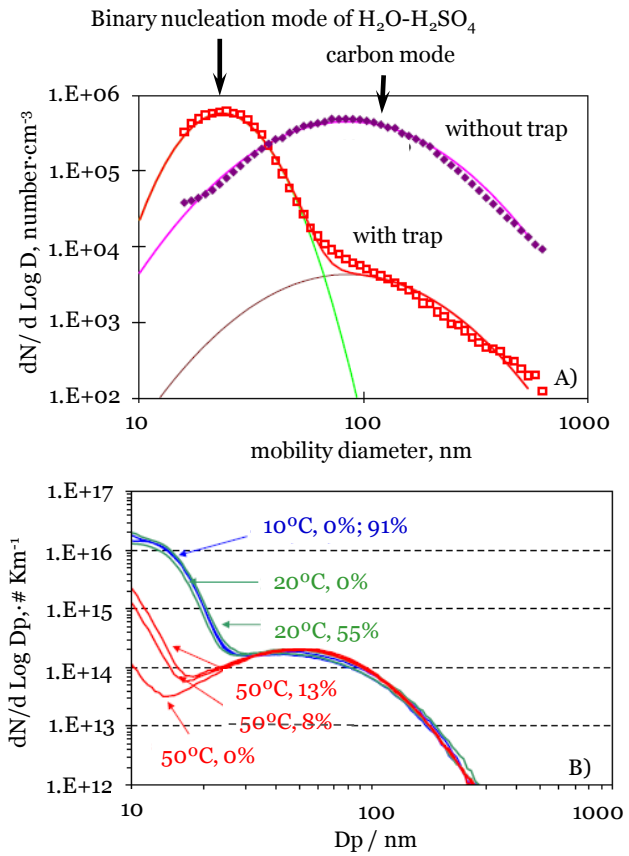

Figure 1.3. A) Size distribution of the particles emitted by vehicle exhaust with and without particle trap. Dp: particle diameter. Source: Burtscher, 2005. *B).* Size distribution of the particles emitted by vehicle exhaust under different conditions of temperature and humidity. Source: Casati et al., 2007

Because of the debate on the need to introduce standards for UFPs (e.g., Franck et al., 2011), several European countries are already performing long term monitoring of total number concentrations (N) in urban ambient air (Reche et al., 2011). Given that the 80 - 90% of the particles are ultrafine, in terms of number, N is considered representative of the UFP concentrations in urban ambient air. These data are already being used for health effects studies (e.g., Wichmann and Peters, 2000; Domínguez-Rodríguez et al., 2011; Franck et al., 2011). Studies performed in Europe and North America are showing that the relationship between ultrafine particles concentrations and PM_{10} and $PM_{2.5}$ is rather complex. As consequence these is not a univocal relationship between different type of aerosol metrics. Some examples:

→ Rodríguez et al. (2007) studied the relationship between number size distribution and $PM_{2.5}$ composition in Milan, Barcelona and London. They found that UFP mostly originated from fresh vehicle exhaust emissions, while $PM_{2.5}$ exhibited high concentrations during events of aged polluted air in the metropolitan areas. As consequence, high concentrations of UFP linked to relatively low PM2.5 events, and vice versa, occurred frequently.

→ In urban areas, UFP tend to exhibits a much higher spatial variability than $PM_{2.5}$ (Hoek et al., 2008).

→ Long range transport of (aged) aerosol may exhibit a much higher influence on PM_{10} and on $PM_{2.5}$ than in UFP concentrations (Ketzel et al., 2004).

→ Processes contributing to the decrease in PM_{10} and/or $PM_{2.5}$, will prompt a decrease in the surface area acting as a condensation sink of aerosol gaseous precursors. This may enhance the new UFP formation rates (Burtscher, 2005; Hamed et al., 2007).

1.2.3 Ultrafine particles in rural and mountain air

A significant fraction of UFPs in rural and mountain sites are linked to the formation of new particles. New particle formation (NPF) due to homogenous nucleation and subsequent growth processes have become a topic of great interest in the atmospheric and environmental sciences, owing to the influence of particles on climate, hydrological cycle and radiative balance. These particles are initially detected at sizes of a few nanometres and may grow until reaching a size within the range of 50 nm to > 100 nm (Kulmala et al., 2004a). The lower detection limit for neutral particles is of about 3 nm with commercial instruments, although some prototypes seem to be able to detect particles down to 1.5 nm (Sipilä et al., 2010).

A major effort is currently undertaken to understand the mechanisms that cause the nucleation and subsequent particle growth. Several theories have been proposed as candidates for the initial cluster formation, such as binary nucleation H_2O-H_2SO_4 (Easter and Peters, 1994), ternary nucleation H_2O-H_2SO_4-NH_3 (Eisele and Mc Murry, 1997), nucleation of organic compounds of low vapour pressure (O'Dowd et al., 2002), ion-induced nucleation (Kim et al., 2002) and more recently the activation of neutral and/or ionic cluster (Kulmala et al., 2006). The condensation of organic vapours onto the cluster / particles includes organic compounds resulting from the oxidation of species linked to biogenic emissions, such as isoprene and terpenes (Marti et al., 1996; Allan et al., 2006; Laaksonen et al., 2008).

Kulmala and Kerminen (2008) pointed out that new particle formation processes require a 'high vapour source rate' provided by photochemistry and a 'low condensation sink' favoured by low surface concentration of pre-existing particles. Two steps are necessary in the NPF processes (Kulmala et al., 2000): i) nucleation of an initial cluster (the nucleation process itself), and ii) activation of the cluster resulting in particle growth to a detectable diameter (3 nm). After a set of

field measurement campaigns, Kulmala and co-workers (Kulmala et al., 2005) observed that the clusters necessary for the initial steps seem to be always present in the atmosphere. They concluded that nucleation of sulphuric acid gas molecules plays a key role in the formation of such stable clusters (0.5 – 1.5 nm size; Fiedler et al., 2005; Kulmala et al., 2006; Kulmala and Kerminen, 2008). The so called 'NPF events' occur when clusters are activated and grow to detectable sizes (≥ 3 nm). It is believed that 'nucleation' and 'cluster and particle growth' may frequently be decoupled processes and that species involved in the nucleation step might not necessarily be the same as those involved in the cluster / particle growth (Kulmala et al., 2004a).

NPF has been observed in the *continental boundary layer* (Weber et al., 1997; Boy and Kulmala, 2002; Stanier et al., 2004; Fiedler et al., 2005; Rodríguez et al., 2005; Kulmala et al., 2006) and in *the mid and upper free troposphere* (Herman et al., 2003; Schröder et al., 2002; Kanawade and Tripathi, 2006; Benson et al., 2008). Moreover, it may also occur in the *outflows of orographic clouds* (Wiedelsohler et al., 1997) and *in proximity to stratus, cirrus and marine cumulus* (Hegg et al., 1991; Perry and Hobbs, 1994; Clarke et al., 1998; Lee et al., 2004). These investigations have shown that NPF is a process strongly dependent on environmental conditions.

The occurrence of nanoparticles (diameter < 10 nm) in the continental boundary layer is highly influenced by solar radiation, temperature, water vapour, relative humidity, and the concentration of pre-existing particles and sulphuric acid and/or organic vapours (Weber et al., 1997; Boy and Kulmala, 2002; Stanier et al., 2004; Fiedler et al., 2005; Rodríguez et al., 2005; Kulmala et al., 2006).

NPF has also been observed on high mountains that reach the *low free troposphere*, such as Jungfraujoch (3,580 m.a.s.l., Switzerland), Monte Cimone (2,165 m.a.s.l., Italy), Mauna Loa (3,400 m.a.s.l., Hawaii), Khumbu (5,079 m.a.s.l., Nepal), Puy de Dôme (1,465 m.a.s.l.; France), Norikura (2,770 m.a.s.l.; Japan) and Lemmon (2,790 m.a.s.l., USA; Weber and McMurry, 1996; Weingartner et al., 1999; Van Dingenen et al., 2005; Shaw et al., 2007; Nishita et al., 2008; Venzac et al., 2007, 2008, 2009). Many of the studies have been based on short campaigns and in many cases did not include measurements of trace gases and other relevant parameters. Owing to this, the conditions favouring the occurrence of nanoparticles in the boundary layer to free troposphere transition region have not been deeply investigated.

1.3 Antecedents and Context

In this work a study on ultrafine particles in the ambient air of Tenerife (Canary Islands) is presented. As already described above, air pollution by UFPs has become in a matter of concern. During the last decade there has been a significant increase in our knowledge on this type of air pollution. However, many uncertainties still remain. Some examples:

→ Studies have mostly focused on the emissions from vehicle exhaust. However, other sources may also contribute to UFPs; for example those releasing gaseous precursors such as sulphur dioxide or organic compounds. What are typical concentrations of UFPs in urban areas affected by SO_2 emissions, such as those linked to oil refineries or ships?.

→ There is lack of techniques for identifying sources of UPFs. Techniques used for source apportionment of PM_{10} and $PM_{2.5}$ (based on sampling in filter and chemical characterisation) are not suitable for UFPs studies, owing to the technical difficulties in their sampling and their chemical characterization (very low amount of sample). There is a lack of techniques/methodologies for quantifying the sources and processes contributing to ultrafine particle concentrations in urban ambient air. Only a few attempts have been made (Rodríguez and Cuevas, 2007; Pey et al., 2009). Is it possible to use the data available from the air quality monitoring networks for detecting the source and processes affecting UFPs concentrations? Is it possible to estimate the contribution from each source?

→ Most of studies on UFPs in rural areas have been performed in *continental boundary layer*, mostly at mid-latitudes (Weber et al., 1997; Boy and Kulmala, 2002; Stanier et al., 2004; Fiedler et al., 2005; Rodríguez et al., 2005; Kulmala et al., 2006). Only a few studies, mostly based on short campaigns have been performed in high mountain observatories (those cited in the previous section). What is the origin of the UFPs observed in the mountain sites entering in the clean low troposphere? Are the gaseous precursors (some key reactive gases) linked to long range transport from distant polluted regions?

In addition to the above cited points of world-wide interest on UFPs, other features of the Canary Islands should be considered. The Canary Islands is an archipelago politically located within the EU territory, but geographically located off the NW coast of Africa. Previous studies have shown that conceptual models for air pollutants, obtained in studies in Europe and/or North America, should not be directly applied to the Canary Islands. Some examples:

→ Events of high concentrations of PM_{10} and $PM_{2.5}$ in Europe and mostly due to anthropogenic emission. In contrast, high PM_{10} and $PM_{2.5}$ events in the Canary Islands are due to the transport of desert dust from the Sahara desert (Viana et al., 2002).

→ The contribution of semi volatile compounds (e.g. ammonium nitrate and some organic species) to PM_{10} and $PM_{2.5}$ is important in Central and Northern Europe. However, because of the high

temperature along the year, it is considered negligible in Europe (Castillo et al., 2006; Rodríguez et al., 2010). This could also influence on the UFPs formation in ambient air and during the dilution and cooling of the vehicle exhausts.

→ Because of the relatively small size of the Islands, the ambient air pollutants are generally fresh. Pollutants are transported to the ocean in some hour periods (Rodríguez and Guerra, 2001; Guerra et al., 2004; Figure 1.4).

Table 1.6 shows a compilation of the studies on air pollution performed in the Canary Islands. It can be observed that there are no previous studies in ultrafine particles, except for the methodological paper of *Rodríguez and Cuevas* (2007) based on data collected in Santa Cruz de Tenerife.

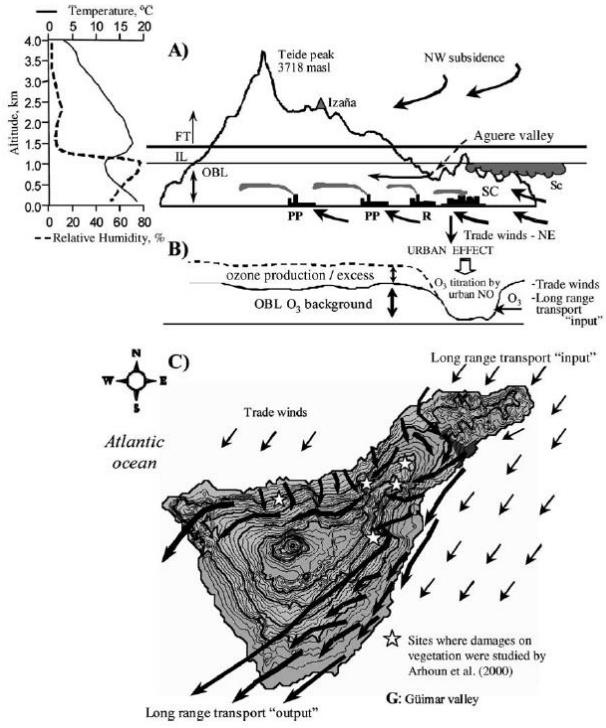

Figure 1.4 Conceptual models for air pollutant dispersion and long-range-transport at Tenerife. (A) Left: Vertical structure of the low troposphere, showing the limit of the oceanic boundary layer (OBL), inversion layer (IL), free troposphere (FT). Right: Vertical contour of Tenerife showing the southward dragging of pollutants and the stratocumulus cloud mantle (Sc) stagnant in the northern side. PP: oil-fired power plant, R: refinery; SC: Santa Cruz city. (B) Scheme of O_3 behaviour, sources and sinks. (C) Trade winds pattern (thin short lines) and pathways of the polluted air masses (long coarse lines) in the boundary layer of Tenerife. Source: Guerra et al., 2004.

Table 1.6 Previous works on Air Quality in SCTF and LPGC. MBL: Marine Boundary layer, FT: free troposphere

AUTHORS	FINDINGS
Rodríguez and Guerra, 2001	High O_3 levels in the MBL at Tenerife associated with fresh oceanic air masses and long-range transport processes
Viana, 2002	Impact of $PM_{2.5}$ and PM_{10} levels related to Saharan dust intrusions in LPGC on the degree of compliance the EU Directives
Rodríguez et al., 2004	At the low FT and MBL at Tenerife, the higher concentrations of O_3 were related to transport from the FT, whereas the lower levels were related to the transport from low altitudes over North Africa and Central North Atlantic
Guerra et al., 2004	The long-range transport and photochemically O_3 formation at Tenerife, contribute to the occurrence of high AOT40 index
Alastuey et al., 2005	Interaction processes of Saharan dust particles and local anthropogenic air pollutants in SCTF: PM_{10}>50 μgm^{-3} and enhancement of the levels of secondary compounds (Ca, Na, sulphates and nitrates)
Hernández et al., 2005	Connection between African dust intense events (PM_{10} > 150 μgm^{-3}) and the increment of the radiotracers ^{137}Cs and ^{40}K
Hernández et al., 2008	High PM_{10} and ^{7}Be levels during winter Saharan dust events: simultaneous effect of downward transport of air masses from mid-troposphere and Saharan dust suspension
López-Villarubia et al., 2008	Seasonality of the levels of gaseous (SO_2, NO_2, CO, O_3) and (PM_{10}, $PM_{2.5}$) particle pollutants measured in air quality cabins during the period 2000-2004 in the cities of LPGC and SCTF: i) SO_2 levels higher in SCTF due to the industrial activity and higher impact of road traffic in NO_2 emissions in LPGC. ii) Seasonal pattern of Saharan dust intrusions: at ground levels from January to March and at high altitude from June to August iii) Marked seasonality between the exposition of PM and O_3
López-Cancio et al., 2008	Analysis of metallic species in the TSP in LPGC
Karlsson et al., 2008	Use of ^{137}Cs measured in filters to identify natural events to reduce the costing of chemical speciation analysis
Nolasco-Torres, 2010	Overview of the emissions of VOCs of road traffic and industry in SCTF
López-Villarrubia et al., 2010	Health effects of PM_{10}, $PM_{2.5}$ and SO_2 concentrations: heart and respiratory mortality
Rodríguez et al., 2010	Origin of PM_{10} and $PM_{2.5}$ in Santa Cruz de Tenerife: vehicle exhaust, ships, refinery, mineral dust and sea salt. Determination of the chemical composition, and contribution of each source to the daily mean and yearly mean concentrations

1.4 Objectives

The objective of this thesis is to study the origin of ultrafine particles, and their relationship with some key trace gases, in different environments of Tenerife (Canary Islands), placed in proximity and distant to emission sources. The first study area, close to the emission sources, is the metropolitan area of Santa Cruz de Tenerife, where several potential sources of ultrafine particles are placed. The second study site is the Izaña Global Atmospheric Watch observatory, placed in a mountain top in the low free troposphere in Tenerife.

The specific objectives are:

1. Implement the Reactive Gases Program of the GAW (WMO) in Santa Cruz Observatory (SCO).
2. Determine typical concentrations of ultrafine particles in the Metropolitan area of Santa Cruz de Tenerife.
3. Identify the sources and processes that contribute to the ultrafine particles in the Metropolitan Area of Santa Cruz de Tenerife.
4. Quantify the contribution of each source to the ultrafine particles concentrations in the Metropolitan area of Santa Cruz de Tenerife. Special attention is paid to the contribution of non vehicle exhaust sources.
5. Determine typical concentrations of ultrafine particles in the Izaña Global Atmospheric Watch observatory.
6. Identifying the processes that contribute to the ultrafine particle concentrations in the Izaña Global Atmospheric Watch observatory.
7. Identifying the processes that contribute to the concentrations of reactive gases in the Izaña Global Atmospheric Watch Observatory.

1.5 Thesis Structure

This study is composed of 6 chapters:

Chapter 1. *Introduction*. This chapter provides an overview of the scientific context and objectives of the thesis. An overview of the state of gaseous and aerosol pollutants on air quality monitoring on local, regional and global scale is presented.

Chapter 2. *Methodology*. In this chapter a brief description of the location of the monitoring sites and well as the experimental techniques used in this study are presented. An important issue of this chapter is that it describes the Reactive Gases program implemented as part of this thesis, in Santa Cruz atmospheric observatory and at Izaña Global atmospheric watch observatory, according to the requirements of the GAW program.

The results of this study are present along the chapters 3, 4, and 5. The content of these chapters have been published or submitted to international journals include in the Science Citation Index.

Chapter 3. *Ultrafine particles in the metropolitan area of Santa Cruz de Tenerife*. In this chapter, the sources of ultrafine particle in this metropolitan area are identified. An estimation of the contribution of each source to the UPF concentrations is presented. Furthermore, the influence of the meteorological parameters is analyzed in order to study the relationship between the different aerosol metrics.

Chapter 4. *Processes affecting the concentrations of reactive gases at Izaña GAW Observatory*. The processes that affect the concentrations of SO_2, NO, NO_X, CO and O_3 are studied. Among other results the study allows identifying the role of upslope winds (transport from the boundary layer to the free troposphere) and long range transport of the concentrations and variability of each studied reactive gas.

Chapter 5. *Atmospheric nanoparticle observations in the low free troposphere during upward orographic flows at Izaña Mountain*. The influence of meteorological parameters and levels of air pollutants on the nanoparticle formation observed at Izaña station is analyzed.

Chapter 6. *Discussion*. The main results obtained in this study are placed in the context of the current state of knowledge.

Chapter 7. *Conclusions*. The most relevant findings of this work are shown.

Chapter 2

Methodology

2.1 Study region

Synoptic-scale-meteorological patterns accounts for the atmospheric stability typically of the subtropical North Atlantic region. This is due to the combination of two synoptic processes (Palmen and Newton, 1969). The descendent branch of the Hadley cell around 30°N results in a NW subsidence regimen in the free troposphere. On the other hand, it results in a quasi-permanent NNE trade wind blowing in the marine boundary layer (MBL; typically < 10000 m a.s.l., see Figure 2.1). The MBL and the FT by an inversion layer (TIL; Figure 2.2) resulted by the large scale subsidence. This causes a strong stratification in the low free troposphere.

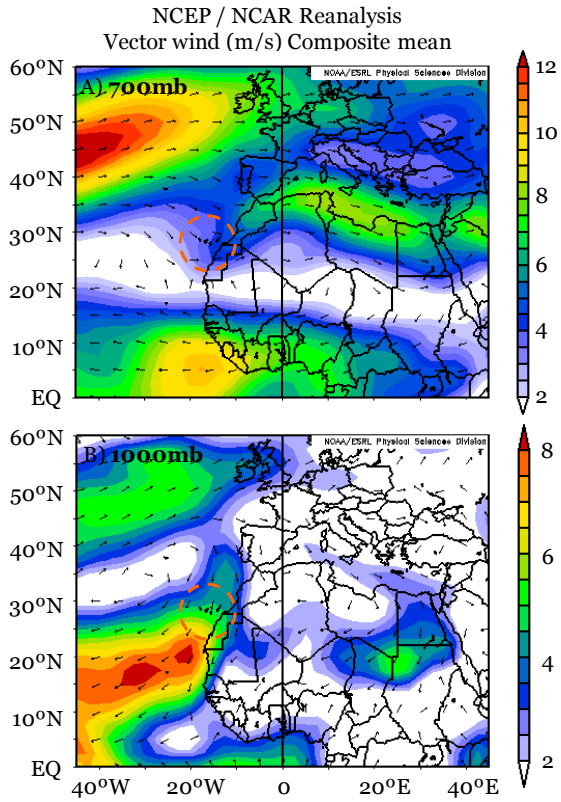

Figure 2.1 Wind vector mean composition at A) 700mb and B) 1000mb centred over the Canary Islands (red dashed circles), during the period 2007 - 2010. Source: NCEP/NCAR reanalysis (http://www.esrl.noaa.gov)

The top of the TIL is generally located around 1,200 metres above sea level (m a.s.l.) in summer and around 1,800 m a.s.l. in winter (Rodríguez et al., 2004). Its seasonal trend is similar to that observed in the Azores (Kleiss et al., 2007). The thickness and temperature gradient of the TIL

reach a maximum in summer (July-August). In this season, the TIL is about 800 m a.s.l., and is characterized by an average thickness of 500 m, and a temperature gradient through 5º C (Torres et al., 2002). The top of the MBL is characterized by a layer of stratocumulus formed by the condensation of water vapour onto pre-existing particles (Figure 2.2b).

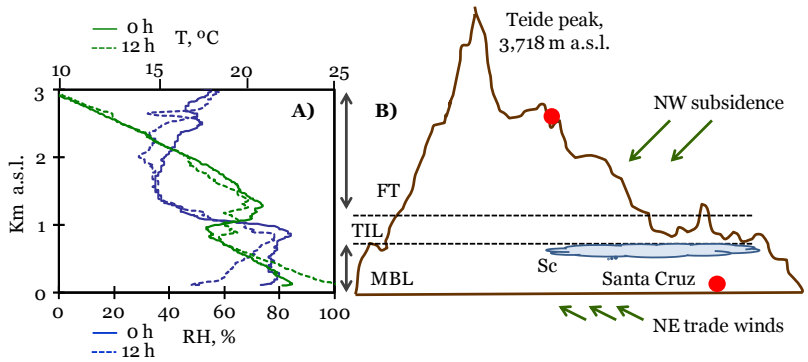

Figure 2.2 A) Vertical profiles of temperature and humidity in Tenerife. B) Location of Izaña and Santa Cruz observatories, the stratification of the troposphere at the island and the wind regimen

The effectiveness of the TIL in isolating the MBL from the FT is evidenced in the relative humidity (RH), which dramatically decrease above the stratocumulus layer. There is a humidity gradient into the layer due to the transport of relatively humid air from the trade winds under the inversion, and the relatively dry air from the subsiding air flow form upper levels.

2.2 Measurement sites

Tenerife Island has a central volcanic caldera (2,000–2,200 m a.s.l.) that serves as a base for the volcano Teide (3,718 m a.s.l., Fig. 2.2). A ridge, crossing SW to NE, divides the island into two main slopes: northern and southern. Tenerife is surrounded by a ring of forest of an endemic species of pine (Pinus canariensis Chr, Sm. ex DC) located between 600 and 2,000 m a.s.l. These species growths owing to the water supply from the 'horizontal rain' linked to the presence of the stratocumulus. Above 2,000 m a.s.l., the terrain is arid and the predominant plant is broom local specie (Spartocytisus supranubius, its local name is retama). Urban areas on the island are mostly located below 600m a.s.l.

Measurements performed in stations located in two different environments have been used. They are Izaña Observatory (IZO) and Santa Cruz Observatory (SCO), which actively participate in the Global Atmosphere Watch (GAW) Programme, and are managed by the Izaña Atmospheric Research Centre (IARC). The location of the stations is shown in figure 2.3. The IARC is an Associated Unit of the 'Consejo Superior de Investigaciones Científicas' (CSIC) through the Earth Science Institute Jaume Almera. The main goal of this Associated Unit is to perform atmospheric pollution research focusing on aerosols.

2.2.1 Santa Cruz Observatory

Santa Cruz Observatory (SCO) is located in the city of Santa Cruz de Tenerife. This metropolitan area has 222,643 inhabitant (National Institute of Statistics, January 2010) distributed in 150 km^2. The topography in the north sector of the island, dominated by the Anaga slope, which protects the city of Santa Cruz de Tenerife (28.31^{o}N, 16.25^{o}W, Figure 2.3) from the prevailing trade winds (NNE, Figure 2.1B).

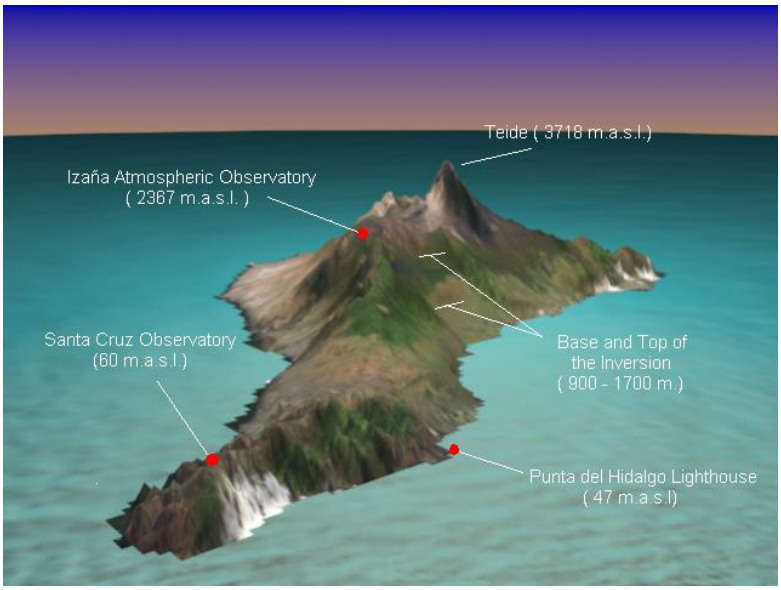

Figure 2.3 Location of SCO and IZO on the Island of Tenerife (Torres et al., 2002)

The main sources of pollutants in this city are:

- Road traffic. 29% of the vehicle fleet in Santa Cruz de Tenerife comprises diesel engines. This fleet consists of 69% of light commercial vehicles, buses and lorries (www.dgt.es, last access October 2010).
- Oil refinery. It operates since 1930. It is located at the SW part of the city, about 3 km far from the measurement site. It covers an area of 500,000 m^2, and it has a distillation capacity of 4.5 million tons·$year^{-1}$ (96,000 barrels per day, www.cepsa.es).
- Ships. The harbour is located less than 1 km of the measurement site at the East of the city. The presence of ships is not continuous, although frequent. These emissions occur during sailing, entries and exits in the harbour, when ships are anchored off shore, and in the port, owing to the engines kept activated for power supply. Between the years 2008 and 2009, the average annual number of merchant ships and cruisers was 16,341 per year and 341 per year, respectively (http://www.puertos.es, last access June 2011).

The pollutant's transport in the city of Santa Cruz is highly influenced by the development of coastal breezes (Guerra et al; 2004). The landward breeze circulation favours the inland transport of the pollutants emitted near the shore during the 10 to 17 GMT period, whereas at night, a slight seaward airflow occurs. The daily PM_{10} aerosol load in Santa Cruz de Tenerife is influenced by the sea

salt, and also by Saharan mineral dust particles during intrusion episodes (>100 mgPM_{10}·m^{-3}, Viana et al., 2002). Other sources of pollutants that could contribute to ultrafine and/or black carbon particles are not present in the city. For example, the fraction of land in the island that is dedicated to agriculture is low, the southern slope is semi-arid and the northern side is a protected forest. Consequently, biomass burning does not practically occur within or close to the city. Moreover, because of the mild weather conditions (temperatures within 15 – 35 ºC throughout the year) house heating is not a common practice.

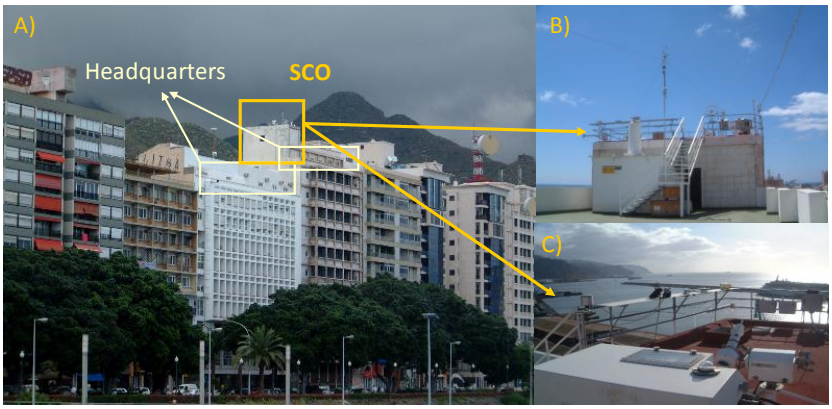

Figure 2.4 A) View of the Santa Cruz Observatory from the Anaga Avenue. B - C) Zoom of the terrace where the inlet lines are placed

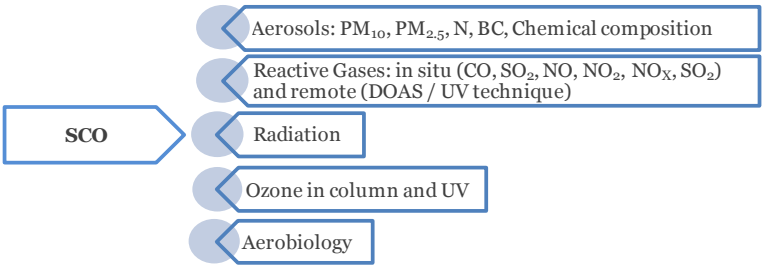

Figure 2.5 Research Program at SCO. N: number of (ultrafine) particles, BC: black carbon

Santa Cruz Observatory (SCO) is a coastal urban background station located in the city of Santa Cruz de Tenerife (Figure 2.4). It is placed at 52 m a.s.l. (at about 45 metres above ground level), on the roof of an 11-storey building at the NE edge of the city, close to the shore, and on the western side of the 4-lane Anaga Avenue; where heavy duty engines account for about 5% of the road traffic intensity (number of vehicles per hour). Different research programs are continuously carried out at this station (Figure 2.5).

2.2.2 Izaña Observatory

Izaña Atmospheric Observatory (IZO) is a mountain top station located in a protected area of Teide National Park (28.31º N, 16.50º W) at an altitude of 2,367 m a.s.l. (average pressure of 770 hPa, Figure 2.6A). This park is protected by the 'sky law'.

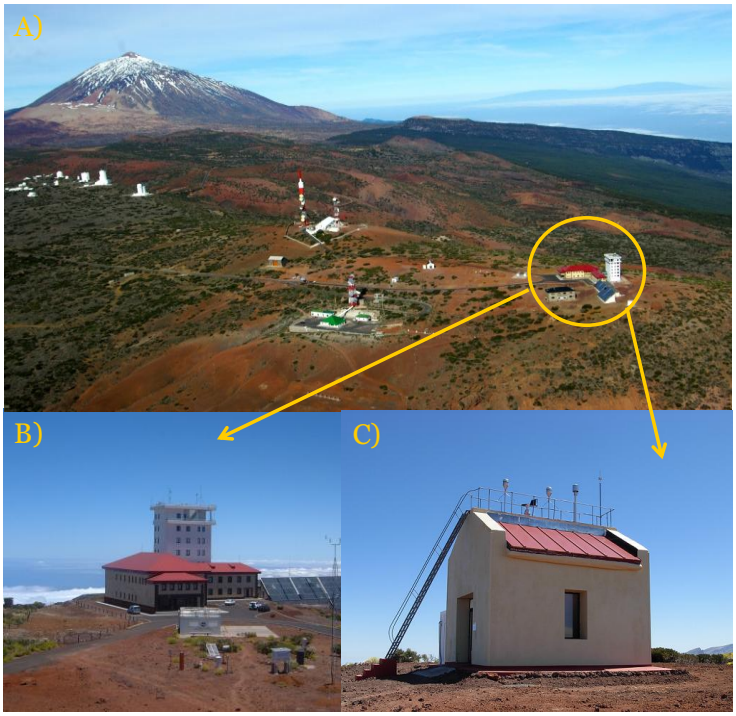

Figure 2.6 A) View of Izaña GAW Observatory, B) Main building and lab - tower for gases program, and C) aerosol laboratory

At IZO, the heating of the air near to the ground generates WNW prevailing winds that blow under strong synoptically driven conditions. These flows influence the daily cycle of gaseous pollutants measured at the station (Cuevas et al., 1991). IZO normally lies above the temperature inversion layer /TIL). Torres at al. (2002) determined that the TIL has a yearly frequency of 78%, with a maximum in June (90%, 00 GMT) and a minimum in March (68%, 00 GMT). IZO is frequently affected by air masses that originate in the North Atlantic mid troposphere, with a maximum number of events in April and June. Secondary, air masses coming from the low and mid troposphere of North African are observed between July and August. Air masses originating in Europe are less frequent. In summer, when the inversion is stronger, air masses coming from North Africa affect the free troposphere but not the marine boundary layer. However, in winter, these air masses may affect both regions simultaneously (Torres et al., 2002).

Different research programs are continuously carried out at this station (Figure 2.7):

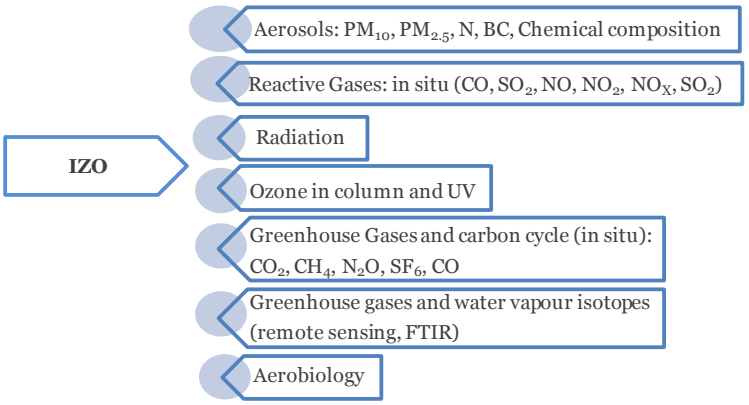

Figure 2.7 Research Program at IZO

2.3 Measurement programs

The measurement program of reactive gases and aerosols at SCO and IZO is described in this section. Because the reactive gases program was implemented under the frame of this thesis (except for O_3), most of the attention is paid on this program.

2.3.1 Reactive Gases

2.3.1.1 QC /QA protocols

The reactive gases program at SCO and IZO includes measurements of SO_2, CO, O_3 and NO_x concentrations. At SCO, O_3 measurements started in 2001; and CO, SO_2 and NO_x measurements were implemented in 2006. At IZO, O_3 measurements started in 1984, CO measurements started in 2004, and SO_2 and NO_x measurements were implemented in 2006 under the frame of this thesis.

Reactive gases monitoring has been performed with instrumentation using the principle methods established at reference by the US Environmental Protection Agency (US EPA) and the European Union (2008/50/CE). These agencies also establish the Quality Assurance / Quality Control (QA / QC) protocols (e.g., US EPA, 600/4-77-027a, 1977; UNE-EN standards). These protocols describe the different steps that must be followed on an air quality program. The requirements go from the sampling environment, to the sampling probes and manifolds, maintenance, calibration and recordings of the systems.

These recommendations have been considered during the implementation of the reactive gases program at SCO and IZO. However, because the IARC belong to the GAW community, some of these parameters follow more restrictive protocols according to the Calibration Centres of GAW. In the following lines the QA / QC program is described. Later, the more restrictive specifications stated by the Calibration Centres of the GAW Program and applied at IARC are developed for each system.

i) Sampling environment

A proper sampling environment demands control of a set of physical parameters external to the samples that might affect sample stability or the function of sampler components. The parameters to be controlled are summarized in Table 2.1. The specifications are usually given by the manufacturer:

Table 2.1 Environment control parameters

Parameter	Method of Control	IARC protocol
Instrument vibration	Design of instrument housings, benches, etc.	Instruments mounted on racks
Light	Shield chemicals or instruments that can be affected by natural or artificial light	Windows covered solar filters and blinds
Electrical voltage	Constant voltage transformers or regulators; separate power lines; isolated high current drain equipment (hi-voltage, heating baths, pumps)	Follows the method
Temperature	Regulated air conditioning, 24-h temperature recorder; electric heating and cooling (US EPA, 20 - 30°C)	20 - 22°C
Humidity	Regulated air conditioning; 24-h temperature recorder	Air conditioning systems and air driers

ii) Sampling probes and manifolds

Some important variables affecting the sampling manifold design are the diameter, length, flow rate, pressure drop, and materials. The last one is important to avoid the reactivity through the inlet lines, whereas the rest are related to the most critical parameter, which is the residence time of the measured compound through the inlet line. The residence time of gaseous pollutants is defined as the interval of time it takes the air sample to travel through the air inlet. The US EPA compendium (US EPA, 1998) indicates that the time that the sample takes by travelling through the air inlet, the manifold and sample lines should be less than 10 seconds. To calculate the residence time (τ_r) the following parameters must be taken into account (equations 2.1 - 2.3):

$$\text{Total Volume} = V_C + V_M + V_L \qquad \text{(eq. 2.1)}$$

$$V = \pi \cdot (d/2)^2 \cdot L \qquad \text{(eq. 2.2)}$$

$$\tau_r = \sum_i Vi \cdot / \text{ flow} \quad \text{(eq. 2.3)}$$

where V_C is the sample volume of the vertical inlet, V_M the manifold volume and V_L the volume of the inlet lines. The volume of each component is measured individually, being V is the component volume, π = 3.14159, d the diameter y L the length of the each component. Each volume is then divided by the corresponding flow rate, obtaining the residence time (τ_r, eq. 2.3., US EPA, 1998).

Manifolds require maintaining a flow rate that is either 3 to 5 times the total sampling requirements (US EPA, 2008). A leak test is necessary, at least after the installation. Manifolds must be cleaned at least each six months (UNE-EN 77-240:2000) or earlier depending on the location, taking care about the products used during the cleaning and their possible residues depending on the measured compound (e.g. the case of volatile organic measures; US EPA, 2008).

Santa Cruz Observatory

At SCO the sampling inlet is located on the roof of the offices at 52 m high (Fig. 2.8A). It consists of a SS316 stainless steel pipe of 7 m, which runs from the roof into the reactive gases laboratory. The air flow passes through the horizontal manifold ($\varnothing_{int}$ = 6 cm and 2.80 m long, Fig. 2.8B) and subsequent teflon lines to the analyzers.

Figure 2.8 A) Design of the sampling inlet line and B) manifold at SCO

From the date of installation to 11-July-2010, a pump with a flow rate of 2,810 l·min^{-1} through an inner diameter of about 6 cm was used. Since 12/07/2010 the pump was replaced by another of lower flow rate (1,587.4 l·min^{-1}) in order to reduce the sensitivity of the CO analyzer to pressure changes (it would be explained in the following lines). In Table 2.2 the parameters involve in the calculation of the residence time at SCO station are shown.

Table 2.2 Residence time of the analyzers placed at SCO. The different periods indicate the change of the pump volume and the length of the lines

Analyzer	Lines lenght (m)	flow (lpm)	Lines vol.(l)	t_r (s)
06/2006-07/2010				
CO	1.9	1.0	0.04	~3
SO_2	1.6	0.5	0.03	~5
NO-NO_2-NO_X	2.5	0.5	0.05	~7
O_3	2.5	0.7	0.05	~5
Since 07/2010				
CO	2.3	1.1	0.03	~2
SO_2	2.3	0.5	0.03	~4
NO-NO_2-NO_X	2.1	2.1	0.03	~3
O_3	3.3	0.6	0.04	~4

Izaña Observatory

At IZO the sampling is located at the top of the tower at 4 m above the terrace, and 30 m above the ground at a height above sea level of 2,397 m. It consists of a stainless steel tube that goes from the terrace of the tower, through the service channel to each of the laboratories. Until April 2010, the reactive gases analyzers were distributed along the second, third, and sixth floor. Then, they were moved to the fifth and sixth floors, in order to reduce the residence time of the sample in the lines. This is important due to the low concentrations of some compounds in this station. A vacuum pump generates an inflow of 2,810 lpm (standard conditions) throughout the sampling line (Fig. 2.9A), which has an inner diameter of 80 mm. The manifold has an inner diameter ($\varnothing_{int}$) of 80 mm and a length of 250 mm (Fig. 2.9B). The analyzers take the air sample using teflon tubes $\varnothing_{int}$ = 4 mm, which go from the manifold to the inlets of the analyzers. The length of the sampling inlet at it passes through each floor of the IZO's tower laboratory is the following: a) 2nd floor, 18m; b) 3rd floor, 15 m; c) 5th floor, 9 m; and d) 6th floor, 6m, respectively. In Table 2.3 the parameters involve in the calculation of the residence time for both stations are shown.

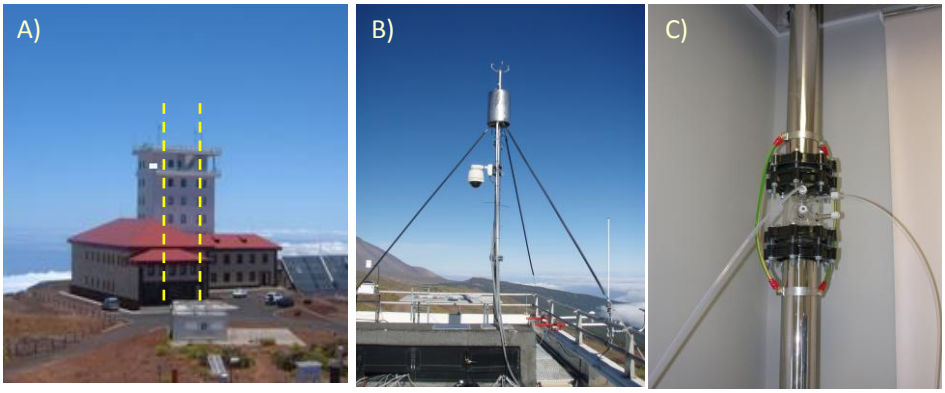

Figure 2.9 Design of the sampling inlet and manifolds at IZO: A) Yellow dashed lines indicate the inlet lines path through the lab-tower, B) top of the inlet line, and C) manifold in each laboratory

Table 2.3 Residence time of the analyzers placed at IZO. The different periods indicate changes in the laboratories.

Analyzer	Lines lenght (m)	flow (lpm)	Lines vol.(l)	t_r (s)
06/2006-04/2010				
CO-TL	11.8	1.0	0.15	~11
SO_2-TL	1.4	0.5	0.02	~4
NO-NO_2-NO_X-TL	1.4	1.0	0.02	~3
O_3 (primary)	2.5	0.6	0.03	~4
O_3 (secondary)	2.0	0.6	0.03	~3
Since 04/2010				
CO-TL	5.1	1.0	0.07	~5
SO_2-TL	3.3	0.5	0.04	~6
NO-NO_2-NO_X-TL	3.9	1.0	0.05	~3
O_3 (primary)	2.4	0.6	0.03	~3
O_3 (secondary)	2.9	0.6	0.04	~5

iii) Calibrations: Zero and span checks

The QC /QA of each instrument includes an appropriate maintenance, as regular checks and calibrations.

The calibration curve relates the analyzer response to the measured concentration. The calibration process requires the determination of: i) the calibration function, ii) the analyzer linearity, iii) the repeatability of measurements; and iv) the lower detection limit; according to the UNE 77-237:1999 or UNE 77-240:2000. The new European Directive on Air quality recommends a multipoint calibration (a zero and 4 upscale points) each 3 months. The US EPA recommends

modifying the internal calibration parameters of the analyzers if a deviation > 3% is observed in the calibration curve with respect the last one.

The calibration procedure of the reactive gases programme at IARC is a 2-step process: 1) the drift of the calibration curve is tested by checking two points: a zero and a span value; and 2) then a multipoint calibration is performed in order to check the linearity of the equipment over a range of concentrations. Before starting the multipoint calibration, the status of the equipment is checked. The particle filters are replaced, pressure sensors are tested, and the efficiency of the zero scrubber are checked. The calibration parameters (background and coefficients of the analyzer) are modified if more than 10% of drift is observed in the calibration curve. The technical specifications of these processes are detailed in the internal protocols of the Reactive Gases Programme at the IARC.

iv) Status of the instrument and records

The criteria for the maintenance and calibration of different analyzers in air quality cabins can be found in the following European Directives: i) SO_2, UNE-EN 14212:2006, ii) NO-NO_2, UNE-EN 14211:2006, iii) O_3, UNE-EN 14625:2005, and iv) CO, UNE-EN 14626:2006.

Table 2.4 General maintenance of the systems

Parameter	**UNE-EN** frequency	**IARC** frequency
Zero check	At least each 2 weeks	Daily
Span check	At least each 2 weeks	Each 3 months
Multi-point calibration	At least each 3 months	Each 3 months
Fan filter cleaning	-	Each week
Particle filter replacement	At least each 3 months	Each 3 months
Manifold and inlet lines	At least each 6 months	Each 6 months

A daily check of the internal variables such as temperature, flow, pressure, automatic zero measurements, the cleanliness of filters and sampling lines, and the efficiency of the scrubbers, allows to quickly respond to possible instrument malfunctions. All the above variables are recorded daily in log-books. Regular maintenance includes the weekly cleaning of fan filters, the monthly replacement of particle filters (before calibration), as well as the cleaning of the sample lines and the intake pipe (manifold) every six months. For every calibration, the identification of the analyser, calibration date, location of the analyser, the calibration standards used, the calibration equation, identification of equipment used in the calibration, as well as the calibrating operator are documented. See in table 2.4 a comparison between the requirements of the European legislation and IARC in terms of calibration frequency and maintenance is shown.

In the following lines a description of the technical specifications for each analyzer implemented at the IARC will be done. A detailed description was performed in the DEA document (González, 2006; Diploma de Estudios Avanzados).

2.3.1.2 Ozone

i) Technical specifications

Surface ozone is measured by UV photometric analyzers, model 49C, provided by Thermo Electron Corporation. The model is based on the principle that ozone molecules absorb UV light at a wavelength of 254 nm. The degree to which the UV light is absorbed is directly related to the ozone concentration as described by the Beer-Lambert Law:

$$I / I_o = e^{-KLC} \qquad \text{(eq. 2.4)}$$

where:

K = molecular absorption coefficient, 308 cm^{-1} (at 0°C and 1 atmosphere)

L = length of cell, 38 cm

C = ozone concentration in parts per million (ppm)

I = UV light intensity of sample with ozone (sample gas)

Io = UV light intensity of sample without ozone (reference gas)

The sample is split into two gas streams, as shown in Figure 2.10. One gas stream flows through an ozone scrubber to become the reference gas (I_o). The reference gas then flows to the reference solenoid valve. The sample gas (I) flows directly to the sample solenoid valve. The solenoid valves alternate the reference and sample gas streams between cells A and B every 10 seconds. When cell A contains reference gas, cell B contains sample gas and vice versa.

The UV light intensities of each cell are measured by detectors A and B. When the solenoid valves switch the reference and sample gas streams to opposite cells, the light intensities are ignored for several seconds to allow the cells to be flushed. The Model 49C calculates then the ozone concentration for each cell and outputs the average concentration.

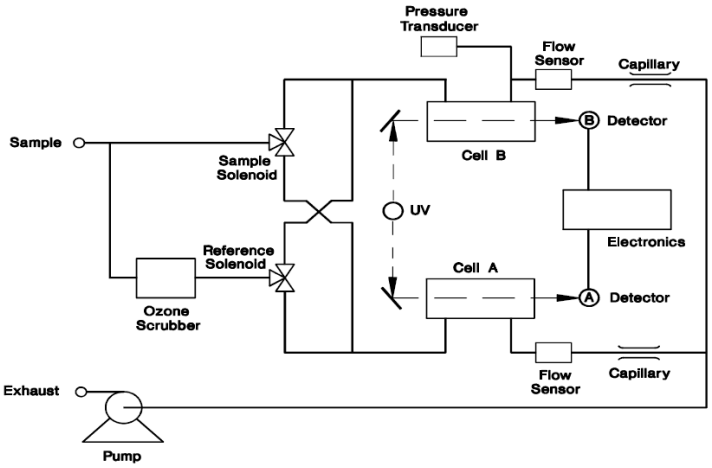

Figure 2.10 Model 49C flow schematic. Source: 49C manual

In Table 2.5 the specifications of this system are summarized.

Table 2.5 Specifications of 49C. Source: 49C manual

Parameter	**Value** (Similar for IZO and SCO stations)
Zero noise	0.5 ppb RMS
Lower detectable limit	1.0 ppb
Zero drift	< 1 ppb / 24h
Span drift	less than 1% per month (including drift of transducers)
Response time	20 seconds
Precision	1 ppb
Linearity	± 1% full scale

ii) Zero Check

This check is carried out every day during 15 minutes, with a scrubber of activated carbon. At SCO this zero is made at 16h GMT, whereas at IZO, the zero on primary analyzer is made at 16h GMT and the secondary at 17h GMT in order to avoid 24-h ozone data at this station. A linear fit between consecutive zeros allows the zero correction of the readings.

iii) Calibration

Ozone analyzers are calibrated with an ozone primary standard (49C - PS). This primary standard is frequently sent (~3 times per year) to the World Calibration Centre of O_3, CO, and CH_4 (EMPA, Switzerland) for being audited. The multipoint calibration consists of a random application of the following concentrations: 0, 10, 30, 45, 60 and 90 ppb. This calibration is preceded by a high concentration (400 ppb) that allows the cleaning of the measuring cells.

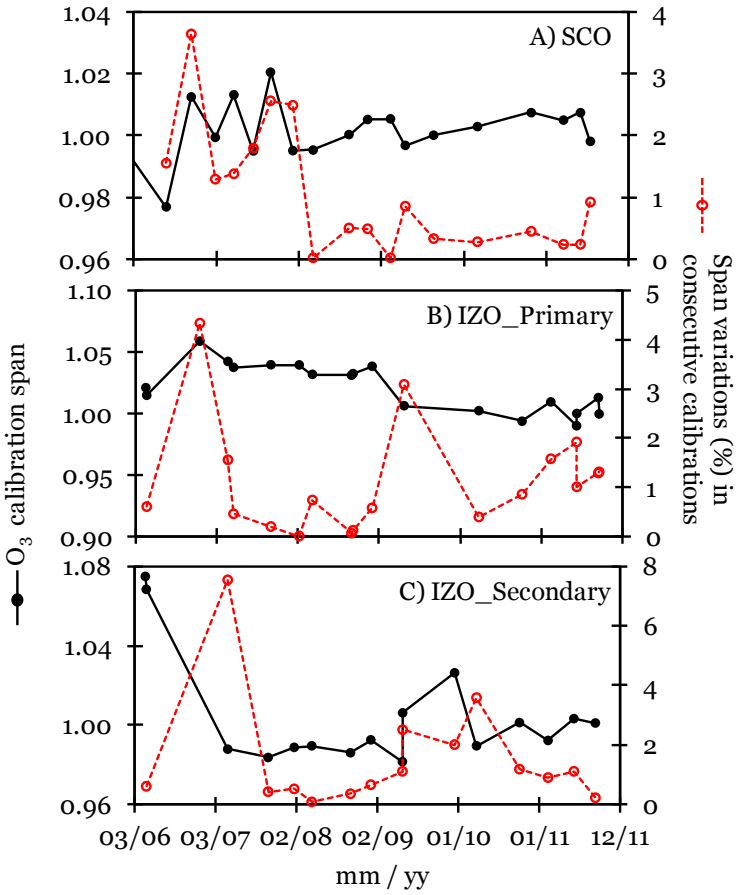

Figure 2.11 Spans and the corresponding variations of the calibrations carried out to the model 49C at SCO (A) and at IZO (B) primary analyzer and C) secondary analyzer (r^2>0.99 is found in all cases)

Figure 2.11 shows the spans obtained at SCO and IZO in the calibrations performed in this thesis. In the secondary y axis, the standard deviations of the spans, give an idea of the stability of these 49C models. For variations lower than 5%, the internal span and zero of the analyzer were not modified. This is the case of the analyzer placed in SCO.

The World Calibration Centre for Surface Ozone, Carbon Monoxide and Methane (EMPA) sets the limits of tolerance for the differences between the analyzers responses and the calibration system responses. These limits allow to check the deviation of the data from the lowest (zero derives or zero scrubber deterioration) to the highest (span derives) values. An example of these plots is shown in Figure 2.12. In these plots, the difference between the analyzers readings and the calibrator readings (axis y) are plotted versus the concentrations fixed in the calibration system (axis x). These data should be fixed between the limits named as "good" imposed by EMPA for the data quality of GAW stations. Surface ozone data at IZO are sent to the Word Data Centre of Greenhouse Gases (WDCGG). The data usually sent are those recorded by the primary analyzer, using the secondary in those cases of lack of data due to failures on the primary system.

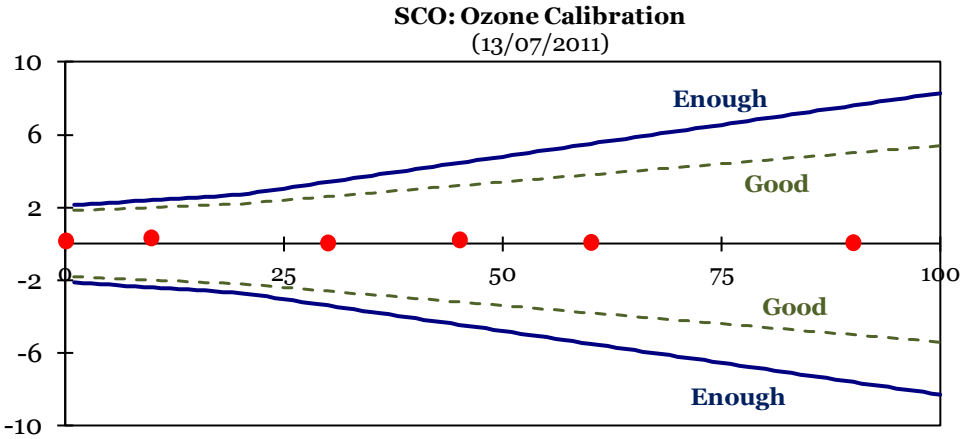

Figure 2.12 Example of the representation of the response of the analyzer 49C on calibration versus the calibration system (49C-PS). Date: 13/07/2011

2.3.1.3 Carbon monoxide

i) Technical specifications

Carbon monoxide is measured by gas filter correlation analyzers, models 48C and 48C-TL (at SCO and IZO respectively), provided by Thermo Electron Corporation. These models are based on the principle that carbon monoxide (CO) absorbs infrared radiation at a wavelength of 4.6 microns. Because infrared absorption is a non-linear measurement technique, it is necessary for the instrument electronics to transform the basic analyzer signal into a linear output. The Model 48C is designed to give a linear response up to a concentration of 10,000 ppm.

The sample flows through the optical bench. Radiation from an infrared source is chopped and then passed through a gas filter alternating between CO and N_2. The radiation then passes through a narrow band pass interference filter and enters the optical bench where absorption by the

sample gas occurs. The infrared radiation then exits the optical bench and falls on an infrared detector (Figure 2.13).

The CO gas filter acts to produce a reference beam which cannot be further attenuated by CO in the sample cell. The N_2 side of the filter wheel is transparent to the infrared radiation and therefore produces a measure beam which can be absorbed by CO in the cell. The chopped detector signal is modulated by the alternation between the two gas filters with an amplitude related to the concentration of CO in the sample cell. Thus, the manufacturer indicates that other gases do not cause modulation of the detector signal since they absorb the reference and measure beams equally, responding specifically to CO.

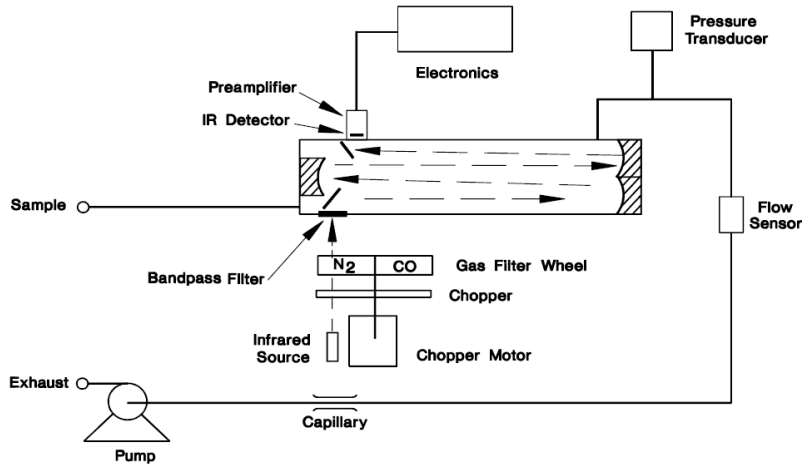

Figure 2.13 Model 48C flow schematic. Source: 48C manual

In Table 2.6 the specifications of this system are summarized.

Table 2.6 Specifications of 48C and 48C-TL. Source: 48C and 48C-TL manuals

Parameter	**Value** (Similar for IZO and SCO stations)
Zero noise	0.02 ppm RMS (30 seconds time setting)
Lower detectable limit	0.04 ppm
Zero drift	< 0.1 ppm (24h)
Span drift	± 1% full scale (24h)
Response time	60 seconds (30 seconds time setting)
Precision	± 0.1 ppm
Linearity	± 1% full scale ≤ 1000 ppm ± 2.5% full scale > 1000 ppm

ii) Zero Check

Previous studies have observed that the infrared techniques are mainly affected by the temperature fluctuations of the laboratory, CO_2 and water vapour content of the air mass. The influence of all these parameters can be minimized with an appropriated zero program:

- The influence of CO_2 is automatically corrected by the zero cycle since CO_2 concentrations in ambient air is almost stable over short periods (approximately several days; Cogan and Lobert, 1998).
- Temperature fluctuations are translated into interferences in the measurement. In order to reduce fluctuations in the measurements, the room temperature should be maintained between 20 - 22º C, and a programme of zeroes is designed for developing zeroes each half an hour. These zeroes can be carried out with a scrubber of molecular-sieve (Na_2O Al_2O_3 $2.45SiO_2$ $6.OH_2O$, desiccant) and sofnocat (a precious metal that in the presence of oxygen, oxidizes the hydrogen to water and converts carbon monoxide to carbon dioxide). The zero check is then carried out each half an hour during 15 minutes. A linear fit between consecutive zeros allows the zero correction of the readings. The relevance of the temperature control can be observed on Figure 2.14. In this figure the zero readings without and with temperature control are shown. As it can be seen, the temperature variability in the laboratory affects the instrument readings. This temperature oscillation is translated in a distortion of the measurements in a 5% on average, reaching in some cases the 40%.

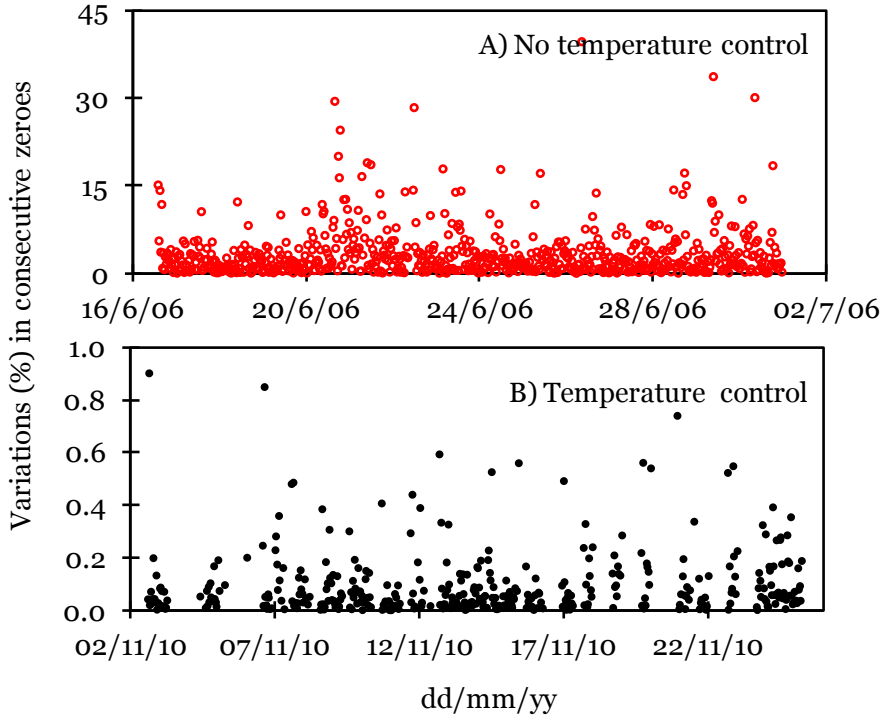

Figure 2.14 Variations (%) of a zero reading with respect its previous one without (A) and with (B) temperature control in the laboratory

- With respect the water vapour influence, at IZO, the sampling air is cryogenically dried using an alcohol bath at a temperature of -65 °C before it is being passed to the analyser. This cryogenic bath was recommended by the World Calibration Centre for Surface Ozone, Carbon Monoxide and Methane (EMPA).

- The last inconvenient found on this technique, is the sensibility to drops of pressure. The design of the models 48C and 48C-TL allows the corrections of the data in terms of temperature and pressure to standard conditions. It was observed that the difference on pressure between the sample and the zero inlets, due to the installation of the scrubber in this second valve, produced also a change in the CO readings. It was observed that variations on the pressure in the zero valve was translated in variations on the CO readings, however, these variations did not attend to a linear behaviour, that is, an enhancement on pressure in the valve was not always related to an enhancement on CO readings or vice versa, which made impossible to correct this type of error. This inconvenient of the pressure variability, in addition to the influence of temperature, provokes a difference of around a 25% between the IR analyzer and the other 2 techniques available at IZO station (see an

example in Figure 2.15). The NOAA/ESRL/GMD CCGG cooperative air sampling network effort began in 1967 at Niwot Ridge, Colorado. Air samples are collected approximately weekly from a globally distributed network of sites. Samples are analyzed in Boulder by CCGG for CO_2, CH_4, CO, H_2, N_2O, and SF_6; and by INSTAAR for the stable isotopes of CO_2 and CH_4 and for many volatile organic compounds (VOCs) such as ethane (C_2H_6), ethylene (C_2H_4) and propane (C_3H_8). Measurement data are used to identify long-term trends, seasonal variability and spatial distribution of carbon cycle gases. On the other hand, gas chromatography with a HgO detector (Trace Analytical RGA-3 GC-system) is used for simultaneous measurements of CO and H_2.

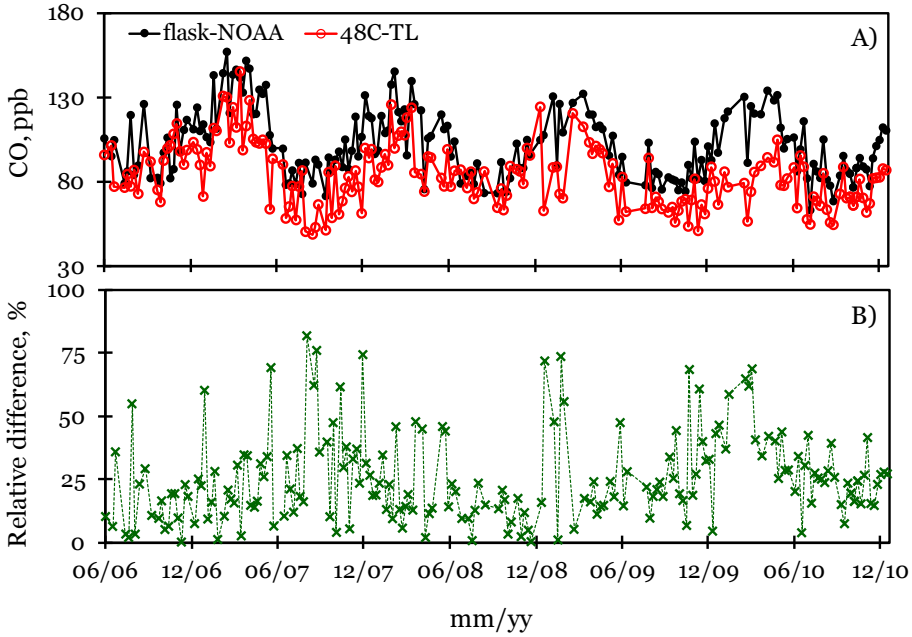

Figure 2.15 A) Temporal series of CO measured with the model 48C-Tl and NOAA flask; B) relative difference between the records of the two techniques in %

At GAW stations, two different designs can be found related to the measurement of carbon monoxide. Some stations such as Hohenpeissenberg (Germany) follow the measurement scheme described by Parrish and co-workers (1994), in which the molecular-sieve + sofnocat scrubber is replaced by a palladium catalyst. This catalyst oxidizes CO to CO_2 with an efficiency exceeding 99.9%. The water-vapour concentration is, however, not being affected, leading to the same amount of water vapour in both the zero line and the sample line, by not using a cryogenic bath for the sample air. The reason for that is because the rapid drop in temperature in the sample line might lead to a transfer of a fraction of the CO molecules into the condensed water phase (Dr. Stefan Gilge, personal

communication, 2010), leading an underestimation of the CO concentration measurements. Both measurement schemes are accepted by EMPA as long as the audits reveal a deviation lower than a 10%.

iii) Calibration

A multigas calibrator (MCZ™) is used to calibrate this analyzer in addition of standard gas bottles provided by Air Liquide s.a. The multigas calibrator is composed of flow controllers (MFC), a zero gas inlet, a span gas inlet, a mixing chamber and an ozone generator.

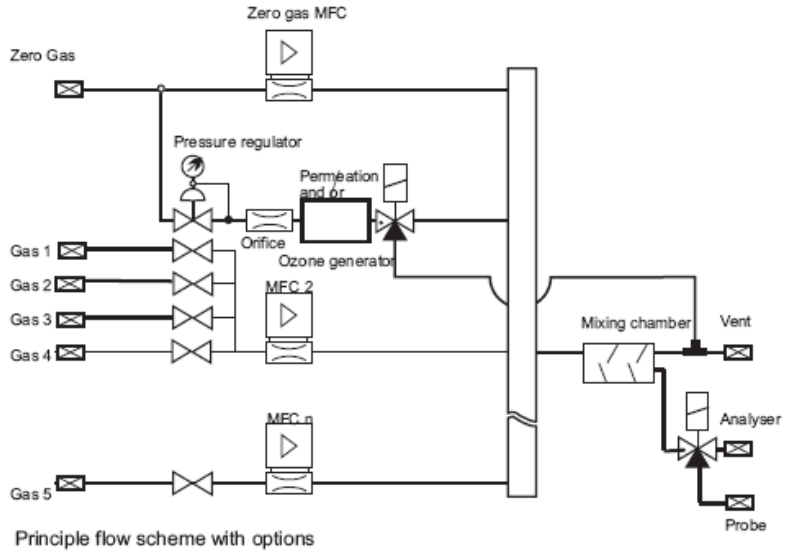

Figure 2.16 MCZ scheme flow. Source: Multigas Calibrator manual

At the beginning a multipoint calibration was done, alternating a zero measurement with synthetic air. After the EMPA audit in 2009, and due to the linearity of the system, they recommended to change the calibration pattern. Thus, the CO calibration consists on a zero check, were zero - CO readings from the scrubber are compared with the zero - CO readings of synthetic air, and the injection of 1,000 ppb (the maxima concentration of the analyzer where linearity is insured) that are alternated with zero scrubbers measures each half an hour during 15 min, as is done in the normal measuring state. In Figure 2.17 the calibrations carried out to the analyzers placed at SCO

and IZO during the period that covers this thesis are shown. For standard deviations lower than 10%, the internal span and zero of the analyzer were not modified.

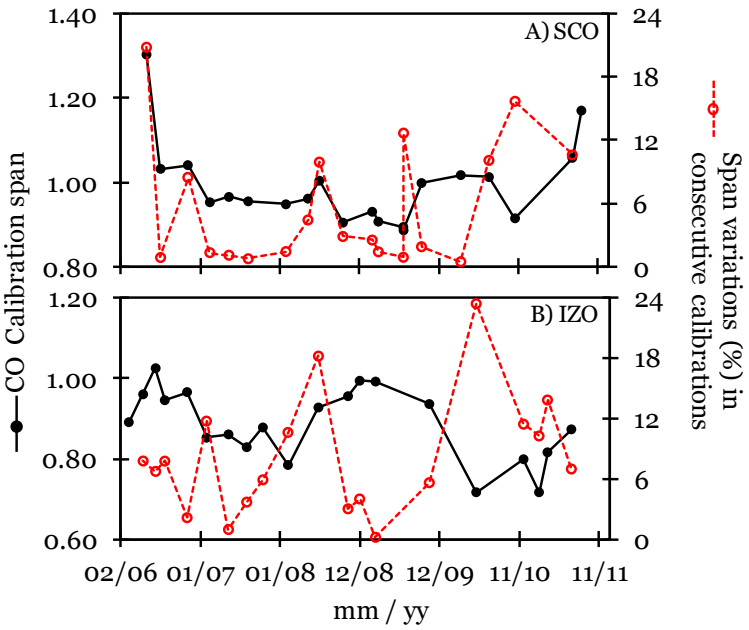

Figure 2.17 Spans and the corresponding variations of the calibrations carried out to A) the model 48C at SCO (A) and (B) the model 48C-TL at IZO (r^2>0.9 is found in all cases)

It can be deduced that these models need a more precise control, and calibrations each three months are not enough. Because of this reason, a new development on the installation is being carried out, that it will allow a span check every day. Furthermore, a new CO analyzer (Horiba), which better features is being installed in that moment at IZO.

2.3.1.4 Sulphur dioxide

i) Technical specifications

Sulfur dioxide is measured by pulsed fluorescence SO_2 analyzers, models 43C and 43C-TL, provided by Thermo Electron Corporation. The model is based on the principle that SO_2 molecules absorb ultraviolet (UV) light and become excited at one wavelength, then decay to a lower energy state emitting UV light at a different wavelength. Specifically,

$$SO_2 + h\nu_1 \rightarrow SO^*_2 + h\nu_1 \qquad \text{(eq. 2.5)}$$

The sample flows through a hydrocarbon "kicker," which removes hydrocarbons from the sample by forcing the hydrocarbon molecules to permeate through the tube wall (Figure 2.18). The SO_2 molecules pass through the hydrocarbon "kicker" unaffected. The sample flows into the fluorescence chamber, where pulsating UV light excites the SO_2 molecules. The condensing lens focuses the pulsating UV light into the mirror assembly. The mirror assembly contains four selective mirrors that reflect only the wavelengths which excite SO_2 molecules.

As the excited SO_2 molecules decay to lower energy states they emit UV light that is proportional to the SO_2 concentration. The bandpass filter allows only the wavelengths emitted by the excited SO_2 molecules to reach the photomultiplier tube (PMT). The PMT detects the UV light emission from the decaying SO_2 molecules. The photodetector, located at the back of the fluorescence chamber, continuously monitors the pulsating UV light source and is connected to a circuit that compensates for fluctuations in the UV light. The sample then flows through a flow sensor, a capillary, and the shell side of the hydrocarbon "kicker."

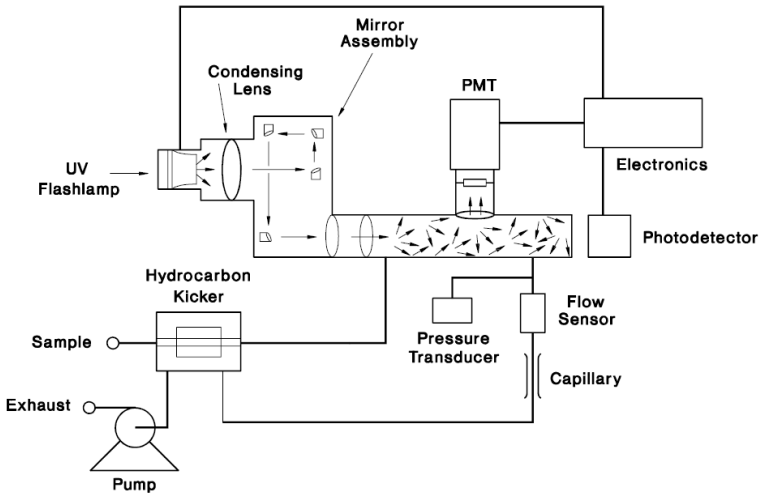

Figure 2.18 Model 43C flow schematic. Source: 43C manual

In Table 2.7 the most specifications of this system are summarized.

Table 2.7 Specifications of 43C and 43C-TL. Source: 43C and 43C-TL manuals

Parameter	Value	
	SCO	IZO
Zero noise	0.5 ppb RMS (60 sec avrg time)	0.05 ppb RMS (60 sec avrg time)
Lower detectable limit	1.0 ppb (60 sec avrg time)	0.10 ppb (60 sec avrg time)
Zero drift	< 1ppb (24h)	< 0.2 ppb (24h)
Span drift	± 1% (24h)	± 1% (week)
Response time	110 sec (60 sec avrg time)	110 sec (60 sec avrg time) 320 sec (300 sec avrg time)
Precision	1% of reading or 1ppb (whichever is greater)	-
Linearity	± 1% of full scale ≤ 100 ppm ± 5% of full scale > 100 ppm	± 1% of full scale

ii) Zero Check

This check is carried out every day during 15 minutes, with a scrubber of activated carbon. It was fixed at 3 am. A linear fit between consecutive zeros allows the zero correction of the readings.

iii) Calibration

A multigas calibrator (MCZ) is used to calibrate this analyzer in addition of standard gas bottles provided by Air Liquide s.a. The multipoint calibration consists in a zero and five concentrations injected in random (25, 50, 75, 100 and 200 ppb). The reason for using such high concentrations at IZO is due to the high concentrations of the standards that would be replaced in the following months. In figure 2.19 the calibrations carried out to the analyzers placed at SCO and IZO during the period that covers this thesis are shown. For standard deviations lower than 10%, the internal span and zero of the analyzer were not modified.

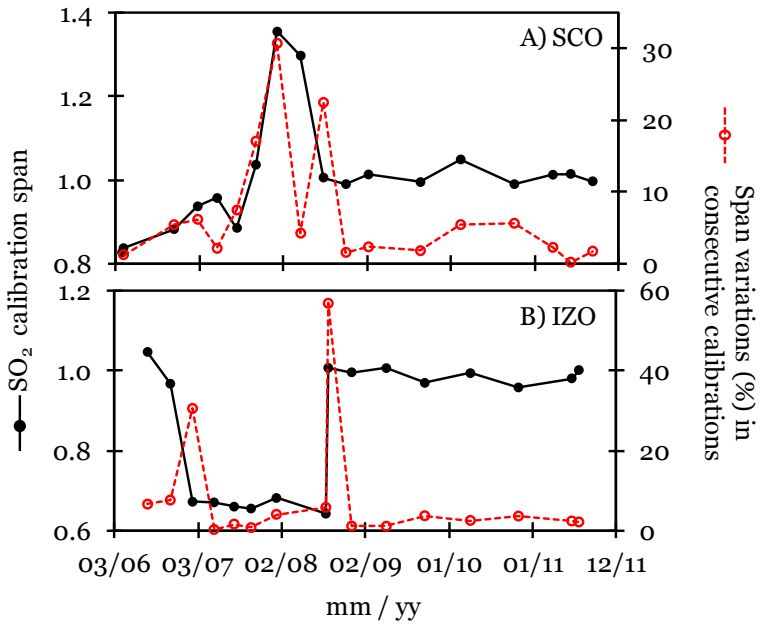

Figure 2.19 Spans and the corresponding variations of the calibrations carried out to A) the model 43C at SCO (A) and (B) the model 43C-TL at IZO (r^2>0.9 is found in all cases)

2.3.1.5 Nitrogen oxides

i) Technical specifications

Nitrogen oxides are measured by chemiluminescence NO - NO_2 – NO_X analyzers, models 42C and 42C-TL, provided by Thermo Electron Corporation. The model is based on the principle that nitric oxide (NO) and ozone (O_3) react to produce a characteristic luminescence with an intensity linearly proportional to the NO concentration. Infrared light emission results when electronically excited NO_2 molecules decay to lower energy states. Specifically,

$$NO + O_3 \rightarrow NO_2 + O_2 + h\nu \qquad \text{(eq. 2.6)}$$

Nitrogen dioxide (NO_2) must first be transformed into NO before it can be measured using the chemiluminescent reaction. NO_2 is converted to NO by molybdenum NO_2 - to - NO converter heated to about 325° C.

In nitrogen oxides analyzers, it has been observed that those built with molybdenum converters; generally overestimate the measured concentration of NO_2. This is due to interferences owing to the oxidation of other nitrogen-containing compounds, e.g. HNO_3 and PAN (Parrish and Fehsenfeld, 2000; Steinbacher et al., 2007). The NO_X analyzer at SCO contains a molybdenum

converter and at IZO a photolytic converter (Fig. 2.20). The photolytic converter uses an array of ultraviolet light emitting diodes (LED), and it converts NO_2 to NO (Blue Light Converter, Manual). The main advantage of this technique is its relatively high conversion efficiency of 50% per second for a flow of 1 $l \cdot m^{-1}$.

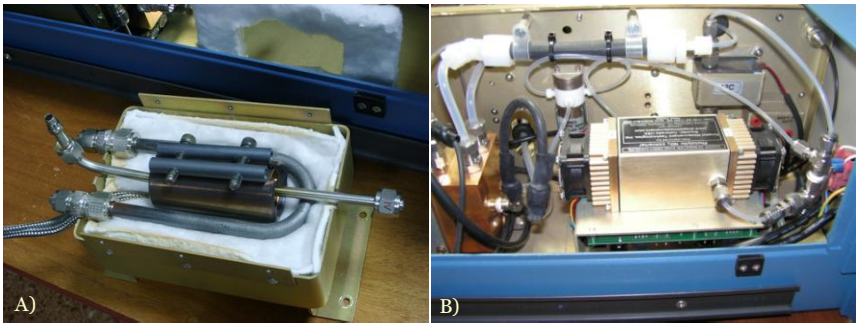

Figure 2.20 Molybdenum and photolytic converters

The flow scheme of these analyzers is shown in Figure 2.21. The sample flows through a particulate filter, a capillary, and then to the mode solenoid valve. The solenoid valve routes the sample either straight to the reaction chamber (NO mode) or through the NO_2 – to - NO converter and then to the reaction chamber (NO_X mode). A flow sensor prior to the reaction chamber measures the sample flow.

Dry air enters the analyzer through a flow sensor, and then through a silent discharge ozonator, that generates the necessary ozone concentration needed for the chemiluminescent reaction. The ozone reacts with the NO in the ambient air sample to produce electronically excited NO_2 molecules. A photomultiplier tube (PMT) housed in a thermoelectric cooler detects the NO_2 luminescence.

The NO and NO_X concentrations calculated in the NO and NO_X modes are stored in memory. The difference between the concentrations is used to calculate the NO_2 concentration.

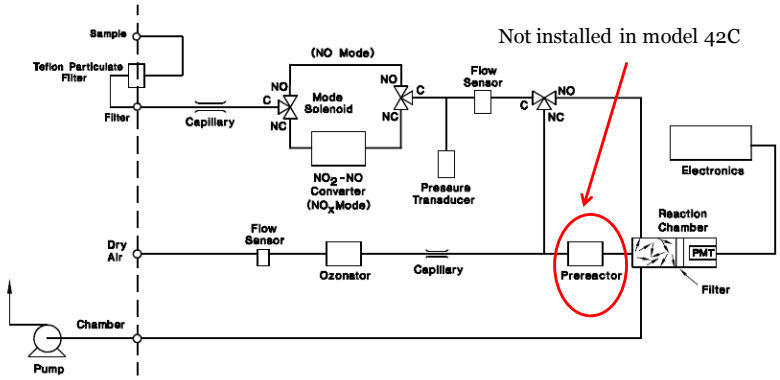

Figure 2.21 Flow Scheme of models 42C and 42C-TL. Source: 42C-TL manuals

In Table 2.8 the most specifications of this system are summarized.

Table 2.8 Specifications of 42C and 42C-TL. Source: 42C and 42C-TL manuals

Parameter	**Value**	
	SCO	IZO
Zero noise	0.20 ppb RMS (60 sec avrg time)	25 ppt RMS (120 sec avrg time)
Lower detectable limit	0.4 ppb (60 sec avrg time)	50 ppt (120 sec avrg time)
Zero drift	< 0.40 ppb (24h)	Negligible (24h)
Span drift	1% (24h)	± 1% of full scale
Response time	80 sec (60 sec avrg time)	90 sec (60 sec avrg time) 300 sec (300 sec avrg time)
Precision	± 0.04 ppb (500 ppb range)	-
Linearity	± 1% of full scale	± 1% of full scale

ii) Zero Check

This check is carried out each 6 hours, by an active carbon scrubber and purafil scrubber, with destroys the NO_x compounds and their interfering compounds. A linear fit between consecutive zeros allows the zero correction of the readings.

NO_X analyzer at IZO requires a system to dry the air mass, in order to avoid that water molecules access to the photomultiplier. Nafion drier desiccant tube was installed for that porpoise (model PD-50T-24-MKS, Perma Pure LLC). Nafion is a copolymer of tetraflouroethylene (Teflon) and perfluoro-3, 6-dioxa-4-methyl-7-octene-sulfonic acid. It is highly resistant to chemical attack, so it can be used with very corrosive gases. The principle of operation is as follows: when gas passes

through Nafion tubing, water is absorbed by and moves through the walls of the tubing. The movement of water is driven by the humidity gradient between the inside and outside of the tubing. A gas stream normally needs to reside in the device for less than one second in order to reach the proper humidity. In figure 2.22, the installation of the nafion dryer at IZO is shown:

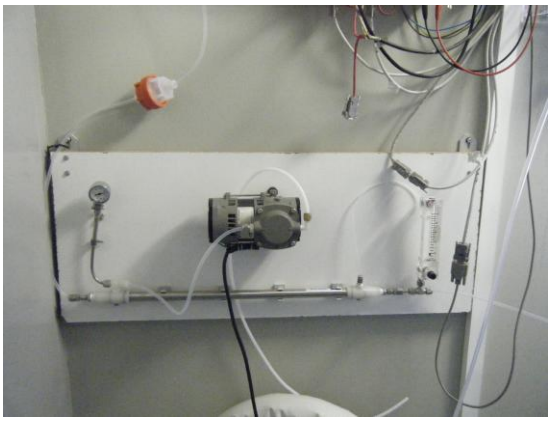

Figure 2.22 Installation of the Nafion dryer for the model 42C-TL at IZO

iii) Calibration

A multigas calibrator (MCZ) is used to calibrate this analyzer in addition of standard gas bottles provided by Air Liquide s.a. The methodology followed during the calibration process depends on the traces of the NO bottle used. It is recommended the use of NO bottle certified and free of NO_2 concentrations. In the other case, these traces should be taken into account during the calibration procedure. In any case, the calibration carried out to the NO_X analyzers is a two-step process.

Firstly, a multipoint calibration is done to the NO and NO_X outputs. This multipoint calibration consists in a zero and five concentrations injected in random (in the range of 25, 50, 75, 150 and 400 ppb). The minimal time fixed in each concentration is 20 min. Again, the reason for using such high concentrations at IZO is due to the high concentrations of the standards that would be replaced in the following months.

In a second step, the calibration of the NO_2 is carried out. This calibration requires the use of a UV lamp, in the gas phase titration (GPT) mode. The procedure described in the following lines is carried out. This procedure takes into account possible NO_2 traces:

1) A NO concentration close to the 90% of the analyzer range is selected. After the reading is stabilized, we record this concentrations as $[NO]_{orig}$, and the corresponding NO_X concentrations as $[NO_X]_{orig}$.

2) A O_3 concentration is generated in order to produce a drop in NO concentration of the 80% of the range, never exceeding the 90%. These stabilized readings will be recorded as $[NO]_{rem}$, y $[NO_X]_{rem}$, respectively.

3) The resulting NO_2 concentrations will be:

$$[NO_2]_{out} = [NO]_{orig} - [NO]_{rem} + \{(F_{NO} \cdot [NO_2]_{imp})/(F_{NO} + F_D)\} \quad \text{(eq. 2.7)}$$

Where F_{NO} = flow of the NO cyclinder and F_D the flow of the synthetic air cylinder. The calibration curve of the NO_2 is obtained by plotting $[NO_2]_{out}$ (axis y) versus the analyzer response $[NO_2]_{exp}$ (axis x).

Finally, the converter efficiency is checked. For this issue, we represent $[NO_2]_{out}$ (axis y) versu $[NO_2]_{conv}$ (axis x). The eficiency of the converter is obtained by multiplying the slope of this linear fit by 100:

$$[NO_2]_{conv} = [NO_2]_{out} - \{[NO_X]_{orig} - [NO_X]_{rem})\} \text{ (eq. 2.8)}$$

In figure 2.23 the calibrations carried out to the analyzers placed at SCO and IZO during the period that covers this thesis are shown. For standard deviations lower than 10%, the internal span and zero of the analyzer were not modified.

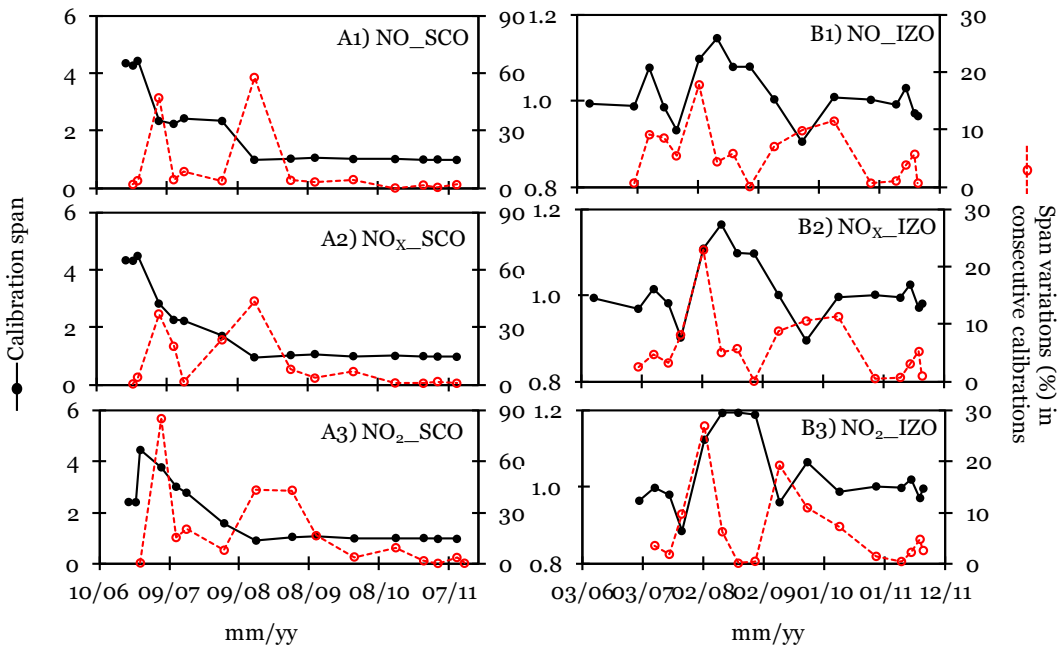

Figure 2.23 Spans and the corresponding variations of the calibrations carried out to A) the model 42C at SCO (A) and (B) the model 42C-TL at IZO (r^2>0.9 is found in all cases)

2.3.2 Aerosols

The in-situ aerosol monitoring programs implemented at SCO and IZO is summarised in Table 2.9. The program will be very briefly described in this section, being the attention focused on the number concentration of (ultrafine) particles and black carbon, the aerosol metrics mostly used for this study.

Table 2.9 Parameters and technique used in the in-situ aerosol programs of IZO and SCO

Aerosol Parameter	**Technique**	**Site**	**Start date**
PM2.5 & PM10 concentrations	24-h, gravimetry 24-h, gravimetry	SCO IZO	2005 2005
PM2.5 & PM10 concentrations	1-h, gravimetry + APS & OPC 1-h, gravimetry + OPC	SCO IZO	2005 2005
Number concentration (UFP)	Condensation Particle Counter (CPC)	SCO IZO	2008 2005
Absorption Coefficient 1 wavelength	Multi-Angle Absorption Photometry (MAAP)	SCO IZO	2006 2006
Scattering Coefficient 3 wavelengths	Integrating Nephelometer	IZO	2008
Number size distribution 10 – 400 nm	Scanning Mobility Particle Sizer (SMPS)	IZO	2008
Number size distribution 0.5 – 20 μm	Aerodynamic Particle Sizer (APS)	IZO	2006

The inlets and sampling systems used in the IZO and SCO programs shows some differences.

At IZO, the in-situ aerosol program is implemented in the building so-called PARTILAB (PARTIcles LABoratory; Figure 2.24). The in-situ aerosol monitoring program of IZO was designed following the recommendations of the Global Atmospheric Watch program (GAW 153, 2003). Three inlets are used here, one for collecting PM_{10} samples on filter, other for collecting $PM_{2.5}$ samples on filter and a third so-called 'general inlet' where the sample for the nephelometer, MAAP, SMPS, APS and CPC is collected. The 'general inlet' collects the sample from the ambient air a flow rate of 4.5 $m^3 \cdot h^{-1}$, which results in a laminar flow with a Reynols of about 1,800. Because RH is usually with the 20 – 30 %, inlets are not heated or dried. Each instrument collects the sample from the general inlet isokinetically. The in-situ aerosol program of IZO was audited in November 2006 by Dr. Thuch and Dr. Nowak, of the World Calibration Centre of Aerosol Physics (Leibniz Institute of Tropospheric Research, Leipzig, Germany).

Figure 2.24 Inlets (A) and indoor view (B-D) of the PARTILAB at IZO

Figure 2.25 Inlets (A) and indoor view (B-D) of SCO

At SCO, no general inlet is used, and each instrument (CPC, MAAP, OPC) has its own inlet (Figure 2.25).

The QA/QC of the aerosol measurement program includes:

1) Airflow checking: frequency weekly. Calibration is performed if a difference ≥ 3%, respect the nominal flow, is observed.

2) Zero check: performed once every three months. This is done by placing an absolute filter in the inlet of each instrument, which allows performing test of leaks and determine the experimental 'instrument noise'.

3) Nephelometer calibration with CO_2 and air. It is done when the clean air test shows background signal higher than 10^{-7} m-1. Usually, 1 -2 calibrations / year.

4) Collection of blank field filters.

5) Intercomparisons. During the development of this study, the instrumentation have participated in the following intercomparisons:

   i) An intercomparison of MAAPs and other absorption photometers in the Word Calibration Centre for Aerosol Physics in November 2005 (Müller et al., 2005).

   ii) An intercomparison of CPCs and MAAPs in the University of Huelva in May 2008 (Fernández Camacho et al., 2010).

   iii) An intercomparison of SMPS in El Arenosillo (Huelva) in May 2010 (Gómez-Moreno et al., 2010).

Different methods are used for determining the aerosol metrics (Table 2.9). A description of the method used by the instruments used in this study is performed below. Focused is paid to number concentration of (ultrafine) particles and black carbon.

2.3.2.1 Number of Particles

As already described in the introduction, the particle number concentration is representative of the number of ultrafine particles in the ambient air. These measurements were performed using three CPCs of TSI™: models 3010, 3025A and 3776.

At SCO, the model 2035A was used for a short campaign in March - April 2006, whereas continuous measurements are being performed since May 2008 with the model 3776. Simultaneous measurements with the models 3025A and 3010 where performed from November 2006 to December 2007. After December 2007, only the 3025A remained operative.

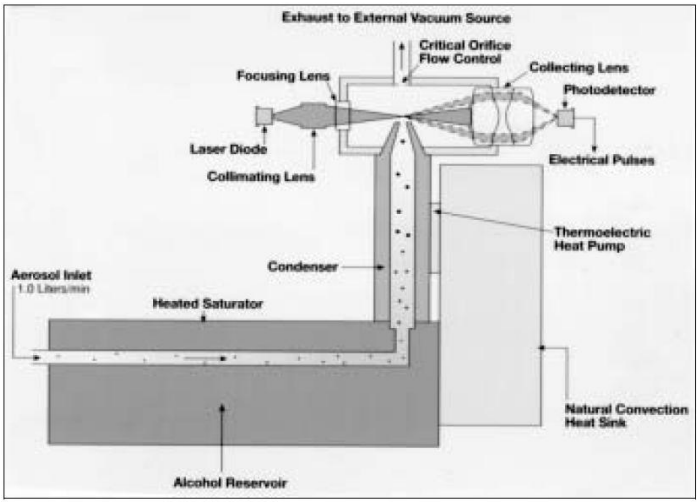

Figure 2.26 Schematic flow of the UCPC model 3010. Source: user manual

The principle of operation of a CPC is detailed in Keady et al. (1986). Figure 2.26 shows the schematic flow of the Condensation Particle Counter model 3010. The sample of ambient air particles passes through the aerosol inlet and is then directed to the heater saturator, where is mixed with vapor of buthanol (heated to 39º C). The aerosol particles and buthanol vapour mixing is then directed to a condenser, where temperature is of 10ºC. The drop in temperature causes the condensation of buthanol onto the particles present in the sample. This results in a growth of particles, from a few nanometers to several microns. Then, the grown particles passed through the optic chamber, where they are illuminated by a focused laser beam, being the signal recorded in a detector. Thus, the number of pulse in time is converted to number of particles by volume of sampled air.

The smallest size of the particles that can be detected in a CPC depends on the degree of supersaturation of the condensing vapour, i.e. buthanol in the case of CPCs. When the vapour surrounding particles reaches a certain degree of supersaturation, it begins to condense onto the particles (heterogeneous condensation). The degree of supersaturation is measured as a saturation ratio (P / P_s), which is defined as the actual vapor partial-pressure (P) divided by the saturation vapour pressure (Ps) for a given temperature:

$$\text{Supersaturation} = P / P_s \quad \text{(eq. 2.9)}$$

For a given saturation ratio, the vapour condense onto particles only if they are large enough. The minimum particle size capable of acting as a condensation nucleus is called the Kelvin diameter and is evaluated from the following relationship:

$$\text{Supersaturation ratio} = P / P_s = \exp(4\gamma M / \rho RTd) \quad \text{(eq. 2.10)}$$

where γ = surface tension of the condensing fluid, M = molecular weight of the condensing fluid, ρ = density of the condensing fluid, R = universal gas constant, T = absolute temperature; and d = Kelvin diameter.

The higher the saturation ratio is, the smaller the Kelvin diameter. Because P_s is defined for a flat liquid surface, for a round liquid surface, such as the surface of a droplet, the actual saturation vapour pressure is greater. That is, the smaller the droplet, the easier it is for the vapour molecules to escape the liquid surface. The Kelvin diameter defines the critical equilibrium diameter at which a pure droplet is stable—there is neither condensation nor evaporation. Smaller liquid particles will evaporate and larger particles grow even larger by condensation. The larger particle will growth until the vapour is depleted, causing the saturation ratio to fall until it is in equilibrium with the particle droplet.

In the CPC model 3010, the minimum particle size that can be detected is 10 nm. Thus, the CPC 3010 provides the number concentrations of particles with a size ≥ 10 nm (N_{10}).

The Ultrafine Condensation Particle Counter (UCPC) models 3025A and 3776 are able to detect particles with a size down to 3 and 2.5 nm, N_3 and $N_{2.5}$, respectively. In order to activate the growth of particles smallest than 10 nm, these two UCPCs models operates at higher supersaturation conditions than the CPC 3010.

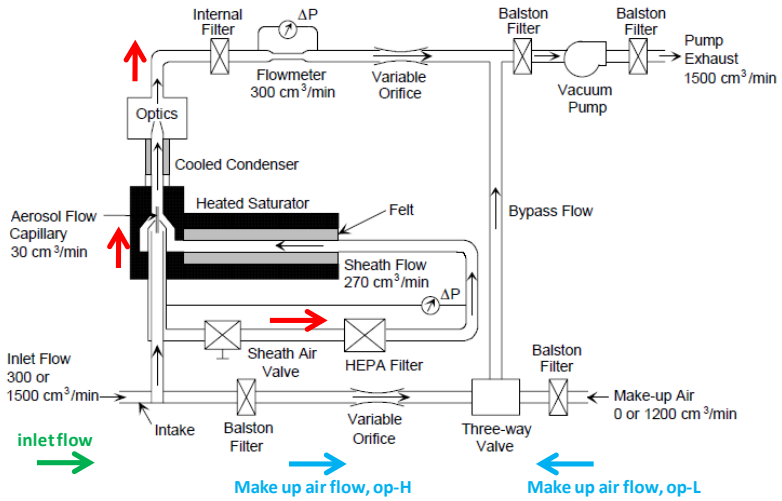

Figure 2.27 Flow schematic of the UCPC (Model 3025 A). Source: user manual

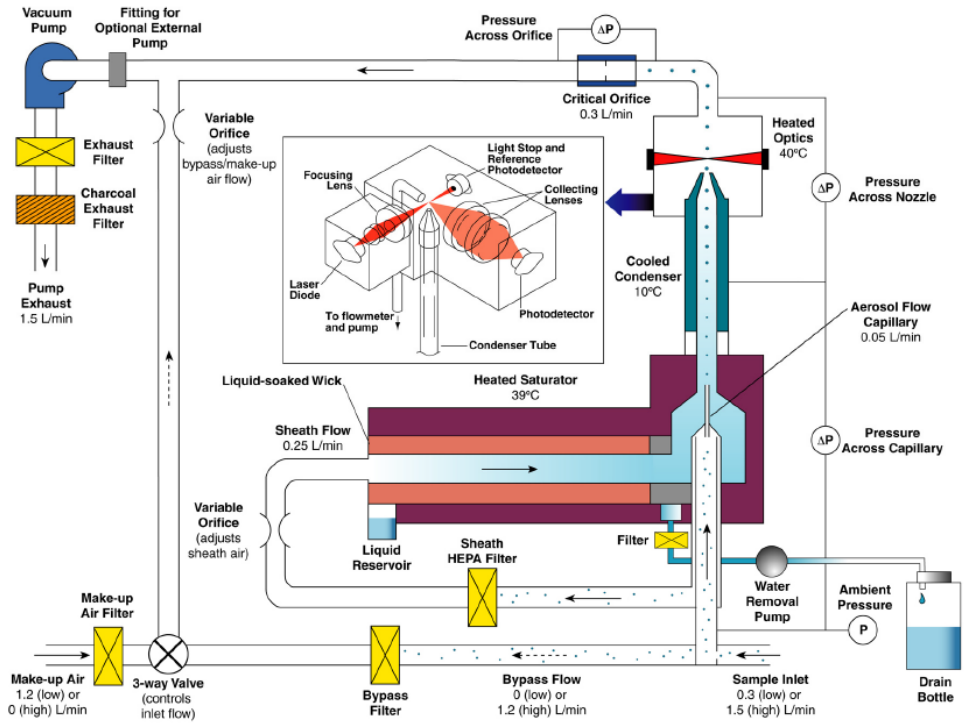

Figure 2.28 Flow schematic of the UCPC (Model 3776). Source: user manual

Figure 2.27 shows the schematic flow of the UCPC 3025A. In the high 'inlet flow' mode, the inlet air flow is 1.5 $l \cdot m^{-1}$. This flow is then divided in two airflow, the makeup air (1.2 $l \cdot m^{-1}$) and the 0.3 $l \cdot m^{-1}$ (300 $cm^3 \cdot m^{-1}$). This latter airflow is again subdivided in an aerosol flow (0.03 $l \cdot m^{-1}$) and a sheath flow (0.270 $l \cdot m^{-1}$). The sheath flow is filtered (particle free) and then passed through the saturator, where it mixes with a buthanol vapor (39°C). Subsequently, the aerosol flow is exposed to sheath flow, resulting, again, in a 0.3 $l \cdot m^{-1}$ flow. This is passed to the condenser, where the low temperature (10°C) results in the condensation of buthanol vapour onto the aerosol particles present in the ambient air sample. The use of the sheath flow increase the supersaturation conditions (with respect to the 3010 model) and in the activation of particles (Kelvin effect) down to 3 nm. In the low 'inlet flow' mode, the inlet flow is 0.3 $l \cdot m^{-1}$, and the makeup air is collected from the backside of the instrument. This has no implication in the sensing zone.

The UCPC 3776 (Figure 2.27) is a new version of the model 3025A, and uses the same principle of measurements.

During the field regularly measurements, all instruments recorded data averaged at 1-min intervals. The two UCPCs units operated in high flow mode (1.5 $l \cdot min^{-1}$) to minimize diffusion losses, whereas the CPC (3010) operated at 1.0 $l \cdot min^{-1}$. In addition to the QA/QC activities, these instruments have participated in several intercomparisons:

- The UCPC 3025A was compared with a reference unit of the World Calibration Centre for Aerosol Physics (WCCAP) in October 2005, where it was obtained that the instrument had an efficiency of 1.0 and a dp50 diameter of 3.2 nm (very close to the value of 3 nm stated by the manufacturer).

- The UCPC 3010 was compared with a reference unit of the World Calibration Centre for Aerosol Physics (WCCAP) in September 2011, where it was obtained that the instrument had an efficiency of 1.0 and a d_{50} diameter of 9.8 nm (very close to the value of 10 nm stated by the manufacturer).

- The UCPC 3776 participated in an intercomparison at the University of Huelva in May 2008. Results show a high linearity between the two instruments and that the differences were of about 0.2% for 10 min averaged data (Fig. 2.29). Experimental measurements performed by Hermann et al. (2007) have shown that the 50% counting efficiency for these instruments is reached at diameters (d_{50}) between 3 and 4 nm.

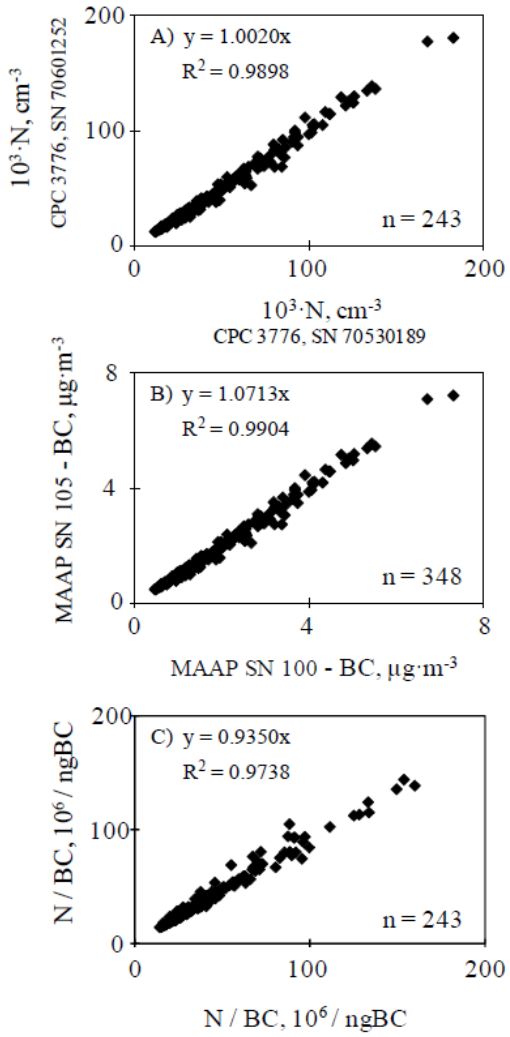

Figure 2.29 Inter-comparison between the 10 min averaged data recorded with two CPCs model 3776, two MAAPs and the N/BC ratio recorded with these instruments. Data plotted in X-axis were collected with the instruments (CPC SN 70601252, MAAP SN 100) used in this study (Fernández-Camacho et al., 2010)

2.3.2.2 Scanning mobility Particle Sizer

A Scanning Mobility Particle Sizer (SMPS) allows measuring the number concentration and size distribution of particles (Figure 2.30). At IZO this instrument was used for measuring from 14 to 600 nm. A very brief description is performed here (see details in Wiedensohler et al., 2012). A SMPS determines the number size distribution of particles according to their electrical mobility (Hinds, 1982):

$$Z= (n \cdot e\ Cs\ (D_p, P))/(3\pi\mu D_p) \qquad (2.11)$$

where n is the number of elementary charges carried by particles, e is the elementary charge, Cs is the Cunningham slip correction factor, μ is the gas viscosity and D_p the particle diameter.

In these instruments, the sample passes through a charger to ionize the particles by exposing them to a bipolar cloud of ions. In this charger a Boltzman charge equilibrium is reached, in which mean charge of particles is zero and a fraction contain ±1, ±2...etc (Fuchs, 1963; Wiedensohler, 1988; Reischl et al., 1996). The contribution of multi-charged particles increases with particle size. The sample (charged and neutral particles) is then conducted to a Differential Mobility Analyzer (DMA), where particles within a narrow interval of electrical mobility are deflected and conducted to a detector. For a given aerosol and sheath flow system in the DMA, the electrical mobility of the selected particles depends on the voltage applied within the DMA. The complete particle size distribution is obtained by applying different voltages. Depending on the applied voltage is increased in discrete steps or in a continuous ramp, these systems are so-called Differential Mobility Particle Sizers (DMPS) or Scanning Mobility Particle Sizers (SMPS), respectively. The most commonly used detector is the Condensation Particle Counter (CPC), which counts singly the monodisperse aerosol deflected by the DMA. The smallest particle size that can be detected is limited by the lower size detection limit of the CPC, which is set to 2.5 nm for neutral charge particles nowadays. The width of the electrical mobility selected for a given voltage depends on the ratio between the sheath and the sampling flows. Usually a sheath flow ten times higher than the aerosol flow is used. Thus, inaccuracies in the flows of the system affects to both concentration and particle sizing. Hermann et al. (2007) presented the efficiency curve for a set of commercially available CPCs. To obtain this curve for each individual CPC unit contribute to improve sizing accuracy close to the lower detection limit. Poly-styrene latex monodisperse spheres, with a sizes ranging from tens to hundred of nanometers, are frequently used for quantification of sizing errors and calibrations.

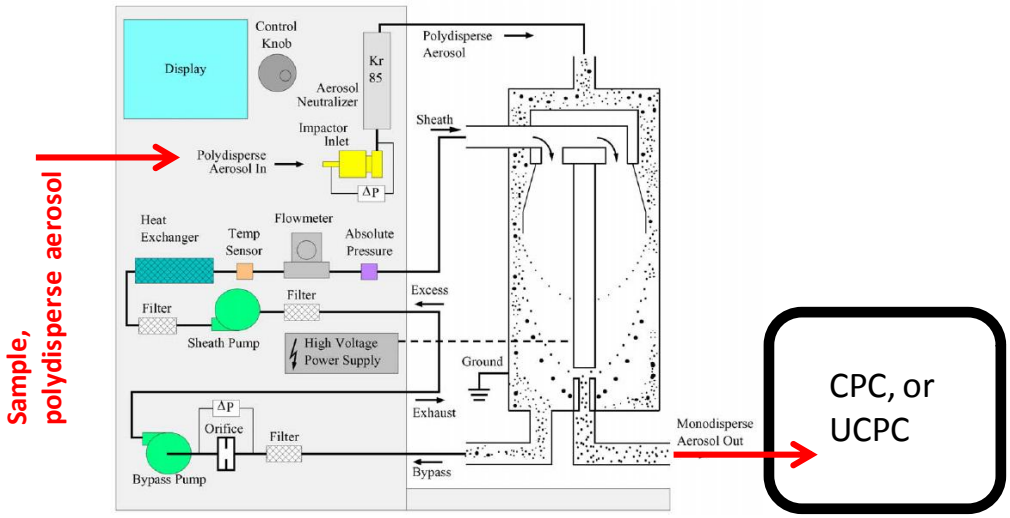

Figure 2.30 Flow schematic of the SMPS. Source: user manual

2.3.2.3 Black Carbon

Measurements of the aerosol absorption coefficient were used for determining black carbon concentrations. The aerosol absorption coefficient was monitored using, the filter based absorption photometer, Multi Angle Absorption Photometer (MAAP), model Carusso 5052 of the manufacturer Thermo™.

In the filter based instruments, ambient air with particles is drawn at a constant volumetric airflow rate through a filter. The optical transmission across the filter is continuously monitored using a source light (located above the filter) and a detector (located below the filter). When particles deposit and accumulate on filter transmission decreases and less light reaches the detector. The derivative in time of the light transmission signal is measured and it is considered related to the aerosol absorption coefficient. A reference (blank) filter is used for zero and for detecting potential changes in the source emission. This is the principle of measurements used by the PSAP (Particle Soot Absorption Photometer) and the Aethaloemter. In practice, the relationship between light transmission and absorption coefficient is affected by other factors, and data corrections are necessary for these instruments. The two most relevant corrections are due to: backscattering of the filter + sample system (back-scattering correction) and decrease in the optical path in a non-linear way due to particles accumulation on the filter (loading correction). These and other corrections are implemented in different ways depending on the instrument design, e.g. PSAP (Bond et al., 1999; Virkkula et al., 2005; Virkkula, 2010) and Aethalometer (Weingartner et al., 2003; Arnott et al., 2002; Schmid et al., 2006; Virkkula et al., 2007; Collaud Coen et al., 2010).

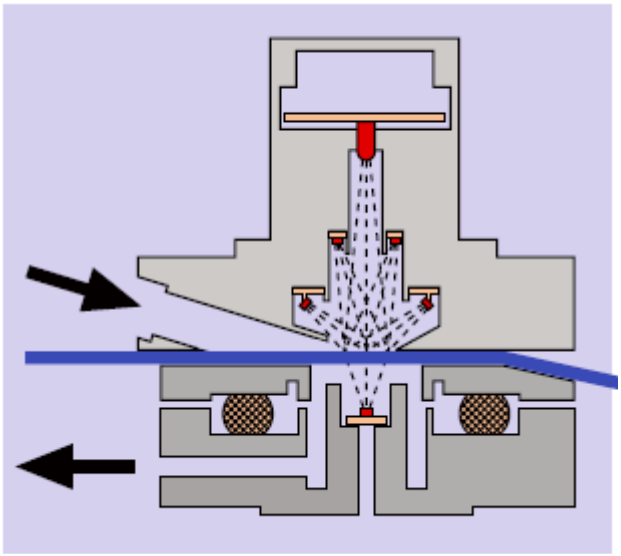

Figure 2.31 Scheme of the sensors of a MAAP

The MAAP includes additional sensors for measuring the backscattering of the filter plus sample system at two angles (Petzold and Schönlinner, 2004). This minimizes the artefact of backscattering in such a way that corrections are not considered necessary (Petzol et al., 2005). A good agreement between measurements of MAAP and photoacoustic method was observed, slope = 0.99 ± 0.01 (Sheridan et al., 2005). However, Müller et al. (2011) observed that the light source of MAAP emits at 637 nm instead of the 670 nm specified by the manufacturer. As a consequence, MAAP measurements should be refereed to 637 nm and then multiplied by 1.05 for considering the wavelength dependence of the absorption coefficient. This is the only correction described for MAAP.

The mass concentration of the aborting material is determined using the absorption coefficient (σ_{ap}; Petzold and Schönlinner, 2004):

$$BC\ (\mu g m^{-3}) = \sigma_{ap}\ (M \cdot m^{-1}) / \sigma\ (m^2 \cdot g^{-1}) \qquad \text{(eq. 2.12)}$$

where σ is the aerosol mass absorption efficiency (expressed in $m^2 \cdot g^{-1}$ units).

At SCO, equation 2.12 was used for converting the absorption coefficient to black carbon (BC) concentrations. The high correlation observed between the absorption coefficient and compounds linked to vehicle exhaust emissions, indicates that absorbing particles in SCO are linked to incomplete combustion processes. Thus, concentrations of Elemental Carbon (EC) were used for determining the aerosol mass absorption efficiency, by cross correlating the absorption coefficient

versus EC (eq 2.12). Concentrations of EC were determined on samples of PM_{10} particles collected in micro quartz fiber filter. These samples were analysed by the Thermo Optical Transmittance technique (Birch and Cary, 1996), using a Sunset Laboratory™ OC-EC analyzer and the default temperature steps of the EUSAAR2 program. These analyses are performed in the Instituto de Diagnóstico del Agua y Evaluación Ambiental (IDAEA) of the Consejo Superior de Investigationes Científicas (CSIC), in the frame of the Joint Research Unit of the Izaña Atmospheric Research Centre and CSIC.

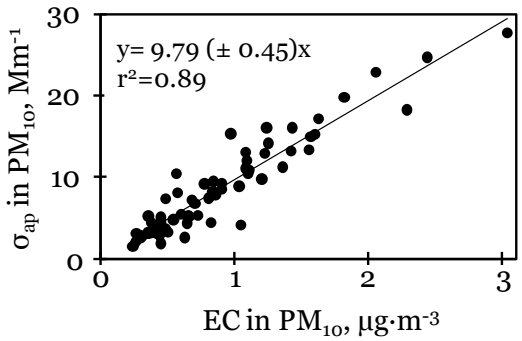

Figure 2.32 Absorption coefficient σ_{ap} versus EC concentrations in PM_{10} particles in SCO (Rodríguez et al., 2010)

At SCO, a mean aerosol mass absorption efficiency of 9.8 $m^2 \cdot g^{-1}$ is observed (Figure 2.32). Because of the low σ values typically associated with other potentially absorbing species, such as mineral dust (0.01 - 0.02 $m^2 \cdot g^{-1}$; Alfaro et al., 2004) or organic aerosols (e.g. humid-like substances σ ~ 0.03 $m^2 \cdot g^{-1}$, Hoffer et al., 2006), and because of the high correlation observed in this study between BC, and, CO and NO_X (discussed in the next chapters), we assume that the measured absorption coefficient is entirely due to absorption by EC.

The MAAP unit used SCO was intercompared with a similar unit in May 2008 at the University of Huelva (Figure 2.29). The 10-min averaged differences between the two units were of about 7%.

This methodology for determining BC concentrations (eq. 2.11) could not be applied in IZO. This is due to the fact that absorption at this site absolutely dominated by the mineral dust particles transported from North Africa. The chemical characterization of PM_{10} and $PM_{2.5}$ in IZO shows that concentrations of EC are below detection limit (5 ng·m^{-3} Rodríguez et al., 2011), and that the absorption coefficient is highly correlated by concentrations of mineral dust (Rodríguez, personal communication). Concentrations of EC at IZO are < 1 ng·m^{-3}, whereas mineral dust is present in concentrations of up to > 500 μg·m^{-3} (Rodríguez et al., 2011). In fact the climatology of the absorption coefficient in IZO is correlated with that of Saharan dust (Andrews et al., 2011).

2.3.2.4 PM_{10} and $PM_{2.5}$

At the two sites, SCO and IZO, PM_{10} and $PM_{2.5}$ were determined by two complementary methods: Gravimetry and size distribution measurements.

i) Gravimetry. Samples of PM_{10} and $PM_{2.5}$ are collected in microfiber quartz filters. For this sample collection, high volume samplers are used (30 m^3·h^{-1}). Before and after sampling, the filters are weighted in a 10^{-5} g precision balance (Metler Toldeo). Before weighting, filters need to be conditioned 48-h at 30% RH and 20ºC. This filter treatment is performed at the Izaña Atmospheric Research Centre (Figure 2.33). At SCO, 24-h samplings are performed, whereas at IZO the sampling is performed only at night in order to avoid the influence of upslope winds. This method allows obtaining PM_{10} and $PM_{2.5}$ data with a 24-h resolution in SCO (sampling 08:00 to 08:00 GMT) and 8-h resolution at IZO (22:00 to 06:00 GTM).

ii) Integration of size distributions. Measurements of number size distributions are used for determining PM_{10} and $PM_{2.5}$ concentrations with 1 minute hour resolution:

$$dV/d\log D_p = \pi/6\, D_p^3\, dN/d\log D_p \quad \text{(eq. 2.13)}$$

$$dM/d\log D_p = \rho_p\, dV/d\log D_p \quad \text{(eq. 2.14)}$$

where, D_p is the diameter, ρ_p particle density. Depending on the instrument used for measuring the size distribution, Dp may refer to a given particle equivalent diameter. The bulk mass concentration of particle below a given cut size is then calculated as:

$$PM_X = \sum_{p=p1}^{p=pn} [dM / d\log D_p]\, d\log D_p \quad \text{(eq. 2.15)}$$

where p_1 and p_n are the lowest and highest particle diameter measured, n is the number of channels in the size distribution measurements and PM_x refer to PM_{10} or $PM_{2.5}$. The use of this technique with APS data was described by Shen et al. (2002) and Peters et al. (2006). Some commercial OPCs already include mass estimations in post processing software. In SCO, size distribution measurements where performed with an OPC (GRIMM™; model 1108). In IZO, size distributions were measured with an APS (TSI™, model 3321). Particle density of Eq 2.15 was determined by cross

correlating mass concentrations (PM_{10} and $PM_{2.5}$), determined by the gravimetric method described above, versus the volume (V_{10} and $V_{2.5}$) concentrations. Typically, volume-to-mass conversion factors (densities) within the range 1.5 to 2.7 are observed.

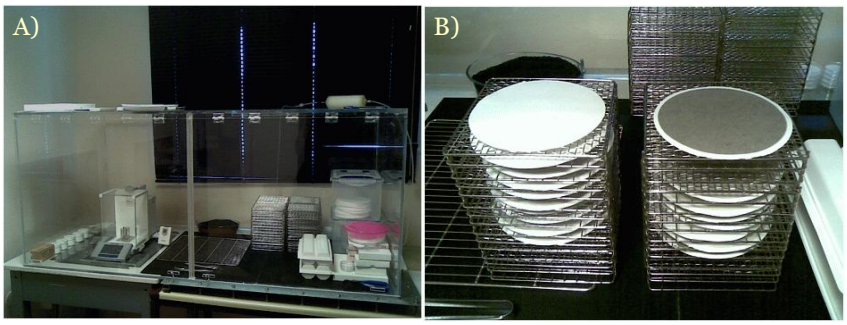

Figure 2.33 A) Room for preparation and weighting of filters of the CIAI (located in SCO). B) On the left side a blank filter (before sampling), and on the right a filter with a sample of PM_{10} particles collected at Santa Cruz de Tenerife are shown

2.4 Additional Parameters

To develop this study, additional data concerning gaseous and aerosol pollutants and meteorology have been used:

(i) Radiation. Several radiation parameters were measured with 1-min resolution: i) Solar radiation was measured with World Meteorological Organisation Class I instruments, ii) UV-B radiation (280 – 320 nm) was measured with a Yankee Environmental System (YES) UVB-1 broadband radiometer; iii) Global radiation (305 – 2,800 nm) and diffuse radiation (305 – 2,800 nm) were monitored with Kipp & Zonen CM21 radiometers, iv) Direct radiation (200 – 4,000 nm) was obtained with a Normal Incidence Pyrheliometer Kipp & Zonen, CH-1 mounted on a Kipp & Zonen 2AP Tracker; and finally, v) Photosynthetic Active Radiation (PAR), the integrated radiation within the 400 – 700 nm range, was measured with a Kipp & Zonen PAR-LITE radiometer.

(ii) Water vapour and relative humidity. Meteorological parameters were measured using a Setra 470 instrument for pressure, a Rotronic for temperature and relative humidity, and a Thies Sonic anemometer for wind. Concentrations of water vapour were calculated with the Magnus equation (equations 2.10 and 2.11). In this study, vertical profiles of temperature, relative humidity and wind speed obtained from meteorological radiosondes (Vaisala RS92+GPS) launched everyday (at 00:00 and 12:00 GMT) at Güimar site (on Tenerife, at ~100ma.s.l.) were also studied. These data allowed monitoring of the marine boundary layer depth. In order to calculate water vapour concentrations, firstly, the saturated water vapour pressure must be calculated:

$$\text{Log } e_w = 10.79574\cdot(1- T_1/T) - 5.02800\cdot\log(T/T_1) + 1.50475\cdot10^{-4}\cdot\{1-10^{-8.2969\cdot[(T/T_1)-1]}\} + 0.42873\cdot10^{-3}\cdot[10^{4.76955\cdot(1-T_1/T)} - 1] + 0.78614 \qquad \text{(eq. 2.10)}$$

where T is temperature (K), $T1$ =273.16 K, is the temperature of the triple point of water, and e_w is the saturation vapour pressure in hPa over water. The water vapour concentration is calculated by using the relative humidity (RH) and the saturated water vapour pressure:

$$e = e_w\,(RH/100) \qquad \text{(eq. 2.11)}$$

(iii) Air Masses. 5 - day backtrajectories calculated at 00:00 UTC using HYSPLIT (Hybrid Single-Particle Lagrangian Integrated Trajectory) 4.0 dispersion model back-trajectories (Draxler and Rolph, 2003; Rolph, 2003) and 50 km × 50 km ECMWF data have been used. The geophysical region covered by the trajectories was divided into 408 grid cells of 5º x 5º latitude and longitude. Ashbaugh et al. (1985) used backward air trajectories, combined with a statistical technique called "residence time analysis" (RTA), to identify source regions for transport of particulate sulfur to the Grand Canyon National Park. This technique, with little modifications, has been used for several investigators to identify the transport corridors and source regions for many pollutants (Poirot and Wishinski, 1986; Comrie, 1994; Poirot et al., 2001). In this method, they first interpolate along each trajectory segment to estimate the fraction of time spent in each grid cell and then the residence time for that cell is assumed. They propose a method to adjust the resulting grid cell values for the geometrical problem of high values in the region immediately adjacent to the receptor site. The potential source regions of gaseous species were identified by analyzing the RTA plots determined for gaseous pollutant analyzed at Izaña.

(iv) Two additional air quality monitoring stations, Los Gladiolos (GL) and Tome Cano (TC), were used in one of the studies as supporting information. These sites belong to the Government of the Canary Islands (Department of Health). They are located in the city centre to the NW of the industrial area of the city (crude oil refinery), and to the NW of the motorway (which links the city to the northern side of the island; Fig. 2.3). At these stations, measurements of PM_{10}, $PM_{2.5}$, SO_2, and wind speed and direction were registered continuously.

2.5 Field measurement strategy

In order to achieve the objectives described in chapter 1, measurements were performed using the following strategy at each site. The specific data treatment will be described in each chapter. In the Santa Cruz Metropolitan Area the following measurements data sets were used:

Data set – 1

March to April 2006 campaign:

Santa Cruz Atmospheric Observatory

- Number of particles coarser than 3 nm with the UCPC 3025A
- Concentrations of black carbon with a MAAP
- Concentrations of PM_{10}, $PM_{2.5}$ and PM_1 using the gravimetric and OPC methods
- Concentrations of CO and O_3
- Meteorological parameters and solar radiation

Complementary measurements were also used:

- Road traffic intensity in the Anaga Avenue, data provided by the city council
- Measurements of PM_{10}, $PM_{2.5}$, NO_X and SO_2 at Tome Cano and Gladiolos at air quality stations (Government of the Canary Islands).

This campaign was used to explore the relationship between different metrics representative of the particle concentrations. Results were used to design a measurement program longer in time.

Data set – 2

May 2008 to December 2010:

Santa Cruz Atmospheric observatory

- Number of particles coarser than 2.5 nm with the UCPC 3776
- Concentrations of black carbon with a MAAP
- Concentrations of PM_{10}, $PM_{2.5}$ and PM_1 using the gravimetric and OPC methods
- Concentrations of CO, NO_x, SO_2 and O_3
- Meteorological parameters and solar radiation

Complementary measurements were also used:

- Road traffic intensity in the Anaga Avenue, data provided by the city council
- Measurements of PM_{10}, $PM_{2.5}$, NO_X and SO_2 at Tome Cano and Gladiolos at air quality stations (Government of the Canary Islands)

Data collected until December 2010 were used in this study. Data collected in this period allowed to estimate how differences sources contribute to the ultrafine particles concentrations.

In the Izaña Global Atmospheric Watch Observatory:

Data set – 3

January 2007 to December 2010:

- Concentrations of CO, NO_X, SO_2 and O_3
- Concentrations of PM_{10} using the gravimetric and APS methods
- Meteorological parameters and solar radiation

This data set was analysed for identifying the processes affecting the concentrations of reactive gases in the low free troposphere. For this analysis, the role of long range transport was studied using 5 - day back-trajectories calculated with the HYSPLIT (Hybrid Single-Particle Lagrangian Integrated Trajectory) dispersion model (Draxler and Rolph, 2003; Rolph, 2003).

Data set – 4

November 2006 to December 2006:

- Number of particles coarser than 3 nm with the UCPC 3025A
- Number of particles coarser than 10 nm with the UCPC 3010
- Concentrations of PM_{10} using the gravimetric and APS methods
- Concentrations of CO, NO_X, SO_2 and O_3
- Meteorological parameters and solar radiation

June to September 2008

- Number size distribution from 14 to 600 nm

Data collected during these two periods were used for studying ultrafine and nanoparticles in the upslope winds at Izaña mount.

Chapter 3

Ultrafine particles in the Metropolitan Area of Santa Cruz de Tenerife

Ultrafine particle (UFP) emissions in urban areas have become in a matter of concern due to their harmful effects on human health. Because of this, there is an open debate about the needed of introducing standards for UFP in ambient air.

As already stated above, most of studies on UFPs in urban air have focused on vehicle exhaust emissions, even if it is well known that other gaseous precursors may be emitted in urban and industrial areas. In this chapter, a study on the origin of the UFPs in the Metropolitan Area of Santa Cruz de Tenerife is presented. This is a good example of city where emissions from vehicle exhausts may be mixed with emissions from other sources. The objectives are to: 1) determine typical concentrations of UFPs in this city, 2) identify the sources and processes that contribute to their concentrations and 3) quantify the contribution of each source. This study is mostly based on data collected at SCO within the frame of this thesis, using the methods descried in chapter 2.

3.1 Sources of ultrafine particles

At SCO, the studied pollutants showed the following mean concentrations: 167 ± 66 $\mu g \cdot m^{-3}$ for CO, 10 ± 23 $\mu g \cdot m^{-3}$ for SO_2, 26 ± 31 $\mu g \cdot m^{-3}$ for NO_X, 56 ± 21 $\mu g \cdot m^{-3}$ for O_3, 900 ± 863 $ng \cdot m^{-3}$ for black carbon (BC) and 15,000 ± 15,086 for the number of concentrations of ultrafine particles (N).

The daily evolution of these pollutants was highly influenced by the coastal sea breeze, which resulted in an inland easterly airflow from 10 to 18 GMT (4 – 5 $m \cdot s^{-1}$) and a slight seaward wind at night (~ 2 $m \cdot s^{-1}$; Figure 3.2A, discussed below). Primary gaseous pollutants exhibited a marked daily evolution. Figure 3.2 shows the hourly mean values of NO_X and SO_2 during working days and weekends at SCO and two other city sites: TC and LG (see location in Figure 3.1A). At all sites, concentrations of NO showed a maximum during the morning of the working days, attributed to vehicle exhaust emissions. This maximum is induced by the sharp increase in road traffic intensity during the early morning (07 - 09 GMT), when low wind conditions (~ 2 $m \cdot s^{-1}$; Figures 3.2A1 - A2) prevail. Inland sea breeze after 10 GMT (~ 5 $m \cdot s^{-1}$) resulted in a drop of NO concentrations. At the three sites (SCO, GL and TC), the daily evolution of SO_2 was markedly different to that of NO (Figures 3.1D - 3.1E).

The highest SO_2 concentrations, recorded from 10 to 18 GMT under the inland sea breeze regime, are attributed to the transport of this pollutant from their emission sources located at the shore (oil refinery and ships; Figure 3.1A). High SO_2 concentrations were recorded at GL and TC under Southeasterly and Southerly winds, respectively, pointing to the oil refinery (Figures 3.1C1 - C2). At SCO, high SO_2 concentrations were recorded under the easterly sea breeze blowing pointing to the harbour, and during the South-westerly winds, pointing to the oil refinery (Figure 3.1C3). NO dependence with wind direction is smoother due to vehicle exhaust emissions occur throughout the city (Figures 3.1C5 - 3.1C7).

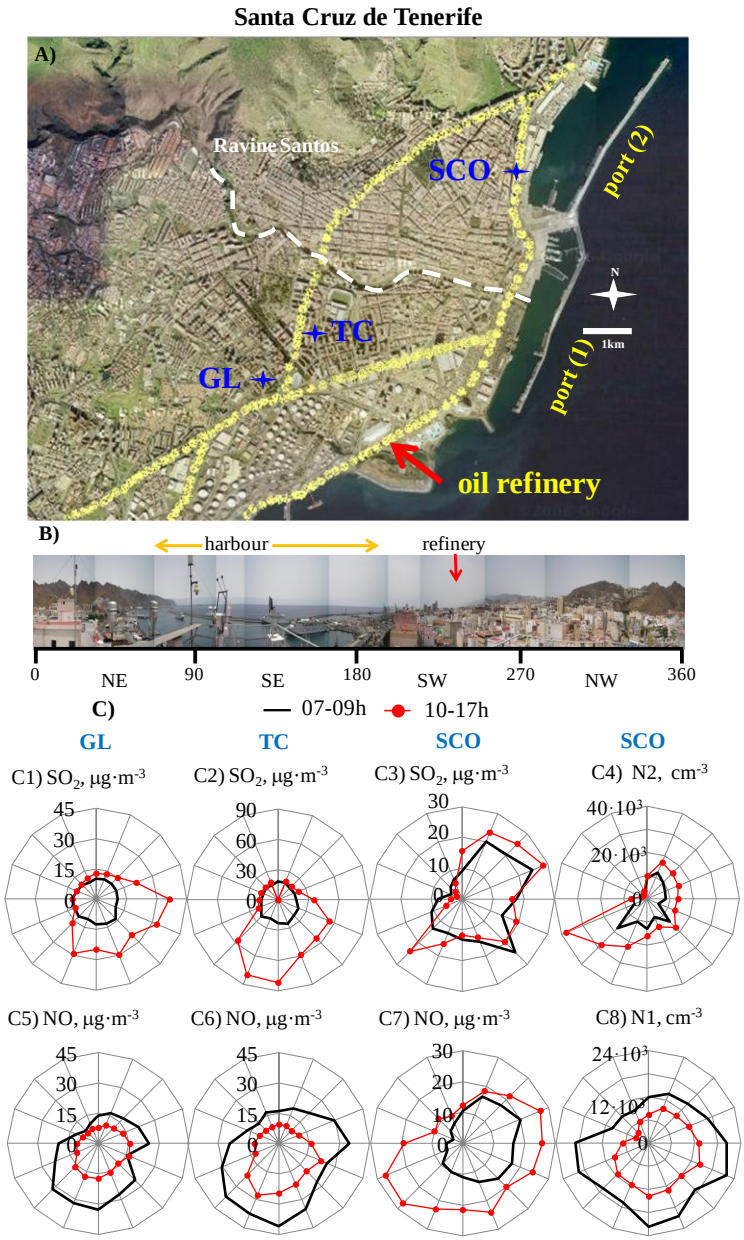

Figure 3.1 A) View of Santa Cruz de Tenerife highlighting the location of the Santa Cruz Observatory (SCO), Tome Cano (TC) and Los Gladiolos (GL) measurement sites. Dotted yellow line indicates main roads. B) 360º view from Santa Cruz Observatory (SCO). C) Wind roses of SO_2 (µg·m^{-3}) and NO (µg·m^{-3}) at GL, TC and SCO. N1 and N2 measured at SCO

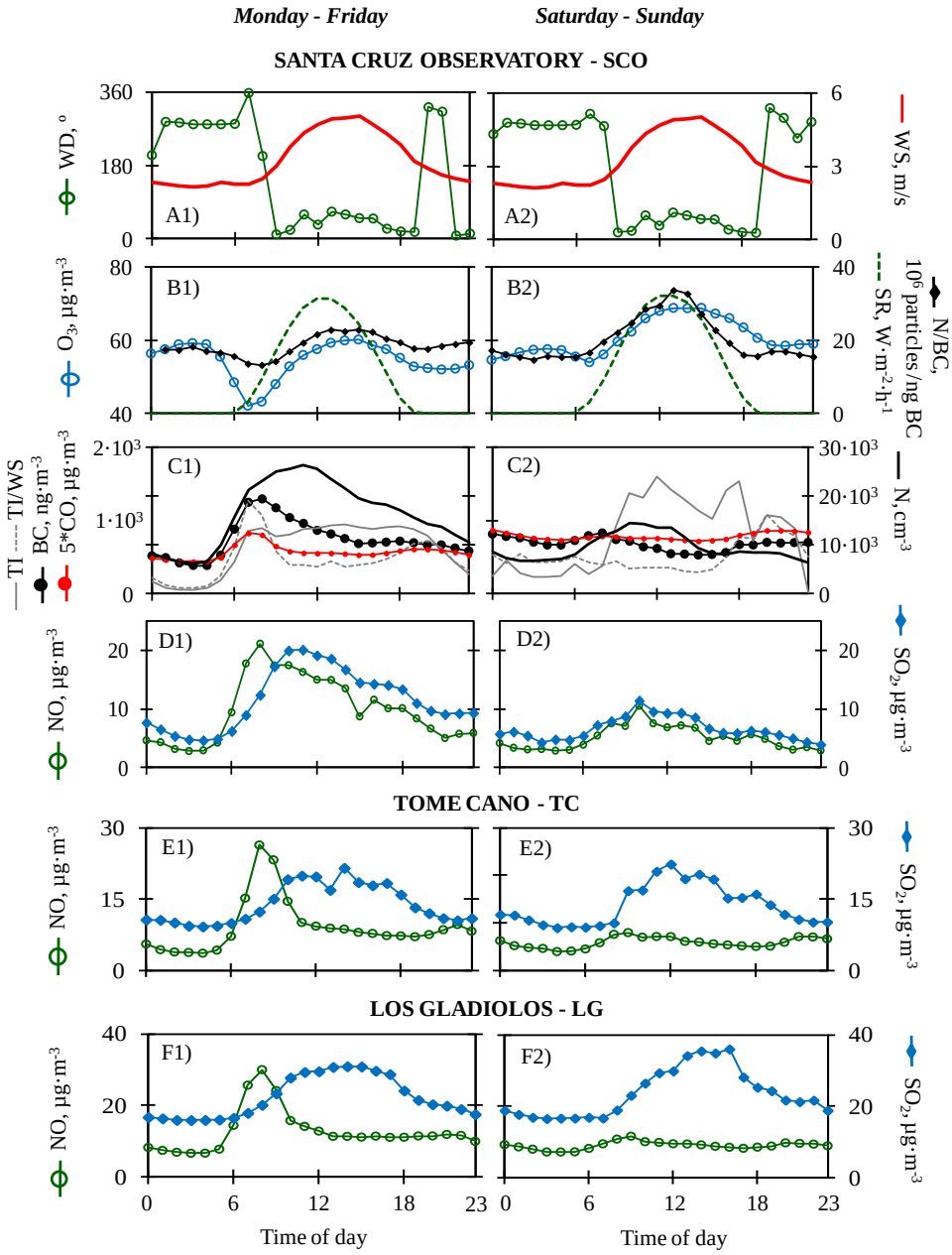

Figure 3.2 Daily evolution (hourly values) of wind speed and direction, solar radiation, road traffic intensity (RTI: vehicles·h^{-1}), road traffic intensity / wind speed (RTI / WS), black carbon (BC), particle number (N) and gaseous pollutants (O_3, CO, SO_2 and NO) in SCO. SO_2 and NO data from TC and GL are also shown

Concentrations of BC and N were only measured at SCO (Figure 3.2C). Weekly evolution of BC was similar to that of NO (Figures 3.2C - D). The correlated weekly evolution of BC and the road traffic/wind speed ratio indicates that the concentrations of this pollutant are mostly modulated by fresh vehicle exhaust emissions and air mass renewal prompted by sea breeze (Figure 3.2C1). This behaviour was observed during the whole study period (Figures 3.2C1, 3.3A1). The abrupt increase in N in the morning evidences a high influence of vehicle exhaust emissions (Figures 3.2C1 and 3.3A1). However, the fact that N reaches maximum concentrations around noon, later than BC concentrations (07 - 09 GMT), suggests than other sources and/or processes contribute to UFP concentrations (Figures 3.2C and 3.3A). The N/BC concentration ratio exhibited a broad maximum during inland sea breeze blowing, correlated with that of SO_2, solar radiation and O_3 (Figures 3.2B1-3.2B2). This suggests that photochemical SO_2 to sulfuric acid - sulfate conversion may be contributing to UFP concentration during the inland sea breeze blowing period.

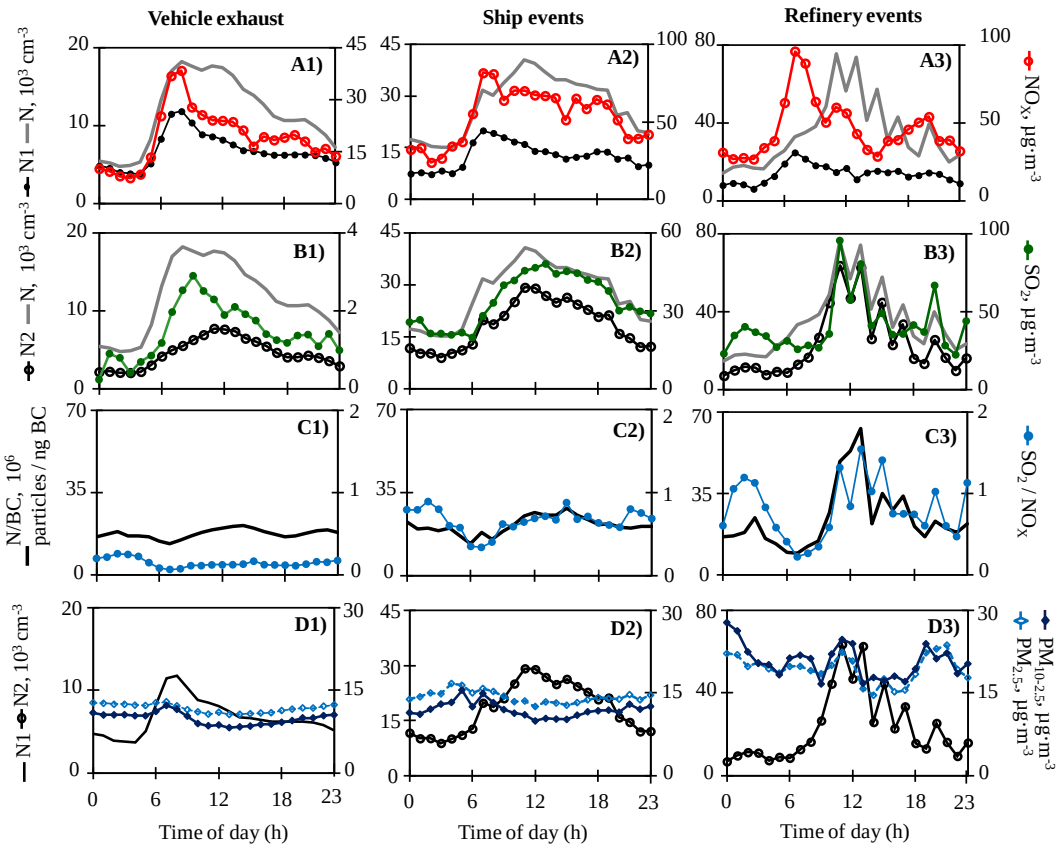

Figure 3.3 Daily evolution (hourly values) of particle number (N, N1 and N2), $PM_{2.5}$, $PM_{10\text{-}2.5}$, gaseous pollutants (SO_2 and NO_X), and the particle number to black carbon (N/BC) and SO_2 / NO_X ratios. Data collected at SCO and classified per event type: vehicle exhaust, ships and refinery

3.2 Segregation of particle number components

Previous studies have shown that in urban areas N and BC tend to show correlated variations (Fruin, Winer & Rodes, 2004; Rodríguez et al., 2007). The observed N / BC relationship is used for identifying the sources of BC (Rodríguez and Cuevas, 2007).

The N-vs-BC data set is usually comprised between two well defined borders. The borders of the N-vs-BC data set, with slopes S1 and S2, represent the minimum (S1) and maximum (S2) N/BC ratios in ambient air. Slope S1 is interpreted as the minimum amount of primary particles emitted/formed, per each unit mass of BC, by the BC prevailing source(s), i.e. vehicle exhausts in Santa Cruz de Tenerife (see Figure 3.4). Increases in the N/BC ratio up to the observed maximum N/BC ratio (S2) are caused by enhancement in the formation or emission rate of UFPs. A study carried out in European cities carried out between the aerosols group at IARC and the Associated unit CSIC, has shown that the relationship between N and BC observed in SCO is similar to that observed in other cities, such as London (UK), Barcelona (Spain) and Lugano (Italy, Reche et al., 2011).

In order to identify the sources and processes that contribute to the UFP concentrations in the metropolitan area of Santa Cruz de Tenerife (SCMA), the methodology developed by Rodríguez and Cuevas (2007) was applied. In this method N is splitting in two components:

$$N1 = BC \cdot S1 \qquad \text{Equation 3.1}$$

$$N2 = N - N1 \qquad \text{Equation 3.2}$$

When road traffic is the predominant source of BC, as the case of the SCMA, component N1 represents the minimum primary particle emissions of the vehicle exhaust and accounts for the emissions of soot mode particles and those components that nucleate immediately after emission, i.e. those components which are in the aerosol phase under typical ambient air conditions. This component includes incomplete fuel combustion products (e.g. black carbon, long-chain organic matter compounds or PAH), condensed trace metals, unburned oil and a fraction of sulfate and organic compounds that nucleate/condensate after emission (Kittelson, 1998; Burtscher, 2005; Arnold et al., 2006; Rose et al., 2006).

Component N2 accounts for those processes resulting in N/BC ratios above S1 (Figure 3.4), such as nucleation and/or growth in ambient air up to detectable sizes (> 2.5 nm in our case) in different contexts: during the dilution and cooling of the vehicle exhaust emissions (Charron and Harrison, 2003; Casati et al., 2007), in ambient air due to photochemistry (Woo et al., 2001; Wehner et al., 2002), and/or in aerosol precursor's plumes (Fernández-Camacho et al., 2010). Some typical sources of BC in Europe, such as biomass burning in house heating or agriculture wastes are not present in our study area.

In Santa Cruz de Tenerife city a slope S1 = $7.9 \cdot 10^6$ particles/ng BC is observed during the morning rush hours (Figure 3.4A). This value is within the range of those observed in other urban areas such as Huelva, Barcelona, Milan, Bern, Lugano and London (Fernández-Camacho et al., 2010; Reche et al., 2011). Reche et al. (2011) did not find city – to - city variations in S1 during the morning rush hours, and showed that the values of this slope depended on the lower cut-off size of the CPC used (~ 8, 5 and $3 \cdot 10^6$ particles/ng BC when measuring number of particles > 2.5, 5 and 7 nm, respectively).

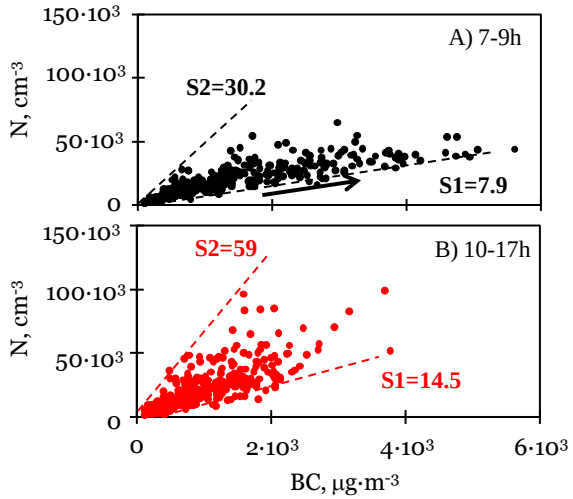

Figure 3.4 Particle number (N) versus black carbon (BC) concentrations at SCO during A) the morning rush hours (07 - 09h) and B) the inland sea breeze blowing (10 - 17h)

The much higher "minimum number of particles per each nanogram of BC" found during the 10 - 17 GMT period, evidences that other sources and/or mechanisms are contributing to UFP concentrations in ambient air during the inland sea breeze blowing. This enhancement in the new particle formation processes also accounts for the higher S2 values found in the same period (Figure 3.4B).

3.3 Ultrafine particle events

Events in which a given source impacted at SCO were identified using wind direction and SO_2 as tracer of the ship and oil refinery plumes. An event was considered as dominated by vehicle exhaust emissions when SO_2 concentrations were lower than 5 $\mu g \cdot m^{-3}$. This threshold is consistent with the concentrations of SO_2 observed when air blew upwind of the refinery and harbour: Northwest at GL (Figure 3.1C1), North at TC (Figure 3.1C2) and NW at SCO (Figure 3.1C3). Increases in SO_2 concentrations at SCO (above 5 $\mu g \cdot m^{-3}$) when air blew from SW (180 - 270º) and East (0 - 180º) were attributed to the refinery and ship emissions, respectively (Figures 3.3B1 and 3.3B3). Measurements when wind blew from 270 to 360 º and SO_2 was > 5 $\mu g \cdot m^{-3}$ were not used due to these could not be unequivocally attributed to (re-circulated) ships or refinery emissions (these cases accounted for 5% of the whole data set). Wind direction and SO_2 concentrations were the parameters used for classifying hourly mean data. Mean concentrations of SO_2 were equal to 3.0 ± 1.9, 37 ± 19 and 38 ±16 $\mu g \cdot m^{-3}$ during vehicle exhaust, ship, and refinery events, respectively. These ranges of SO_2 concentrations are consistent with those observed in other studies, e.g. in European cities for the case of vehicle exhaust events (Reche et al., 2011) or downwind of ship (Lowles and ApSimon, 1996) or refinery (Prtenjak et al., 2009) emissions.

The daily mean evolution (hourly average) of N, NO_X and SO_2 concentrations during the vehicle exhaust, ships and refinery events is plotted in Figures 3.3A-B. The profile of each type of UFP episode was studied by performing a set of Principal Component Analyses (PCAs), followed by a varimax rotation, with 1-h average data (Table 3.1). The PCAs were performed segregating the study period (07:00 – 09:00 and 10:00 – 17:00 GMT) and the type of event (vehicle exhaust dominated, ship and oil refinery). Different combinations of variables were tested. In the morning vehicle exhaust events (07:00 - 09:00 GTM), only two Principal Components (PCs) were persistently obtained (Table 1A):

The profile of each type of UFP episode was studied by performing a set of Principal Component Analyses (PCAs), followed by a varimax rotation, with 1-h average data (Table 3.1). The PCAs were performed segregating the study period (07 - 09 and 10 - 17 GMT) and the type of event (vehicle exhaust dominated, ship and oil refinery). Different combinations of variables were tested. During the morning rush hours (07 - 09 GTM), when vehicle exhaust events predominate, only two Principal Components (PCs) were persistently obtained (Table 3.1A):

- PC-1 is associated with N1, CO, NO_2 and road traffic intensity/wind speed ratio. This profile agrees with the above interpretation of the N1 component, i.e. mostly soot (Rose et al., 2006) including light absorbing particles and some species that nucleate during the emission.

- PC-2 shows high loading factors for N2 and SO_2. This PC accounts for the nucleation of sulfuric acid during the dilution and cooling of the vehicle exhaust (Arnold et al., 2006). Note that SO_2 concentrations during vehicle exhaust events reached a maximum in the morning (~ 3.5 $\mu g \cdot m^{-3}$;

Figure 3.3B1). The above described simultaneous emission of soot and nucleation particles accounts for the presence of N1 in this component.

Table 3.1. Loading factors of the Principal Components Analysis (followed by varimax rotation) obtained with hourly averaged values of the study parameters. The analysis was performed for Vehicle Exhaust (V.E.), ship and refinery events. Data were segregated for time (07 - 09 and 10 - 17 GMT). Eigenvalues >1 and a maximum number of principal components equal to 4 were set.

	A) 07-09 GMT		*B) 10-17 GMT*		*C) 10-17 GMT*			*D) 10-17 GMT*		
	V.E.		**V.E.**		**Ships**			**Oil refinery**		
	PC-1	PC-2	PC-1	PC-2	PC-1	PC-2	PC-3	PC-1	PC-2	PC-3
N1	**0.74**	**0.60**	**0.85**	0.25	0.35	0.16	**0.70**	**0.69**	-0.03	0.40
N2	0.00	**0.72**	**0.67**	-0.05	0.29	**0.78**	0.14	0.17	**0.88**	-0.20
SO_2	0.20	**0.79**	**0.77**	-0.08	**0.77**	0.30	0.08	**0.87**	0.31	-0.31
NO	0.59	**0.61**	**0.67**	0.01	**0.90**	0.13	0.09	**0.81**	-0.23	0.44
NO2	**0.80**	0.47	**0.68**	0.53	**0.68**	-0.09	0.34	**0.94**	-0.05	0.28
CO	**0.81**	0.21	0.02	0.55	-0.15	-0.27	**0.75**	0.24	-0.11	**0.94**
O3	-0.46	**-0.66**	-0.40	0.34	**-0.67**	0.04	0.36	-0.61	**0.71**	0.07
WS	**0.82**	0.31	-0.02	**-0.82**	-0.12	**0.82**	-0.27	-0.04	**0.97**	-0.05
Variance %	40	30	36	18	32	21	22	42	30	17

During the inland sea breeze blowing (10 - 17 GMT, Tables 3.1B - 3.1D):

- N1 and N2 tend to be included in PCs that also contain primary gases linked to combustion. This indicates that fresh combustion emissions are the main sources that affect UFPs variability.

- A PC-2 with high factor loading of N2 and wind speed is observed. This represents entry of nucleation sulfuric acid / sulfate particles from the harbour (East) during ship events, and from the Southwest in the refinery episodes over the NE of the city (Figures 3.1A and 3.1C4). Consumption of SO_2 during the oxidation processes accounts for the moderate loading factor (~ 0.3) of this precursor gas in this PC. Associations between wind speed and nucleation particles are frequently observed (Rodríguez et al., 2005; Hamed et al., 2007). The correlation with O_3 suggests a significant involvement of photochemistry during the refinery events. This fact is observed during refinery events and not during the ship episodes, which may be due to the involvement of key organic species (Metzger et al., 2010; Cheung et al., 2011). Several studies showed that some of these compounds may enhance the nucleation rates of sulfuric acid and may also participate in the nucleation particles growth (Zhang et al., 2004).

The daily mean evolution (hourly average) of the N, NO_X and SO_2 concentrations and of the N/BC and SO_2 /NO_X ratio during the vehicle exhaust, ship, and refinery events are shown in Figure 3.3. Increases in N during the morning, were associated with increases in NO_X concentrations due to vehicle exhaust emissions in all type of events (Figure 3.3A). During ship events, the daily evolution of N is correlated to that of SO_2 and NO_X after the early morning, due to the inland transport of the ship plumes by the sea breeze (Figures 3.3A2 and B2). Similarly, during refinery episodes, the fumigations of SO_2 plumes resulted in high N concentrations (Figure 3.3B3).

The daily evolution of N1 and N2 are shown Figure 3.3. Several issues of interest are observed in these events:

- Fumigations of the ship and refinery plumes have a lower impact on N1 than on N2 concentrations (Figure 3.3). During the three types of events the highest N1 concentrations were recorded during the morning rush hours (as the case of CO and NO_X). This indicates that vehicle exhausts is the mayor source of N1 particles, even if ship and oil refinery emissions may also contribute.

- Component N2 exhibits a daily evolution correlated with that of SO_2, solar radiation and O_3 (Figures 3.2B and 3.3C). This component typically reaches the highest concentrations in the 10:00 – 15:00 GMT period, i.e. later than N1 (07:00 – 09:00 GMT). The fact that N2 is predominantly influenced by SO_2 concentrations is illustrated in Figures 3.3B - C. Observe how the daily evolution of the N/BC and SO_2/NO_X ratios are significantly correlated, and how these ratios increase across the sequence of events of vehicle exhaust, ships and oil refinery during the 10:00 – 17:00 GMT period.

- N1 and N2 tend to exhibit a high association with NO_X and SO_2, respectively. These parameters tend to exhibit a correlated evolution and a significant linearity (Figures 3.5A1 and 3.54B1).

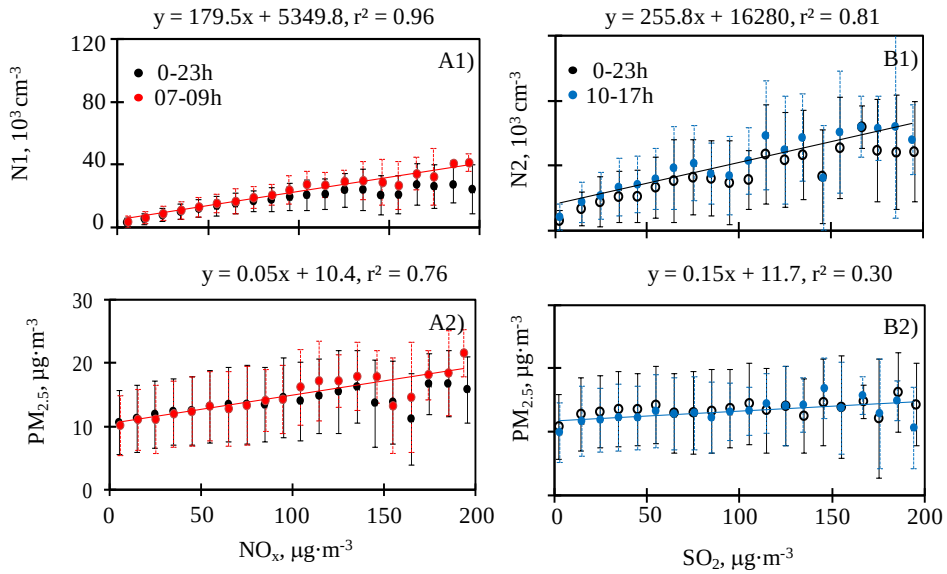

Figure 3.5 N1 and $PM_{2.5}$ versus NO_x concentrations, and N2 and $PM_{2.5}$ versus SO_2 concentrations at SCO

3.4 Contribution of sources to ultrafine particles

Figure 3.6 shows the daily evolution of the typical range of N concentrations (between 25th and 75th percentiles) during each type of episode. The contributions of the refinery and ships were calculated considering only the component N2, whereas for the vehicle exhausts both, N1 and N2 were considered. Each hourly N2 value was attributed to each source using the above describe criteria (SO_2 concentrations and wind direction).

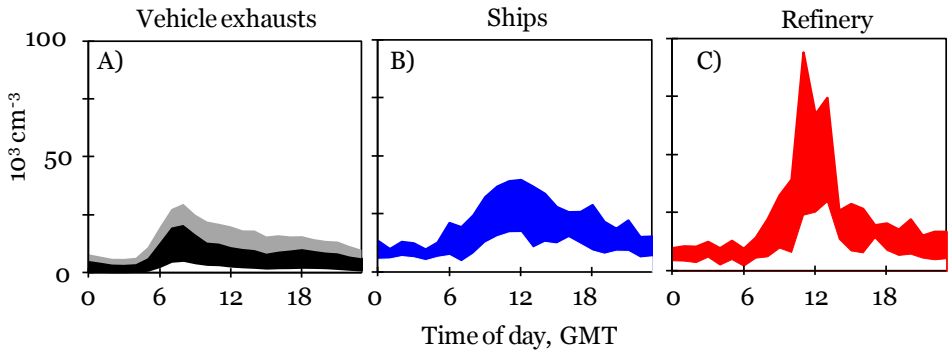

Figure 3.6 Daily evolution (hourly values) of the particle number concentration during vehicle exhaust, ships and refinery pollution events. Lower and upper border of each shadowed area represent the 25th and 75th percentiles, respectively. For vehicle exhaust events, black and grey area highlights N1 and N2, respectively

Different diurnal profiles are observed:

- UFP from vehicle exhausts showed the maximum concentrations in the morning, with frequent concentrations within the range 5,000-25,000 cm^{-3} (25th – 75th percentile; Figure 3.6A). This daily evolution is similar to that observed in cities of Central and Northern Europe, where vehicle exhausts is considered the most important source of UFP, e.g. Helsinki, Leipzig, London, Belfast, Barcelona and Milan (Harrison & Jones, 2005; Kaur et al., 2005; Laakso et al., 2003; Rodríguez et al., 2007; Wehner &Wiedensohler, 2003).

- UFP from ships showed the maximum concentrations in the 10 - 17 GMT period, typically within the range 15,000–45,000 cm^{-3} (25th - 75th). This cycle is induced by the inland transport of the SO_2 and ultrafine-sulfate plumes from the shore / harbour to the conurbation by the easterly sea breeze (Figure 3.6B).

- UFP linked to the refinery emissions exhibits the highest concentrations also in the 10 - 17 GMT, with frequent values within the range 25,000–95,000 cm^{-3} (Figure 3.6C). This daily evolution is prompted by fumigations of the SO_2 and ultrafine-sulfate plume over the north-eastern side of the city (prompted by synoptic southerly winds coupled with daylight inland sea breeze) and the photo-chemically induced nucleation (probably including organic compounds).

Figure 3.7 shows the UFP concentrations classified from the highest to the lowest levels, highlighting the contribution of each source. Table 3.2 shows the sources contribution in different ranges. At any time scale (07 - 09 GMT, 10 - 17 GMT or 24-h) vehicle exhausts result in moderate UFP concentrations, with a well defined maximum. Concentrations above such maximum are only recorded when ships and/or the oil refinery contribute. For example, the maximum contribution of

vehicle exhausts to the 24-h concentrations is of about 25,000 cm^{-3}; however, when other sources contribute (ships and refinery), N may reach 24-h values of up to 56,000cm^{-3} (Figure 3.7C and Table 3.2C). This is also observed in the 07 - 09 GMT and the 10 - 17 GMT periods.

Table 3.2. Mean concentrations and mean contribution of N1 and N2 to N during different periods and for the three types of sources: refinery (Ref.), ships, and vehicle exhausts (V.E.). Contributions higher than 20% are highlighted in bold.

	UFP (N)	**Refinery**	**Ships**	**V.E.**	**V.E. Components**	
					N1	**N2**
A) **07 - 09 GTM**	cm^{-3}	%	%	%	%	%
all data set, mean:	23,590	1.7	**21**	**77**	51	26
< 70^{th}	1,800–2,8900	1.3	12	**86**	54	33
70^{th} - 100^{th}	28,900–79,400	2.8	**42**	**55**	46	9
B) **10 - 17 GTM**	cm^{-3}	%	%	%	%	%
all data set, mean:	21,700	4.2	**22**	**74**	40	35
< 55^{th}	2,300–19,500	1.1	8	91	46	45
55^{th} - 90^{th}	19,500–46,700	1.9	**39**	**59**	34	25
95^{th} - 100^{th}	46,700–99,100	**59**	13	**28**	24	4
C) ***0-24 h***	cm^{-3}	%	%	%	%	%
all data set, mean:	16,540	4.1	19	77	47	30
< 70^{th}	2,000-20,380	2.5	12	**85**	50	35
70^{th} - 95^{th}	20,380-39,900	5.8	**37**	**57**	39	18
95^{th} - 100^{th}	39,900-56,100	**21**	**38**	**41**	35	5

A summary of key findings:

- In the morning (07 - 09 GMT), vehicle exhausts accounted for 86% of the N values < 70^{th} percentile (28900 cm^{-3}). Above this value (i.e. the range 70^{th} – 100^{th} = 28900 – 79400 cm^{-3}) ships accounted for 42% of N (Figure 3.9A and Table 2A).

- In the 10 - 17 GMT period, vehicle exhausts accounted for 91% of the N values < 55^{th} percentile (19500 cm^{-3}). Within the range 55^{th} – 90^{th} percentiles (N: 19500 – 46700 cm^{-3}) ships accounted for 39% of N (59% vehicle exhausts). The most intense UFP pollution episodes (95^{th} – 100^{th} percentiles: 46700 – 99100 cm^{-3}) were prompted by the refinery emissions, which accounted for ~60% of the concentrations of such particles in ambient air.

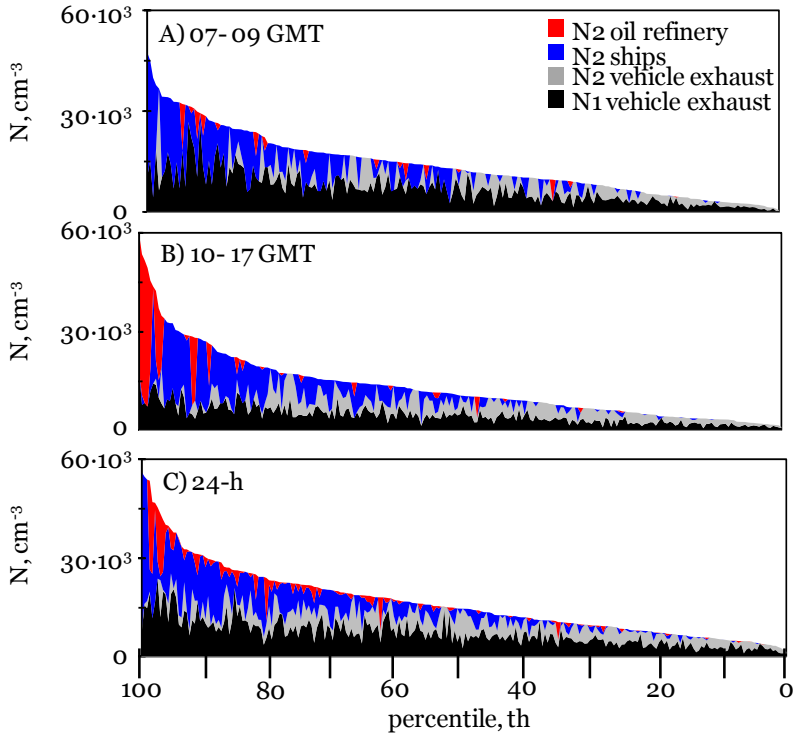

Figure 3.7 Particle number concentrations classified from the highest to the lowest concentration (100^{th} – 0.1^{th} percentile). Data averaged in three periods: 07 – 09 GMT, 10 – 17 GMT and 24-h

The very different nature of the sources of UFPs, can be observed in Figure 3.8, where the daily averaged source contribution of UFP is shown. Observe how the contribution of vehicle exhaust is almost permanent, whereas that of the ship and the refinery is more sporadic, although it results in much higher concentrations of UFPs.

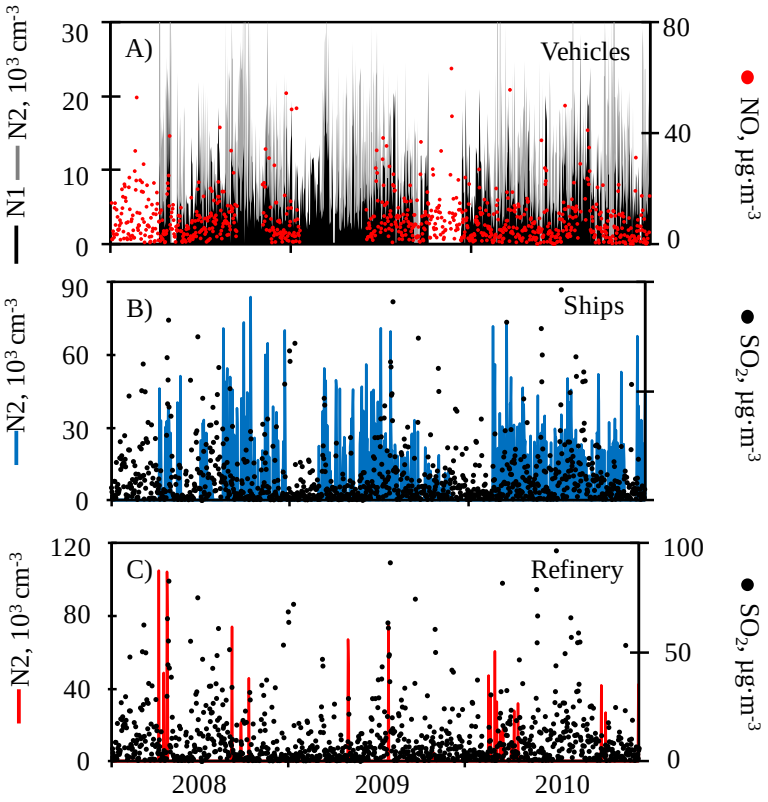

Figure 3.8 Daily averaged values of NO, SO_2 and the particle number linked to each source from 2008 to 2010. Data collected at SCO

3.5 UFPs in a port city: vehicle exhaust versus ships

As shown in the previous section, ships may significantly contribute to air quality impairment due to emissions of gaseous pollutants and UFPs. In this section, it is aimed to 'simulate' what the concentrations of UFPs would be in the northern side of Santa Cruz de Tenerife (at the North of Santos Ravine) if the oil refinery would not be present in the study area. A special attention is paid to compare the contribution of vehicle exhaust versus that of ships to UFPs. This study attempts to illustrate how ships result in urban air quality impairment in port cities. The analysis was performed using the data set generated in the previous section, after removing the contribution of the refinery to UFPs.

Figure 3.9 View of the harbour from SCO. Date: 12/11/2010 08:30 am

3.5.1 Daily inland transport of ship plumes

Figure 3.10 shows the daily evolution of the study pollutants observed in SCO after removing the contribution of the oil refinery. Fresh vehicle exhaust emissions and dilution /ventilation conditions modulate the regular variations of NO_X and BC (Figure 3.10). Concentrations of BC and NO_X reached the highest values during the morning rush hours (07 – 09 GMT) of working days. During the activation of the sea breeze (10 - 17 GMT), the ship plumes are transported into the city, and the highest concentrations of SO_2 are recorded. Particle N concentrations experience also a sharp increase (correlated with BC and NO_X) linked to fresh vehicle exhaust emissions. Because of the predominant role of ship emissions, daily evolution of pollutants does not change. The N/BC ratio evolves with SO_2, wind speed, radiation and O_3 concentrations.

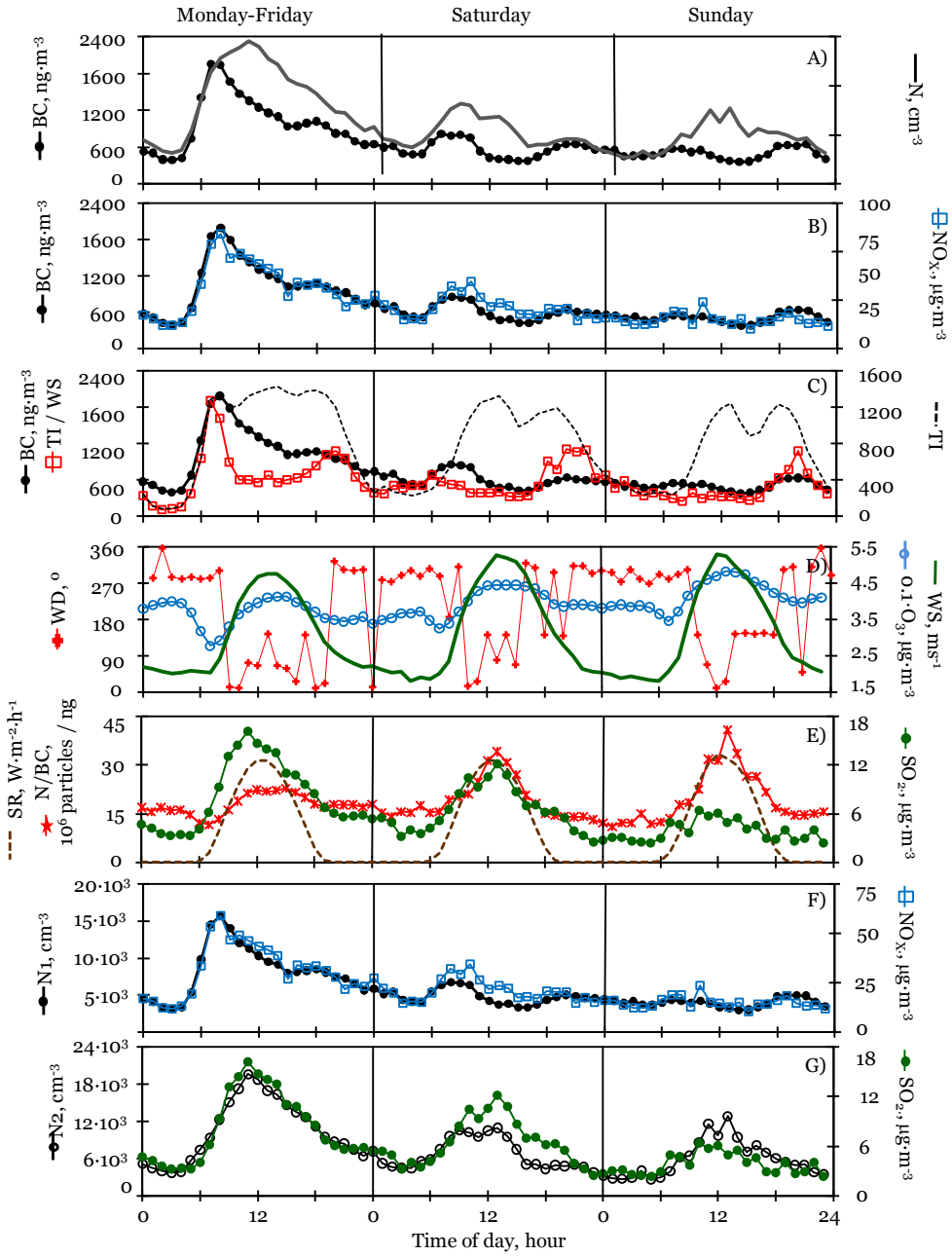

Figure 3.10 Hourly mean values of particles (N and BC) and gaseous (NO_X, SO_2 and O_3) concentrations, N/BC ratio, N1, N2, TI (number of vehicles hour^{-1}) after removing refinery events; and TI/WS ratio for working days and weekends. WS: wind speed, WD: wind direction, SR: solar radiation. Hourly data of air pollutants drive by southern winds have not been taken into account

3.5.2 Components contributing to UFPs

The relationship between N and BC concentrations in this case showed the same behaviour described in section 3.3 (Figure 3.4). Table 3.3 shows the results obtained in a PCA followed by a varimax rotations performed in two periods: 07 – 09 GMT and 10 - -17 GMT. Eigenvalues >1 and a maximum number of principal components equal to 4 were set. Only two principal components (PCs) were obtained.

Table 3.3. Mean concentrations and mean contribution of N1 and N2 to N during different periods and for the three types of sources: refinery (Ref.), ships, and vehicle exhausts (V.E.). Contributions higher than 20% are highlighted in bold.

	07 - 09 GTM		**10 - 17 GTM**	
	PC-1: vehicle exhaust	PC-2: vehicle exhaust 2	PC-1: ships	PC-2: vehicle exhaust
N1	**0.81**	0.44	**0.78**	0.35
N2	-0.05	**0.89**	**0.79**	-0.12
CO	**0.90**	0.04	0.00	**0.80**
SO_2	0.21	**0.86**	**0.90**	-0.08
NO_X	**0.83**	0.46	**0.86**	0.24
RTI / WS	**0.82**	-0.18	0.09	**0.76**
Variance %	48%	33%	46%	24%

In the morning (07 – 09 GMT):

- a PC associated with N1, CO, NO_X and road traffic intensity / wind speed is observed. This profile points to vehicle exhaust emissions of particle carbonaceous material (Arnold et al., 2006). In this study, the daily evolution of N1 was similar to that of NO_X, with a maximum value from 07 to 09 GMT on working days (Figure 3.10).
- the PC associated with N2 and SO_2 points to the formation of nucleation sulphuric acid particles (Burtscher, 2005).

In the inland sea breeze blowing (10 – 17 GMT):

- PC-1, associated with N1, N2, NO_X, and SO_2, is attributed to the inland transport of ship plumes,
- PC-2 evidence the impact of vehicle exhausts emissions (modulated by wind speed) on CO concentrations. In Figure 3.10 is shown the similar behaviour found between N2and SO_2, with high values during the inland sea breeze blowing.

3.5.3 Impact of ship emissions on UFP concentrations in urban ambient air

The daily evolution of the hourly values of N, N1, N2, SO_2, and NO_X during events in which SO_2 concentrations (in the 10 – 17 GMT period) were within the following ranges (0 – 3, 3 – 10, 10 – 30, 30 – 50, 50 - 200 $\mu g \cdot m^{-3}$, Figure 3.11) was studied.

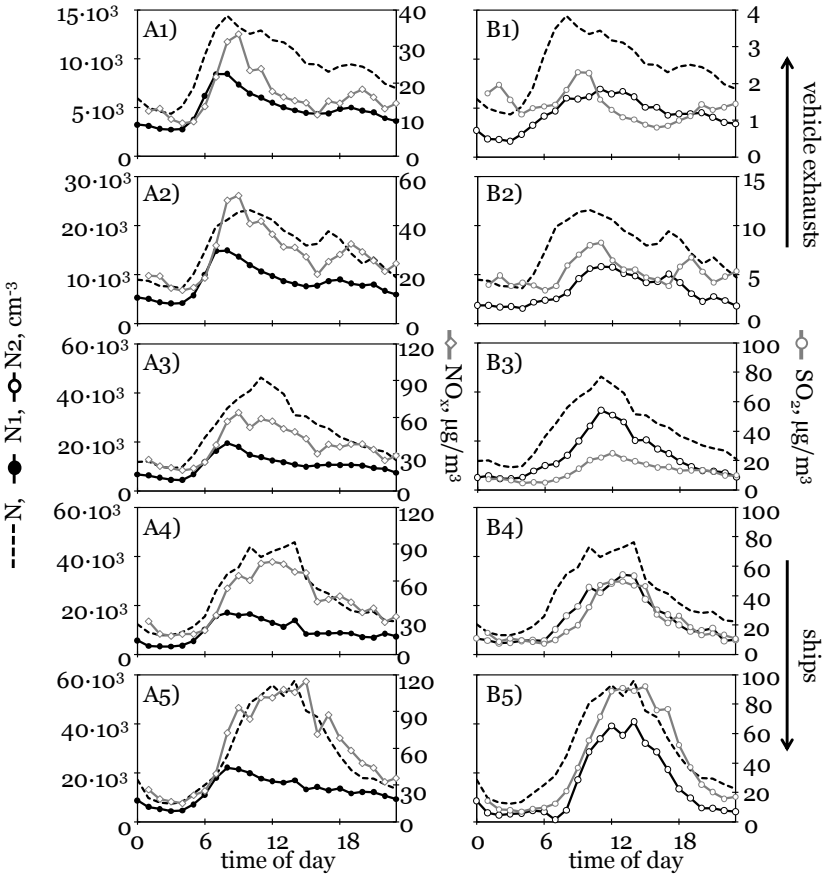

Figure 3.11 Hourly mean daily evolution of N2, N1, SO_2 and NO_X for events of different SO_2 concentration ranges (during the 10 - 17 GMT): 0 - 3 $\mu g \cdot m^{-3}$ (A1 - B1), 3 – 10 $\mu g \cdot m^{-3}$ (A2 - B2), 10 – 30 $\mu g \cdot m^{-3}$ (A3 - B3), 30 - 50 $\mu g \cdot m^{-3}$ (A4 - B4), 50 - 250 $\mu g \cdot m^{-3}$ (A5 - B5)

In this analysis several important features are observed:

→ For any SO_2 concentration range, N1 showed a maximum during the morning rush hours (Figures 3.11A1 - A5), indicating that N1 is dominated by vehicle exhaust emissions, even if ships may emit BC particles.

→ During events of SO_2 concentrations < 10 $\mu g \cdot m^{-3}$, the behaviour of SO_2, NO_X and N was predominantly influenced by vehicle exhaust emissions, with a maximum during the morning rush hours (Figures 3.11A1 - B2). At this time period, N1 showed values within the range 15 – 30 $\cdot 10^3$ cm^{-3}. The contribution of N1 and N2 to N was very close, both typically accounting for 55 - 65% of total UFP (Figures 3.12B1); and N showed an increasing trend with NO_X (Figures 3.12A1 and 3.12C1).

→ During events of SO_2 concentrations > 10 $\mu g \cdot m^{-3}$, the behaviour of SO_2, NO_X and N is predominantly influenced by ship emissions, reaching the highest concentrations during the inland sea breeze blowing time period (Figures 3.11A3 - B5).

The contribution of N1 and N2 to N concentrations were very different in events dominated by "vehicle exhaust" (low SO_2 levels) and in events dominated by "ships" (high SO_2 levels) emissions (Figures 3.12). The highest contribution of N1 to N occurred during the morning rush hours (07-09 GMT), when N was dominated by vehicle exhaust emissions and it showed values within the range 15 – 30$\cdot 10^3$ cm^{-3}. In this context the contribution of N1 and N2 to N was very close, each of them typically accounting for 55-65% of total UFP each (N). The highest contribution of N2 to N occurred during the inland sea breeze blowing period (10-17 GMT), when both, vehicle exhausts and ships emissions, may contribute to UFP concentrations. In this period mean N concentrations showed a monotonic increase throughout the SO_2 sequence showed in Figures 3.11B1 - B5 when mean ± standard deviations showed he following values: 10,900 ± 9,400, 19,250 ± 13,870, 35,400 ± 21,600, 37,160 ± 26,300 and 48,350 ± 37,500 cm^{-3}. This increase in N concentrations is prompted by an increase in the N2 contribution: 53 ± 3, 53 ± 2, 66 ± 5, 68 ± 4 and 70 ± 4%, respectively.

The strong impact of ship emissions on UFP concentrations in urban air is easily recognized in Figure 3.12. In this Figure, the hourly mean N data are classified from the highest to the lowest value, highlighting the contribution of N1 and N2 to N (Figures 3.12A1 – B2). SO_2 and NO_X concentrations (Figures 3.12A1 – B2) recorded during the morning rush hours and during the inland sea breeze blowing period are also shown. Under the predominant influence of vehicle exhaust emissions in the morning, N shows an increasing trend with NO_X (Figures 3.12A1 and 3.12C1). In this period, the contribution of N1 and N2 to N is very close, ranging between 40 and 60% each for the whole percentile range (Figure 3.12B1). Under the influence of ship emissions during the inland sea breeze blowing period, N also shows an increasing trend with SO_2 and NO_X (Figures 3.12A2, C2 and D2), and it may reach much higher concentrations than in the morning (~twice; Figure 3.12A2).

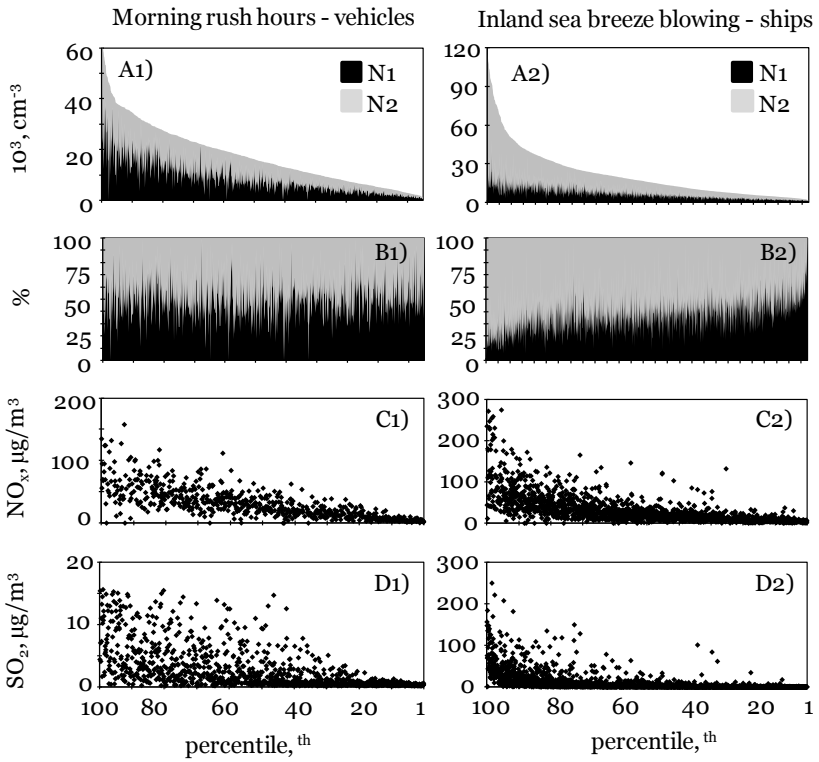

Figure 3.12 Hourly mean values of total number concentration (N = N1 + N2) classified from the highest (100th) to the lowest (1th) value. The contributions of N1 (black) and N2 (grey) to N, in absolute (cm^{-3}; A1 and A2) and relative (%; B1 and B2) concentrations, are highlighted. NO_X (C1 and C2) and SO_2 (D1 and D2) concentrations associated with the decreasing N values (from 100th to 1th) are plotted

Observe in Figure 3.13 how N1 and N2 tend to increase with NO_X and SO_2, respectively. The increase in N concentrations is prompted by an enhancement in N2, whose contribution is prompted by an enhancement in N2, whose contribution accounts for 46 ± 16%, 58 ± 14%, and 70 ± 14% for the N percentiles ranges < 20^{th,} 20 – 80th and >80th (Figure 3.12B2). These much higher N2 concentrations are prompted by the much higher SO_2 concentrations under the influence of ship plumes than vehicle exhausts (up to 10 times higher; Figure 3.12D1 and D2).

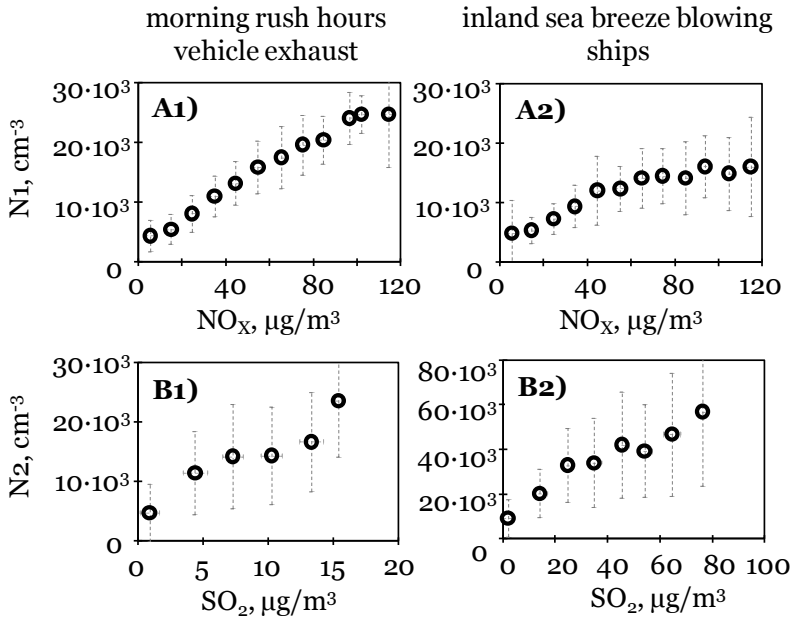

Figure 3.13 N1–vs-NO_X and N2–vs-SO_2 concentrations during the morning rush hours (07 - 09 GMT; A1 and B1, respectively) and the inland sea breeze period (10 - 17 GMT; A2 and B2, respectively). In order to reduce the variability of other influencing parameters, data of NO_X and N1 were averaged in bins of 10 µg m^{-3} of NO_X, whereas data of SO_2 and N2 were averaged in bins of 3 (B1) and 10 µg m^{-3} of SO_2 (B2). Mean ± 1 standard deviation is included in the plots

3.6 Relationship between PM_{10}, $PM_{2.5}$, BC and UFPs

Studies performed during the last decades related the exposure to urban ambient PM_{10} and $PM_{2.5}$ (mass concentrations of particulate matter – PM < 10 μm and <2.5 μm aerodynamic diameter, respectively) with an increased risk to suffer of respiratory and cardiovascular diseases (Dockery and Pope, 1996). As a result, PM_{10} and $PM_{2.5}$ are currently used as urban air quality reference metrics. More recently researches have highlighted the effects on human health of some component of PM such as UFPs (e.g., Peters et al. 1997; Highwood and Kinnersley, 2006). These studies have derived in an open debate on whether additional (to PM_{10} and $PM_{2.5}$) metrics related to ambient air particle concentrations should be monitored to improve human health protection. Under this debate, several studies focused on characterising aerosol physical properties have been carried out, since the PM working group of the European commissions recognised that more studies are necessary on other metrics of the aerosol concentration in order to consider a possible regulation of metrics complementary to PM_{10} and $PM_{2.5}$ (Second Position Paper on PM, 2004). Thus, much more attention is being paid to UFPs in cities lately.

A first drawback is that those processes affecting PM_1, $PM_{2.5}$ are $PM_{2.5-10}$ are significantly different from those affecting the UFP number concentration. Accumulation mode particles (0.1 – 1 μm) are the most important contributors to PM_1 and $PM_{2.5}$, even if they account for a marginal fraction of the number concentration (10 – 15%). Although some primary emissions may contribute (e.g. soot due to heavy diesel engines or mineral dust), most of the accumulation mode mass is due to gas to particle conversion processes onto pre-existing particles and to UFP growth (Cabada et al., 2004). In contrast, coarse particles (> 1 μm) are mainly made up of mineral dust, abrasion products from tyre and brake wear, and sea salt at coastal sites. Ultrafine, accumulation and coarse particles also differ in life time. Coarse particles are relatively rapidly removed through sedimentation, whereas UFPs rapidly grow through condensation and coagulation. In contrast, accumulation mode particles exhibit a long residence time (from days to a few weeks) and consequently, they may significantly contribute to the urban and regional aerosol background.

In order to understand the processes affecting the relationship between metrics representative of the particle concentrations in urban air, the relationship between PM_{10} and number concentration has been studied in several cities (Ruuskannen et al., 2001; Ketzel et al., 2004, Mönkönen et al., 2004; Harrison and Jones, 2005; Rodríguez et al., 2007; Puustinen et al., 2007). However, understanding such relationship is not an easy task. For example, long range transport of (aged) aerosol may exhibit a much higher influence on PM_{10} and $PM_{2.5}$ than in number concentrations (Ketzel et al., 2004). On the other hand, processes contributing to the decrease in PM_{10} and / or $PM_{2.5}$ (e.g. meteorology) may enhance the new particle formation rates owing to the fact that reductions in PM_X may decrease the surface area of acting as a condensation sink for the aerosol gaseous precursors (Burtscher, 2005, Hamed et al., 2007). In a recent study, Hoek et al.

(2008) observed that in urban areas the number of concentration exhibits a much higher spatial variability than PM2.5, soot and sulphate - aerosol.

This study was developed with the instrumentation and during the period described in data set -1 (section 2.5, chapter 2).

3.6.1 Mean daily evolution of aerosols

Figure 3.14 displays the regular daily evolution of the road traffic intensity and the particle and some gaseous pollutant concentrations at SCO, TC and GL urban air quality stations. At SCO coastal site, particle (PM_X, BC and N_3) and CO concentrations exhibited a maximum during the morning rush hours of working days , and a subsequent decrease (09:00 – 19:00) associated with the easterly entry of marine air (Figures 3.14A - F). At night, a smooth increase in the PM_X concentrations associated with slight westerly winds bringing air masses from the city centre was observed at SCO.

At TC and GL city centre sites, after the maximum recorded in PM_X and NO_X concentrations recorded during the morning rush hours, a decrease in the PM_X concentrations such as that described above at SCO (09:00 – 19:00) was not observed. However, PM_{10} and $PM_{2.5}$ at TC and GL showed an increasing trend until 21:00 (local time). This contrasting behaviour between the PM_X concentrations at the coastal (SCO) and the city centre (TC and GL) sites is a consequence of the easterly inland sea breeze blowing during daylight, which prompts the entry of “clean” marine air masses along the coast and favours the inland transport of the pollutants (emitted in the eastern part of the city) to the city centre. This is one of the reasons because PM_{10} concentrations are much lower at the coastal SCO than at the TC and GL city centre sites. In fact, this daylight breeze results in the inland transport of the (refinery) SO_2 plumes, giving rise to higher concentrations during daylight than at night at the TC and GL city centre sites (Figures 3.14G - I).

At SCO, N_3 and BC concentrations also exhibited a well defined daily cycle (Figures 3.14A - C). During working days, N_3 and BC presented a maximum during the morning rush hours. The morning maximum in the vehicles$\cdot h^{-1}$ / wind speed ratio indicates that the morning maximum in the particle concentrations is favoured by the coupled effect of an increase in the road traffic intensity and low wind speed in the morning (owing to the fact that the inland sea breeze has not yet started blowing). Observe that the daily evolution of N_3 and BC during weekdays is different from that recorded at weekends because of the change in road traffic patterns.

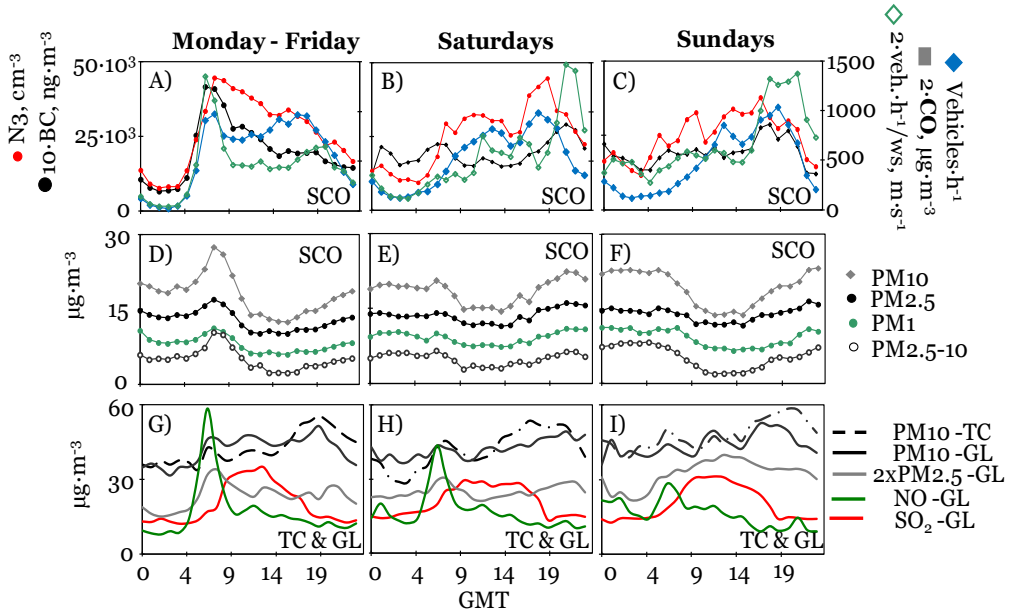

Figure 3.14 Mean daily cycles. Hourly averaged concentrations of CO and the particle N_3, BC and PM_X concentrations at SCO (A – C) and of PM_{10}, $PM_{2.5}$ and gaseous pollutants at the Tome Cano (TC) and Gladiolos (GL) city centre sites (G – I) during weekdays, Saturdays and Sundays

3.6.2 Processes affecting urban coastal aerosols concentrations

The relationship between road traffic intensity, meteorology and particle concentration at SCO (coastal urban background site) was examined using Principal Component Analysis (PCA) followed by a varimax rotation. This analysis was performed at several times of the day: morning (07:00 – 09:00), central daylight (11:00 – 17:00) and night (00:00 – 05:00). Three principal components, accounting for 81, 66 and 72% of the variance for the three daytime periods selected, were found (Table 3.4):

- PC-1 is positively correlated with PM_X and BC and negatively correlated with wind speed. The fact that PC-1 does not exhibit a significant correlation with road traffic intensity indicates that fresh road traffic emissions do not exhibit a major influence on PM_X variance. Furthermore, the negative factor loading of wind speed indicates that this component accounts for the influence on the aerosol mass (BC and PM_X), of the dilution and the air mass renovation prompted by wind blowing over the study city.

- PC-2 is positively correlated with road traffic intensity, BC and N_3. This component represents the influence of fresh vehicle exhaust emissions on the particle concentration.

○ PC-3 is present during daylight (i.e. morning rush hours 07 – 09 GMT and central daylight period 10 – 17 GMT). The positive correlation of the N_3/BC ratio and solar radiation intensity suggests that nucleation of photo-oxidized vapours contributes to increasing the above ratio by enhancing new particle formation in ambient air. Further details are provided below.

Table 3.4 Factor loading of the PCA performed with data from selected periods

	Morning rush hours 07-09 GMT			*Central daylight 10 – 17 GMT*			*Night 00 – 05 GMT*	
	PC - 1	**PC - 2**	**PC - 3**	**PC - 1**	**PC - 2**	**PC - 3**	**PC - 1**	**PC - 2**
Vehicles·h^{-1}	-0.11	**0.89**	0.14	0.29	**0.51**	-0.04	-0.01	**0.85**
BC	**0.56**	**0.70**	-0.33	0.39	**0.82**	-0.22	**0.75**	0.59
N_3	0.17	**0.90**	-0.07	0.32	**0.81**	0.28	0.30	**0.80**
N_3/BC	**-0.59**	-0.05	**0.61**	-0.23	-0.18	**0.77**	**-0.77**	-0.04
PM_1	**0.95**	0.06	-0.07	**0.86**	0.27	-0.08	**0.86**	0.36
$PM_{2.5}$	**0.96**	0.04	-0.08	**0.89**	0.21	-0.05	**0.86**	0.37
$PM_{2.5\text{-}10}$	**0.88**	0.16	-0.08	**0.52**	-0.16	**0.55**	**0.85**	0.46
wind speed	-0.42	-0.15	**0.81**	**-0.63**	0.07	0.12	-0.49	-0.09
Radiation	0.24	0.03	**0.73**	-0.08	0.20	**0.72**		
variance, %	38%	24%	19%	29%	20%	17%	46%	26%

3.6.3 Influence of wind speed

The PCA indicates that wind speed exerts: (1) a major influence on PM_X, (2) a moderate influence on BC and (3) a relatively low influence on N_3. In fact, wind speed exhibited Pearson's correlation coefficients (r) of -0.50, -0.44, -0.41, -0.33 and 0.0 with $PM_{2.5\text{-}10}$, $PM_{2.5}$, PM_1, BC and N, respectively (values calculated using 3,092 10-min observations; Figure 3.15). The fact that high N_3 concentrations (> $45{\cdot}10^3$ cm^{-3}) may still be recorded under high wind speed conditions (> 5 ms^{-1}), may be accounted for new particle formation processes.

Charron and Harrison (2003) found that increases in wind speed produced much higher decreases in the concentration of accumulation mode particles (0.1 – 1 μm) than in the concentration of nucleation mode particles (< 30 nm). They argued that this was caused by the fact that "clean atmospheres" (favoured by high wind speeds) tend to favour new particle formation owing to the low aerosol surface area (mostly occurring in the accumulation mode) available for condensation of the aerosol gaseous precursors. They concluded that the lack of correlation between wind speed and number concentration is a feature of new particle formation. Similar results were found by Rodríguez et al. (2005) at a rural site influenced by nearby town emissions in Northern Italy. The analysis of the N_3 / BC ratios shown below supports this involvement of the new particle formation processes during the periods of high wind speed (typically associated with inland sea breeze blowing).

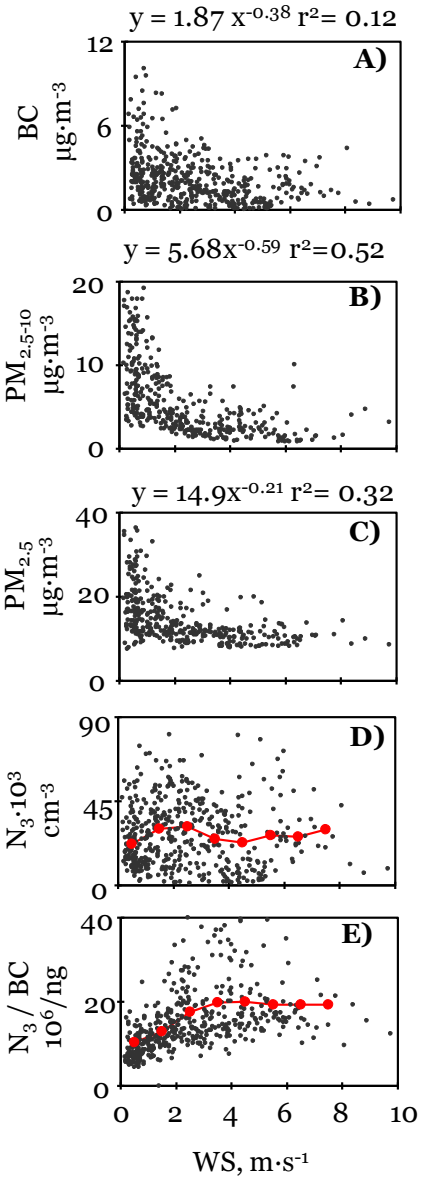

Figure 3.15 Concentration of particles (A – D) and N_3/BC ratio (E) versus wind speed at the SCO site. Red dots and line in plots D and E represent mean N_3 and N_3/BC values for each 1 m·s^{-1} bin

3.6.4 Quantification of the impact of road traffic emissions

The impact of fresh road traffic emissions on the particle concentration was quantified at several times of the day. Figures 3.16A1 – F1 present the mean BC, N_3 and PM_X concentrations measured for each 100 vehicles·h^{-1} bin during the morning (07:00 – 09:00), the central part of the day (11:00 – 17:00) and at night (00:00 - 05:00). The use of 100 vehicles·h^{-1} bins smoothes the variability in the concentrations due to other influencing parameters (mainly meteorology). The concentrations of BC and N_3 tend to increase when road traffic intensity (Figures 3.16A1 and B1). This behaviour is not observed for $PM_{2.5}$ and PM_1 (Figures 3.16C1 and D1). During the morning, the $PM_{2.5-10}$ concentrations also tend to increase when road traffic intensity increases, this being most probably due to road dust re-suspension (Figure 3.16E1).

The much lower "direct influence" of the road traffic emissions in $PM_{2.5}$ and PM_1 (Figures 3.16C1 and D1) than in N_3 and BC (Figures 3.16A1 and B1) may account for the coming into forced of the European standards EURO 1 - 5 (progressively since 1992) for vehicle exhausts emissions. Because EURO 1 - 4 have been established in terms of particle mass (g·Km^{-1}), they have decreased the emissions of the accumulation (0.1 – 1 μm) and coarse (> 1 μm) mode particles, which are the main contributors to PM_X. In contrast, N_3 and BC tend to increase when road traffic intensity increases. This is due to the fact that vehicle exhaust mostly emits ultrafine and soot particles and these are the main contributors to N_3 and BC (Burtscher, 2005; Harris and Maricq, 2001; Rose et al., 2006). Thus, in the recently EURO 5b (September 2005) emission standards for UFPs based on particle total number concentrations are scheduled.

Although BC concentrations tend to increase with road traffic intensity, different BC concentrations are observed for a given number of vehicles·h^{-1} bin at different times of the day (Figure 3.16A1). For example, a road traffic intensity within the range of 1,100 – 1,200 vehicles·h-1 is associated with 3.7 μg·m^{-3} during the 07:00 – 09:00 period, and with 1.5 μg·m^{-3} during the 11:00 – 17:00 period. The lower BC concentrations during the 11:00 – 17:00 period are a consequence of the higher wind speeds during that period of daylight (because of the inland breeze blowing). For this a normalization of the road traffic intensity data by dividing them by wind speed has been done (Figure 3.16A3). It can be observed how BC concentrations tend to increase in a more regular way (monotonic growth) when increasing the vehicles·h^{-1} / wind speed ratio that when increasing the vehicles·h^{-1} ratio (Figures 3.16A1 and A3). The results show how a increase in 200 vehicles·h^{-1}·m^{-1}·s are associated with BC increases of about 0.50 ± 0.29 μg·m^{-3} (on average) at any time of the day.

This analysis of particle concentration versus vehicles·h^{-1} / wind speed was also applied to the PM_X and N_3 concentrations (Figures 3.16A3 - F3). The most important results are:

(1) N_3 also exhibits an increasing trend of 3250 ± 2395 cm^{-3} every 200 vehicles·h^{-1}·m^{-1}·s during the 07 – 09 GMT period and of about 6523 ± 1437 cm^{-3} every 200 vehicles·h^{-1}·m^{-1}·s in the 10 – 17 GMT period (Figure 3.16B3). These higher values in the 11:00 – 17:00 period in

comparison with the 07:00 – 09:00 period suggest an enhancement in the particle formation at noon and during the afternoon. This interpretation is supported by the results shown in the following section.

(2) $PM_{2.5}$ and PM_1 do not exhibit a strong association with the vehicles·h^{-1} / wind speed ratio (as that described for BC and N_3).

(3) $PM_{2.5\text{-}10}$ exhibits a clearly increasing trend of about 1.20 ± 0.90 μg $PM_{2.5\text{-}10}$·m^{-3} every 200 vehcicles·h^{-1} during the morning rush hours (07:00 – 09:00), most probably due to road dust re-suspension. The weaker association observed during the 11:00 – 17:00 period (Figure 3.16E3) is probably due to the influence of sea salt transported inland during daylight.

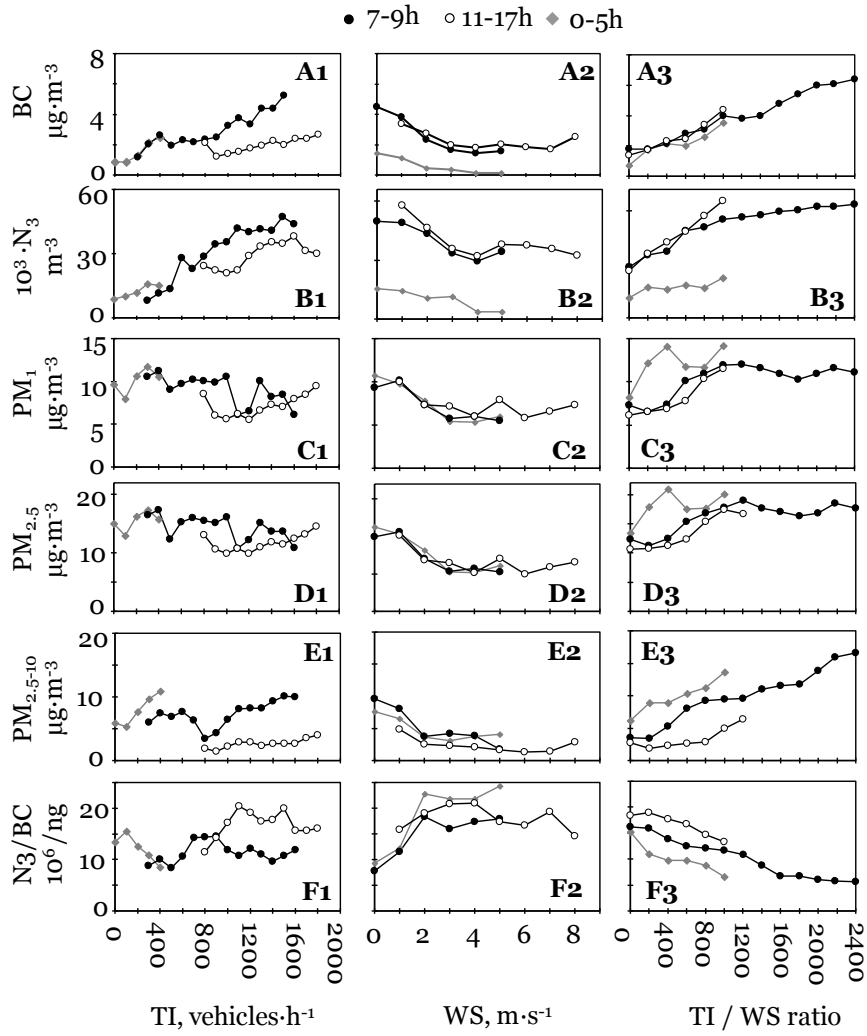

Figure 3.16 Particle concentration and N_3/BC ratio averaged for each "100 vehicles·h^{-1}" bin (A1 – F1), for each "1 m·s^{-1}" bin (A2 – F2) and for each "200 vehicles·h^{-1}" bin (A3 – F3)

3.6.5 The number-to-black carbon ratios

The relationship between N_3 and BC concentrations at SCO site has been used to identify periods of enhancement of new particle formation rates, which would lead to an increase in the N_3 / BC ratio. At SCO, N_3 and BC exhibited a significant correlation because of the vehicle exhaust emissions: r = +0.70 during the whole measurement campaign (based on 3,092 10 – min average data).

All the points on the plot of the N_3 versus BC data appear comprised between two well defined borders at each time of the day, that again manifest the minimum contribution of the fresh vehicle emissions to particle number concentration (minimum slope, S_{min}) and the enhancement of the new particle formation during daylight (maximum slope, S_{max}, higher during the 11:00 - .17:00 period).

In Figure 3.17 is can be observed how the N_3 / BC ratio exhibits a daily evolution with a maximum during daylight, when the highest temperature and the highest wind speed are measured. This result is in opposition to those founds in other studies, where enhancement of new particle formation N_3 / BC ratios seen to be favoured by low ambient temperature (e.g. Olivares et al., 2007) and / or low wind speed leading to lees dilution (Casati et al., 2007). At SCO the N_3 / BC ratio reaches the hghest values during the noon and afternoon period when:

(1) Solar radiation intensity reaches the highest values. In fact, in the PCA discussed above, it was shown how PC-3 is correlated with the N_3 / BC ratio and the solar radiation (PC-3 in Table 3.3),

(2) PM_1 and $PM_{2.5}$ concentrations (where most of the aerosol surface area is comprised) are minima (3.14 and 3.17). The fact that the N_3 / BC ratio exhibited a much higher anti – correlation with PM1 and PM2.5 than with PM2.5-10 during the 11:00 – 17:00 period (plot not shown), suggest a more active role of the accumulation mode particles (which typically accounts for most of the aerosol surface area) as condensation sink for the aerosol gaseous precursors,

(3) It is positively correlated with wind speed for wind speed values between 0 and 4 $m \cdot s^{-1}$ (Figures 3.15E and 3.16F3).

These features suggest that, in addition to the new particle formation during the dilution and cooling of the vehicle exhaust, there is a contribution to N_3 concentrations due to new particle formation in ambient air described above fit very well with those of the new particle formation in ambient air, such is has been described in the previous sections and the works of Boy and Kulmala (2002), Rodríguez et al. (2005), Hamed et al. (2007) and Fernández-Camacho et al. (2010). The behaviour observed at SCO site indicates that the increase in wind speed (due to the inland sea

breeze blowing), results in a decrease in the aerosol surface area concentrations. This would favour nucleation, rather than condensation onto pre-existing particles, for those aerosol gaseous precursors formed by photo-oxidation processes. Observed in Figure 3.17 how the daily variation of the N_3 / BC ratio is much better modulated by the daily evolution of the inverse of the PM_1 (which typically comprises most of the aerosol surface) than by the daily evolution of the $PM_{2.5-10}$. An example of one of these events (8th April 2006) is shown in Figure 3.18: observe the correlated increases in the N_3 / BC ratio and in solar radiation intensity from 10:00 to 16:00. This contribution to N_3 due to nucleation in ambient air during the central part o the daylight accounts for: (1) the faster decrease in the BC than in the N_3 concentrations after the morning rush hours (Figure 3.14A), and (2) the higher increase in N_3 concentrations for every 200 vehicles·h^{-1}·/ m·s^{-1} bin during the 11:00 – 17:00 period than during the 07:00 – 09:00 period (described above; 3,250 cm^{-3} during the 07:00 – 09:00 and about 6,523 cm^{-3} during the 11:00 – 17:00 periods).

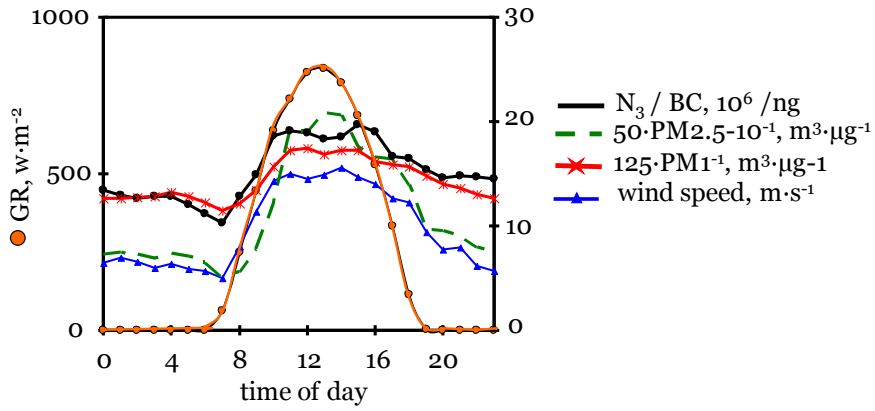

Figure 3.17 Daily mean cycle (hourly averaged values) of the global radiation, wind speed, the N_3/BC ratio, and the inverse of the PM_1 (PM_1^{-1}) and $PM_{2.5-10}$ ($PM_{2.5-10}^{-1}$) concentrations

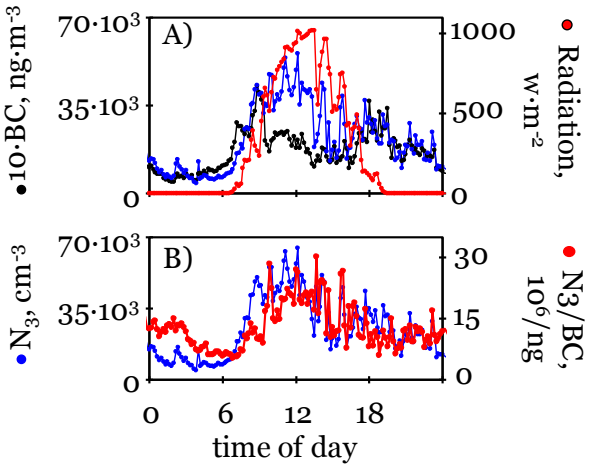

Figure 3.18 10 - min averaged values of the solar radiation, N_3 / BC ratio, black carbon (BC) and number N_3 concentrations at SCO during 8th April 2006

3.6.6 Day – to - day particle events

Figure 3.19 shows the hourly BC, N_3 and PM_X concentrations at SCO and the road traffic intensity during the measuring period. Figure 3.20 shows the median of the BC, N_3 and PM_X concentrations for each wind direction for the 07:00 – 09:00, 11:00 – 17:00 and 00:00 – 05:00 time periods during the whole campaign. These data (Figures 3.19 and 3.20) clearly illustrate how N_3, BC and PM_X concentrations are influence in different ways by sea breeze circulation, vehicle exhaust emissions and ageing processes given that:

1. High BC and N_3 concentrations are recorded during the morning rush hours due to fresh vehicle exhaust emissions (07 – 09 GMT; Figs. 3.19A - B and 3.20A - B), the highest being BC and N_3 concentrations registered when wind blows from the city centre (Southwest; Figure 3.20A1) or from the coastal Anaga Avenue (East; Figure 3.19A1).

2. High N_3 concentrations (associated with high N_3/BC ratios) during the central part of daylight (10 – 17 GMT) are associated with easterly winds (inland breeze; Figure 3.20B2) due to the above described new particle formation in ambient air. Examples of these events occurred during the periods 22 -24 and 28 – 31 March 2006, when N_3 / BC ratios of 15 – $25{\cdot}10^6$ particles $ngBC^{-1}$ and $<10{\cdot}10^6$ particles were recorded during daylight and at night, respectively (Figure 3.19; N_3 / BC ratios not shown); and

3. The highest PM_1 and $PM_{2.5}$ and the lowest N_3 and BC concentrations are recorded at night when the wind blows from the city centre, bringing aged particulate pollutants to the shore owing to the seaward airflow associated with nocturnal breeze circulation (Figures 3.20C3 -

D3). See examples of these PM_1 and $PM_{2.5}$ nocturnal events associated with the outflows from the city centre during the periods 23–26 March and 30 March–2 April 2006 (Figure 3.19).

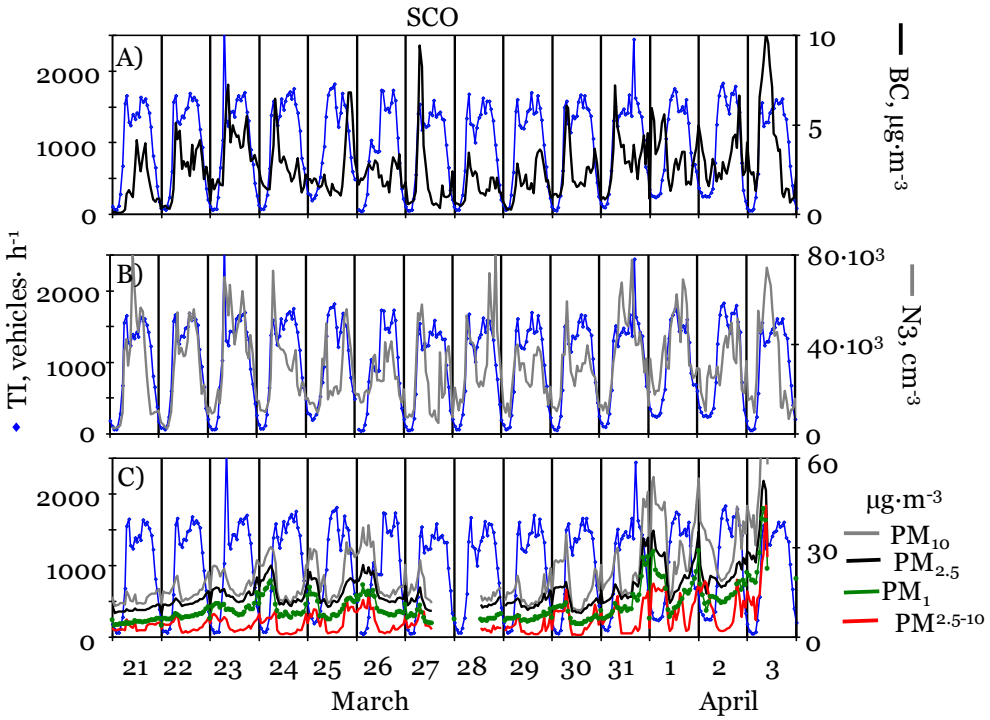

Figure 3.19 Hourly mean values of road traffic intensity at the coastal Anaga Avenue (vehicles h^{-1}) and of the particle BC, N_3 and PM_x concentrations at the SCO site from March 21st to April 3rd 2006

BC and N_3 tend to exhibit patterns correlated with those of the road traffic intensity, evidencing the high influence of "fresh emissions" (Figure 3.19). In contrast, PM_1 and $PM_{2.5}$ tend to exhibit high concentrations at night, when road traffic emissions are not significant. The nocturnal conditions (e.g. decrease in the boundary layer depth resulting in an increase of the concentrations of aerosols and its gaseous precursors, or decrease in temperature decreasing the equilibrium vapour pressure and consequently favouring condensation) favour particle growth by coagulation and condensation processes and this contributes to the increase in the particle mass in the accumulation mode and consequently to the increase in PM_1 and $PM_{2.5}$ concentrations.

Observed in Figure 3.21 how $PM_{2.5}$ experiences low spatial variations across the city (slope and intercept of about 1.0). In contrast, PM_{10} experiences a much higher spatial variability across the city because of the local contribution of coarse particles in the city centre (~20 $\mu g \cdot m^{-3}$): see the high value of the intercept (18 - 21 $\mu g \cdot m^{-3}$) of the scatter plots "PM_{10}: GL versus SCO (Figure 3.21B) and

the TC versus SCO (Figure 3.21C)" and the "$PM_{2.5-10}$: GL versus SCO (Figure 3.21D)". This supports the idea that $PM_{2.5}$ is mostly representative of the urban background (accumulation mode aged aerosols formed by condensation / reaction of gases onto pre – existing particles) whereas $PM_{2.5-10}$ is mostly affected by local (street) emissions.

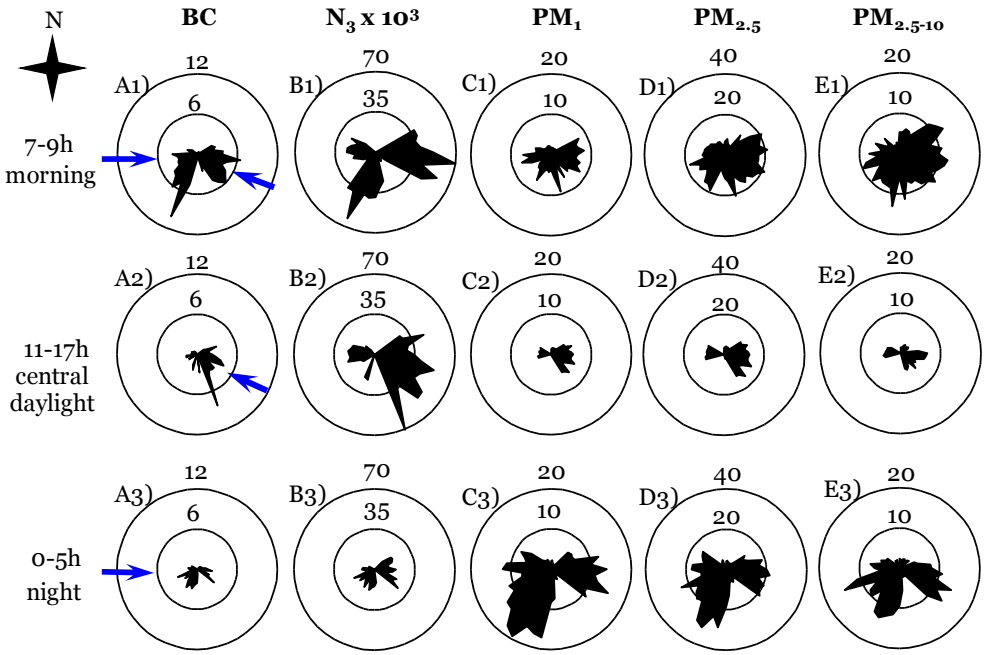

Figure 3.20 Hourly mean concentrations of the particle BC, N_3 and PMx for each wind direction at several times of the day at the SCO site

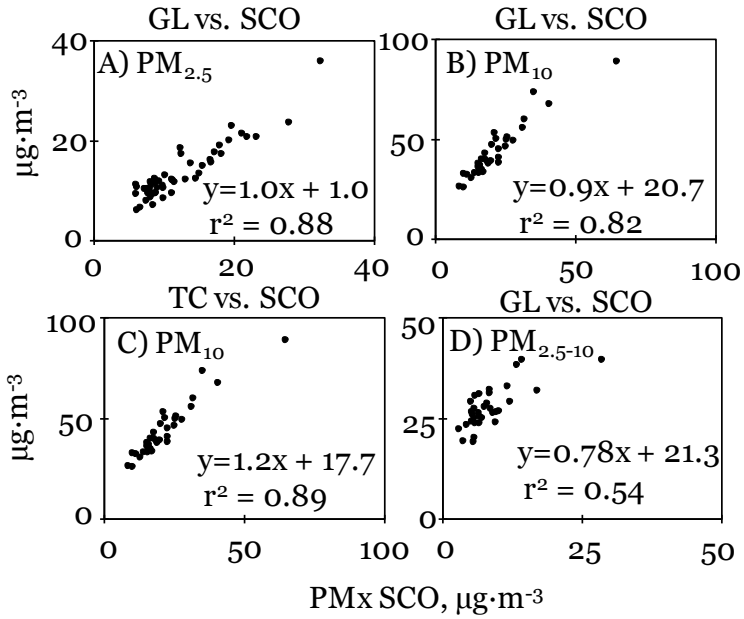

Figure 3.21 Daily mean concentrations of the $PM_{2.5}$, $PM_{2.5-10}$ and PM_{10} at city centre sites (TC and GL) versus at SCO coastal urban background

3.7 Summary and Conclusions

The impact of vehicle exhausts, ships, and crude oil refinery emissions on the UFP concentrations in ambient air was studied using two years of hourly concentration data of number of particles coarser than 2.5 nm (N), black carbon (BC) and gaseous pollutants (NO, NO_2, SO_2, CO and O_3). N was split into two components, N = N1 + N2. Component N1 accounts for the emissions of light absorbing carbonaceous material and some compounds that nucleate immediately after the emission. It is strongly linked to the vehicle exhaust emissions. N2 is dominated by SO_2 concentrations.

According to Kulmala et al. (2004a), new particle formation rates in a coastal environment as high as those in industrial plumes are frequently recorded. This could, in part, be due to the fact that some of the factors which may favour nucleation are present in the coastal environment: (i) enough high relative humidity to favour binary H_2O–H_2SO_4 nucleation (Easter and Peter, 1994; Olivares et al., 2007), (ii) relatively clean air conditions (low aerosol surface area concentration) due to the marine air entries) and (iii) the mixing of two air parcels with different temperature and different relative humidities (Nilsson and Kulmala, 1998).

In this study has been observed that the concentration of UFP linked to vehicle exhausts reached a maximum in the morning (07–09 GMT), with typical values (25^{th}–75^{th} percentiles) in the range 5,000–25,000 cm^{-3}. UFP linked to ships (15,000–45,000 cm^{-3}) and the refinery (25,000–95,000 cm^{-3}) exhibited a maximum in the 10–17 GMT period. When UFP (24-h mean) were present in concentrations within the range 2,000–20,000 cm^{-3} (0.1^{th}-70^{th} percentile), vehicle exhausts were the predominant source, accounting for 85% of the observed UFP. Higher concentrations (i.e. >70^{th} up to 56,000 cm^{-3}, 24-h mean) were prompted by the contributions of ship and refinery emissions. The highest UFP concentrations were recorded in pollution events during 10-17 GMT, and prompted by the refinery and ships and the influence of the inland sea breeze blowing. Ship emissions accounted for 39% of N when their concentrations were within the range 55^{th} – 90^{th} percentiles (19,500–46,700 cm^{-3}), whereas the refinery accounted for 60% of N when their concentrations were within the range 95^{th} – 100^{th} percentiles (46,700–99,100 cm^{-3}). Below the 55^{th} percentile (19,500 cm^{-3}), vehicle exhausts accounted for 91% of UFPs.

This study has shown that emissions of SO_2 (and probably some key gaseous hydrocarbons) in large combustion installations (power plants, industry, ships, etc...) result in high concentrations of UFPs in downwind urban areas. UFP concentrations above the background levels due to vehicle exhausts (10,000-2,000 cm^{-3}) are prompted by these emissions, which may result in up to 56,000 cm_{-3} (24-h average). Because of the variety of hydrocarbons and SO_2 emitted in crude oil refineries, this source has a great potential to result in very high concentrations of UFPs.

It is also important to highlight that the inland sea breeze circulation and road traffic emissions, also exert a great, but differentiated, influence on the particle black carbon (BC), number (N_3, >3 nm) and PMx (PM_1, $PM_{2.5}$ and $PM_{2.5–10}$) concentrations. Whereas BC and N_3 concentrations are greatly influenced by fresh vehicle exhaust emissions, PM_X (especially PM_1 and $PM_{2.5}$) reaches the highest values at night due to the seaward transport of aged particulate pollutants to the shore, and the lowest values during daylight due to the inland entry of clean marine air.

Chapter 4

Processes affecting the concentrations of reactive gases at Izaña GAW Station

Understating the long term evolution of reactive gases in the free troposphere is a crucial task for assessing how human activities are influencing on climate (IPCC, 2007; Laj, 2009). The long term evolution of reactive gases is being studied in some specific regions, e.g. mountain sites of Europe (Gilge et al., 2010). There is a clear lack of knowledge on how the concentrations of reactive gases are evolving in other regions. The reactive gases program at Izaña GAW station was complemented within the frame of this work by adding measurements of SO_2 and NO_X since 2007. Measurements of other gases started earlier, CO in 2001 and O_3 in 1987.

In this chapter, data of reactive gases collected at Izaña GAW station between 2007 and 2010 are analysed. The objective is to identify the processes that contribute to the concentrations of reactive gases at Izaña Observatory.

4.1 Insular versus background contribution

4.1.1. Daily cycle

Figure 4.1 shows a topographic map of Tenerife, highlighting the location of Izaña, el Teide National Park and the main motorways and power plants/refinery in the Island. In order to investigate how the transport of air from the boundary layer contributes to the concentrations of reactive gases, the following analysis were performed:

- study of the location of the temperature inversion (Figure 4.2)
- determination of the daily evolution of the concentrations of water vapour and reactive gases, segregating weekdays and weekends (Figure 4.3)
- calculation of the daylight / nighttimes ratios and of the daylight increase fraction (Figure 4.4)
- determination of the variability in the concentrations of reactive gases with wind direction (Figure 4.5)

Mean levels of the study pollutants during the period 2007 – 2010 are shown in Table 4.1.

Table 4.1 Mean levels of reactive gases and data availability in the period 2007-2010

Pollutant	mean ± std	% hourly data
CO	103 ± 24 ppb	91.4 %
NO	43 ± 93 ppt	87.3 %
NO_2	39 ± 64 ppt	67.3 %
NO_X	77 ± 849 ppt	67.5 %
SO_2	66 ± 161 ppt	97.2 %
O_3	46 ± 11 ppb	96.0 %

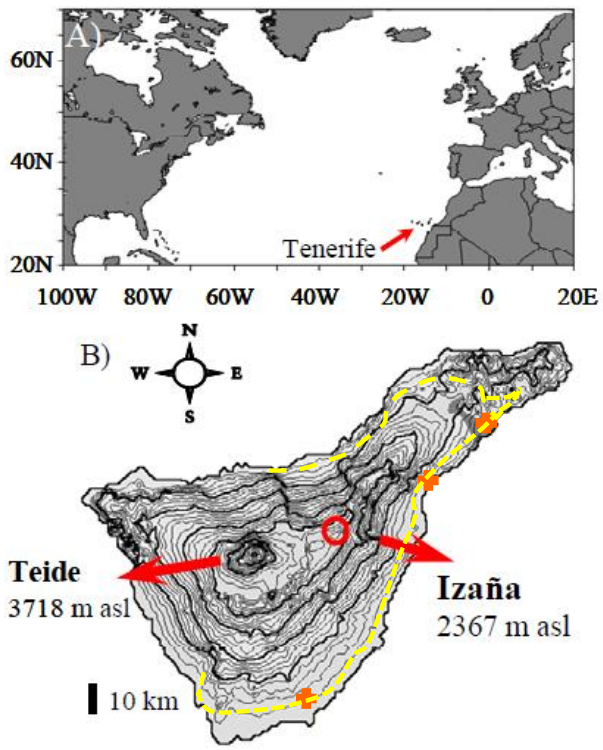

Figure 4.1 A) Map showing the location of Tenerife at the North Atlantic Ocean. B) Map of Tenerife, indicating the location of IZO station, power plants (orange crosses) and the highway. Map B includes 100 and 500 m height lines (grey and black lines respectively)

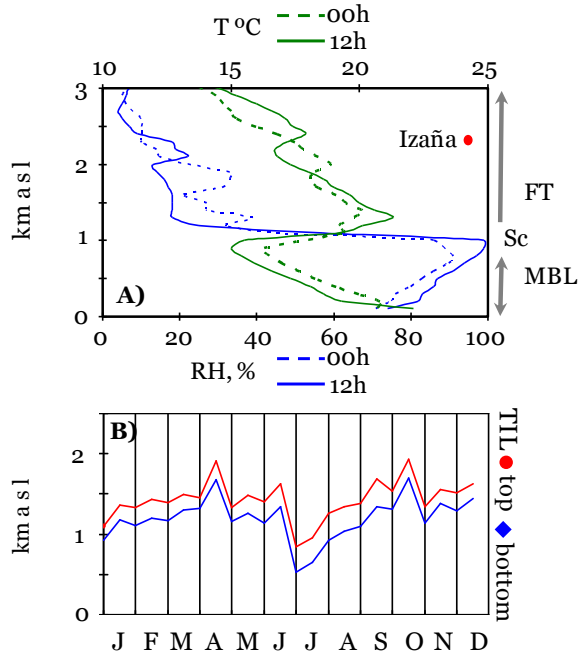

Figure 4.2 A) Vertical profile of temperature and relative humidity at Tenerife, highlighting the location of Izaña, the marine boundary layer (MBL), top and bottom of the temperature inversion layer, stratocumulus layer (Sc) and the free troposphere (FT). B) Monthly average values of the location of the top and the bottom of the temperature inversion layer at 12:00 GMT and 00:00 GMT

At Izaña mountain site, air tends to move upward during daylight and downward at night. For this reason, concentration of water vapour tends to be higher during daylight than at night (Figure 4.3B). The diurnal upward flows that prompt this cycle are caused by two main processes:

- Thermally driven vertical growth of the marine boundary layer (MBL) depth, caused by the expansion of the MBL volume. Owing to this, the top and the bottom of the temperature inversion layer (TIL) are located at higher altitudes during daylight (1,200 and 1,700 m.a.s.l., respectively) than at night (900 and 1,300 m.a.s.l., respectively; Figure 4.2). These vertical movements are also observed in the location of the stratocumulus layer (Font, 1956), and are also shown in the soundings launched over the ocean (Figure 4.2). This data set indicates that vertical growth of the MBL depth is not linked to vertical motions of air over the island, but a general behaviour over the ocean.

- Buoyant air flows caused by the heating of the air located just above the terrain of the Island. The predominance of WNW winds (Figure 4.7 C) indicates that this upward transport of air is mostly linked to the development of buoyant flows on the northern slope of the Island.

Mechanically forced upslope winds may occur under strong wind synoptic conditions, however, these may not account for the observed regular daily evolution of the water vapour at Izaña. Upward winds linked to mechanically forced and buoyant airflows have also been observed at the Pico Observatory in the Azores (Kleiss et al., 2007).

The prevailing subsidence conditions (linked to the North Atlantic anticyclone) result in downward transport of free troposphere air at night, whereas the development of the described upward flows during daylight results in the daily cycles of water vapour observed at Izaña (Figure 4.3B).

Primary reactive gases (NO_X, SO_2 and CO) show strongly marked daily cycles, similar to those of water vapour, with much higher values during daylight than at night (Figure 4.3). Moreover, there are differences between working days and weekends. This increase during daylight is attributed to the transport of pollutants from the boundary layer. In the case of NO, soil emissions from the vegetation ring surrounding the island may also contribute (Kesik et al., 2005). It is important to highlight that, although this transport occurs, concentrations are extremely low. In air quality units, SO_2, NO_X and CO are typically within the ranges 2-200, 10-100 and 100-500 $\mu g \cdot m^{-3}$ in Santa Cruz and within the ranges 0.1-0.5, 0.05-0.5 and 70-300 $\mu g \cdot m^{-3}$ in Izaña, respectively. The readings of the SO_2, NO and NO_X analysers typically showed concentrations of about 20, 5 and 30 ppt at night and of about 50, 80 and 600 ppt during daylight, respectively. Many of instruments readings are frequently below the detection limit. The 5-min average SO_2, NO and NO_X concentrations were above detection limit (60 ppt for SO_2 and 50 ppt for NO and NO_X) only the 7, 3 and 63% of time at night, and the 40, 38 and 92% of time during daylight. This daily cycle we observed in Izaña for NO_2 has also been described for other mountain sites, such as Gilge et al. (2010).

Figure 4.4A shows the daylight / nighttimes ratio for each study pollutant. These ratios are much higher for NO_X and SO_2 (2 - 3) than for CO (~ 1.1) and O_3 (~ 0.9). This indicates that the concentrations of NO_X and SO_2 are 2-3 times higher than the nocturnal background representative of the free troposphere. Figure 4.4B shows the daylight increase fraction for each pollutant, calculated as the difference between the daylight and night mean concentrations divided by the daylight averaged concentration. Observe how the daylight increase accounts for ~ 70% of the average concentrations of NO_X, NO_2 and NO and for ~ 50% of the average concentrations of SO_2 observed during daylight. In contrast, this daylight increase only accounts for ~ 4 % of the average concentrations of CO observed in the daylight.

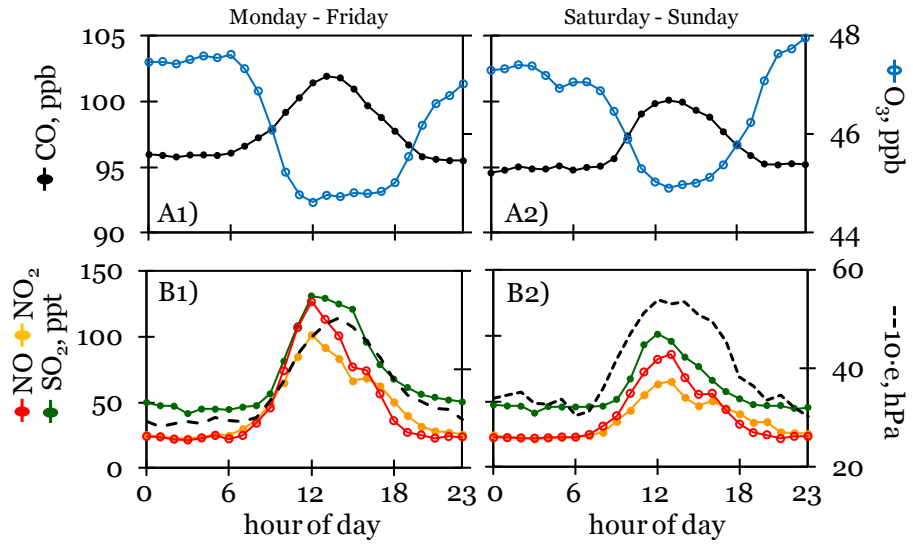

Figure 4.3 Daily cycle of reactive gases measured at IZO (CO, SO_2, NO, NO_2 and O_3) and water vapour, during working days (Monday-Friday) and weekends (Saturday-Sunday)

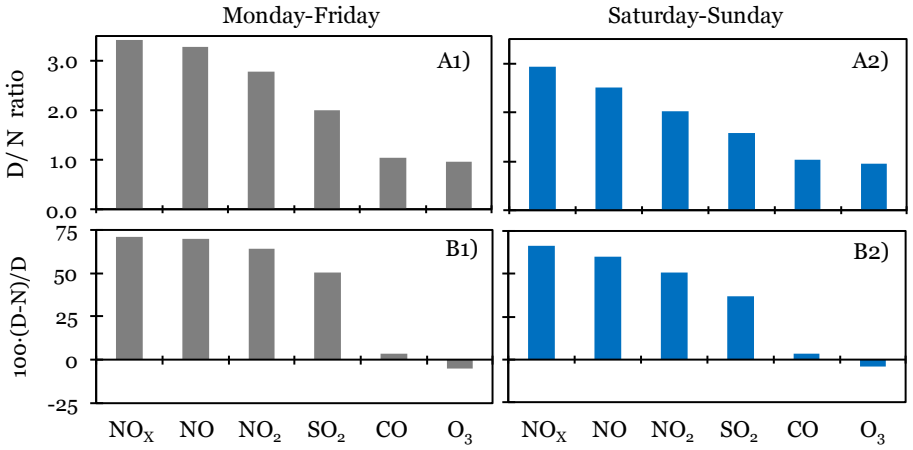

Figure 4.4 A) Daylight /night (D/N) ratio time of reactive gases. B) Daylight increase fraction [100·(D-N)/D] of reactive gases. Analysis segregated for working days and weekends. D=daylight, N=night-time

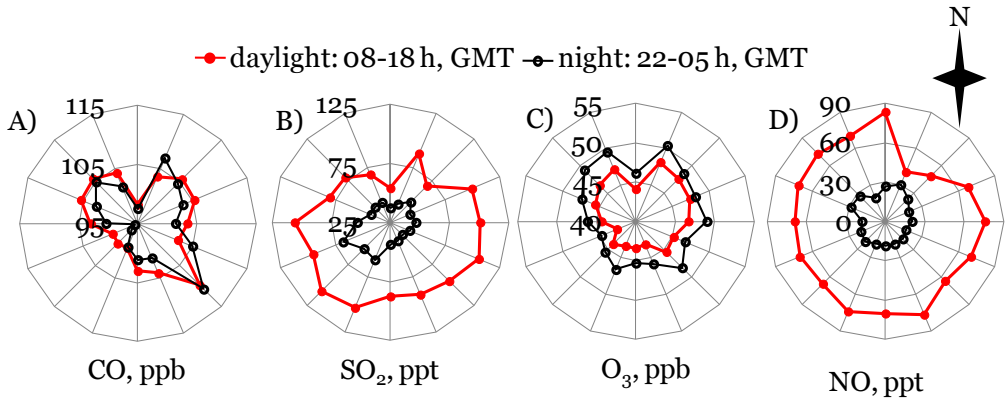

Figure 4.5 Gaseous (CO, SO_2, O_3 and NO) concentrations as a function of wind direction and time period (Red dots indicated 08 -18h GMT, and black dots 22 – 05h GMT)

The behaviour of O_3 is markedly different (Figure 4.3. and 4.4). The concentration of this gas decreases during daylight (Figure 4.3 B). The strong increase in the concentrations of this gas with altitude, typically observed in this region of the North Atlantic (Oltmans et al., 1996) and the regular daily airflow (upward during daylight and downward at night) accounts for this behaviour observed in Izaña. This cycle is opposite to that observed in Europe and North America, where a maximum during daylight is observed due to the photo-chemical daylight production (e.g. Millán et al., 1997).

These results demonstrate that SO_2 and NO_X during daylight are more influenced by the upward transport from the boundary layer than CO and O_3. Figure 4.5 shows the wind rose for the study trace gases. The dependence with wind direction is rather smooth. The slightly higher values of SO_2 when wind blows from southwest are probably related to the emission of buses exhaust in Las Cañadas del Teide National Park. In the next section it is shown how the somewhat higher values of O_3 and CO with northern winds are associated with long range transport.

CO and O_3 concentrations at Izaña (Table 4.1) are on the same order of magnitude that those observed in other remotes stations around the world. As an example, CO and O_3 background values for Jungfraujoch are in the range of 93 – 111 ppb for CO and 55 – 58 ppb for O_3 (Balzani - Lööv et al., 2008). At Mount Waliguan (China), Wang and co-workers (2006) found mixing ratios of 103 – 133 ppb for CO, and 61 – 58 ppb for O_3 for spring and summer, respectively. A comparison of the SO_2 and NO_X concentrations registered at Izaña under free troposphere conditions (night-time) with those recorded in other remote sites is a difficult task. This is due to the fact that readings of the SO_2 and NO_X analysers are frequently below detection limit at Izaña at night. During ACE-2 project, samples collected in flights performed between 1,100 and 7,000 m.a.s.l. above Tenerife observed SO_2 concentrations within the range 20 – 30 ppt (Andreae et al., 2000).

4.1.2. Seasonal evolution

In order to study the seasonal evolution of the reactive gases, the following analyses were performed:

- daily evolution per month of the study pollutants (Figure 4.6)
- daylight increase fraction for each month (Figure 4.7)

Differences in the seasonal evolution are observed (Figure 4.6):

- the seasonal evolution of the pollutants significantly influenced by transport from the boundary layer occurs by an enhancement of the in the amplitude of their daily cycle. This is the case of NO_X and SO_2:

  - NO_X concentrations reached their maximum in winter. This behaviour is frequently observed in rural and background sites and is attributed to the lower photo-oxidation rates, e.g. in Alpine stations (Steinbacher et al., 2007; Gilge et al., 2010). Observe in Figure 4.7B how the higher amplitude of the NO_X daily cycles tend to occurs in autumn and winter. The seasonal evolution at Izaña contrast with that observed Pico mountain station in Azores (Val Martin et al., 2008) where the maximum is observed in summer.

  - SO_2 concentrations exhibited a maximum in July and August. This behaviour is attributed to the frequently occurrence of Eastern and SE winds in this season, associated with the arrival of Saharan dust. This may favour the transport of this pollutant, during daylight, from the emission sources located in the eastern side of Tenerife (see power plants in Figure 1). Observe in Figure 4.7B how the higher amplitude of the SO_2 daily cycles tend to occurs in July and August.

- the seasonal evolution of the CO and O_3 is induced by a change nocturnal concentrations (free troposphere background), rather than for a change in the daily cycle:

  - At night, CO concentrations reached a maximum February – April. This behaviour is close to the winter typically observed in rural and background sites and is attributed to the lower photo-oxidation rates of the atmosphere (Novelli et al., 1998; Gilge et al., 2010).

  - At night, O_3 concentrations reached a maximum from March – July. This behaviour is markedly different to that observed in the continental boundary layer of Europe and North America, where the maximum tend to occur in summer due to an enhancement in the photo-chemical formation rates of this gas (Millán et al., 1997). The origin of this maximum in late spring- early summer at Izaña, has been a matter of controversy on what the influence of transport from continental regions or from upper

troposphere are (e.g. see references in Rodríguez et al., 2004). In the next section, the origin of the high ozone concentrations registered at Izaña is analysed on the basis of long range transport.

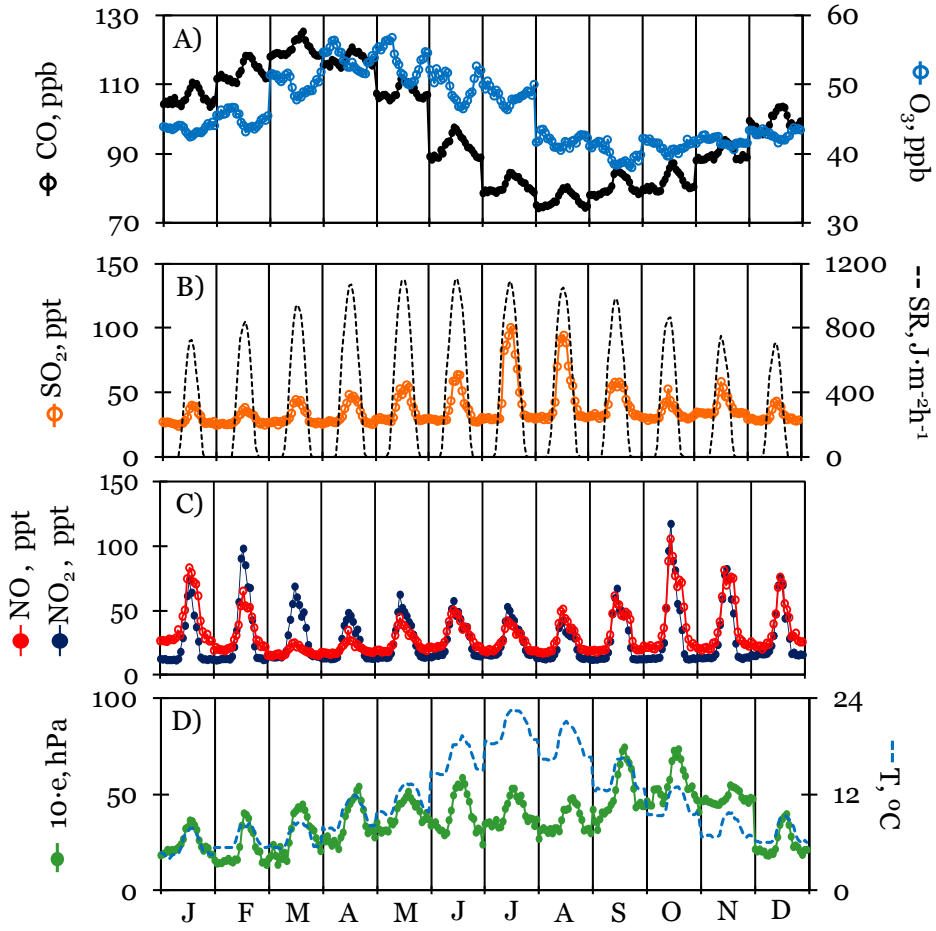

Figure 4.6 Daily median cycle (0 -23 h) for each month of the year (2007 – 2010) of the next parameters: (A) CO and O_3, (B) SO_2 and global radiation (C) NO and NO_2, and (D) water vapour and temperature (T)

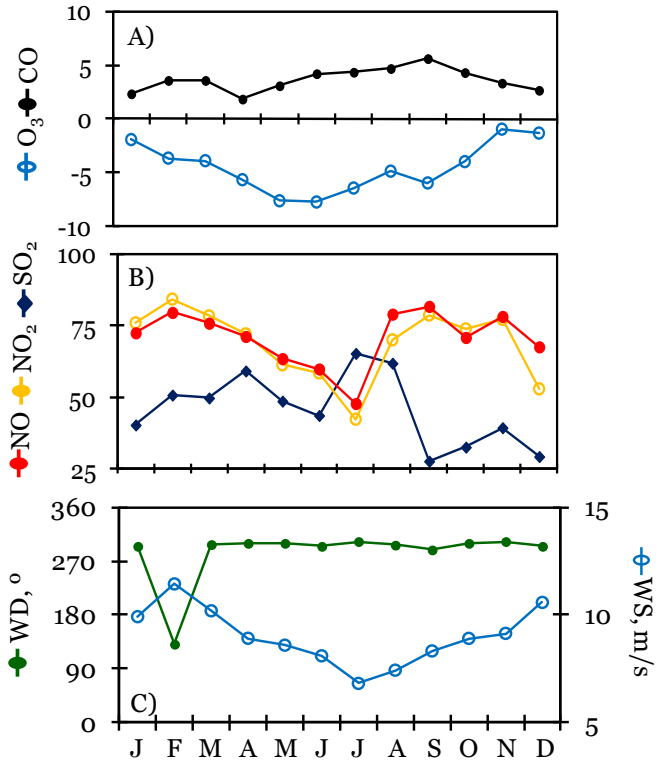

Figure 4.7 A-B) Daylight increase fraction [100·(D-N)/D] of reactive gases per month. C) Seasonal cycle of wind direction and speed at Izaña

4.2 Processes affecting background concentrations

In this section the influence of long range transport on the concentrations of reactive gases under free troposphere conditions is analysed. This is based on night-time data. Because the SO_2 and NO_X analysers are mostly below detection limit at night, this analysis was performed for O_3 and CO.

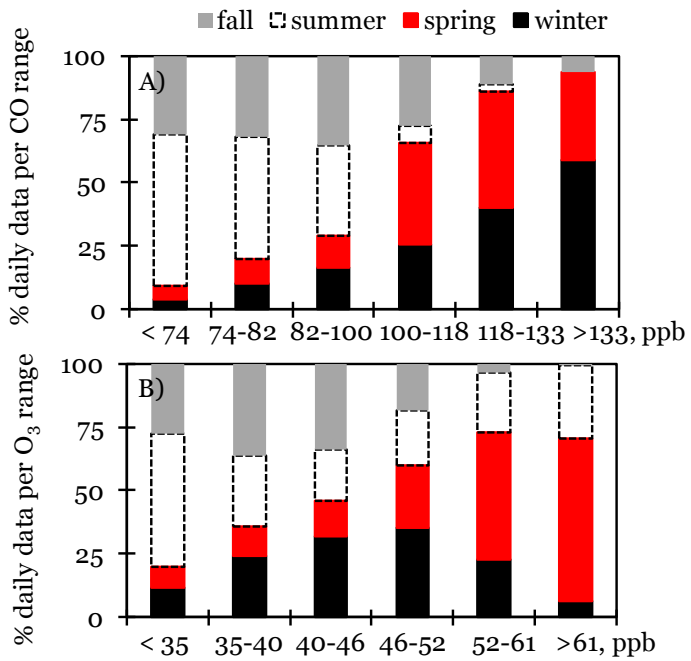

Figure 4.8 Frequency distribution O_3 and CO concentrations

The following method was used for analysing the 2007 – 2010 night-time data (22 – 06h, GMT)

1. Percentiles 10th, 25th, 50th, 75th and 90th were determined for each gas (O_3 and CO). Then, each night-time data was included within the intervals (<P10th, P10th - P25th, P25th – P50th, P50th – P75th, P75th – P90th, >P90th). The frequencies of data within those intervals, and for each season, are shown in Figure 4.8 for O_3 and CO.

2. Back-trajectories were calculated for each night-time data.

3. For the set of back-trajectories included in each percentile group in each season 'transport pathways' and 'potential source regions' were determined. The transport pathway represent the most common pathway of the back-trajectories that reached Izaña for the data set

(concentrations range and season), including the vertical component. Transport pathways are strongly influenced by the meteorological conditions (synoptic patterns in this case). Potential source regions are determined by giving a higher weighting to the most distant points of the transport pathways. Details on this method were provided in chapter 2.

The plots obtained with these methods are shown in Figure 4.9 – 4.14 for O_3 and Figure 4.15 – 4.20 for CO.

4.2.1 Long range transport on ozone

The analysis of the transport pathways plotted in Figures 4.9 – 4.13 (columns 2 and 3) lead to results similar to those obtained by Rodríguez et al. (2004) for the 1991-1994 data:

→ for a given season, an increase in ozone concentrations (across the different percentiles ranges) is associated with transport pathways showing transport from increasing latitudes and altitudes. This evidences the well known northward latitudinal gradient in ozone concentrations in the North Atlantic (Creilson et al., 2003).

→ because of the above described northward gradient, the lowest ozone concentrations (< 35 ppb) are registered with transport pathways showing transport from the Central North Atlantic (at low latitudes) and North Africa (Figure 4.9).

→ increasing ozone levels are associated with a reinforcement of a N–NW subsiding transport pathway (e.g. see column 2 across Figures 4.11 to 4.13). In summer, high ozone events (P^{th}> 90^{th}) are associated with a relatively "short" northern subsiding transport pathway, which results from depressions located just at the north of Tenerife, frequently at pressure levels above 700 hPa (Figure 4.14C2).

In summary, this analysis of the transport pathways does not allow to get new conclusions with respect to the previous study of Rodríguez et al. (2004). New contributions on how to differentiate ozone transported from the upper troposphere or from polluted continental regions will be proposed in further section. The 'potential source regions' for ozone concentrations shown in some plots, e.g. within the percentile ranges 50^{th} – 75^{th}, 75^{th} – 90^{th} in winter (Figures 4.12A1 and 4.13A1), suggest that these anthropogenic contributions may occurs.

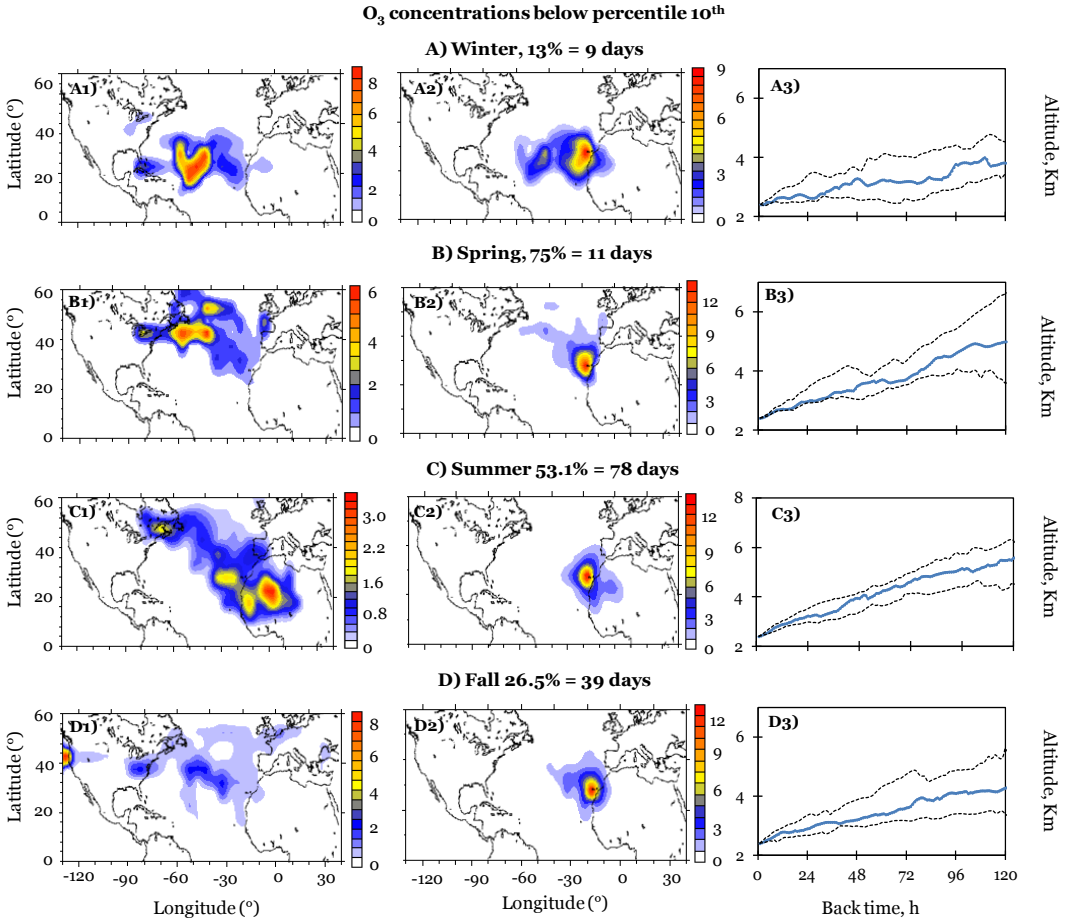

Figure 4.9 Potential source regions (column 1) and transport pathways (columns 2 and 3) for O_3 concentrations within the range < 10th (<35 ppb)

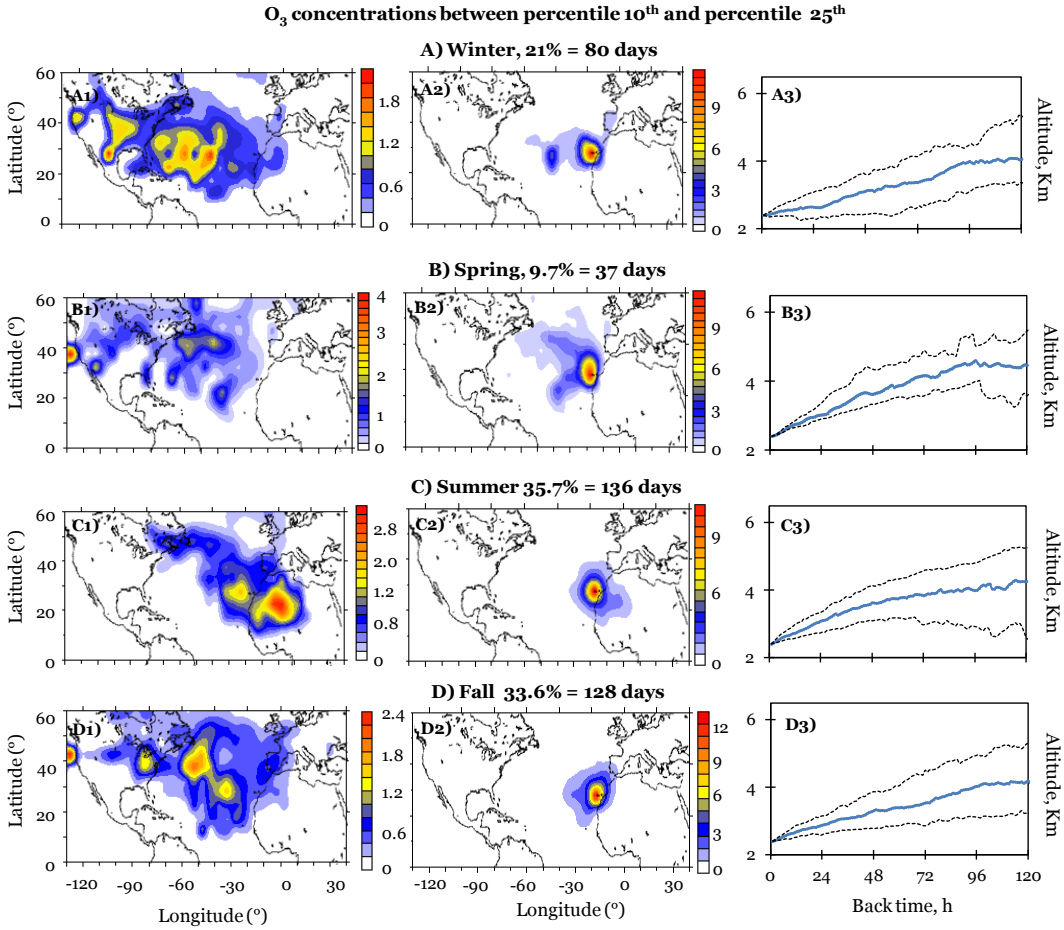

Figure 4.10 Potential source regions (column 1) and transport pathways (columns 2 and 3) for O_3 concentrations within the range 10th – 25th (35 - 40 ppb)

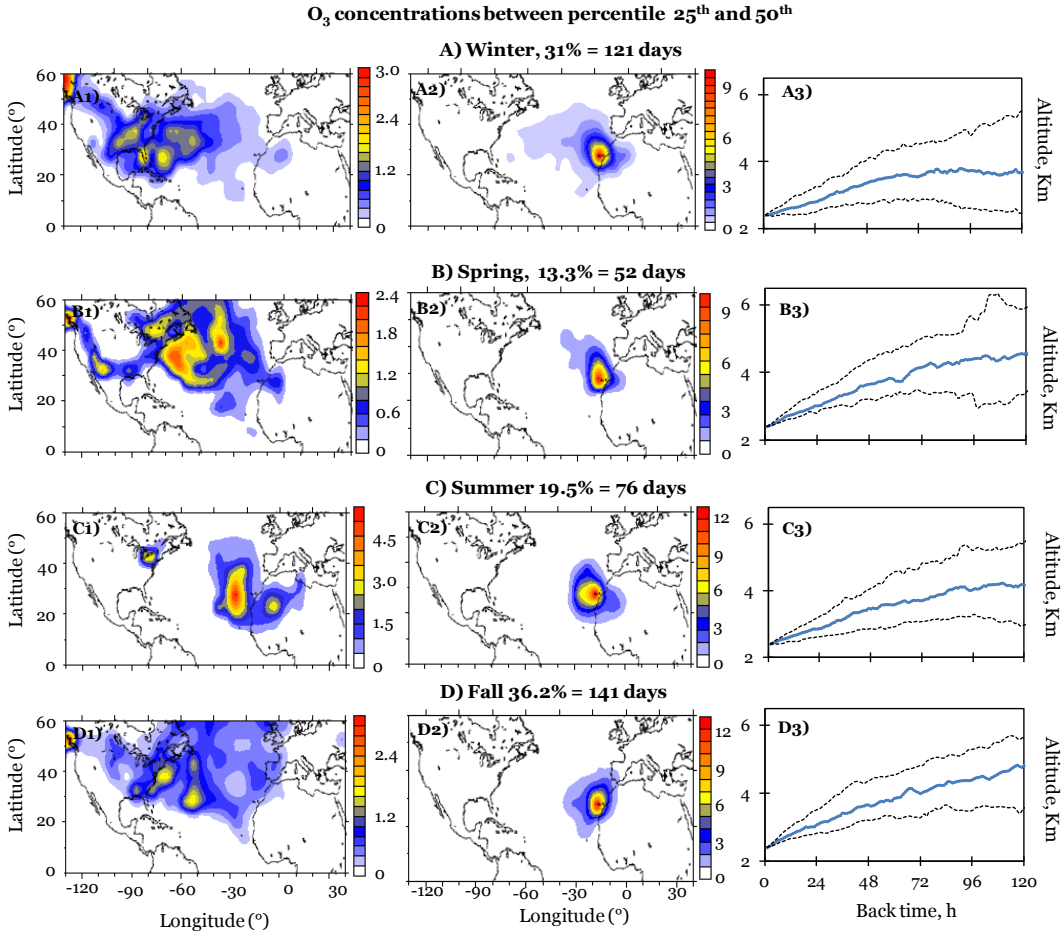

Figure 4.11 Potential source regions (column 1) and transport pathways (columns 2 and 3) for O_3 concentrations within the range 25th – 50th (40 - 46 ppb)

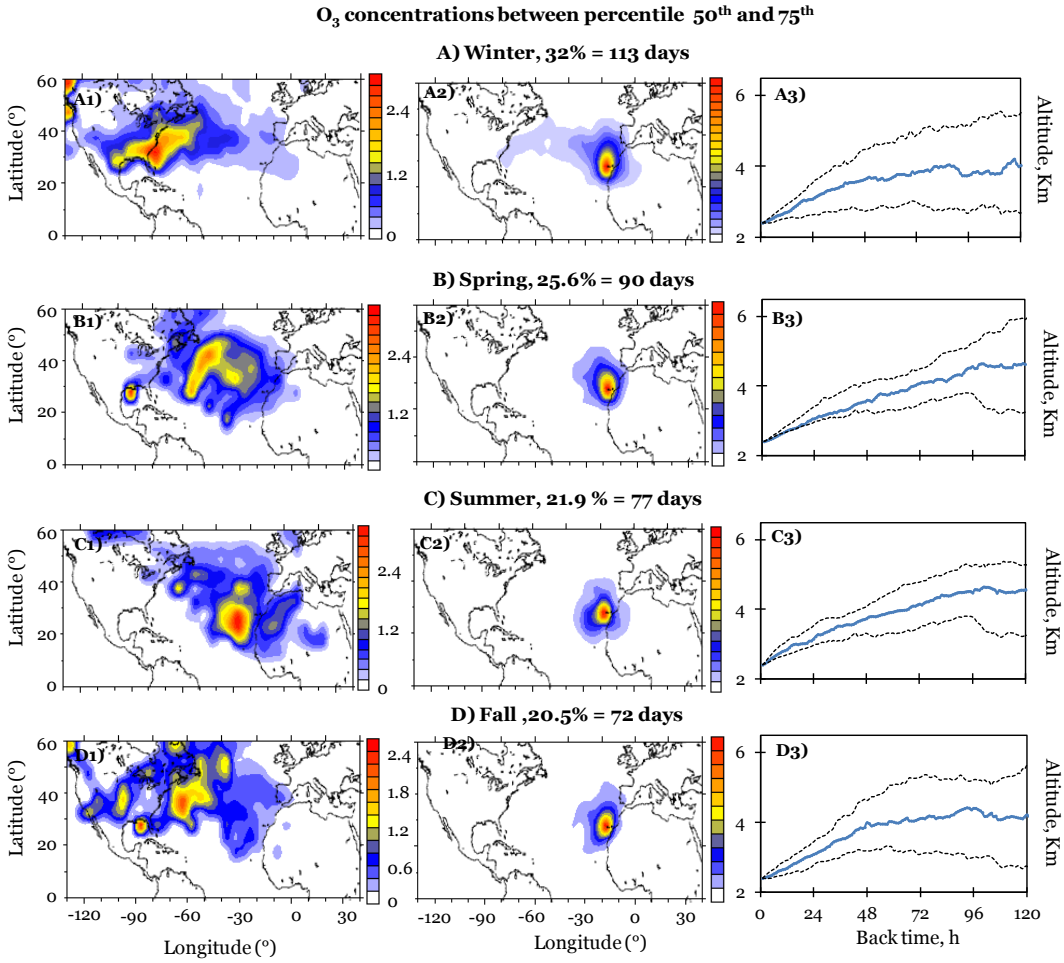

Figure 4.12 Potential source regions (column 1) and transport pathways (columns 2 and 3) for O_3 concentrations within the range 50th – 75th (46 - 52 ppb)

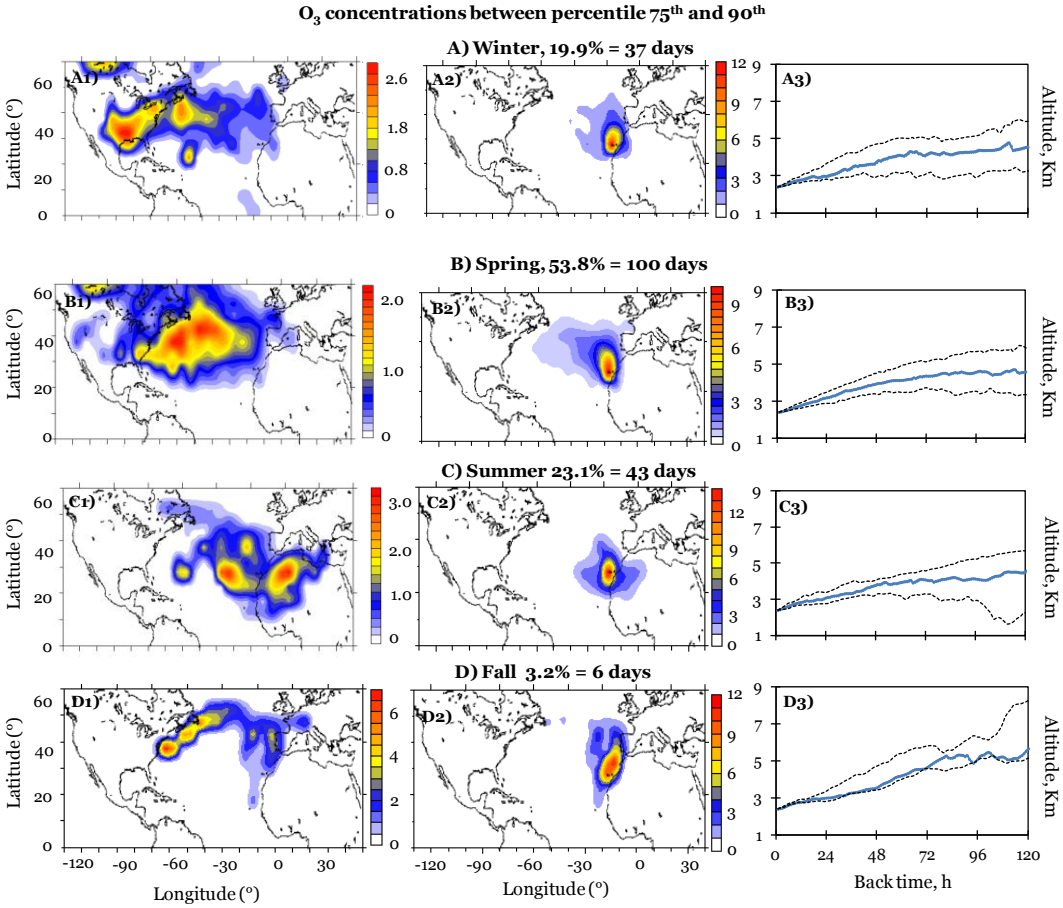

Figure 4.13 Potential source regions (column 1) and transport pathways (columns 2 and 3) for O_3 concentrations within the range 75th – 90th (52 - 61 ppb)

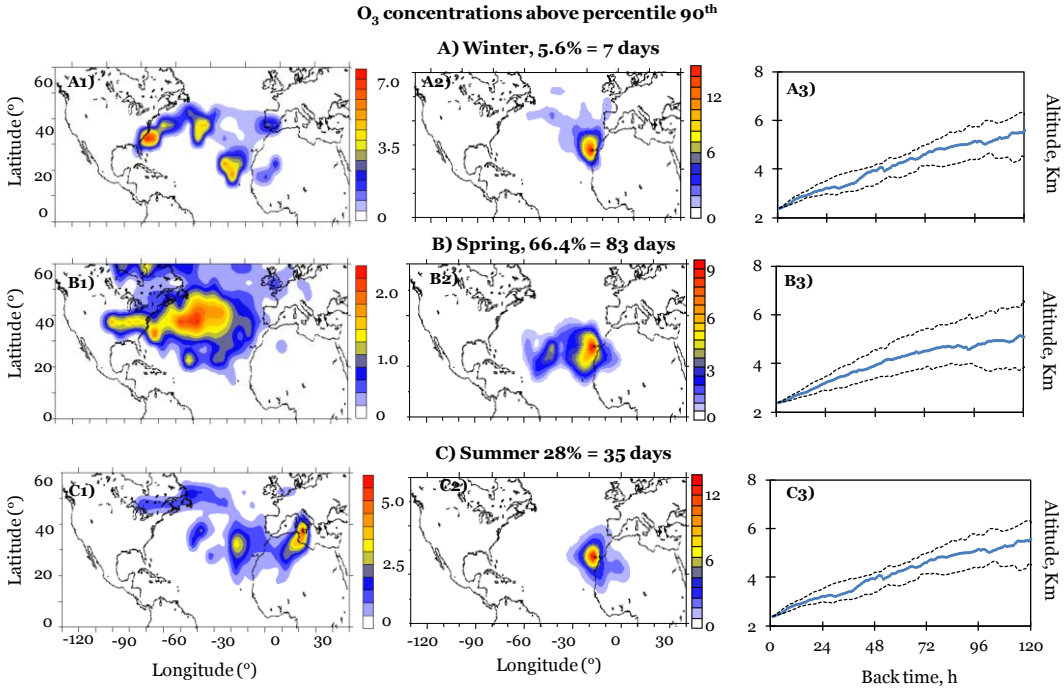

Figure 4.14 Potential source regions (column 1) and transport pathways (columns 2 and 3) for O_3 concentrations within the range >90th (> 61 ppb)

4.2.2 Long range transport on carbon monoxide

Transport pathways and potential source regions for CO are plotted in Figures 4.15 – 4.19. This is the first analysis performed for CO data from Izaña. It can clearly be observed that:

→ for a given season, moderate to low CO concentrations (<50th = 100 ppb) are associated with transport from the Central North Atlantic at low latitudes (Figures 4.15 and 4.16). In summer, the transport of air masses from North Africa is also associated low CO concentrations (Figure 4.15 B1). These two regions, where low CO emission occurs, were also associated with low ozone concentrations (Figure 4.9 and 4.10).

→ an increase in CO concentrations (across the percentiles ranges 25th – 50th, 50th -75th and 75th; i.e. from 82 to 118 ppb) is associated with transport pathways showing transport from increasing latitudes (Figure 4.17 and 4.18). This behaviour resembles to what is previously described for O_3 (Figure 4.11 and 4.12).

→ high CO concentrations (>90th = 133 ppb) are clearly associated with transport from North America (Figure 4.19), where emissions of CO are important.

In this analysis, it is important to observe that high CO concentrations are also associated with transport pathways from the mid troposphere, where, it would be expected that CO concentrations should be low. Stolh et al. (2002) showed how the convective activity occurring in the in the warm side of frontal systems that typically crosses North America, result in the upward transport and exportation to the North Atlantic free troposphere of North-American pollutants. Exportation of North American CO to the North Atlantic free troposphere has also been observed in Pico observatory, in the Azores (Honrath et al., 2004)

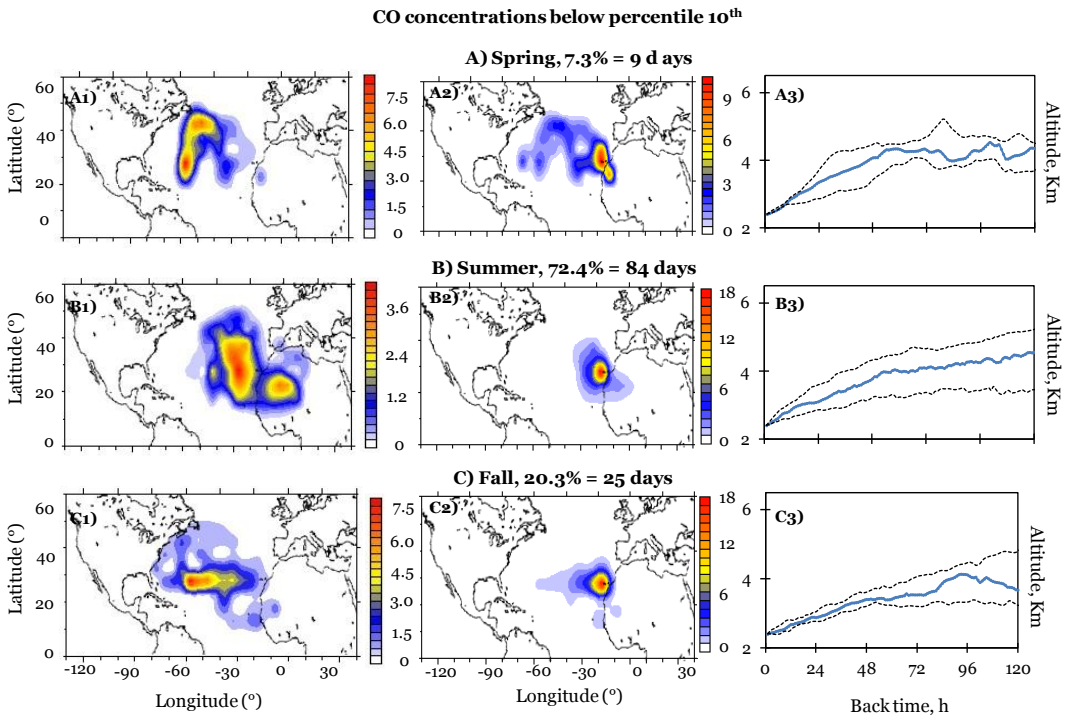

Figure 4.15 Potential source regions (column 1) and transport pathways (columns 2 and 3) for CO concentrations within the range < 10th (< 74 ppb)

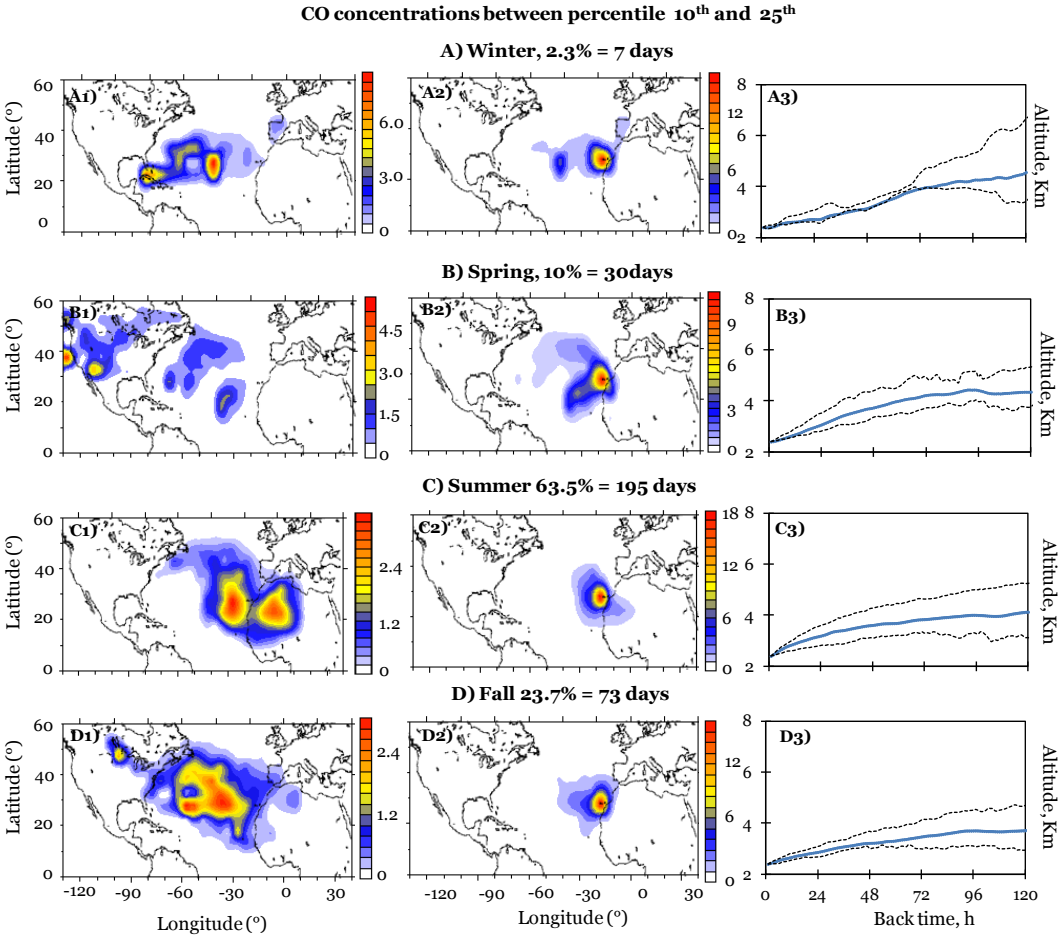

Figure 4.16 Potential source regions (column 1) and transport pathways (columns 2 and 3) for CO concentrations within the range 10th and 25th (74 – 82 ppb)

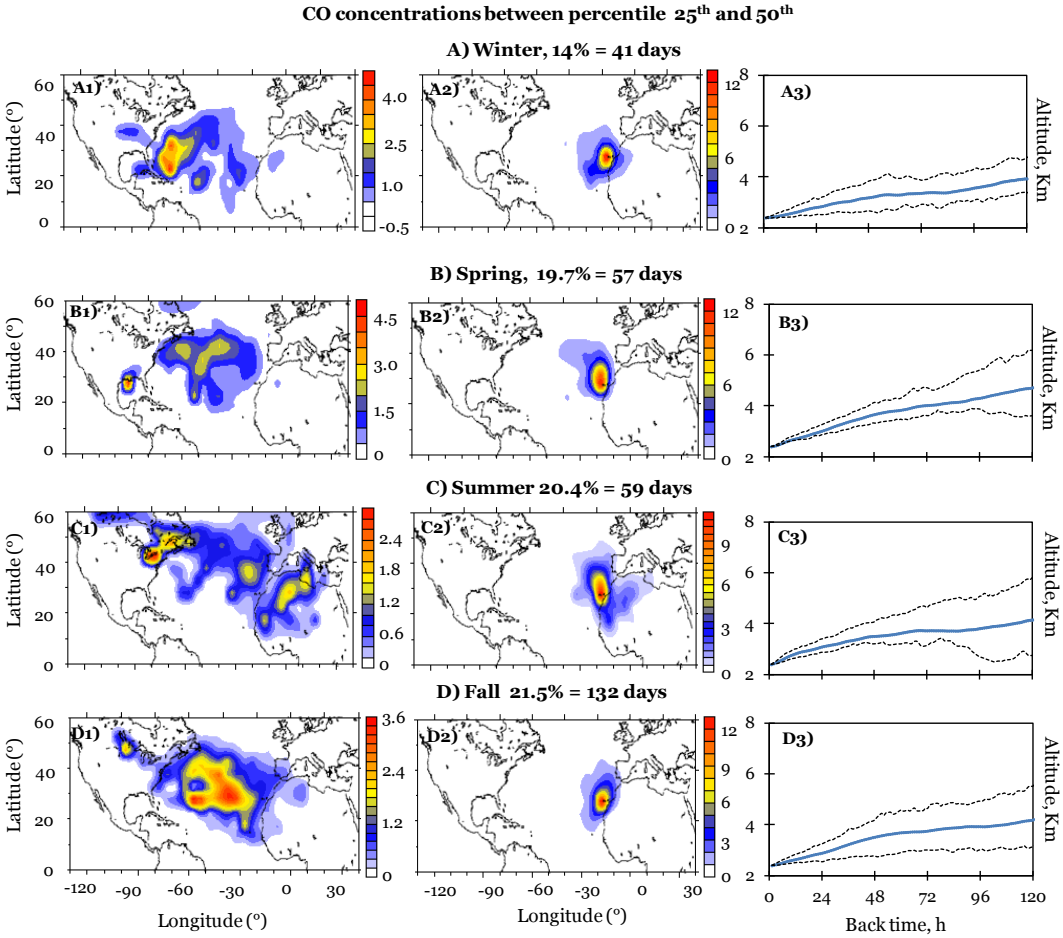

Figure 4.17 Potential source regions (column 1) and transport pathways (columns 2 and 3) for CO concentrations within the range 25th and 50th (82 – 100 ppb)

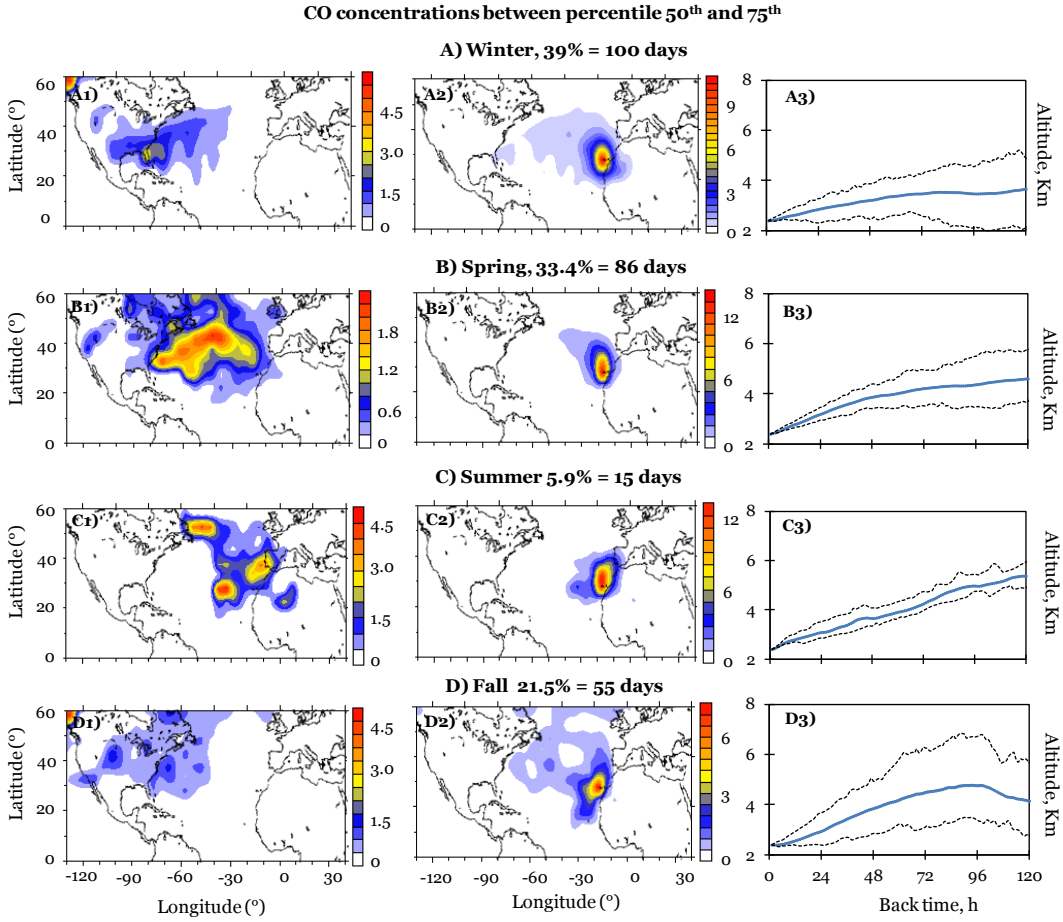

Figure 4.18 Potential source regions (column 1) and transport pathways (columns 2 and 3) for CO concentrations within the range 50th and 75th (100 - 118 ppb)

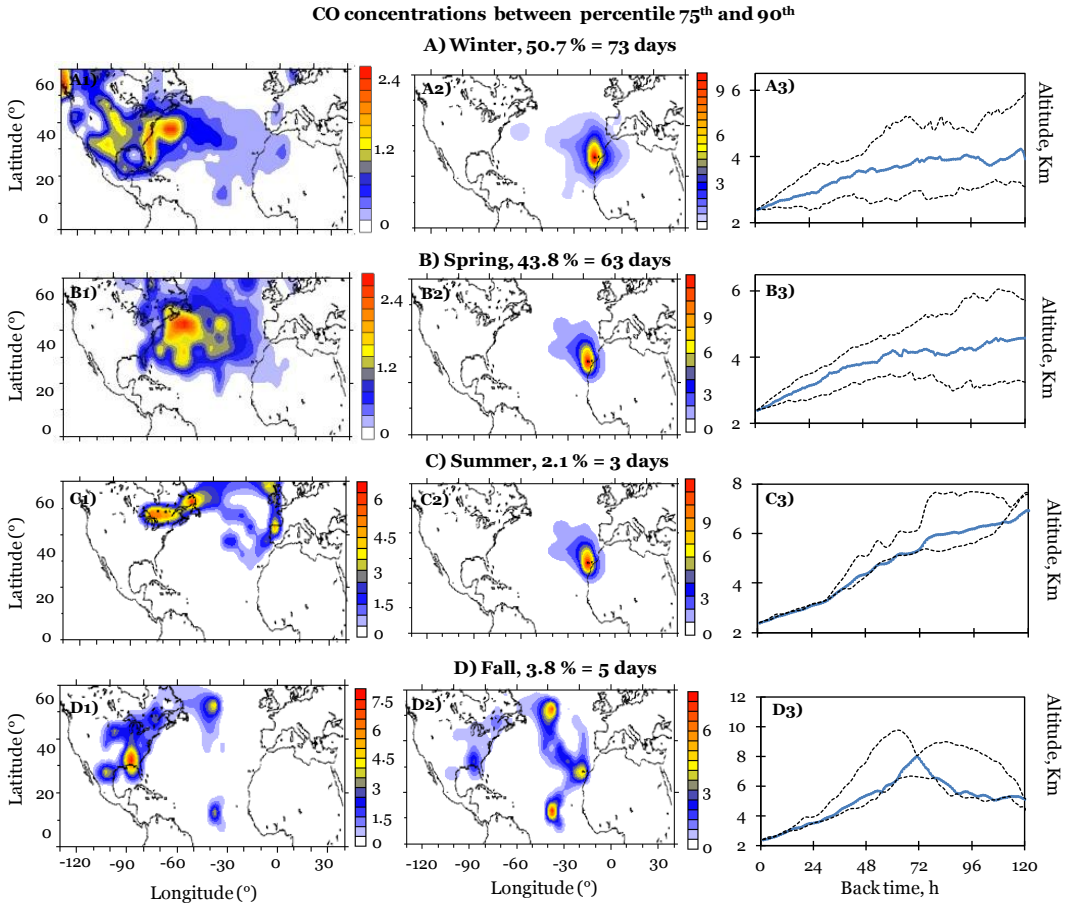

Figure 4.19 Potential source regions (column 1) and transport pathways (columns 2 and 3) for CO concentrations within the range 75th and 90th (118 - 133 ppb)

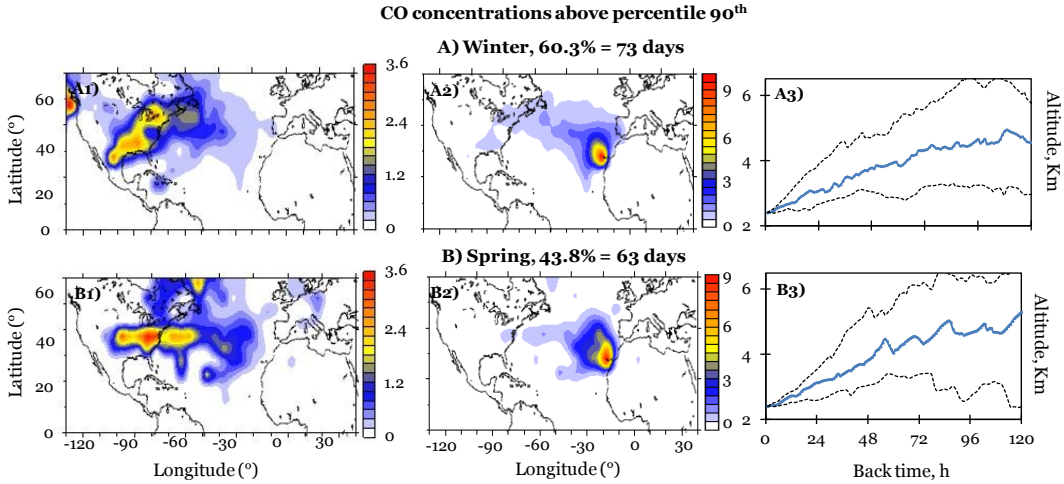

Figure 4.20 Potential source regions (column 1) and transport pathways (columns 2 and 3) for CO concentrations within the range > 90th (> 133 ppb)

4.2.3 Long range transport of ozone and carbon monoxide

The correlation between O_3 and CO has frequently been used for distinguishing O_3 episodes attributed to anthropogenic emissions of precursors or downward transport from upper troposphere / low stratosphere (Parrish et al., 1998; Li et al., 2002b).

Figure 4.21 shows the scatter plot of the O_3 versus CO concentrations recorded at night in Izaña from 2007 to 2010. Although the scattering is high, data tend to be comprised between two lines with slopes between 0.2 and 0.6. The linearity between O_3 and CO is high, except in autumn, when O_3 concentrations are in the minimum of the seasonal evolution (Figure 4.22). A progressive increase across winter (0.16), spring (0.20) and summer (0.37) is observed. These results points that the background of O_3 in the North Atlantic free troposphere may be modulated by anthropogenic emissions of precursors.

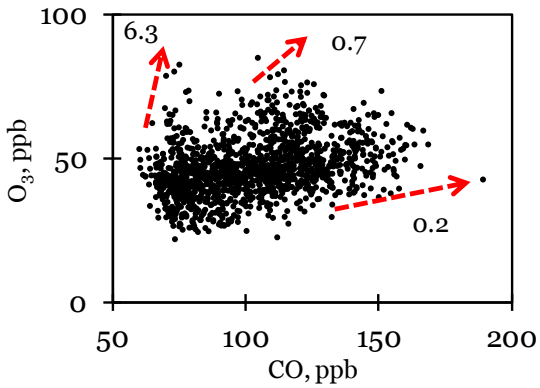

Figure 4.21 O_3 vs. CO. Night-time data collected from 2007 to 2010. The slope of the data aligned in the arrow is shown

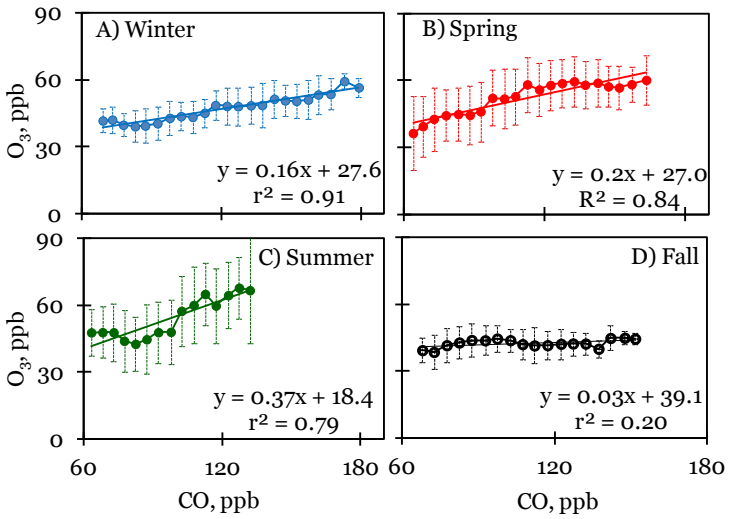

Figure 4.22 CO vs. O_3: Night time CO concentrations have been grouped in 10 ppb bin ranges. Standard deviations of night time O_3 concentrations for each bin are also shown

Table 4.2 Type of events selected for studying the origin of the events of high correlation between O_3 and CO. winter = Jan – Mar, spring = Apr- Jun, summer = Jul – Sep, fall = Oct – Dec

Type	O_3 range	O_3 - CO correlation, r	Ratio O_3/CO	Cases
1	Outliers: 47-87 ppb	<0.1	>0.75	41 days: 10% late spring + 90% summer
2	75-100th: 52 - 76 ppb	>0.75	0.53 ± 0.09	40 days: 100% spring
3	50-75th: 46 - 52 ppb	>0.75	0.42 ± 0.06	11 days: 54.5% winter + 45.5% spring
4	25-50th: 41 - 45 ppb	>0.75	0.46 ± 0.10	17 days: 45.5% winter + 45.5% fall
5	0 -25th: 34 - 39 ppb	>0.75	0.35 ± 0.03	11 days: 100% fall

In order to identify the origin of those events in which a high correlation between O_3 and CO occurs the following type of events were defined (Table 4.2):

→ Type 1: events in which O_3 / CO ratios are > 0.75 and the correlation between the two species is low (r<0.1) was found. These events have a ratio between 0.75 and 6 (Figure 4.21).

→ Type 2: events in which O_3 remained within the percentile ranges 75th - 100th and the correlation of this gas with CO was high (r>0.75).

→ Type 3: events in which O_3 remained within the percentile ranges 50th - 75th and the correlation of this gas with CO was high (r>0.75).

→ Type 4: events in which O_3 remained within the percentile ranges 25th - 50th and the correlation of this gas with CO was high (r>0.75).

→ Type 5: events in which O_3 remained within the percentile ranges <25th and the correlation of this gas with CO was high (r>0.75).

For each type of event, the transport pathway and the residence time was determined (Figure 4.23).

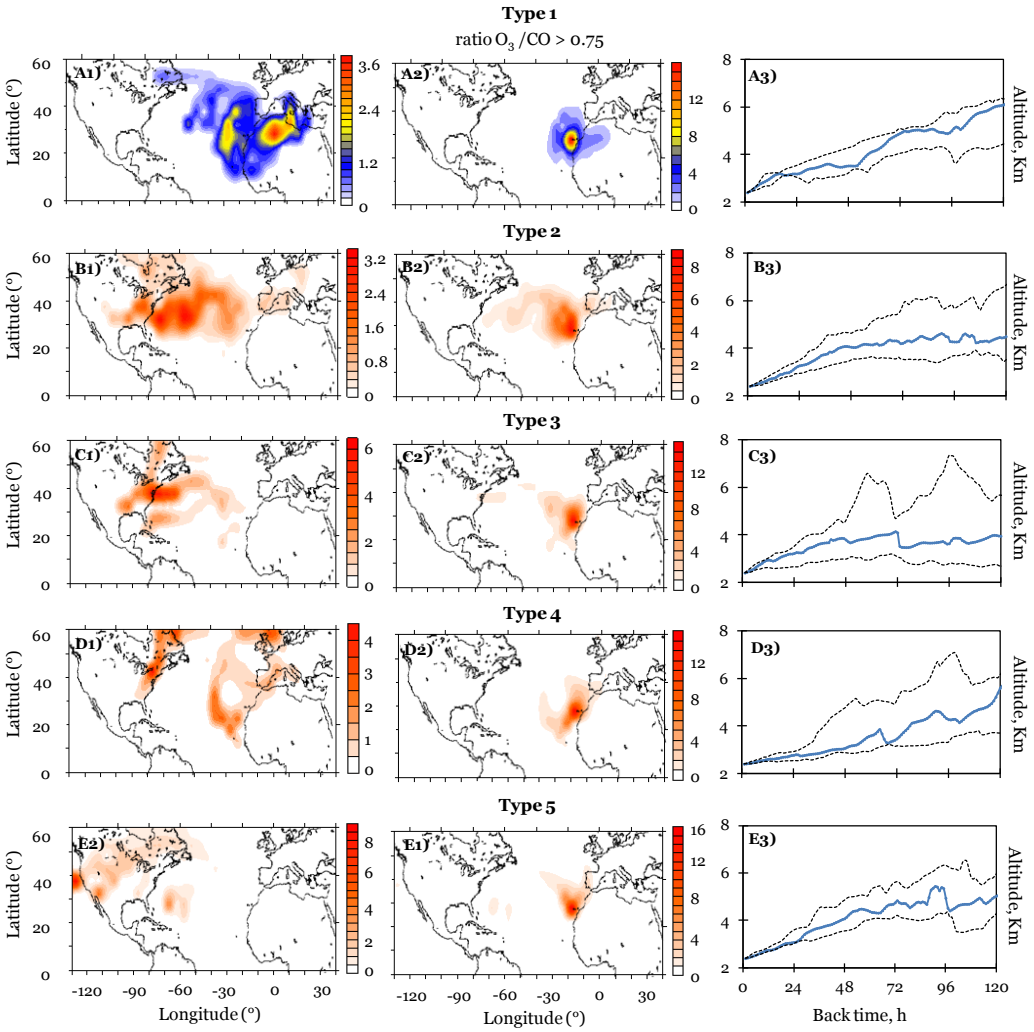

Figure 4.23 Potential source regions (column 1) and transport pathways (columns 2 and 3) for events type 1 to 5. Column 3: mean (blue line), P25th and P75th (dashed black lines) of the travelling altitude of the air masses for each type of events. Colour bars indicate the residence time

The analysis of the data plotted in Figure 4.23 shows that:

→ Events type 1 (high O_3, 47-87 ppb, - and low CO concentrations) are associated with subsidence of air masses over the Eastern North Atlantic and North Africa (Figure 4.23A). Rodríguez et al. (2004) also found this scenario for the high ozone events (>58 ppb) and concluded that were they caused by the subsidence linked to depressions that developed over Tenerife at altitudes above 700hPa. This scenario may account for the events of high ozone and Be^7 concentrations observed in this region and attributed to downward transport of air from the upper troposphere / low stratosphere (Prospero et al., 1995; Kentarchos et al., 2000). The 90% of these events occurred in summer (Table 4.2).

→ In events type 2 (O_3 within the ranges 52 - 76 ppb) the high correlation between O_3 and CO is linked to the transport of polluted air from North America and Europe (Figure 4.23B). These events occurred in spring (Table 4.2).

→ In events type 3 (O_3 within the ranges 46 - 52 ppb) the high correlation between O_3 and CO is linked to the transport of polluted air from North America. These events occurred in winter and spring (Table 4.2).

→ In events type 4 and 5 (O_3 within the ranges 34 - 45 ppb), which occurs in fall and winter (Table 4.2), an influence of continental pollution from Europe and North America is observed.

These results are consistent with the observations of O_3 and CO in Pico –Azores (Honrath et al., 2004; Owen et al., 2006) and Sable Island (Parrish et al., 1998). The important role of the zonal transport of North American pollutants across the Atlantic is discussed in previous studies (Hudman et al., 2007; Choi et al., 2009; Li et al., 2002; Stohl et al., 2002; Stohl and Trickl, 1999; Atherton et al., 1996; Parrish et al., 1993).

4.3 Summary and Conclusions

The processes that affect the concentrations of reactive gases (NO_X, SO_2, CO and O_3) at Izaña Global Atmospheric Watch Observatory were studied. Special emphasis was paid on segregating and quantifying how upward transport from the boundary layer and the how the free troposphere background contribute to the concentrations of the studied gases.

The concentrations of the study reactive gases show a strongly marked daily cycle induced by the upward transport of air (from lower levels than Izaña) during daylight and the downward transport of air from the free troposphere at night. This diurnal airflow is induced by the development of buoyant air flows around Tenerife. The air that arrives to Izaña is mostly linked to vertical movements in the northern side of Tenerife.

The mean daylight to night-time ratios were ~3 for NO_X, ~2 for SO_2, ~1 for CO and <1 for O_3. As average, the 75% of NO_X, 50% of SO_2 and 4% of the CO recorded during daylight are attributed to the upward transport from the boundary layer to Izaña Mountain. This contribution results in concentrations above the free troposphere background during daylight. In contrast, the concentrations of O_3 are regularly lower during daylight than at night due to the strong vertical gradient of this trace gas in this region.

The long range transport processes that contribute to the free troposphere concentrations of CO and O_3 were studied using some products (transport pathways and potential source regions) determined with back-trajectories. The analysis of these products and the correlation observed between O_3 and CO during the four study years (2007 – 2010) point that exportation of polluted air from North America exerts a significant influence on the concentrations and variability of O_3 in the North Atlantic free troposphere. In these cases, O_3 showed concentrations within the range 34 - 76 ppb and O_3 / CO ratios typically within the range 0.2 - 0.7. In addition to these events, episodes of high O_3 concentrations (47 – 87 ppb), high O_3 / CO ratios (0.7 – 6.5) and low correlations between O_3 and CO occur in late spring and summer. These events are associated with downward transport of air from the upper troposphere in the eastern side of depressions developing in the Eastern North Atlantic.

The contribution of the long range transport processes to NO_X and SO_2 concentrations observed under free troposphere conditions could not be studied due to the fact that these gases exhibits concentrations below the detection limit of the used analysers (60 ppt for SO_2 and 50 ppt for NO and NO_X for 5 min averages) during the 37% and 92% of night-time period/year, respectively.

Chapter 5

Atmospheric nanoparticles observations in the low free troposphere during upward orographic flows at Izaña Mountain

New particle formation (NPF) by nucleation and subsequent growth processes has become a topic of great interest in atmospheric and environmental sciences, since they may influence the climate (by acting as cloud condensation nuclei) and playing a role in the hydrological cycle and radiative balance.

NPF have been studied in different scenarios. This formation process depends on environmental conditions, such as solar radiation, temperature, water vapour, relative humidity and the concentration of pre-existing particles and sulphuric acid and/or organic vapours (Weber et al., 1997; Boy and Kulmala, 2002; Fiedler et al., 2005; Rodríguez et al., 2005; Kulmala et al., 2006).

The aim of this study is to investigate the processes and conditions that favour the formation of 3 – 10 nm particles observed on high mountains entering the low free troposphere. For this purpose data collected during daylight at Izaña Mountain Observatory (Tenerife, Canary Islands) has been analyzed (see data set 4, section 2.5 in chapter 2). Understanding the formation of particles < 10 nm has become a crucial matter to understand the initial steps of the growth processes that may result in particles of 50 – 100 nm in size.

5.1 Development of diurnal upward flows

Because of the occurrence of the upslope winds during daylight and downslope winds at night, the concentrations of SO_2 and nitrogen oxides exhibited clearly marked daily cycles similar to those of water vapour (Figures 4.2, 5.1a-b). This diurnal cycle is caused by the upward transport of pollutants emitted at the lower levels of the island. During the study period, the readings of the SO_2, NO and NO_y analysers typically showed concentrations of about 20, 5 and 30 ppt at night and of about 50, 80 and 600 ppt during daylight, respectively (Fig. 5.1.b). The 5-min average SO_2, NO and NO_y concentrations were above detection limit (60 ppt for SO_2 and 50 ppt for NO and NO_y) only the 7, 3 and 63% of time at night, and the 40, 38 and 92% of time during daylight. The objective of the data plotted in Fig. 5.1.b (obtained by averaging data collected both above and below detection limit) is simply to illustrate the strong night – to - daylight changes in the SO_2 and NO_y concentrations due to the developments of the upward flows.

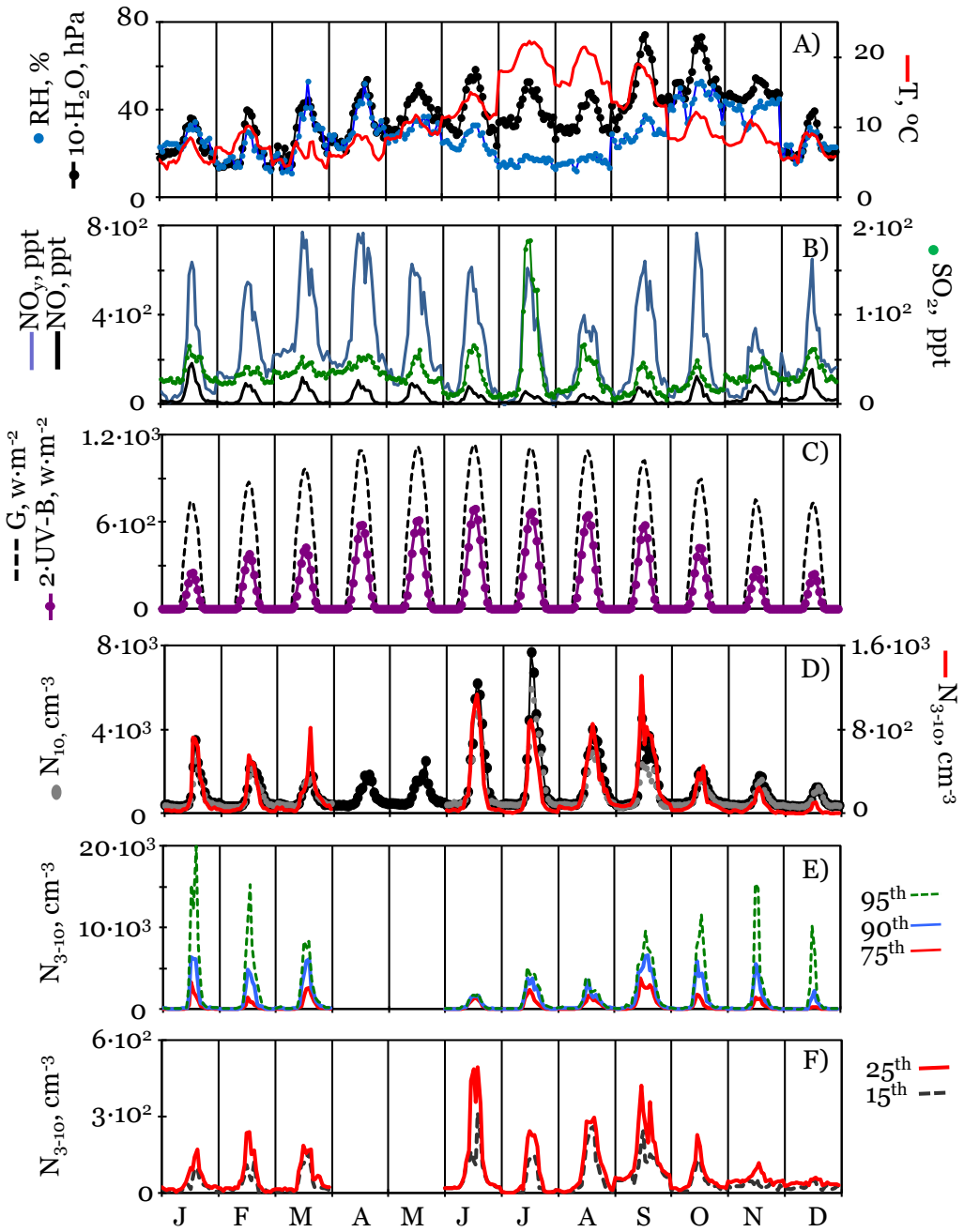

Figure 5.1 Hourly median values and percentiles for each month of 2007 of: (A) relative humidity (RH), water vapour (H_2O) and temperature (T), (B) SO_2 and NO_y concentrations, (C) global, and (G) UV-B radiation, (D) N_{10}, N_3 and N_{3-10} concentrations, (E) percentiles 70th, 90th and 85th of N_{3-10}; and (F) percentiles 15th and 25th of N_{3-10}.

5.2 Particle size distributions

N_{3-10} measured from November 2006 to December 2007 using two Condensation Particle Counters (CPC): a CPC model 3025A (TSI™) to measure the number of particles >3 nm (N_3), and a CPC model 3010 (TSI™) to measure the number of particles >10 nm (N10). N_{3-10} was determined as the difference between N_3 and N_{10}. The accuracy of the measurements was assessed comparing data from both CPCs. The readings from the instruments were almost identical at night owing to the extremely low concentrations of 3 – 10 nm particles in this period, whereas N_3 and N_{10} differed during daylight due to new 3 – 10 nm particle formation (Fig. 5.2).

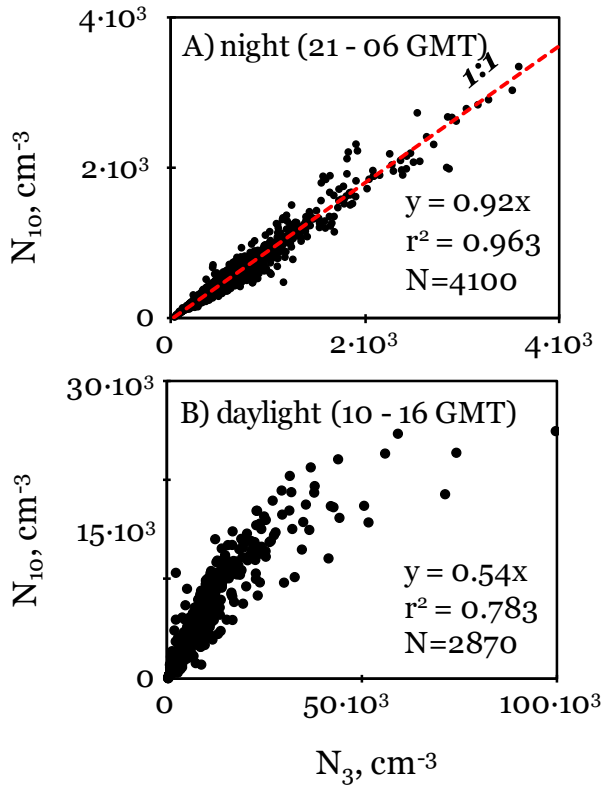

Figure 5.2 N_{10} versus N_3 concentrations registered at Izaña during nocturnal (A) and diurnal (B) periods of 2007. N: Number of hourly data used.

Complementary aerosol measurements were performed. The number size distribution of particles with sizes between 14 nm and 20μm were measured with a Scanning Mobility Particle Sizer (TSI™) within the range 14 – 660 nm (an electrostatic classifier model 3080 connected to a CPC model 3025A; 24 June to 30 September, 2008) and an Aerodynamic Particle Sizer (APS model 3321 of TSI™; 2007–2008). Moreover, daily averaged PM_{10} concentrations were determined during 2007

– 2008 by sampling on filter, whereas 1-min average PM_{10} concentrations were determined by converting the aerosol volume (calculated with the APS data) to aerosol mass concentrations using experimentally determined aerosol effective density.

At Izaña, particle concentration exhibit daily cycles as those described for the trace gases. N_3 and N_{3-10} typically show concentrations of about 480 cm^{-3} and 25 cm^{-3} at night and of about 4,600 cm^{-3} and 600 cm^{-3} during daylight (Fig. 5.1.d). The particle size distribution also exhibits a marked daily evolution (Fig. 5.3 and Table 5.1). During the night, a mean number concentration of 480 cm^{-3} was recorded and the dN/dlogD size distribution showed a 50 nm mode (Fig. 5.3.a). Similar size distribution and number concentration were observed in the free troposphere at Mauna Loa (Weber and McMurry, 1996), Jungfraujoch (Weingartner et al., 1999), Puy de Dôme (Venzac et al., 2009) and Khumbu (Venzac et al., 2008). This was also observed by Raes et al. (1997) and Maring et al. (2000) at Izaña in July 1994 and July 1995, respectively. They observed that, particles with a size of 50 – 60 nm were predominant during events of downward transport of air from the middle and upper troposphere, and that they also correlated well with ^{7}Be. These facts supported the idea that these aerosols are originally formed in the mid to upper troposphere.

Table 5.1 Statistics of the hourly particle number concentrations recorded at Izaña during the periods 17th November 2006 to 31st December 2007 (for N_3, N_{10} and N_{3-10}) and 24th June 2008 to 1st October 2008 (for N_{13-660} and its subsets). Units: N (cm^{-3}), hour (GMT)

	Particle number range									
0-5h	3	10	3-10	13-660	13-20	20-50	50-100	100-200	0-500	500-660
mean	479	445	38	362	7	126	102	103	23	0.5
%		92	8		2	35	28	28	6	<0.1
25th	316	293	3	166	2	39	73	44	8	<0.1
50th	401	371	28	246	4	64	92	66	20	0.3
75th	526	490	64	352	9	94	119	97	32	0.6
90th	759	711	99	472	17	139	149	124	4241.52	1. 5
11-16h	3	10	3-10	13-660	13-20	20-50	50-100	100-200	0-500	500-660
mean	4594	3179	1379	1498	201	848	292	122	35	0.6
%		70	30		13	57	19	8	2	<0.1
25th	942	828	78	404	20	157	130	76	22	0.0
50th	1891	1575	284	818	88	410	182	108	30	0.3
75th	5304	4040	1068	1841	263	1114	285	139	40	0.7
90th	11419	8428	3226	3335	555	2104	429	183	63	1.4

The night-to-daylight increase in the particle number concentration is associated with a predominant increase in the concentrations of nucleation particles (< 20 nm). Observe in Table 5.1 that mean daylight-to-night concentration ratios were equal to 37 for N_{3-10}, 29 for N_{13-20}, 7 for N_{20-50}, 3 for N_{50-100} and <2 for the concentration of particles >100 nm during the study period. The greatest increase in particle concentrations were observed for particles < 20 nm, that indicates that the daily evolution of the particle number concentration is highly influenced by NPF during daylight. Thus, the

mode diameter of the dN/dlogD spectrum is lower during daylight (20 to < 50 nm) than at night (50 nm).

Moreover, the mode of the size distribution during daylight shifts towards lower diameters when the particle number concentration increases, in such a way that the dN/dlogD mode diameter exhibits values of about 53 nm, 27 nm and 23 nm when N_{13-660} exhibits values within the ranges <500, 500 – 1000, 1000 – 6000 cm^{-3}, respectively (Fig. 5.3b). This indicates that increases in particle number concentration are associated with increases in NPF rates.

There is a marked difference between the nocturnal and diurnal particle number size distributions. In the unperturbed free troposphere at night, the Aitken mode is predominant. The development of buoyant flows during daylight results in upward transport of vapours and in NFP. Three different cases are shown in Fig. 5.4. NPF followed by marked particle growth during daylight was observed on 25th July, 2008 (Fig. 5.4a). On 16th August, 2008 moderate particle growth occurred (Fig. 5.4b), whereas on 17th July no particle growth was observed after the 13 – 20 nm event registered in the afternoon (Fig. 5.4c).

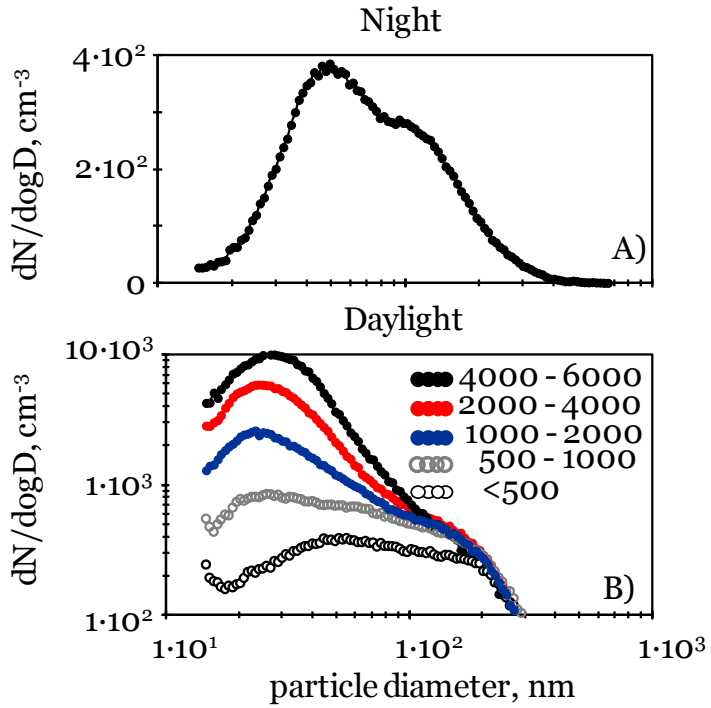

Figure 5.3 Averaged dN/dlogD size distribution recorded at Izaña: (A) at night (00 – 05 GMT), and (B) daylight episodes (10 – 17 GMT) of N_{13-660} concentrations within the ranges <500, 500 – 1000, 2000 – 4000 and 4000 – 6000 cm^{-3}.

Daily cycles of the particle number concentration similar to those we observed at Izaña (prompted by NPF in the daylight upslope winds) were also observed at Jungfraujoch, Monte Cimone, Mauna Loa, Khumbu and Puy de Dôme (Weber and McMurry, 1996; Weber et al., 1997; Weingartner et al., 1999; Van Dingenen et al., 2005; Venzac et al., 2007).

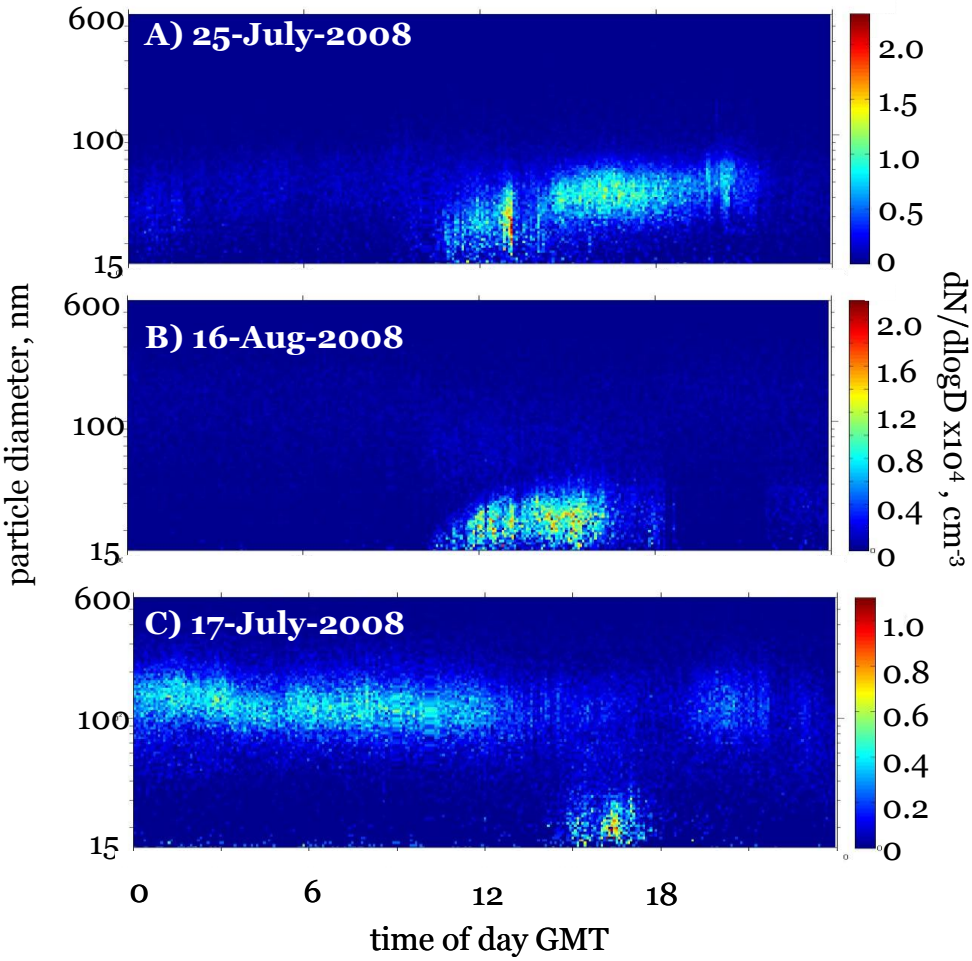

Figure 5.4 5-min values of the dN/dlogD size distribution during three events.

5.3 3 - 10 nm particle events

In this section, the conditions that favour the formation of 3 – 10 nm particles necessary for the growth process resulting in NPF episodes is investigated. As described in Chapter 1, the formation of a 3 – 10 nm particle is a two-step processes: nucleation of an initial cluster and activation of such cluster resulting in particle growth to detectable sizes (≥ 3 nm).

5.3.1 Short time variations of 3 – 10 nm particles

The processes that influence on the short time variations of N_{3-10} were identified by performing a Principal Component Analysis (PCA) followed by varimax rotations using 5-min averaged data (e.g. as those plotted in Figures 5.5 to 5.7). For the PCA, the data set was first normalised (by subtracting to each value the mean value of that variable in the whole data set, and then dividing it by the standard deviation). A minimum value of 1.0 was set for the eigenvalues, whereas the maximum number of principal components allowed (PC) was set to 5. Usually, 3 to 4 PC were obtained in each PCA. An initial PCA was performed with the whole data set (~1 year). Subsequently, PCAs were performed month-by-month in order to study how the processes that influence on the 3 – 10 nm particle formation change along the year. Such PCAs were performed only with those months with more than 22 days of available data. In order to avoid the influence of the common daily patterns exhibited by some variables (e.g. those plotted in Fig. 5.1) the PCA was performed only during daylight (09 – 16 GMT). Owing to the PC obtained depends on the number and types of variables introduced in the PCA, a number of tests were performed by introducing different combinations of variables.

Only SO_2, NO and NO_y data recorded above detection limit were used. Thus, about 25 PCAs were performed. For the sake of brevity, only two examples are shown (Table 5.2). In the PCA performed in the summer months three PCs were usually found (e.g. July 2007; Table 5.2):

- *PC-1* is positively correlated with N_{3-10} and direct (DI) radiation. This PC indicates that NPF by nucleation of photo-oxidized species may significantly contribute to N_{3-10}. The negative association of PM_{10} and diffuse radiation (DF) with this PC indicates that high concentrations of pre-existing particles do not favour the occurrence of 3 – 10 nm particles. The negative correlation of temperature is attributed to the fact that the condensation processes involved in the NPF are favoured under low temperature conditions, whereas the negative association of pressure is probably linked to the slight pressure drops during upward flows periods.

Table 5.2 Factor loading of the Principal Components Analysis (followed by a varimax rotation) obtained with 5-min averaged data from 08 to 16 GMT in July and November 2007. Only trace gases concentrations above detection limit were used.

	July 2007			*November 2007*		
	PC-1	*PC-2*	*PC-3*	*PC-1*	*PC-2*	*PC-3*
N_{3-10}	**0.51**	**0.50**	0.06	**0.76**	-0.06	0.22
PM_{10}	**-0.83**	0.02	-0.01	-0.09	**0.55**	**0.69**
SO_2	0.18	**0.67**	0.05	**0.89**	0.07	0.24
NO_y-NO	0.18	**0.57**	**0.75**	**0.86**	-0.01	-0.27
NO	-0.02	0.00	**0.97**	**0.91**	0.06	-0.13
H_2O	-0.04	0.60	0.16	-0.07	**-0.40**	-0.10
DF-Rad	**-0.93**	0.03	-0.04	0.14	**0.82**	0.22
DI-Rad	**0.88**	-0.02	0.07	-0.03	**-0.80**	0.02
P	**-0.68**	-0.39	0.05	-0.04	0.38	**0.83**
Temp	**-0.76**	0.48	-0.06	0.16	-0.36	**0.71**
Wind speed	0.12	**-0.83**	-0.01	-0.24	0.79	-0.12
Var. %	34	21	14	28	24	18

- *PC-2* is positively correlated with N_{3-10} and SO_2. This PC represents NPF in relatively sulfur-rich (tens to hundreds of ppt) air masses. The correlation of the NOy - NO difference with this PC evidences that these air masses are relatively enriched in aged nitrogenous compounds. The positive temperature and water vapour and negative wind speed associations indicate that buoyant upward flows are favoured by increases in temperature and decreases in synoptic wind speed.

–*PC-3* is positively correlated with NO and the NO_y - NO difference and represents the influence of the upward flows on the concentrations of nitrogenous species.

In the PCA performed in the winter months, it was observed that N_{3-10} and trace gases were associated with the same PC (e.g. November 2007; Table 5.2). The origin of the apparently lesser influence of PM_{10} and radiation on N_{3-10} is discussed below in detail. In the PCA performed with the whole data set, the most important association was that of N_{3-10} with SO_2 and with NO_y (~ 1 year).

5.3.2 Classification of 3 – 10 nm particle events

A day-to-day analysis of the 5-min average time series was performed. Three types of event were found (Table 5.3):

– *Type I*. During these events, N_{3-10} concentrations higher than 500 cm^{-3} and correlations between N_{3-10} and SO_2 were observed. Most of these episodes occurred from 10 to 13 GMT (Table 5.3) and were caused by the arrival at Izaña of air from lower altitudes resulting in simultaneous increases in N_{3-10}, SO_2 and water vapour. Figure 5.5 shows some of these events occurred on 16th November 2007, from 10:50 to 12:40 GMT, (Fig. 5.5a) and on 15th December

2007, from 11 to 14 GMT (Fig. 5.5c). In this type of episode, the "N_{3-10} versus SO_2" concentrations exhibited a linear relationship (see examples in Figs. 5.5c and d). The "N_{3-10} versus SO_2" slope of this first order equation ranged between 2 and 40 cm^{-3} ppt^{-1} (r^2 coefficient was between 0.70 and 0.95) and showed an averaged value of 11 cm^{-3} ppt^{-1} during the whole study period. This "N_{3-10} versus SO_2" slope is a measure of the NPF rates related to the SO_2 to H_2SO_4 conversion, cluster activation and subsequent activation and growth to detectable sizes (≥ 3 nm). A total of 58 events (with an average duration of 2h 48') were observed in the January to December 2007 period (264 days with available data).

All analyses of the "N_{3-10} versus SO_2" slope shown below are based on slopes obtained from fittings with an r^2 coefficient > 0.7. In all cases SO_2 concentrations were above detection limit (60 ppt).

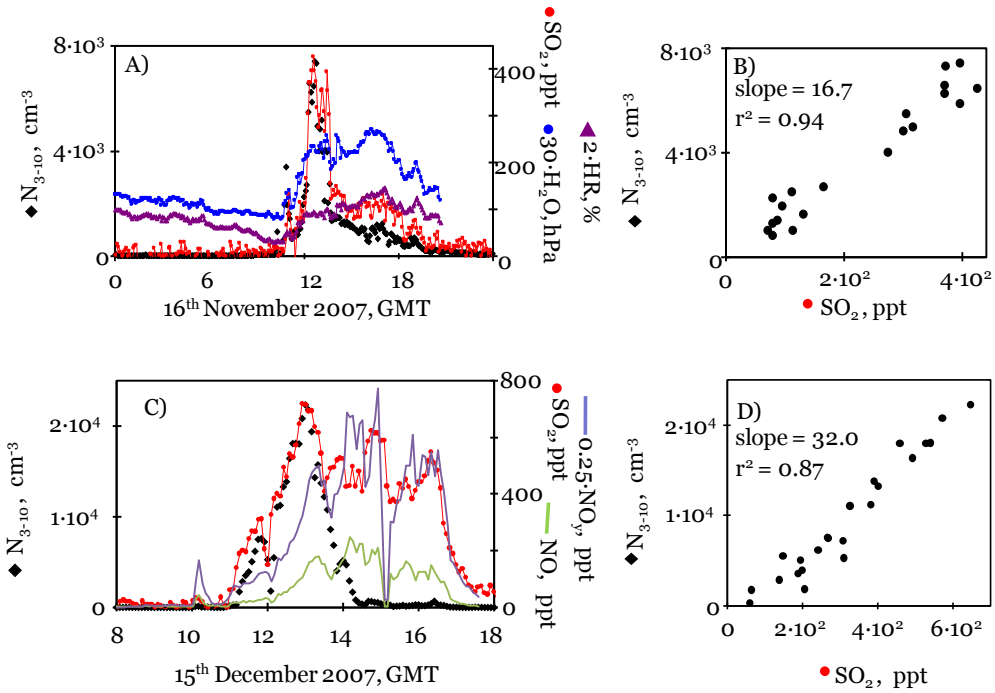

Figure 5.5 5-min averaged values of N_{3-10}, SO_2 and water vapour concentrations and RH during two events Type I events (16th November 2007 and 15th December 2007).

-*Type II*. During these episodes N_{3-10} concentrations were higher than 500 cm^{-3} and correlations between N_{3-10} and SO_2 were not observed. Most of these episodes occurred from 12 to 16 GMT (later than Type I events; Table 5.3), when N_{3-10} concentrations experienced significant increases not observed in SO_2 levels. In most of these events, increases in NO_y concentrations were observed. Figure 5.6 shows some of these episodes occurred on 22nd

September, 2007 during the whole daylight period (Fig. 5.6a) and 4th March, 2007 during the central part of daylight (Fig. 5.6b). A total of 87 events (with an average duration of 3h 36') were observed in the January to December 2007 period (264 days with available data). During the 60% of these events, SO_2 concentrations were above detection limit.

-*Type III*. In these episodes no significant night - to - daylight increases in N_{3-10} were registered. Examples are not shown for the sake of brevity.

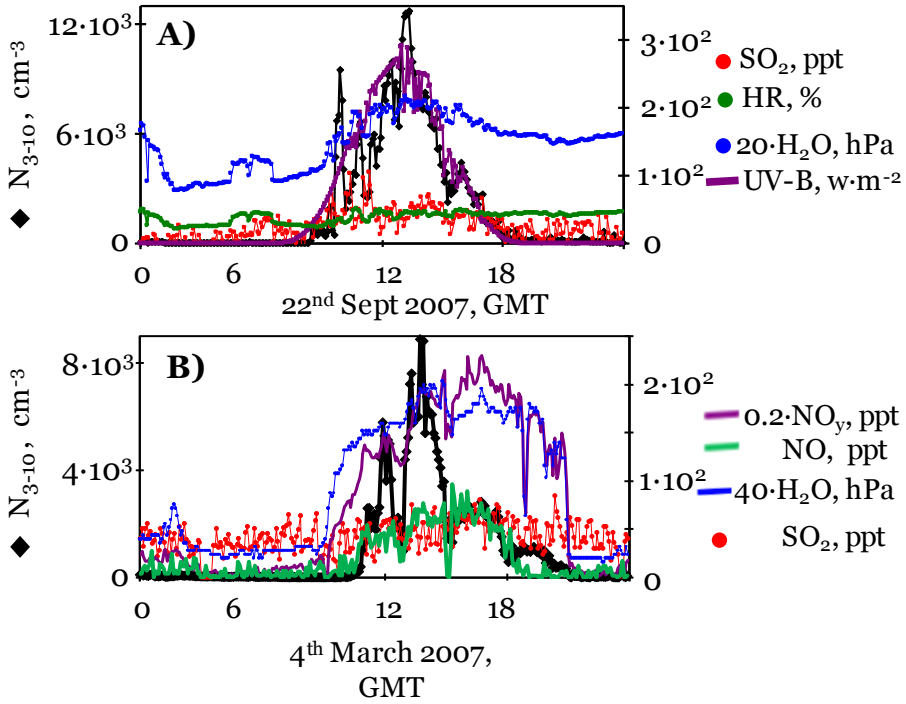

Figure 5.6 5-min averaged values of N_{3-10}, SO_2 and water vapour concentrations, relative humidity and UV-B radiation during two Type II events (22nd September 2007 and 4th March 2007).

The fact that the relationship between N_{3-10} and SO_2 is linear in Type I events, suggests that the N_{3-10} and SO_2 correlation is caused by cluster/particle growth to ≥ 3 nm size due to sulfuric acid condensation, even if SO_2 concentrations are low (tens to hundreds of ppt). Fiedler et al. (2005) observed linear relationships between H_2SO_4 and the number of particles > 3 nm, and it has been proposed that this behaviour is accounted for by the cluster activation theory (Kulmala et al., 2006).

Table 5.3 Data of N_{3-10} Types I, II and III events registered at Izaña from January to December 2007. Data availability expressed in number of days. Number of events registered every month. Average start time and ending time of the events for every month. Start and ending time for Type III events are not provided because they generally occurred during the whole daylight period.

Number of valid days in each moth	**Type I**			**Type II**			**Type III**
	events	*start*	*end*	*events*	*start*	*end*	*events*
Jan. 29	3	10:05	12:15	19	12:32	15:23	16
Feb. 28	2	11:00	11:45	11	11:37	16:08	13
Mar. 22	2	10:00	13:45	7	11:52	15:52	9
Apr. 0							
May. 0							
Jun. 5	2	11:15	14:40	1	11:00	15:00	1
Jul. 31	12	09:40	13:06	6	12:00	14:40	10
Aug. 27	2	10:00	13:00	16	12:34	16:53	8
Sep. 28	7	09:20	12:04	16	11:08	16:04	6
Oct. 30	12	09:50	13:24	4	11:00	14:30	17
Nov. 29	10	10:10	12:27	6	12:30	15:40	15
Dec. 17	6	10:45	12:22	1	13:00	15:00	11
Total 246	*58*			*87*			*106*

During Type II events, no correlation between N_{3-10} and SO_2 was observed. These events mostly occurred from 12 to 16 GMT, when solar radiation intensity is high and significant correlations between N_{3-10} and solar radiation were frequently observed (e.g. PC-1 in July 2007 in Table 5.2; Figs. 5.6a, 5.7a and b). This suggests that condensation of vapours brought about by photochemistry (not measured) plays a significant role in 3 – 10 nm particle formation. Two types of vapour may be involved: sulfuric acid and organic compounds. The fact no correlation is observed between SO_2 and N_{3-10} does not rule out that sulfuric acid condensation may contribute to N_{3-10} in these events. Indeed, Weber et al. (1997) observed H_2SO_4 formation during daylight correlated with 3 – 4 nm particles, with no association with SO_2 variations. However, the contribution of organic vapours (not measured in this study) of natural or anthropogenic origin to N_{3-10} should also be considered (Marti et al., 1996; Allan et al., 2006; Laaksonen et al., 2008). At Izaña, Fischer et al. (1998) observed that the concentrations of anthropogenic and biogenic (e.g. isoprene) organic compounds exhibited daily cycles similar to those we observed in N_{3-10}, SO_2, NO and NO_y, indicating that natural biogenic and anthropogenic substances are mixed in the upward flows that reach Izaña. The mixing is caused by biogenic (e.g. forests of pines and other species around the island) and soil (e.g. NO) emissions during the upward flow regime that results in the transport of pollutants (e.g. SO_2 and a fraction of NO and NO_y). In this air mass, organic compounds may contribute to N_{3-10} by "nucleation and condensation of pure organic substance" or by "condensation of organic compounds onto sulfuric acid containing droplets or clusters". The fact that the association between N_{3-10} and SO_2 was observed in all PCA performed in this study suggests that this latter scenario is plausible.

Finally, it is important to highlight that although increases in NO and NO_y concentrations are observed during Type II events, the oxidation product of these gases (nitrate) may not account for

the observed 3 – 10 nm particles in the Type II events. Nitrate is typically observed at particle diameters ≥ 50 nm (Tolocka et al., 2004). As far as we know, this compound has not been detected in the 3 – 10 nm size and none theory has been proposed for this.

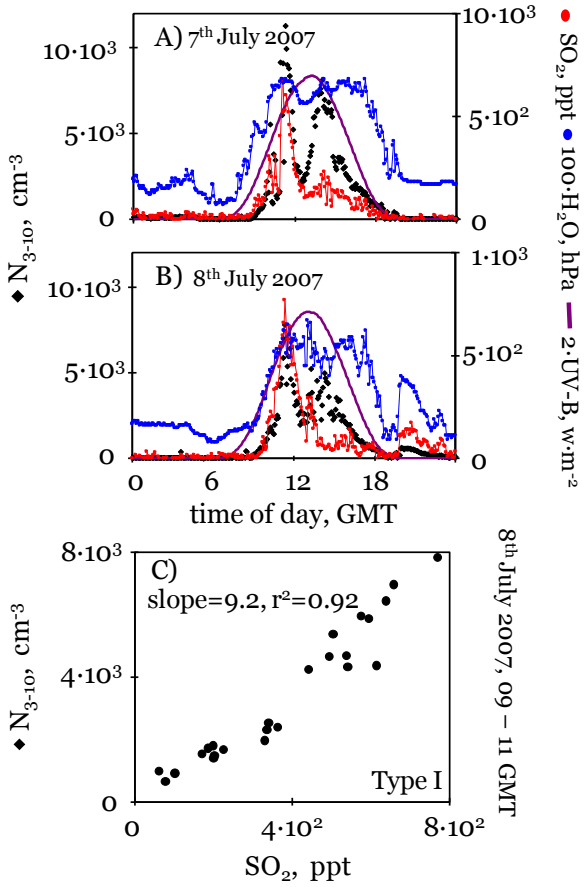

Figure 5.7 5-min average values of N_{3-10}, SO_2 and water vapour concentrations and UV-B radiation during two days on which Type I and Type II events were registered on a single day (7th and 8th July 2007). N_{3-10} versus SO_2 concentrations during the Type I event recorded the 8th July 2007 from 09:30 to 11:30GMT (C).

In summary, Type I events are attributed to 3 – 10 nm particle formation during the upward transport of air mass with relatively high SO_2 concentrations (plumes of hundreds of ppt). In contrast, Type II events seem to be associated with fresh 3 – 10 nm particles formed in-situ due to the condensation of vapours recently formed. In both type of events, gaseous precursors are attributed to emissions on the island. Figure 5.7 shows examples of two days on which Type I and II events occurred on a single day. The strong decoupling between Type I and II events in these examples supports the idea that these are different in nature.

5.4 Influence of environmental parameters

In this section, the environmental conditions favouring the formation of 3 – 10 nm particles have been analyzed. Part of this analysis is based on the results shown in Tables 5.3 and 5.4 and Figures 5.8 and 5.9.

Table 5.4 Statistics of the hourly particle surface area (24th June 2008 to 1st October 2008) and particle PM_{10} (17th November 2006 to 31st December 2007) concentrations recorded at Izaña.

S $\mu m^2 cm^{-3}$	0.014 - 0.1 µm ultrafines	0.014 - 1 µm fines	1 - 10 µm coarse	0.014 - 10 µm Total	PM_{10} μgm^{-3}
mean	4	20	25	45	13
%	8	44	56	-	-
25th	2	10	0	11	0.4
50th	2	18	7	28	1.3
75th	4	27	43	71	7.9
90th	8	36	72	103	40.2

5.4.1 SO_2 and NO_y concentrations

As stated above, correlations between SO_2 and N_{3-10} were only observed during Type I events. SO_2 concentrations (Fig. 5.8b) were higher during Type I events (monthly averages 100 – 300 ppt) than during Types II (35 – 70 ppt) and III (30 – 150 ppt) events. Concentrations of NO_y (not shown in Fig. 5.8 for the sake of brevity) were almost the same during Types I (300 – 800 ppt) and II (430 – 900 ppt) events, and much lower during Type III episodes (250 – 500 ppt). The fact that NO_y concentrations were relatively high during Type II events suggests that these air masses may bring organic compounds that may contribute to N_{3-10} with two possible origins (Marti et al., 1996): i) anthropogenic emissions at low altitude on the island (< 600 m a.s.l., well below the stratocumulus layer) and subsequent upward transport, and ii) biogenic emission (in the forest between 600 and 2,000 m a.s.l.) mixed with polluted air during upward transport.

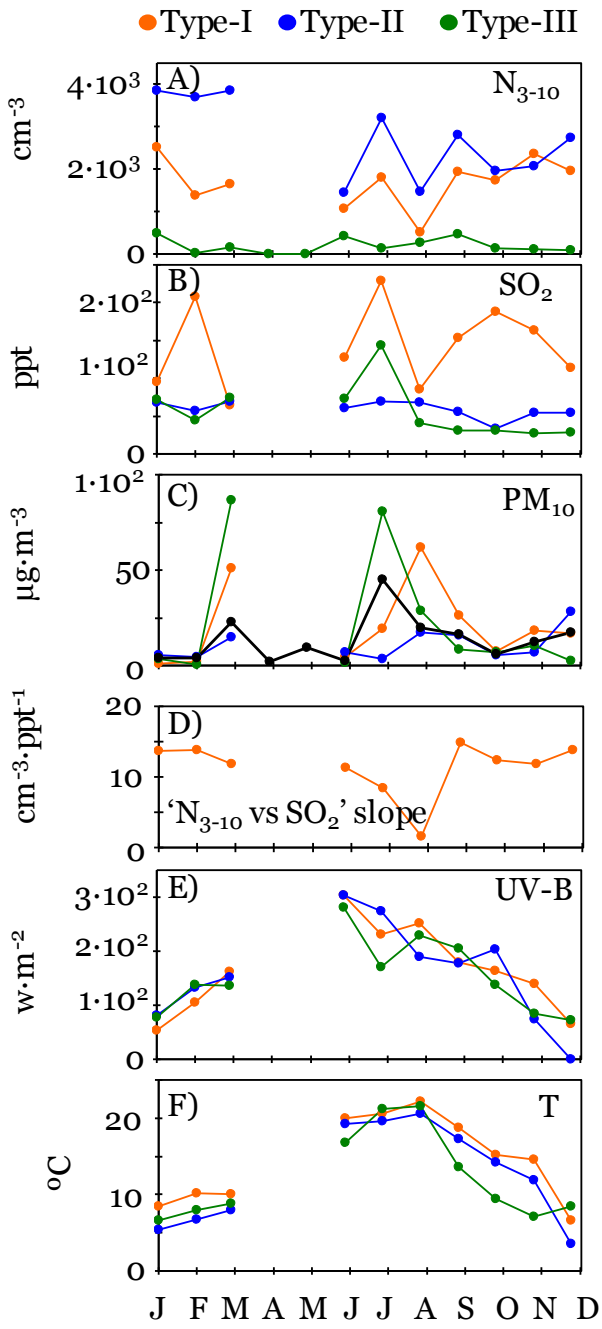

Figure 5.8 Monthly averaged values of N_{3-10}, SO_2, PM_{10}, the 'N_{3-10} versus SO_2" slope, UV-B radiation and temperature during the Type I, II and III events recorded during 2007. Black dot for PM_{10} (C) indicates monthly average calculated with all days/month

5.4.2 Surface of pre-existing particles as condensation sinks

The negative association of PM_{10} with PC-1 (Table 5.2) indicates that high surface area concentration (S) of pre-existing PM_{10} particles hinders the formation of 3 – 10 nm particles. Observe that S_{10} (surface area of particles less than 10 μm) is highly correlated with PM_{10} (Fig. 5.9a; owing to the fact that accumulation 0.1 – 1μm and coarse 1 – 10 μm mode particles are the main contributors to both the particle mass and surface area), whereas N_{3-10} concentrations and the "N_{3-10} versus SO_2" slope are negatively correlated with PM_{10} (Figs. 5.9a and b).

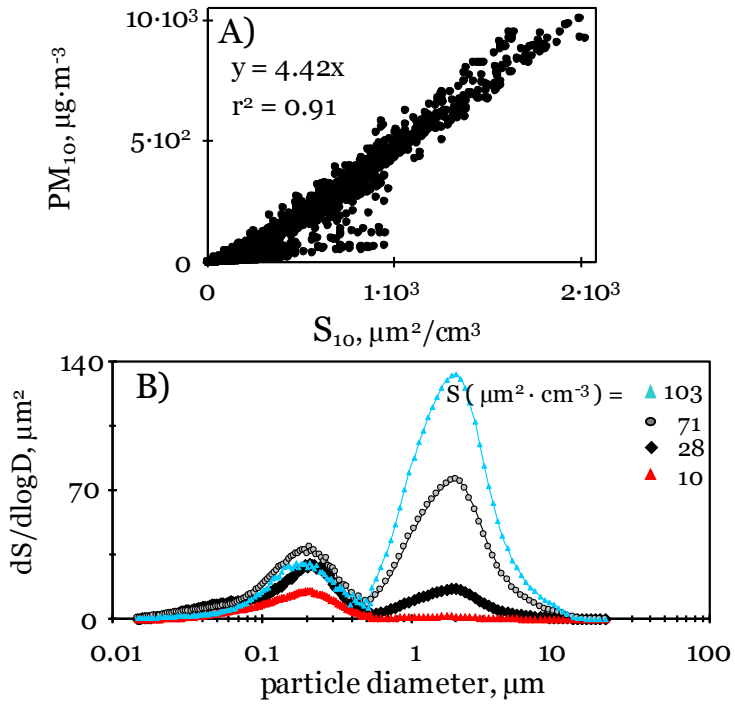

Figure 5.9 (A) PM_{10} versus S10 concentrations, and (B) dS/dlogD particle surface area size distribution associated to S values corresponding to percentiles 90th (103 m^2Ecm^{-3}), 75th (71 m^2Ecm^{-3}), 50th (23 m^2Ecm^{-3}) and 25th (10 μm^2Ecm^{-3}). Data recorded at Izaña from June to September 2007

NPF is observed on an almost day – to - day basis at Izaña (Fig. 5.3d), which is, in part, aided by the low S concentrations typically registered in the upward flows where these 3 – 10 nm particles are formed. The S_{10} concentrations typically registered at Izaña (median ~ 25 $\mu m^2\ cm^{-3}$; Table 5.4) are close to those observed in the mid and upper troposphere (S_{10}: 2 – 20 $\mu m^2\ cm^{-3}$; Schröder et al., 2002) and much lower than those registered in the boundary layer (e.g., S1 (S for submicron particles) ~ 450 $\mu m^2\ cm^{-3}$ in Northern Italy; Rodríguez et al., 2005). These low S concentrations (favouring nucleation in the upward flows) are facilitated by two main processes:

1) The low background S concentration in the free troposphere air masses found when the MBL air experiences the upward transport (mixes with it),

2) The cloud processing resulting in the aerosol activation, cloud droplet formation and scavenging, in the stratocumulus clouds during the upward transport of MBL air. This process typically results in the scavenging of particles ≥ 100 nm which is the most important contributors to the aerosol mass and surface area (Weber and Mc Murry, 1996; Henning et al., 2002). This "pre-existing particle" scavenging process in the upward flows (which is favoured by the fact that Izaña is regularly above cloud condensation level) accounts for two facts: i) the low PM_{10} concentrations (e.g. a median of 1.3 μg m^{-3} during 2007, Table 5.4) and low night-to-daylight increases in PM_{10} due to the upward flow regimen (~ 1 $\mu g m^{-3}$; Fig. 4.2D) at Izaña, and that ii) sea salt particles are not detected in the aerosol chemical composition at Izaña, even if sea salt concentrations are high in the marine boundary layer (~ 10 $\mu g m^{-3}$ in PM_{10} as an annual mean, Putaud et al., 2000; Alastuey et al., 2005). This in-cloud particle scavenging process was also observed in Mauna Loa and Puy de Dôme mounts (Weber and Mc Murry, 1996; Venzac et al., 2007). Moreover, this NPF link to low S concentrations in the outflows and/or surrounding area of clouds was also described by Kanawade and Tripathi (2006) and by Perry and Hobbs (1994) and Clarke et al. (1998) close to marine cumulus.

At Izaña, significant increases in the particle mass (PM_{10}) and surface (S_{10}) concentrations are registered during Saharan dust events (Chiapello et al., 1999; Maring et al., 2000; Alastuey et al., 2005), when hourly PM_{10} and S_{10} concentrations as high as 1,000 $\mu g \cdot m^{-3}$ and 200 $\mu m^2\ cm^{-3}$ have been recorded (e.g., Summer 2008, Fig.5.9a). These dust transport episodes typically occur in summer and sporadically in March (see monthly averaged PM_{10} levels in black dots in Fig. 5.8c). Observe in Fig. 5.9b and Table 5.4 that increases in S concentrations are mostly caused by an increase in surface area of coarse particles because of the coarse nature of the dust (coarse particles account for > 70% of S_{10} during dust events when S_{10} is > 100$\mu m^2 \cdot cm^{-3}$ and for < 20% of S when S_{10} is < 20 $\mu m^2 \cdot cm^{-3}$; Table 5.4). These high S concentrations of coarse particles during Saharan episodes hinder nucleation and favour condensation of gaseous precursors onto pre-existing particles. Furthermore, the surface of mineral dust has a strong affinity to absorb SO_2 and H_2SO_4 and consequently to decrease the concentrations of an important 3 – 10 nm particle precursor (Dentener et al., 1996; Alastuey et al., 2005). These processes result in a decrease in the "NPF rates" in the presence of dust particles and account for the observed negative correlation between PM_{10} and N_{3-10} (Fig. 5.10a) and between PM_{10} and the "N_{3-10} versus SO_2" slope (Fig. 5.9b). Observe that high PM_{10} concentrations: i) resulted in Type III events (low N_{3-10} concentrations) in July 2007, even when SO_2 levels during these episodes were high (~ 150 ppt; Fig. 5.8a, b and c), and ii) in August 2007 resulted in a decrease in the "N_{3-10} versus SO_2" slope and low N_{3-10} concentrations (Fig. 5.8a, c and d).

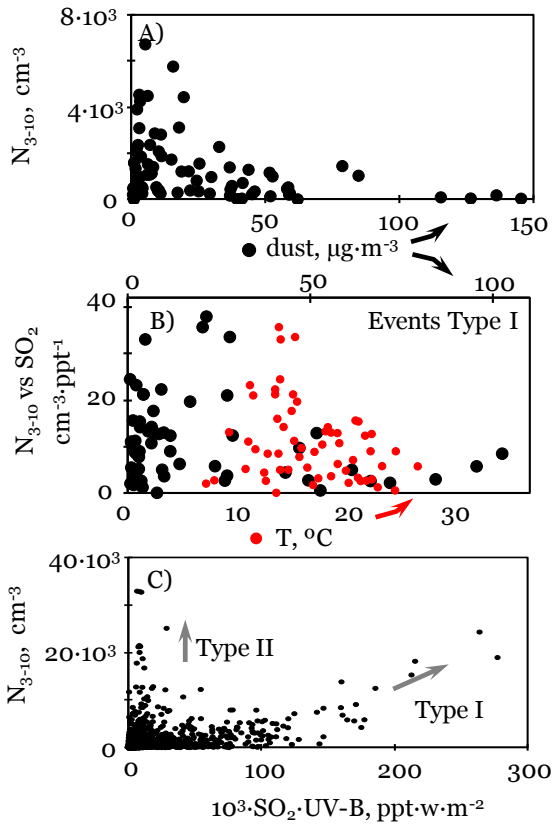

Figure 5.10 (A) $N_{3\text{-}10}$ versus PM_{10} concentrations (July to September 2007). (B) "$N_{3\text{-}10}$ versus SO_2" slope (events with $r^2 > 0.7$) versus PM_{10} and temperature. (C) $N_{3\text{-}10}$ versus SO_2·UV-B product.

5.4.3 Solar radiation

Solar radiation (G, DI, PAR and UV-B) did not show significant variations during the different types of event (e.g. UV-B in Fig. 5.7e). This is attributed to the fact that solar radiation intensity remains high above the stratocumulus layer. In the "N_{3-10} versus SO_2·UV-B product" plot shown in Fig. 5.10c, two regions are well defined. In the region attributed to Type I events, a linear relationship between N_{3-10} and the SO_2·UV-B product is observed. This linear relationship agrees with the results obtained in model simulations by Pirjola (1999), who showed that an increase in UV-B radiation results in an enhancement of SO_2 oxidation and new H_2SO_4 - H_2O particle production. These results suggest that radiation is not a limiting factor in activating OH production and the reactions resulting in the photo-oxidation of particle precursors in the free troposphere.

5.4.4 Temperature

Temperature had a clear influence on the NPF rates. Observe in Fig. 5.10b that high "N_{3-10} versus SO_2" slopes (> 20 cm^{-3} ppt^{-1}; indicating high NPF rates) were only registered when the temperature was ≤ 15ºC, whereas low "N_{3-10} versus SO_2" slopes (< 10 cm^{-3} ppt^{-1}) were observed when the temperature was > 20ºC. These results fit with those found by Easter and Peters (1994), who showed that the NPF rates due to binary H_2SO_4 - H_2O nucleation and condensational growth (which is considered an important NPF mechanism in the free troposphere; Kulmala and Kerminen, 2008) increased when temperature decreased. If it is assumed that stable clusters are always present in the atmosphere (as suggested by Kulmala and co-workers; Kulmala et al., 2005; Kulmala and Tammet, 2007), then the increase we observe in the "N_{3-10} versus SO_2" slope would indicate that clusters activation and growth is favoured at low temperature.

The influence of temperature on NPF in upslope winds has also been observed in other mountaintop observatories. At Norikura mount, high NPF rates were observed when upslope winds mixed with northern cold air above (Nishita et al., 2008). In Jungfraujoch mount, nucleation particles reached a maximum in winter (Weingartner et al., 1999). Siebert et al. (2004) observed high concentrations of 5 – 10 nm particles close to an inversion layer that attributed to the strong change in temperature and humidity experienced by the air mass when it crossed. This may occur in the inversion layer typically located below Izaña (just above the stratocumulus clouds).

5.5 N_{3-10} concentrations and seasonal evolution

N_{3-10} concentrations were significantly different during the different type of events. The monthly averaged values of N_{3-10} were within the range 1,000 – 2,500 cm^{-3} during Type I events, 2,000 – 4,000 cm^{-3} during Type II events and 400– 600 cm^{-3} during Type III events (Fig. 5.8a). Several processes may account for the fact that N_{3-10} concentrations are higher during Type II events than during Type I events:

i) PM_{10} and S_{10} concentrations were higher during Type I events (this favours condensation rather than nucleation in these events; Fig.5.8c),

ii) the temperature was higher during Type I events (this increases equilibrium vapour pressure and consequently hinders the gas to aerosol phase conversion; Fig. 5.8f), and

if Type I events are attributed to particle formation during upward transport and Type II attributed to in-situ formation, then coagulation processes during the transport may contribute to the drop in N_{3-10} concentrations.

Type III events occurred under free troposphere (low SO_2 and NO_y concentrations; Fig. 5.8b) or Saharan dust (high PM_{10} and surface area concentrations favourable for condensation; Fig. 5.8c) conditions. Conditions for reaching high rates of 3 – 10 nm particle formation were more favourable in winter than in summer.

The slightly higher values of the hourly "15^{th}, 25^{th} and 50^{th} percentiles of N_{3-10}" and the "averaged values of N_{3-10}" (Fig. 5.1d and f) recorded in the summer were caused by the lower frequency of Type III events (6 – 10 events·month^{-1} in summer and 11 – 17 events·month^{-1} in the other seasons; Table 5.3). In contrast, the "95^{th} and 90^{th} percentiles of N_{3-10}" reached higher values in autumn and winter (10,000 – 20,000 cm^{-3}) than in summer (5,000 cm^{-3}; Fig. 5.1e). This higher efficiency in the NPF mechanisms in winter is favoured by the lower temperature and the lower surface area of pre-existing PM_{10} particles (Fig. 5.8c). Observe that the monthly means of the "N_{3-10} versus SO_2" slope were lower in summer (2 – 8 cm^{-3} ppt^{-1}) than in autumn and winter (15 cm^{-3} ppt^{-1}; Fig. 5.7d).

5.6 Summary and Conclusions

A data set of aerosol size distribution, trace gases, a set of radiation components and meteorological data collected during 2007 – 2008 at Izaña Mountain observatory has been analysed with the aim of identifying the processes and conditions favouring the formation of 3 – 10 nm particles.

The development of orographic thermal-buoyant upward flows during daylight results in the upward transport of water vapour and trace gases emitted at low altitudes on the island by biogenic and anthropogenic sources. These airflows perturb the low free troposphere and result in high concentrations of 3–10 nm particles (N_{3-10} > 10,000 cm^{-3} have been recorded several times) due to new particle formation (NPF).

Two types of N_{3-10} event were observed. In Type I events, a linear relationship between N_{3-10} and SO_2 was observed (r^2 coefficients 0.70 – 0.95, a mean slope of 11 cm^{-3} ppt^{-1} and SO_2 concentrations within the range from tens to hundreds of ppt). These particles seem to be formed during the upward transport process, most probably within or after the outflows of the cloud layer (marine cumulus slightly perturbed by the topography of the island) typically located well below Izaña. During Type II events, 3 – 10 nm particles are formed in-situ around noon and during the afternoon probably due to condensation of vapours linked to photochemistry.

In both types of events, the low surface area (S) of pre-existing particles favoured NPF in the upward flows. Such low S concentrations are favoured by the scavenging of pre-existing particles in the stratocumulus layer typically located below Izaña.

Variations in temperature and in concentration of pre-existing particles influenced 3 – 10 nm particle formation. Because of the lower temperature and lower surface area of pre-existing particles, N_{3-10} concentrations were higher in Type II events than in Type I (even if SO_2 concentrations were higher in Type I events).

Moreover, the NPF efficiency was greater in winter owing to the lower temperature and the presence of coarse (Saharan) dust particles in summer. This resulted in higher "N_{3-10} versus SO_2" slopes in autumn-winter (up to 40 cm^{-3} ppt^{-1} in some events) than in summer (down to 2 cm^{-3} ppt^{-1} in some events). Our observations show that NPF is favoured in the boundary layer to the free troposphere transition region by the low surface area of pre-existing particles (prompted by in-cloud particle scavenging), the gaseous precursor transport during the upward flow regime, and the high solar radiation conditions above the marine cloud layer. The overall data analysis suggests that, although sulfuric acid participates in 3 – 10 nm particle formation, other vapours are likely involved in the particle formation during at least one of the two types of events segregated.

The few aerosol observations at elevated mountains reaching the low free troposphere worldwide, suggest that NPF is favoured in the boundary layer to free troposphere transition region. The influence of the environmental conditions on the nanoparticles formation observed in the upslope winds at Izaña, were also observed at other high mountain observatories (mentioned above). These field observations suggest that elevated mounts reaching the low free troposphere may act as source regions for new particles.

Chapter 6

Discussion

6. Discussion

Sources and processes contributing to ultrafine particles in ambient air

Two main sources and processes that contribute to ultrafine particles (UFPs) have been found in the study area: vehicle exhaust emissions and conversion of SO_2 to ultrafine sulphate.

Conversion of SO_2 to UFP was observed in sites close to the emission sources (in SCO at 200 metres and 2.5 km distant to the harbour and refinery, respectively) and in Izaña observatory (at 2.4 km above the emissions sources, usually located in the boundary layer). Figure 6.1 shows the daily evolution of the particle number (N) concentration, gaseous pollutants and solar radiation in Santa Cruz de Tenerife and in Izaña Observatories. In Santa Cruz, components N1 (related to primary emissions from vehicle exhausts) and N2 (linked to SO_2) are shown. In Izaña, components N1 and N2 were not determined for two reasons: 1) the N vs. BC relationship that allows the determination of N1 and N2 is not observed (Figure 6.2). This is attributed to the decrease in the UFP number concentration due to aging of the aerosol population by coagulation during the transport from the source emission (into the boundary layer) to Izaña, and 2) the absorption coefficient measurements at Izaña are not only affected by black carbon, but also by the iron oxides (hematite and goethite) contained in the Saharan dust frequently transported to the observatory (Andrews et al., 2011). Thus, the segregation of N1 and N2 in Izaña has no physical meaning. As shown in the previous section, UFPs observed in the upslope wind in Izaña are dominated by nucleation of the sulphate / sulphuric acid linked to the SO_2 photo-oxidation. Concentrations of SO_2 and NO_X (Figure 6.1) in Izaña Observatory (where these gases are linked to transport from the boundary layer) are 70 – 100 lower than in Santa Cruz Metropolitan Area (where these gases are linked to urban scale emissions). In Izaña total UFPs (N) exhibits a strongly marked daily evolution with a maximum during daylight. In Santa Cruz Metropolitan Area, component N2 exhibits a similar daily evolution. These results shows that photo-oxidation of SO_2 is a significant source of UFPs in the ambient air of sites located close and distant to the emission sources of SO_2.

These conclusions are supported by results obtained in other studies. In rural areas of the Po Valley (Italy), Hamed et al. (2007) found that SO_2 was involved in the ultrafine particle formation episodes. In Huelva (SW Spain), Fernández – Camacho et al. (2010) observed that the highest UFPs episodes were linked to fumigations of SO_2 of industrial origin. In Mauna Loa observatory, Weber et al. (1996) observed an increase in 2 - 5 nm particles, correlated with sulphuric acid, linked to the arrival of air from the boundary layer of Hawaii Island. The results of this study show that new particle formation is favoured when polluted air from boundary layer enters in the free troposphere. This is in agreement with UFP observations in mountain observatories such as Jungfraujoch (3,580ma.s.l., Switzerland), Mauna Loa (3,400ma.s.l., Hawaii), Khumbu (5,079ma.s.l., Nepal), Puy de Dôme (1,465ma.s.l.; France), Norikura (2,770ma.s.l.; Japan) and Lemmon (2,790ma.s.l., USA;

Weber et al., 1996; Weber and McMurry, 1996; Weingartner et al., 1999; Shaw et al., 2007; Nishita et al., 2008; Venzac et al., 2008, 2009).

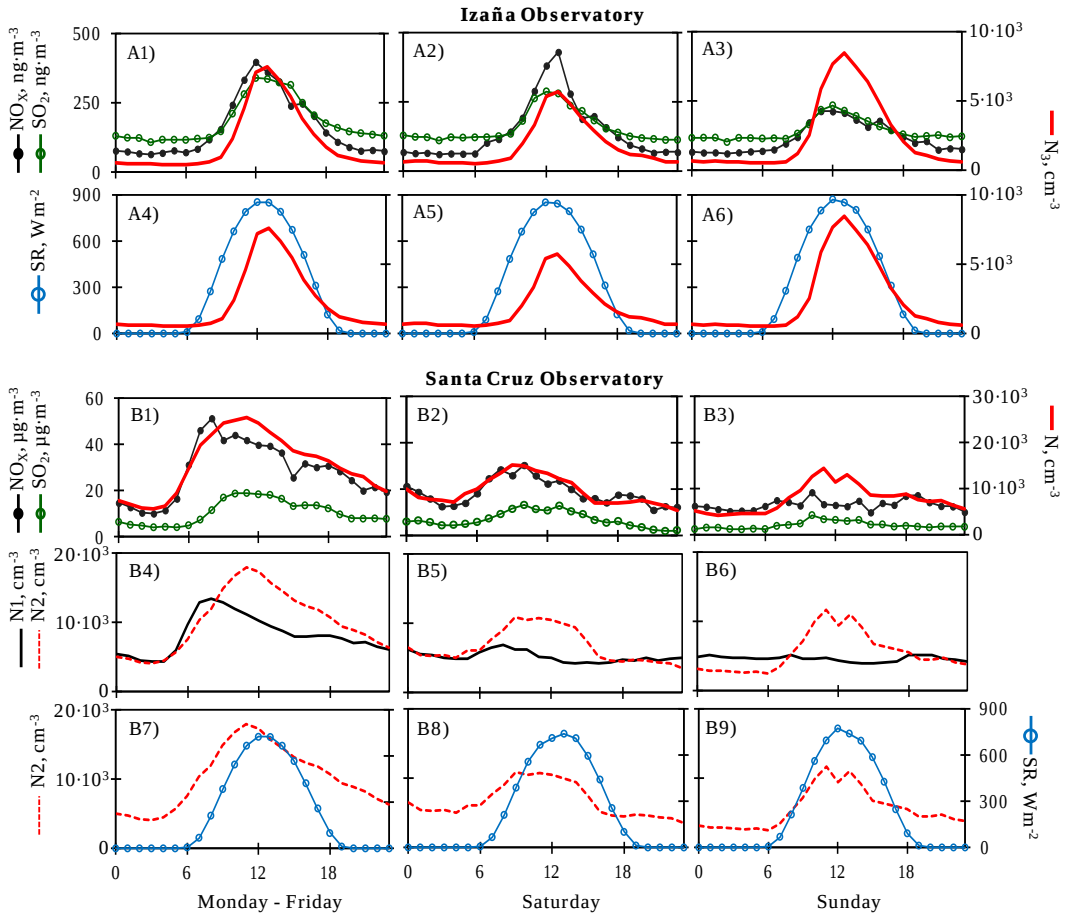

Figure 6.1 Daily cycle of SO_2, NO_X and N concentrations and solar radiation observed at Izaña and Santa Cruz Observatories. N1 and N2 particle number components at Santa Cruz are also shown

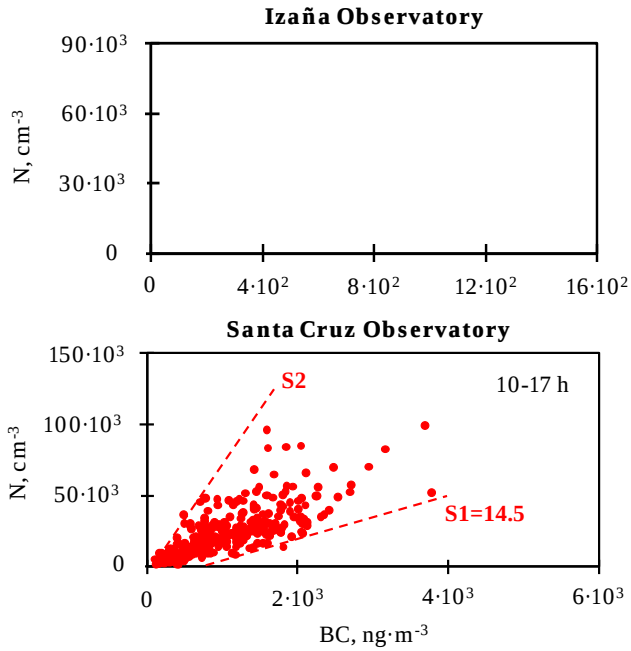

Figure 6.2 Relationship between BC and N concentrations observed at Izaña and Santa Cruz Observatories

The fact that photochemical processes may significantly contribute to UFPs also in urban ambient air seem to be a feature of the territories located in the southern part of Europe and/or the European Union. A recent research (Reche et al., 2011), to which this study also contributed, focused on identifying the processes affecting UFPs and black carbon (BC) concentrations in several cities (London - UK, Bern and Lugano in Switzerland, and Barcelona, Huelva and Santa Cruz de Tenerife in Spain), found that in cities of Central and Northern Europe UFPs and BC are linked to vehicle exhaust emissions, whereas in Barcelona, Huelva and Santa Cruz de Tenerife UFPs tend to show a maximum during the central part of the daylight not linked to vehicle exhausts. These results suggest that SO_2 to particle conversion may preferably occur by photochemistry (Seinfeld and Pandis, 1998) in the South of the EU and by wet chemistry processes (in cloud; Seinfeld and Pandis, 1998) in areas of Central and Northern Europe. This last case would not contribute to UFPs.

Ultrafine particles and urban air quality management

The results of this study show that additional emission sources to vehicle exhausts significantly contribute to UFPs in urban ambient air. In the Santa Cruz Metropolitan Area, the background of UFPs is dominated by vehicle exhaust emissions (typically associated with hourly means within the range 8,000- 15,000 cm^{-3}), being UFPs pollution events caused by the emissions of

the refinery (contributing with 5,000 – 70,000 cm^{-3}) and ships (contributing with 3,000 – 45,000 cm^{-3}). This has implications for the air quality management. Several studies have concluded that the exposure to UFPs is associated with an increased risk to suffer cardiovascular diseases (e.g., Stolzel et al., 2007; Araujo et al., 2009). This has also been observed in the Metropolitan Area of Santa Cruz de Tenerife. A recent study (Rodríguez-Domínguez et al., 2011) performed in this city by scientists of the University Hospital of the Canaries and the Izaña Atmospheric Research Centre, and based on the data set presented in this work, concluded that there is an association between hospital admission by heart failure and exposed UFPs in the ambient air.

Because of these adverse effects linked to exposure to UFPs, there is an opened debate about the need to introduce limit values for UFP concentrations in ambient air, and complement the current standards for PM_{10} and $PM_{2.5}$ (Second Position Paper on PM, 2004; COST 633 Report, 2009). In fact, vehicle exhaust emissions are already subject to limit values of UFPs in all the EU territory since September 2011 (EURO 5b). The results of this work indicate that at least two actions should be undertaken for decreasing UFP concentrations in the Metropolitan Area of Santa Cruz de Tenerife:

1) A reduction of SO_2 emissions from the refinery and ships. A drop in the emissions of this gaseous precursor of UFP would contribute to decrease UFP concentrations during pollution events linked to adverse meteorological conditions. This could also be applied to other areas with industrial emissions of SO_2. For example, in Huelva industrial city, it has been observed that vehicle exhausts also accounts for the urban background of UFPs, being the pollution events prompted by the fumigations of the SO_2 plume linked to the emissions from a refinery, a Cu smelter and a phosphoric acid production plants. The works of Yu (2010) and Stevens et al. (2012) also highlights the relevance of the industrial SO_2 emissions in the UFPs formation.

2) A reduction of the vehicle exhausts emissions. This would contribute to decrease the urban background concentrations of UFPs along the year, or in a long term basis. Some of the measurements that are already being taken in some European cities are: the creation of Low Emission Areas, the prohibition of entry to old vehicles in the city centre, and the reduction of sulfur in fuels. The benefits of these actions have been clearly demonstrated some cities, such as London and Birmingham (Jones et al., 2012). These actions, including the use of the so-called 'sulphur free fuels' (< 10 ppm of S in diesel and super-unleaded petrol) resulted in a decrease in UFPs between 30 and 60% in a period of few months in these two British cities. The fuels currently used in the Santa Cruz Metropolitan Area have a sulphur content of about 10 ppm (Directive 2002/80/EC).

It is believed that different type of particles may exhibit different type of health effects, depending on their size and chemical composition (Araujo et al., 2009). As result of this works, it is

recommended to implements air quality monitoring programs for particulate matter based on the simultaneous monitoring of:

- Ultrafine particles (<0.1 µm), measured in terms of total number concentration. This metric present high values in scenarios of fresh vehicle exhaust emissions and during formation of particles in SO2 plumes. These particles typically exhibit a short live time due to coagulation and deposition processes. They allow identifying fresh emissions.

- Black Carbon, measured in terms of light absorption and then converted to mass concentration. Although in some periods and some locations, emissions from ships and industrial sources may also contribute to black carbon, this metric is mostly representative of fresh vehicle exhaust emissions of solid particles, mostly with an initial size of about 0.1 µm (Rose et al., 2006). Because of the fast deposition processes, these particles also exhibit a short live time (they accounts for the black soiling of building).

- $PM_{2.5}$. This metric is representative of (i.e. tend to show high values) of aged polluted air, in which high mass concentrations of the accumulation mode particles occurs due to condensation and coagulation processes (Raes et al., 2000). It is complementary to ultrafine and black carbon concentrations. In a study performed in Milan, Barcelona and London, Rodríguez et al. (2007) observed that low ultrafine and high concentrations of $PM_{2.5}$ particles were observed when urban polluted air stagnated over the study cities, being in these cases observed a high particle growth due to coagulation and condensation of ammonium-nitrate, ammonium-sulphate and organic matter.

- PM_{10}. This metric includes $PM_{2.5}$ plus coarse mode particles (2.5 – 10 µm) linked to anthropogenic (road dust, demolition mass, cement factories, etc...) and natural (desert dust or sea salt) emissions.

Some of these metrics, such as PM_{10} and $PM_{2.5}$ are already included in the air quality monitoring programs of the European Union, whereas other metrics such as UFP and black carbon are not mandatory. The simultaneous measurements of these metrics would allow a better understating, for the air quality manager, on the sources and processes that contribute to the urban air quality impairment by particulate matter. Moreover, such data base in a long term basis (years) would allow to epidemiologist to better understand how different type of particles may prompt different cardiovascular diseases.

Long range transport

The results if this study shows how long range transport processes in the low free troposphere in Tenerife influence on levels of O_3 and CO. Because of the short life time of SO_2 and NO_X, these long range transport processes from North America and/or Europe do not result in concentrations of SO_2 and NO_X above the detection limit of the analyzers used in this study. At Izaña, night time concentrations of UFPs are similar to those registered in other mountain sites placed in the free troposphere, i.e. ~500 cm^{-3} (Weber and McMurry, 1996; Schröder et la., 1997, Weingartner et al., 1999; Venzac et al., 2008; 2009).

This is the first study in which long term time series (4 years) of O_3 and CO are analysed in the North Atlantic free troposphere. Previous analysis have focused only in long term O_3 concentrations (Rodríguez et al., 2004) or in the relationship between O_3 with radio-nuclei tracers of the high troposphere (^{7}Be) and the earth's crust (^{210}Pb) in short periods (Reiter et al., 1983; Cuevas, 1995; Prospero et al., 1995; Cuevas et al., 2000a, Li et al., 2002). The results show that westward exportation of pollution from the North America exert a significant influence in the variability of O_3 and CO in the North Atlantic free troposphere. Moreover, rapid downward transport of O_3 from the upper troposphere results in high concentrations and high O_3/CO ratios. The contribution of these two sources was also identified during the North Atlantic Regional Experiment (NARE) in the flights sampling the low free troposphere over the western North Atlantic Ocean (e.g., Parrish et al., 2000). The westward exportation of O_3 from North America contributes to O_3 levels in Europe (e.g. Li et al., 2002; Prather et al., 2003). This westward O_3 trans-Atlantic transport, also observed in Pico observatory (at 2,225 m.a.s.l. in Azores, Honrath et al., 2004), mostly occurs between 30°N and 45°N (Hegarty et al.; 2009), being more efficient in the middle and upper free troposphere due to higher wind speeds (Stohl, 2001; Stohl et al., 2002).

Chapter 7

Conclusions

7.1 Conclusions

SOURCES AND PROCESSES AFFECTING CONCENTRATIONS OF REACTIVE GASES IN TENERIFE

Concentrations of the studied primary reactive gases (SO_2, NO_X and CO) are affected by fresh emissions and atmospheric transport.

In the Metropolitan Area of Santa Cruz de Tenerife, vehicle exhausts, ships and the oil refinery are the main sources of primary reactive gases. Transport and dispersion in the city is predominantly influenced by the coastal sea breeze circulation (inland during daylight and slight seaward transport at night). Air pollutants transport through the Island is influenced by orographic circulations coupled with trade winds, which typically results in southward transport.

At the Izaña mountain observatory, concentrations of SO_2, NO_X, CO are 54, 167 and 1.6 times lower than in the Metropolitan Area of Santa Cruz de Tenerife as average, respectively. At this site, concentrations of reactive gases are influenced by two main processes: upward transport from the boundary layer and a synoptic scale long range transport. The upward transport from the boundary layer to the low free troposphere is linked to the development of buoyant orographic upward flows during daylight. This upward transport results in a sharp increase in the concentrations of NO_X and SO_2. Mean daylight to night-time ratios of ~3 for NO_X, ~2 for SO_2, ~1 for CO and <1 for O_3 are observed. As average, the 75% of NO_X, 50% of SO_2 and 4% of the CO recorded during daylight are attributed to the upward transport from the boundary layer to Izaña. At night, the downward transport of air from the free troposphere results in extremely low concentrations of NO_X (< in 50 ppt 37% of time) and SO_2 (< in 50 ppt 92% of time). This results in a slight decrease in CO concentrations and in increases in O_3 concentrations prompted by the vertical gradient of this grace gas in this region.

PROCESSESS AFFECTING CARBON MONOXIDE AND OZONE CONCENTRATIONS IN THE FREE TROPOSPHERE

The results obtained in the analysis of 4 years data (2007-2010) shows that the variability in the concentrations of CO and O_3 in the free troposphere is modulated by the eastward exportation and trans-Atlantic transport of pollutants from North America. In this frequent scenario, O_3 typically shows concentrations within the range 34 - 76 ppb and O_3 / CO ratios within the range 0.2 - 0.7. In addition to these O_3 pollution episodes, events of high O_3 concentrations (47 – 87 ppb), high O_3 / CO ratios (0.7 – 6.5) and low correlations between O_3 and CO occur in late spring and summer. These events are associated with downward transport of air from the upper troposphere in the eastern side of depressions developing in the Eastern North Atlantic.

SOURCE CONTRIBUTION TO ULTRAFINE PARTICLES IN THE METROPOLITAN AREA OF SANTA CRUZ DE TENERIFE

In urban areas, other sources than vehicle exhaust may significantly contribute to ultrafine particles (UFPs) concentrations. This is the case of the Metropolitan Area of Santa Cruz de Tenerife, where it is concluded that vehicle exhaust emissions dominate the urban background of UFPs, being UFPs episodes induced by the emissions of ships and the refinery:

- when UFPs (24-h mean) are present in concentrations within the range 2,000–20,000 cm^{-3} (0.1^{th}-70^{th} percentile), vehicle exhausts is the dominant source, accounting for 85% of the observed ultrafine particle concentrations. Higher concentrations (i.e. >70^{th} up to 56,000 cm^{-3}) are linked to the contributions of ship and refinery emissions.

- UFP pollution events tend to occur during daylight (10:00 to 17:00 GMT), when ship emissions typically accounts for 39% of UFPs when their concentrations are within the range 19,500 – 46,700 cm^{-3} (percentile 55^{th} – 90^{th}), whereas the refinery typically accounts for 60% of UFPs with concentrations within the range 46,700 – 99,100 cm^{-3} (percentile 95^{th} – 100^{th}). Below 19,500 cm^{-3} (percentile 55^{th}), vehicle exhausts accounted for 91% of UFPs in this period.

SOURCES AND PROCESSES AFFECTING ULTRAFINE PARTICLES IN TENERIFE

Although ultrafine particles (UFPs) have a short life time (~hours), they may be formed in sites close and distant to the source emission of the gaseous precursors. The overall results of this study show that emissions of SO_2 play a key role as agent that tend to increase UFP concentrations. In the Metropolitan Area of Santa Cruz de Tenerife, the fraction of UFPs linked to SO_2 (as gaseous precursor) shows a daily evolution with a broad maximum during daylight. At Izaña mountain observatory, total UFP concentrations also exhibit a daily evolution with a maximum during daylight. This maximum is linked to the arrival of SO_2 from the boundary layer, owing to the development of diurnal buoyant airflows. In both cases, photochemical conversion of SO_2 to ultrafine sulphate is an important source of UFPs.

The field observations of this study points that elevated mounts that reaches the low free troposphere may act as source regions for new particles. New particle formation is favoured in the boundary layer to the free troposphere transition region by the low surface area of pre-existing particles (prompted by in-cloud particle scavenging), the gaseous precursor transport during the upward flow regime, and the high solar radiation conditions above the marine cloud layer typical of subtropical oceanic regions. This may contribute to the fact that the 'Izaña to Santa Cruz de Tenerife' ratio is higher for UFPs (0.25) than for SO_2 (0.02).

STRATEGIES FOR AIR QUALITY MANAGMENT

These results have important implications to be considered by air quality managers. First, most of studies on UFPs and urban air quality have focused on vehicle exhaust emissions. In fact, vehicle exhaust is the only source subject to limit values for emissions of UFPs. The results of this research clearly demonstrate that SO2 emissions result in high concentrations of UFPs (frequently higher than those linked to vehicle exhaust emissions). Because of these high SO2 emissions, UFPs in Santa Cruz Metropolitan Area exhibit features (e.g. daily evolution, typical concentrations ranges, UFP to black carbon ratio) different to those observed in cities where vehicle exhausts are the predominant UFPs source (e.g. London, Milan, Lugano or Bern). The influence of SO2 emissions on UFPs concentrations is observed even at distant sites from the SO2 emission sources, as it is demonstrated with the data collected at Izaña observatory. Second, about the open debate on if the current limit values for PM_{10} and $PM_{2.5}$ should be complemented, this study concludes that the simultaneous monitoring of ultrafine, black carbon, PM_{10} and $PM_{2.5}$ particles is a suitable strategy for tracing aerosol pollutants of different nature (fresh vs. aged) and of different sources: 1) UFPs are a better tracer of the fresh emissions of vehicle exhaust, ship and refinery, than $PM_{2.5}$ and $PM_{2.5-10}$, 2) $PM_{2.5}$ is significantly influenced by aged aerosols, 3) black carbon was found to be the better tracer of solid particles emitted by vehicle exhausts. To include UFPs measurements is of especial relevance. A recent research, based on the data set produced in this study, concluded that there is an association between hospitalizations due to heart failure and exposure to UFPs in the ambient air of the study city.

7.2 Future Research lines

The next steps that are considered to be followed right after this work are numbered in the following lines:

1) Identification of organic gaseous compounds linked to ship and refinery emissions that may contribute to ultrafine particles
2) Quantification of the contribution of organic gaseous compounds (linked to ship and refinery emissions) to ultrafine particles
3) Standardization of methods of ultrafine particle measurements for air quality purposes
4) Quantification of the contribution of role of biogenic emissions to ultrafine particles in Izaña
5) Quantification of the new particle formation and growth rates

References

Agrawal, H., Malloy, Q.G.J., Welch, W.A., Miller, J.W., Cocker III, D.R., In-use gaseous and particulate matter emissions from a modern ocean going container vessel, Atmospheric Environment, 42, 5504-5510, 2008.

Alastuey, A., Querol, X., Castillo, S., Escudero, M., Avila, A., Cuevas, E., Torres, C., Romero, P. M., Expósito, F., García, O., Díaz, J. P., Van Dingenen, R., and Putaud, J. P., Characterization of TSP and $PM_{2.5}$ at Izaña and Santa Cruz de Tenerife (Canary Islands, Spain) during a Saharan Dust Episode (July 2002), Atmos. Environ., 39, 4715–4728, 2005.

Alfaro, S.C., Lafon, S., Rajot, J.L., Formenti, P., Gaudichet, A., and Maille, M., Iron oxides and light absorption by pure desert dust: An experimental study. J. Geophys. Res.-Atmos., 109, 8, D08208, doi: 10.1029/2003JD004374, 2004.

Allan, J. D., Alfarra, M. R., Bower, K. N., Coe, H., Jayne, J. T., Worsnop, D. R., Aalto, P. P., Kulmala, M., Hÿotyläinen, T., Cavalli, F., and Laaksonen, A., Size and composition measurements of background aerosol and new particle growth in a Finnish forest during QUEST 2 using an Aerodyne Aerosol Mass Spectrometer, Atmos. Chem. Phys., 6, 315–327, 2006, http://www.atmos-chem-phys.net/6/315/2006/.

Andreae, M.O., Elbert, W., Gabriel, R., Johnson, D.W., Osborne, S., and Wood, R., Soluble ion chemistry of the atmospheric aerosol and SO_2 concentrations over the eastern North Atlantic during ACE-2, Tellus, 52B, 1066–1087, 2000

Andrews, E., Ogren, J.A., Bonasoni, P., Marinoni, A., Cuevas, E., Rodríguez, S., Sun, J.Y., Jaffe, D.A., Fischer, E.V., Baltensperger, U., Weingartner, U., Collaud Coen, M., Sharma, S., Macdonald, A.M., Leaitch, W.R., Lin, N.H., Laj, P., Arsov, T., Kalapov, I., Jefferson, A., Sheridan, P., Climatology of Aerosol Radiative Properties in the Free Troposphere, Atmospheric Research, 102, 365–393, 2011.

Araujo, J. A. and Nel, A. E., Particulate matter and atherosclerosis: role of particle size, composition and oxidative stress, Particle and Fibre Toxicology, 6(24), doi:10.1186/1743-8977-6-24, 2009.

Araujo, J.A., Barajas, B., Kleinman, M., Wang, X., Bennett, B.J., Gong, K.W., Navab, M., Harkema, J., Sioutas, C., Lusis, A.J., Nel, A.E., Ambient particulate pollutants in the ultrafine range promote early atherosclerosis and systemic oxidative stress, Circulation Research, 102, 5, 589-596, 2008.

Arnold, F., Pirjola, L., Aufmhoff, H., Schuck, T., Lähde, T., and Hämeri, K., First gaseous sulphuric acid measurements in automobile exhaust: Implications for volatile nanoparticle formation, Atmos. Environ., 40, 7097–7105, 2006.

Arnott, W. P., Hamasha, K., Moosmüller, H., Sheridan, P. J., Ogren, J. A., Towards aerosol light-absorption measurements with a 7-wavelength aethalometer: Evaluation with a photoacoustic instrument and 3-wavelength nephelometer, Aerosol Sci. Tech., 39, 17–29, 2002.

Ashbaugh, L.L., Malm, W.C., Sadeh, W.Z., A residence time probability analysis of sulfur concentrations at Grand Canyon National Park, Atmos. Environ., 19,1263-1270, 1985.

Atherton, C.S., Sillman, S. and Walton, J., Three-dimensional global modeling studies of the transport and photochemistry over the North Atlantic Ocean, J. Geophys. Res. 101 (D22), 1996; doi: 10.1029/96JD01062. issn: 0148-0227.

Balzani Lööv, J.M., Henne, S., Legreid, G., Staehelin, J., Reimann, S., Prévôt, A.S.H., Steinbacher, M. and Vollme M.K., Estimation of background concentrations of trace gases at the Swiss Alpine site Jungfraujoch (3,580 m asl), J. Geophysical Res., vol. 113, D22305, doi:10.1029/2007JD009751, 2008.

Benson, D. R., Li-Hao Young, , Shan-Hu Lee, , Campos, T. L., Rogers, D. C., and Jensen, J., The effects of air mass history on new particle formation in the free troposphere, case studies, Atmos. Chem. Phys., 8, 3015–3024, 2008.

Birch, M.E. and Cary, R.A., Elemental carbon-based method for monitoring occupational exposure to particulate diesel exhaust, Aerosol Sci. Tech., 25, 221–241, 1996.

Bond, T. C., Anderson, T. L., and Campbell, D., Calibration and intercomparison of filter-based measurements of visible light absorption by aerosols, Aerosol Sci. Tech., 30, 582–600, 1999.
Bond, T.C., Bergstrom, R.W., Light absorption by carbonaceous particles: An investigative review. Aerosol Science and Technology 40, 1, 27-67, 2006, doi: 10.1080/02786820500421521.
Boy, M., and Kulmala, M., Nucleation events in the continental boundary layer: influence of physical and meteorological parameters, Atmos. Chem. Phys., 2, 1–16, 2002.
Brown, L.M., Collings, N., Harrison, R.M., Maynard, A.D. and Maynard, R.L., Ultrafine particles in the atmosphere: introduction, Phil. Trans. R. Soc. Lond. A 358, 2563 - 2565, 2000, doi: 10.1098/rsta.2000.0668
Burtscher, H. Physical characterization of particulate emissions from diesel engines: a review, Aerosol Sci. Tech., 36, 896–932, 205.
Cabada, J., Khlystov, A., Wittig, A., Pilinis, C. and Pandis, S., Light scattering by fine particles during the Pittsburgh Air Quality Study: Measurements and modeling. Journal of Geophysical Research 109 (D16): doi: 10.1029/2003JD004155. issn: 0148-0227, 2004.
Casati, R., Scheer, V., Vogt, R., and Benter, T., Measurement of nucleation and soot mode particle emission from a diesel passenger car in real world and laboratory in situ dilution, Atmos. Environ., 41, 2125–2135, 2007.
Castillo, S., PhD, Impacto de las masas de aire africano sobre los niveles y composición del material particulado atmosférico en Canarias y en la Península Ibérica, Polytechnic University of Catalonia, 2006.
CEPSA, Industrial Group web page, www.cepsa.es., Last access: February 2011.
Charron, A. and Harrison, R.M., Primary particle formation from vehicle emissions during exhaust dilution in the roadside atmosphere, Atmospheric Environment, 37, 4109–4119, 2003.
Cheung, H. C., Morawska, L., and Ristovski, Z. D., Observation of new particle formation in subtropical urban environment. Atmos. Chem. Phys., 11, 3823-3833, 2011; doi:10.5194/acpd-11-3823-2011.
Chiapello, I., Prospero, J. M., Herman, J. R., and Hsu, N. C., Detection of mineral dust over the North Atlantic Ocean and Africa with Nimbus 7 TOMS, J. Geophys. Res., 104, 9277–9291, 1999.
Choi, Y., Kim, J., Eldering, A., Osterman, G., Yung, Y.L., Gu, Y., Liou, K.N., Lightning and anthropogenic NO_X sources over the United States and the western north Atlantic Ocean: impact on OLR and radiative effects. Geophysical Research Letters 36, L17806, 2009.
Clarke, A. D., Varner, J. L., Eisele, F., Maudin, R. L., Tarnner, D., and Litchy, M., Particle production in the remote marine Atmosphere, cloud outflow and subsidence during ACE-1, J. Geophys. Res., 103, 16396–16409, 1998.
Clarke, A. D., Varner, J. L., Eisele, F., Maudin, R. L., Tarnner, D., and Litchy, M., Particle production in the remote marine Atmosphere, cloud outflow and subsidence during ACE-1, J. Geophys. Res., 103, 16396–16409, 1998.
Collaud Coen, M., Weingartner, E., Apituley, A., Ceburnis, D., Fierz-Schmidhauser, R., Flentje, H., Henzing, J. S., Jennings, S. G., Moerman, M., Petzold, A., Schmid, O., and Baltensperger, U., Minimizing light absorption measurement artifacts of the Aethalometer: evaluation of five correction algorithms, Atmos. Meas. Tech., 3, 457–474, 2010, doi:10.5194/amt-3-457-2010.
Comrie, A.C., Tracking ozone: air-mass trajectories and pollutant source regions influencing ozone in Pennsylvania forests, Annals of the Association of American Geographers, 84, 635-651, 1994.
COST Report 633, Particulate matter: Properties related to health effects, 2009
Creilson, J.K., Fishman, J., and Woznia, A.E., Intercontinental transport of tropospheric ozone: a study of its seasonal variability across the North Atlantic utilizing tropospheric ozone residuals and its relationship to the North Atlantic Oscillation, Atmos. Chem. Phys., 3, 2053–2066, 2003

Cuevas, E., Diamantino V.H., Sancho, J.M., Stratosphere-Troposphere Exchange events over North Atlantic subtropical region, Proc. 2ª Asamblea Hispano Portuguesa de Geodesia y Geofisica, Lagos (Portugal), 8-12 febrero 2000, 451-452, 2000a.

Cuevas, E., Díaz, A., Martín, F., Atmospheric Carbon Dioxide Concentration at Izaña BAPMoN Observatory, Canary Islands, 1984-90, Proceedings 19th ITM on Air Pollution Modelling and its Application, NATO/CCMS, Ierapetra, Greece, 1991.

Cuevas, E., Estudio del Comportamiento del Ozono Troposférico en el Observatorio de Izaña (Tenerife) y su relación con la Dinámica Atmosférica, Memoria de Tesis Doctoral, Facultad de Ciencias Físicas, Universidad Complutense de Madrid, 1995.

Dentener, F., Carmichael, G. R., Zhang, Y., Lelieveld, J., and Crutzen, P. J., Role of mineral dust as a reactive surface in the global Atmosphere, J. Geophys. Res., 101, 22869–22889, 1996.

DGT Report, Dirección General de Tráfico, Informe de parque de vehículos, 2010. http://www.dgt.es/portal/es/seguridad_vial/estadistica/.

Dockery, D., Pope, A., Epidemiology of acute health effects: summary of time-series studies. In: Wilson, R., Spengler, J.D. (Eds.), Particles in Our Air: Concentration and Health Effects. Harvard University Press, Cambridge, MA, USA, pp. 123–147, 1996.

Domínguez-Rodríguez, A., Abreu-Afonso, J., Rodríguez, S., Juárez-Prera, R. A., Arroyo-Ucar, E., Jiménez-Sosa, A., González, Y., Abreu-González, P., Avanzas, P., Comparative Study of Ambient Air Particles in Patients Hospitalized for Heart Failure and Acute Coronary Syndrome, Rev. Esp. Cardiol.;64, 8, 661–666, 2011.

Draxler, R. R. and Rolph, G. D., HYSPLIT (HYbrid Single-Particle Lagrangian Integrated Trajectory), NOAA Air Resources Laboratory, Silver Spring, MD, 2003. Model access via NOAA ARL READY Website: http://www.arl.noaa.gov/ready/hysplit4.html.

Easter, R.C., Peters, L.K., Binary homogeneous nucleation: temperature and relative humidity fluctuations, nonlinearity and aspects of new particle production in the atmosphere. J. Applied Meteorology 33, 775–784, 1994.

Eisele, F.L., and Mc Murry, P.H., Recent Progress in Understanding Particle Nucleation and Growth, Philos, T. Roy. Soc. London B., 352, 1350, 191–200, 1997.

EU Directive 2008/50/EC of the European parliament and of the council of 21 May 2008 on ambient air quality and cleaner air for Europe.

Farman, J.C., Gardiner, B.G., and Shanklin, J.D., Large losses of total ozone in Antarctica reveal seasonal ClO_X/NO_X interaction, Nature 315, 207 – 210, 1985; doi:10.1038/315207a0

Fernández-Camacho, R., Rodríguez, S., de la Rosa, J., Sánchez de la Campa, A.M., Viana, M., Alastuey, A., and Querol, X., Ultrafine particle formation in the inland sea breeze airflow in Southwest Europe, Atmos. Chem. Phys., 10, 9615-9630, 2010.

Fiedler, V., Dal Maso, M., Boy, M., Aufmhoff, H., Hoffmann, J., Schuck, T., Birmili, W., Hanke, M., Uecker, J., Arnold, F., and Kulmala, M., The contribution of sulphuric acid to atmospheric particle formation and growth, a comparison between boundary layers in Northern and Central Europe, Atmos. Chem. Phys., 5, 1773–1785, 2005.

Franck, U., Odeh, S., Wiedensohler, A., Wehner, B., Herbarth, O., The effect of particle size on cardiovascular disorders — The smaller the worse, Science of the Total Environment, Sci. Total Environ., 409 (20) 4217-21.

Fruin, S.A., Winer, A.M., & Rodes, C.E., Black carbon concentrations in California vehicles and estimation of in-vehicle diesel exhaust particulate matter exposures. Atmospheric Environment, 38, 4123–4133, 2004.

GAW, Strategy for the Implementation of the Global Atmosphere Watch Programme (2001 – 2007). No 142, A contribution to the Implementation of the WMO Long-Term Plan WMO TD. No 1077, 2001a.

GAW, WMO Global Atmosphere Watch, No. 172, Strategic Plan: 2008 – 2015, 2007.

GAW, World Meteorological Organization Global Atmosphere Watch. No. 165. Report of the CAS WORKING GROUP on Environmental Pollution and Atmospheric Chemistry and the GAW 2005 Workshop (Geneva, Switzerland, 14-8, March 2005.

Gilge, S., Plass-Duelmer, C., Fricke, W., Kaiser, A., Ries, L., Buchmann, B., and Steinbacher, M., Ozone, carbon monoxide and nitrogen oxides time series at four alpine GAW mountain stations in central Europe, Atmos. Chem. Phys., 10, 12295 – 12316, 2010

Gómez-Moreno, F.J., Sastre, M., Artíñano, B., Piñeiro, M., López Mahía, P., Pey, J., Ripoll, A., Alastuey, A., Sorribas, M., Fernández, M., De la Morena, B., Trujillo de Cabo, J.L., Rodríguez, S. The Spanish Network on Environmental DMAs: Introduction and main activities, IV Reunión Española de Ciencia y Tecnología de Aerosoles. Granada, Spain, 28-30 June 2010.

González Y., Implantación y Operación de un Programa de Observación de Gases Reactivos para Estudios Atmosféricos y Vigilancia de la Calidad del Aire: Resultados Preliminares. Diploma de Estudios Avanzados, Departamento de Física Básica, Universidad de La Laguna, 2006.

Guerra, J.-C.¸Rodríguez, S., Arencibia, M.-T., García, M.-D., Study on the formation and transport of ozone in relation to the air quality management and vegetation protection in Tenerife (Canary Islands), Chemosphere 56, 1157–1167, 2004.

Hamed, A., Joutsensaari, J., Mikkonen, S., Sogacheva, L., Dal Maso, M., Kulmala, M., Cavalli, F., Fuzzi, S., Facchini, M.C., Decesari, S., Mircea, M., Lehtinen, K.E.J., Laaksonen, A., Nucleation and growth of new particles in Po Valley, Italy, Atmos. Chem. Phys., 7, 355-376, 2007.

Hamed, A., Joutsensaari, J., Mikkonen, S., Sogacheva, L., Dal Maso, M., Kulmala, M., Cavalli, F., Fuzzi, S., Facchini, M.C., Decesari, S., Mircea, M., Lehtinen, K.E.J., Laaksonen, A., Nucleation and growth of new particles in Po Valley, Italy; Atmos. Chem. Physic., 7, 335-376, 2007.

Harris, J.S., and Maricq, M.M., Signature size distributions for diesel and gasoline engine exhaust particulate matter, J. Aerosol Sci., 32, 749-764, 2001.

Harrison, R.M., Jones, A.M., Multisite study of particle number concentrations in urban air. Environmental Science and Technology 39, 6063–6070, 2005.

Hegg, D. A., Radke, L. F., and Hobbs, P. V., Measurements of aitken nuclei and cloud condensation nuclei in the marine Atmosphere and their relation to the DMS- cloud-climate hypothesis, J. Geophys. Res., 96, 18727–18733, 1991.

Henning, S.,Weingartner, E., Schmidt, S.,Wendisch, M., Gäggeler, H. W., and Baltenspenger, U., Size-dependent aerosol activation at the high-alpine site Jungfraujoch (3580ma.s.l.), Tellus, 54B,82–95, 2002.

Hermann, M., Heintzenberg, J., Wiedensohler, A., Zahn, A., Heinrich, G., and Brenninkmeijer, C. A. M., Meridional distributions of aerosol particle number concentrations in the upper troposphere and lower stratosphere obtained by Civil Aircraft for Regular Investigation of the Atmosphere Based on an Instrument Container (CARIBIC) flights, J. Geophys. Res., 108, 4114, 2003, doi,10.1029/2001JD00107.

Hernández, F., Alonso-Pérez, S., Hernández-Armas, J., Cuevas, E., Karlsson, L., Romero-Campos, P.M., Influence of major African dust intrusions on the 137Cs and 40K activities in the lower atmosphere at the island of Tenerife, Atmospheric Environment 39, 4111–4118, 2005b.

Hernández, F., Rodríguez, S., Karlssona, L., Alonso-Pérez, S., López-Pérez, M., Hernández-Armas, J.¸ Cuevas, E., Origin of observed high 7Be and mineral dust concentrations in ambient air on the Island of Tenerife, Atmospheric Environment, 42, 4247–4256, 2008.

Hidy G.M., Atmospheric Sulphur and Nitrogen Oxides, Eastern North American Source-Receptor Relationships, Academic Press, San Diego, 447, 1994.

Highwood, E.J., Kinnersley, R.P., When smoke gets in your eyes: the multiple impact of atmospheric black carbon on climate, air quality and health, Environment International, 32, 560–566, 2006.

Highwood, E.J., Kinnersley, R.P., When smoke gets in your eyes: the multiple impact of atmospheric black carbon on climate, air quality and health, Environment International, 32, 560–566, 2006.

Hinds, William C., Aerosol technology: Properties, behaviour, and measurement of airborne particles, J. Wiley (New York), 1982. ISBN 0471087262

Hoek, G., Kos, G., Harrison, R., de Hartog, J., Meliefste, K., ten Brink, H., Katsouyanni, K., Karakatsani, A., Lianou, M., Kotronarou, A., Kavouras, I., Pekkanen, J., Vallius, M., Kulmala, M., Puustinen, A., Thomas, S., Meddings, C., Ayres, J., vanWijnen, J., Hameri, K., Indoor–outdoor relationships of particle number and mass in four European cities, Atmospheric Environment, 42, 156–169, 2008.

Hoffer, A., Gelencsér, A., Gyon, P., Kiss, G., Schmid, O., Frank, G. P., Artaxo, P., and Andreae, M. O., Optical properties of humic-like substances (HULIS) in biomass-burning aerosols, Atmos. Chem. Phys., 6, 3563–3570, 2006. doi:10.5194/acp-6-3563-2006

Honrath, R.E., Owen, R.C., Val Martín, M., Reid, J.S., Lapina, K., Fialho, P., Dziobak, M.P., Kleiss, J., Westphal, D.L., Regional and hemispheric impacts of anthropogenic and biomass burning emissions on summertime CO and O_3 in the North Atlantic lower free troposphere, J. Geophysical Research, vol. 109, D24310, 17 PP., 2004, doi:10.1029/2004JD005147

Hudman, R.C., et al., Surface and lightning sources of nitrogen oxides over the United States: Magnitudes, chemical evolution, and outflow, J. Geophys. Res., 112, D12S05, 2007, doi:10.1029/2006JD007912.

ICRP, Human respiratory tract model for radiological protection, Ann., 24(1–3), 66, 1994.

IPCC, Climate Change 2007 – the Physical Science Basis; Working Group I Contribution to the Fourth Assessment Report of the IPCC, Intergovernmental Panel on Climate Change, 2007.

Jones, A.M., Harrison, R.M. Barratt, B., Fuller, G., A large reduction in airborne particle number concentrations at the time of the introduction of “sulphur free” diesel and the London Low Emission Zone, Atmospheric Environment, 50, 129.138, 2012.

Kanawade, V. and Tripathi, S. N., Evidence for the role of ion-induced particle formation during an Atmospheric nucleation event observed in Tropospheric Ozone Production about the Spring Equinox (TOPSE), J. Geophys. Res., 111, D02209, doi:10.1029/2005JD006366, 2006.

Karlsson, L., Hernández, F., Rodríguez, S., López-Pérez, M., Hernández-Armas, J., Alonso-Pérez, S., Cuevas, E., Using 137Cs and 40K to identify natural Saharan dust contributions to PM_{10} concentrations and air quality impairment in the Canary Islands, Atmospheric Environment, 42, 7034–7042, 2008.

Kasper, A., Aufdenblatten, S., Forss, A., Mohr, M., Burtscher, H., Particulate emissions from a low-speed marine diesel engine, Aerosol Science and Technology, 41, p. 24, 2007.

Kaur, S., Nieuwenhuijsen, M., Colvile, R., Personal exposure of street canyon intersection users to $PM_{2.5}$ ultrafine particle counts and carbon monoxide in Central London, UK, Atmos. Environ., 39, 3629-3641, 2005.

Keady, P.B., Quant, F.R. and Sem, G.J., A Condensation Nucleus Counter for Clean Rooms, Proc. Institute of Environmental Sci., Annual Technical Mtg, pp. 445-451, 1986

Kentarchos,A.S., Roelofs, G.L., Leiveld, J.,Cuevas, E., On the origin of elevated surface ozone concentrations at Izaña Observatory,Tenerife during late March 1996, Geophysical Research Letters 27 (22),3699–37 02, 2000.

Kesik, M., Ambus, P., Baritz, R., Brüggemann, N., Butterbach - Bahl, K., Damm, M., Duyzer, J., Horváth, L., Kiese, R., Kitzler, B., Leip, A., Li, C., Pihlatie, M., Pilegaard, K., Seufert, S., Simpson, D., Skiba, U., Smiatek, G., Vesala, T., and Zechmeister - Boltenstern, S., Inventories of N_2O and NO emissions from European forest soils, Biogeosciences, 2, 353–375, 2005

Ketzel, M., Wàhlin Kristensson, A., Swietlicki, E., Berkowicz, R., Nielsen, O.J., Palmgren, F., Particle size distribution and particle mass measurements at urban, near-city and rural level in the

Copenhagen area and Southern Sweden, Atmospheric Chemistry and Physics, 4, 281–292, 2004.

Kim, C. S., Adachi, M., Okuyama, K., and Seinfeld, J. H., Effect of NO2 on Particle Formation in SO2/H2O/air Mixtures by Ion- Induced and Homogenous Nucleation, Aerosol Sci. Tech., 36, 941–952, 2002.

Kittelson, D.B., Engines and nanoparticles: a review, Journal of Aerosol Science, 29, 575-588, 1998.

Kleiss, J., Honrath, R. E., Dziobak, M. P., Tanner, D., Val Martín, M., Owen, R. C., and Helmig, D., Occurrence of upslope flows at the Pico mountaintop observatory: A case study of orographic flows on a small, volcanic island, J. Geophys. Res., 112, D10S35, doi:10.1029/2006JD007565, 2007.

Kulmala, M. and Kerminen, V. M., On the formation and growth of Atmospheric nanoparticles, Atmos. Res., 90, 132–150, 2008.

Kulmala, M., Lehtinen, K. E. J., and Laaksonen, A., Clúster activation theory as an explanation of the linear dependence between formation rate of 3nm particles and sulphuric acid concentration, Atmos. Chem. Phys., 6, 787–793, 2006, http,//www.atmos-chem-phys.net/6/787/2006/.

Kulmala, M., Lehtinen, K. E. J., Laakso, L., Mordas, G., and Hämeri, K., On the existence of neutral atmospheric clústeres, Boreal Environ. Res., 10, 79–87, 2005.

Kulmala, M., Pirjola, L., Mäkela, J.M., Stable sulphate clusters as a source of new atmospheric particles, Nature, 404, 66.69, 2000.

Kulmala, M., Tammet, H., Finnish–Estonian air ion and aerosol workshops. Boreal Environ. Res., 12, 237–245, 2007

Kulmala, M., Vehkamäki, H., Petäjä, T., Dal Maso, M., Lauri, A., Kerminen, V.-M., Birmili, W., and McMurry, P., Formation and growth rates of ultrafine atmospheric particles: a review of observations. Journal of Aerosol Science 35, 143-176, 2004a.

Laakso, L., Hussein, T., Aarnio, P., Komppula, M., Hiltunen, V., Viisanen, Y. et al., Diurnal and annual characteristics of particle mass and number concentrations in urban, rural and Arctic environments in Finland, Atmospheric Environment, 37, 2629–2641, 2003.

Laaksonen, A., Kulmala, M., O'Dowd, C. D., Joutsensaari, J., Vaattovaara, P., Mikkonen, S., Lehtinen, K. E. J., Sogacheva, L., Dal Maso, M., Aalto, P., Petäjä, T., Sogachev, A., Yoon, Y. J., Lihavainen, H., Nilsson, D., Facchini, M. C., Cavalli, F., Fuzzi, S., Hoffmann, T., Arnold, F., Hanke, M., Sellegri, K., Umann, B., Junkermann, W., Coe, H., Allan, J. D., Alfarra, M. R., Worsnop, D. R., Riekkola, M. -L., Hy¨otyl¨ainen, T., and Viisanen, Y., The role of VOC oxidation products in continental new particle formation, Atmos. Chem. Phys., 8, 2657–2665, 2008.

Laj, P., et al., Measuring atmospheric composition change, Atmos. Environ., 43, 5351–5414, 2009, doi:10.1016/j.atmosenv.2009.08.020

Lee, S.-H., Wilson, J. C., Baumgardner, D., Herman, R. L., Weinstock, E. M., LaFleur, B. G., Kok, G., Anderson, B., Lawson, P., Baker, B., Strawa, A., Pittman, J. V., Reeves, J. M., and Bui, T. P., NPF observed in the tropical/subtropical cirrus clouds, J. Geophys. Res., 109, 2004, doi 10.1029/2004JD005033.

Li, Q., D. J. Jacob, I. Bey, P.I. Palmer, B. N. Duncan, B. D. Field, R. V. Martin, A. M. Fiore, R. M. Yantosca, D. D. Parrish, P. G. Simmonds, and S.J. Oltmans, Transatlantic transport of pollution and its effects on surface ozone in Europe and North America, J. Geophys. Res., 107(D13), 4166, doi:10.1029/2001JD001422, 2002a.

Li, Q., Jacob, D.J., Fairlie, T.D., Liu, H., Yantosca, R.M., Martin, R.V., Stratospheric versus pollution influences on ozone at Bermuda: reconciling past analyses, Journal of Geophysical Research D22, 2002JD002138, 4611, 2002b.

Likens, G.E. and Bormann, F.H., Acid rain: a serious regional environmental problem, Science, 184, 4142, 1176–1179, 1974.

Lippman, M., Environmental Toxicants, Human Exposures and Their Health Effects, second edition, Wiley-Interscience, ISBN 0-471-29298-2
Logan J. A., Tropospheric ozone: seasonal behavior, trends and anthropogenic influence, J. Geophys. Res., 90, 10,463-10,482, 1985.
Logan, J. A., The rural ozone problem in North America, in Tropospheric Ozone: Regional and Global Scale Interactions, ed. I.S.A. Isaksen, NATO ASI Series C, Volume 227, pp 327-344, D. Reidel Publishing Company, Holland, 1988.
López Cancio, J., Vera Castellano, A., Chaar Hernández, M., García Bethencourt, R., Macías Ortega, E., Metallic species in atmospheric particulate matter in Las Palmas de Gran Canaria, Journal of Hazardous Materials, Volume 160, Issues 2-3, 521-528, 2008.
López-Villarrubia, E., Ballester, F.¸ Iñiguez, C., Peral, N., Air pollution and mortality in the Canary Islands: a time-series analysis, Environmental Health, 9:8, 2010.
López-Villarrubia, E., García Pérez, M.-D., Peral Pérez, N.¸Ballester Díez, F., Iñiguez Fernández, C., Pita Toledo, M.-L., Caracterización del ambiente atmosférico en Las Palmas de Gran Canaria y Santa Cruz de Tenerife, 2000 a 2004. Rev Esp Salud Pública, 82: 493-507, 2008.
Maring, H., Savoie, D. L., Izaguirre, M. A., McCormick, C., Arimoto, R., Prospero, J. M., and Pilinis, C., Aerosol Physical and optical properties and their relationship to aerosol composition in the free troposphere at Izaña, Tenerife, Canary Islands, during July 1995, J. Geophys. Res., 105, 14677 – 14700, 2000.
Markham, A., A Brief History of Pollution. New York: St. Martin's Press, 162 pp, 1994.
Marti, J. J, Weber, R. J., Mc Murry, P. H., Eisele, F., Tanner, D., and Jefferson, A., New particle formation at a remote continental site, Assessing the contributions of SO2 and organic precursors, J. Geophys. Res., 102, 6331–6339, 1997.
Metzger, A., Verheggen, B., Dommen, J., Duplissy, J., Prevot, A.S.H., Weingartner, E., Riipinen, I., Kulmala, M., Spracklen, D.V., Carslaw, K.S., and Baltensperger, U., Evidence for the role of organics in aerosol particle formation under atmospheric conditions, Proceedings of the National Academy of Sciences of the United States of America, 107, 15, 6646–6651, 2010.
Millán, M.M., Salvador, R., Mantilla, E., Kallos, G., Photo-oxidant dynamics in the Mediterranean basin in summer: results from European research projects, Journal of Geophysical Research 102, 8811-8823, 1997.
Moldanová, J., Fridell, E., Popovicheva, O., Demirdjian, B., Tishkova, V., Faccinetto, A., Focsa, C., Characterisation of particulate matter and gaseous emissions from a large ship diesel engine, Atmospheric Environment 43, 2632-2641, 2009.
Mönkkönen, P., Umac, R., Srinivasan, D., Koponen, I.K., Lehtinen, K.E.J., Hämeri, K., Suresh, R., Sharma, V.P., Kulmala, M., Relationship and variations of aerosol number and PM10 mass concentrations in a highly polluted urban environment, New Delhi, India, Atmospheric Environment 38, 425–433, 2004.
Müller, T., Henzing, J.S., de Leeuw, G., Wiedensohler, A., Alastuey, A., Angelov, H., Bizjak, M., Collaud Coen, M., Engström, J.E., Gruening, C., Hillamo, R., Hoffer, A., Imre, K., Ivanow, P., Jennings, G., Sun, J.Y., Kalivitis, N., Karlsson, H., Komppula, M., Laj, P., Li, S.-M., Lunder, C., Marinoni, A., Martins dos Santos, S., Moerman, M., Nowak, A., Ogren, J.A., Petzold, A., Pichon, J.M., Rodríguez, S., Sharma, S., Sheridan, P.J., Teinilä, K., Tuch, T., Viana, M., Virkkula, A., Weingartner, E., Wilhelm, R., Wang, Y.Q., 2011. Characterization and intercomparison of aerosol absorption photometers: result of two intercomparison workshops, Atmos. Meas. Tech., 4, 245-268, 2011.
Nilsson, E.D., Kulmala, M., The potential for atmospheric mixing processes to enhance the binary nucleation rate, Journal of Geophysical Research 103, 1381–1389, 1998.Olivares, G., Johansson, C., Strom, J., Hasson, H.-C., The role of ambient temperature for particle number concentrations in a street canyon, Atmos. Environ., 41, 10, 2145–2155, 2007.
Nishita, C., Osada, K., Kido, M., Matsunaga, K., and Iwasaka, Y., Nucleation mode particles in upslope valley winds at Mount Norikura, Japan, Implications for the vertical extent of new

particle formation events in the lower troposphere, J. Geophys. Res., 113, D06202, doi,10.1029/2007JD009302, 2008.
Nolasco-Torres, D., Emisiones e Inmisiones de Compuestos Orgánicos Volátiles (COVs) en Tenerife, Ph.D. Thesis, Facultad de Ciencias Físicas, Universidad de La Laguna, 2010.
Novelli, P.C., Masarie, K.A., and Lang, P.M., distributions and recent changes of carbon monoxide in the lower troposphere, J. Geophys. Res., vol. 103, no. D15, pages 19,015 – 19, 033, August 20, 1998.
O'Dowd, C.D., Hoffmann, T., Coastal new particle formation: a review of the current state-of-the-art. Environmental Chemistry 2, 245–255, 2005, doi:10.1071/EN05077
Oberdörster G, Sharp Z, Atudorei V, Elder A, Gelein R, Lunts A, et al., Extrapulmonary transloction of ultrafine carbon particles following whole-body inhalation exposure of rats, J Toxicol Environ Health, 65 A, 1531–1543, 2002.
Oberdörster, G., Sharp, Z., Atudorei, V., Elder, A., Gelein, R., Kreyling, W., and Cox, C., Translocation of Inhaled Ultrafine Particles to the Brain, Inhal. Toxicol., 16, 1–9, 2004.
Olivares, G., Johansson, C., Strom, J., Hasson, H.-C., The role of ambient temperature for particle number concentrations in a street canyon, Atmos. Environ., 41, 10, 2145–2155, 2007.
Oltmans, S.J., Levy, H., Harris, J.M., Merrill, J.T., Moody, J.L., Lathrop, J.A., Cuevas, E., Trainer, M., O'Neill, M.S., Prospero, J.M., Vomel, H., Johnson, B.J., Summer and spring ozone proÞles over the North Atlantic from ozonesonde measurements, Journal of Geophysical Research, 1996, 101, 29,179-29,200.
Owen, R.C., Cooper, O.R., Stohl, A., and Honrath, R.E., An analysis of the mechanisms of North American pollutant transport to the central North Atlantic lower free troposphere, J. Geophys. Res., vol. 111, D23S58, doi:10.1029/2006JD007062, 2006
Palmen, E., and Newton, C. W., Atmospheric Circulation, Academic Pres, pp 603, 1969
Parrish, D.D., Holloway, J.S., Trainer, M., Murphy, P.C., Fehsenfeld, F.C., and Forbes, G.L., Export of North American ozone pollution to the north Atlantic Ocean, Science, 259, 1436-1439, 1993; doi: 10.1126/science.259.5100.1436
Parrish,D.D., Trainer, M., Holloway, J.S., Yee, J.E., Warshawsky, M.S., Fehsenfeld, F.C., Relationship between ozone and carbon monoxide at surface sites in the North Atlantic region, Journal of Geophysical Research, 103 (13), 357–376, 1998.
Perry, K.D. and Hobbs, P.V., Further evidence for particle nucleation in clean air adjacent to marine cumulus clouds, J. Geophys. Res., 99, 22803–22818, 1994.
Peters, A., Wichmann, H.E., Tuch, T., Heinrich, J., Heyder, J., Respiratory effects are associated with the number of ultrafine particles, American Journal of Respiratory and Critical Care Medicine, 155, 1376–1383, 1997.
Petzold, A. and Schönlinner, M.: Multi-angle absorption photometry-a new method for the measurement of aerosol light absorption and atmospheric Black Carbon, J. Aerosol Sci., 35, 421–441, 2004.
Petzold, A., Feldpausch, P., Fritze, L., Minikin, A., Lauer, P., Kurok, C., Bauer, H., Particle emissions from ship engines, Journal of Aerosol Science, 2004.
Pey J., Querol X., Alastuey A., Rodríguez S., Putaud J.P., Van Dingenen R., Source apportionment of urban fine and ultra-fine particle number concentration in a Western Mediterranean city, Atmos. Environ., 43, 29, 4407-4415, 2009.
Pirjola, L., Effects of the increased UV radiation and biogenic VOC emissions on the ultrafine sulphate aerosol formation, J. Aerosol Sci., 30, 355–367, 1999.
Poirot, R.L., Wishinski, P.R., Hopke, P.K., Polissar, A.V., Comparative application of multiple receptor methods to identify aerosol sources in northern Vermont, Environmental Science and Technology 35, 4622–4636, 2001.
Poirot, R.L.,Wishinski, P.R., Visibility, sulfate and air-mass history associated with summertime aerosol in northern Vermont, Atmos. Environ., 20, 1457-1469, 1986.

Prospero, J.M., Schmitt, R., Cuevas, E., Savoie, D., Graustein, W., Turekian, K., Volz-Thomas, A., Díaz, A., Oltmans, S., Levy, H.: Temporal Variability of ozone and Aerosols in the Free Troposphere Over the Eastern North Atlantic; Geophys. Res. Letts., 22, 21, 2925-2928, 1995.

Putaud, J. P., Van Dingenen, R., Mangoni, M., Virkkula, A., Raes, F., Maring, H., Prospero, J. M., Swietlicki, E., Berg, O. H., Hillamo, R., and Mäkela, T., Chemical mass closure and assessment of the origin of the submicron aerosol in the marine boundary layer and the free troposphere at Tenerife during ACE- 2, Tellus, 52B, 141–168, 2000.

Puustinen, A., Hämeri, K., Pekkanen, J., Kulmala, M., de Hartog, J., Meliefste, K., ten Brink, H., Kos, G., Katsouyanni, K., Karakatsani, A., Kotronarou, A., Kavouras, I., Meddings, G., Thomas, S., Harrison, R., Ayres, J.G., van der Zee, S., Hoek, G., Spatial variation of particle number and mass over four European cities. Atmospheric Environment 41, 6622–6636, 2007.

Querol, X., Alastuey, A., Rodríguez, S., Plana, F., Mantilla E., Ruiz C.R., Monitoring of PM_{10} and $PM_{2.5}$ around primary particulate anthropogenic emission sources, Atmos. Environ., 35, 845–858, 2001.

Raes, F., Van Dingenen, R., Cuevas, E., Van Velthoven, F. J. V., and Prospero, J. M.: Observations of aerosols in the free troposphere and marine boundary layer of the subtropical Northeast Atlantic: discussion of processes determining their size distribution, J. Geophys. Res., 102, 21315–21328, 1997.

Reche, C, Querol, X., Alastuey, A., Viana, M., Pey, J., Moreno, T., Rodríguez, S., González, Y., Fernández-Camacho, R., Sánchez de la Campa, A.-M., de la Rosa, J., Dall'Osto, M., Prévôt, A. S. H., Hueglin, C., Harrison, R.-M., and Quincey, P., New considerations for PM, Black Carbon and particle number concentration for air quality monitoring across different European cities, Atmos. Chem. Phys., 11, 6207–6227, 2011; doi:10.5194/acp-11-6207-2011.

Reiter, R., Munzert, K., Kanter, H.J., Poetzl, K., Cosmogenic radionuclides and ozone at a mountain station at 3.0 km a.s.l., Archive Meteriology Geophysik and Bioclamatologic 32B, 131-160, 1983.

Rodhe, H., An atmospheric sulphur budget for NW Europe, in Nilioqen, Phosphorus and Sulphur Global Cycles, Svensson, B.H., and Soderlund, R. (eds.), SCOPE, Report 7, Ecol. Bull. (Stockholm), 22, 123-134, 1976.

Rodríguez, C. Torres, J.C. Guerra, E. Cuevas, Transport Pathways to Ozone to Marine and Free-Troposphere Sites in Tenerife, Canary Islands, Atmos. Environ., 38, 4,733-4,747, 2004.

Rodríguez, S. and Guerra, J.C., Monitoring of ozone in a marine environment in Tenerife (Canary Islands), Atmos. Environ., 135, 1829-1841, 2001.

Rodríguez, S., Alastuey, A., Alonso-Pérez, S., Querol, X., Cuevas, E., Abreu-Afonso, J., Viana, M., Pérez, N., Pandolfi, M., de la Rosa, J., Transport of desert dust mixed with North African industrial pollutants in the subtropical Saharan Air Layer, Atmospheric Chemstry and Physics,11, 6663–6685, 2011.

Rodríguez, S., Alastuey, A., Viana, M. et al., Instituto de Diagnóstico Ambiental y Estudios del Agua (IDÆA – CSIC), el Centro de Investigación Atmosférica de Izaña (Agencia Estatal de Meteorología - AEMET) y la Universidad de Huelva, Estudios de contaminación por material particulado en Canarias durante los años 2007 a 2010, Informe elaborado por el, para la Consejería del Medio Ambiente y ordenación Territorial del Gobierno de Canarias, 2010.

Rodríguez, S., and Cuevas, E., The contributions of 'minimum primary emissions' and 'new particle formation enhancements' to the particle number concentration in urban air, J. Aerosol Sci., 38, 1207–1219, 2007.

Rodríguez, S., Van Dingenen, R., Putaud, J. P., Martins-Dos Santos, S., and Roselli, D., Nucleation and growth of new particles in the rural Atmosphere of Northern Italy – Relationship to air quality monitoring, Atmos. Environ., 39, 6734–6746, 2005.

Rodríguez, S., Van Dingenen, R., Putaud, J.P., Dell'Acqua, A., Pey, J., Querol, X., Alastuey, A., Chenery, S., Kin-Fai, H., Harrison, R.M., Tardivo, R., Scarnato, B., and Gianelle, V., A study on the relationship between mass concentrations, chemistry and number size distribution of urban fine aerosols in Milan, Barcelona & London, Atmos. Chem. Phys., 7, 2217-2232, 2007.

Rolph, G. D., Real-time Environmental Applications and Display sYstem (READY) Website: http://www.arl.noaa.gov/ready/hysplit4.html, NOAA Air Resources Laboratory, Silver Spring, MD, 2003

Rose, D., Wener, B., Ketzel, M., Engler, C., Voigtländer, J., Tuch, T., Wiedensohler, A., Atmospheric number size distributions of soot particles and estimation of emission factors, Atmos. Chem. Phys., 6, 1021-1031, 2006

Ruuskanen, R., Tuch, Th., Ten Brink, H., Peters, A., Khlystov, A., Mirme, A., Kos, G.P.A., Brunekreef, B., Wichmann, H.E., Buzorius, G., Vallius, M., Kreyling, W.G., Pekkanem, J., 2001. Concentrations of ultrafine, fine and $PM_{2.5}$ particles in three European cities, Atmospheric Environment, 35, 3729–3738, 2001.

Schmid, O., Artaxo, P., Arnott,W. P., Chand, D., Gatti, L. V., Frank, G. P., Hoffer, A., Schnaiter, M., and Andreae, M. O., Spectral light absorption by ambient aerosols influenced by biomass burning in the Amazon Basin. I: Comparison and field calibration of absorption measurement techniques, Atmos. Chem. Phys., 6, 3443–3462, 2006, doi:10.5194/acp-6-3443-2006.

Schröder, F. P., Kärcher, B., Fiebig, M., and Petzold, A., Aerosol states in the free troposphere at northern midlatitudes, J. Geophys. Res., 107 (D21), 8126, doi:10.1029/2000JD000194, 2002.

Second Position Paper on Particulate Matter, CAFE working group on particulate matter, 2004.

Seinfeld, J.H., and Pandis, S.N., Atmospheric Chemistry and Physics, From Air Pollution to Climate Change, A Wiley- Interscience Publication, Jonh Wiley & Sons, inc. 1998.

Shaw, G. E., Aerosols at a mountaintop observatory in Arizona, J. Geophys. Res., 112, D07206, 2007, doi,10.1029/2005JD006893.

Siebert, H., Stratmann, F. and Wehner, B., First observations of increased ultrafine particle number concentrations near the inversion of a continental planetary boundary layer and its relation to ground-based measurements, Geophysical Research Letters, 31, L09102, doi:10.1029/2003GL019086, 2004

Sipilä, M., Berndt, T., Petäjä, T., Brus, D., Vanhanen, J., Stratmann, F., Patokoski, J., Mauldin, R. L., Hyvärinen, A. P., Lihavainen, H., and Kulmala, M., The Role of Sulphuric Acid in Atmospheric Nucleation, Science, 327, 1234–1246, 2010

Stanier, C. O., Khlystov, A. Y., and Pandis, S. N., Ambient aerosol size distributions and number concentrations measured during the Pittsburgh Air Quality Study (PAQS), Atmos. Environ., 38, 3275–3284, 2004.

Steinbacher, M., Zellweger, C., Schwarzenbach, B., Bugmann, S., Buchmann, B., Ordóñez, C., Prevot, A.S.H., and Hueglin, C., Nitrogen oxide measurements at rural sites in Switzerland: Bias of conventional measurement techniques, J. Geophys. Res., vol. 112, D11307, doi:10.1029/2006JD007971, 2007

Stevens, R.G., Pierce, J.R., Brock, C.A., Reed, M.K., Crawford, J.H., Holloway, J.S., Ryerson, T.B., Huey, L. G., and Nowak, J.B., Nucleation and growth of sulfate aerosol in coal-fired power plant plumes: sensitivity to background aerosol and meteorology, Atmos. Chem. Phys., 12, 189–206, 2012; doi:10.5194/acp-12-189-2012

Stohl, A., A 1-year Lagrangian "climatology" of airstreams in the Northern Hemisphere troposphere and lowermost stratosphere, J. Geophys. Res., 106, 7263–7279, 2001.

Stohl, A., and Trickl, T., A textbook example of long-range transport: Simultaneous observation of ozone maxima of stratospheric and North American origin in the free troposphere over Europe, J. Geophys. Res., 104, 30,445 – 30,462, 1999.

Stohl, A., Eckhardt, S., Forster, C., James, P., and Spichtinger, N., On the pathways and timescales of intercontinental air pollution transport, J. Geophys. Res., 107 (D23), 4684, 2002, doi:10.1029/2001JD001396

Stölzel M, Breitner S, Cyrys J, Pitz M, Wolke G, Kreyling W, et al., Daily mortality and particulate matter in different size classes in Erfurt, Germany., J Expo. Sci. Environ. Epidemiol.,17:458–467, 2007.

Tolocka, M. P., Lake, D. A., Johnston, M. V., andWexler, A. S., Ultrafine nitrate particle events in Baltimore observed by real-time single particle mass spectrometry, Atmos. Environ., 38, 3215– 3223, 2004.

Torres, C., E. Cuevas y J. C. Guerra, Caracterización de la capa de mezcla marítima y de la atmósfera libre en la región subtropical sobre Canarias, 3ª Asamblea Hispano-Portuguesa de Geodesia y Geofísica, Valencia, 4-8 febrero, 2002.

UK Ministry of health, Mortality and morbidity during the London fog of December 1952. Her Majesty's Stationary Office, 1954

UNE-EN 14211:2006. Calidad del aire ambiente. Método normalizado de medida de la concentración de dióxido de nitrógeno y monóxido de nitrógeno por quimioluminiscencia.

UNE-EN 14212:2006. Calidad del aire ambiente. Método normalizado de medida de la concentración de dióxido de azufre por fluorescencia de ultravioleta.

UNE-EN 14625:2005. Calidad del aire ambiente. Método normalizado de medida de la concentración del ozono por fotometría ultravioleta.

UNE-EN 14626:2006. Calidad del aire ambiente. Método normalizado de medida de la concentración de monóxido de carbono por espectroscopia infrarroja no dispersiva.

UNE-EN 14907:2006. Calidad del aire ambiente. Método gravimétrico de medida para la determinación de la fracción másica $PM_{2.5}$ de la materia particulada en suspensión

UNE-EN 77-237:1999. Calidad del aire. Determinación de las características de funcionamiento de los métodos de medida.

UNE-EN 77-240:2000. Calidad del aire. Evaluación de las características de funcionamiento de los analizadores de gas.

US EPA, Quality Assurance Handbook for Air Pollution Measurement Systems, Volume II - Ambient Air Specific Methods EPA 600/4-77-027 and 40 CFR 50, Appendix C. 2; Available from Purafil, Inc., POB 80434, Atlanta, GA 30366. 3. 40 CFR 58, Appendix A, B, 1977

US EPA, Quality Assurance Handbook for Air Pollution Measurement systems, Volume II: part 1, Ambient Air Quality monitoring Program, Quality System Development, EPA-454/R-98-004, 1998.

US EPA, Report on the Environment (Final Report), 2008

Val Martin, M., Honrath, R.E., Owen, R.C., and Li, Q.B., Seasonal variation of nitrogen oxides in the central North Atlantic lower free troposphere, J. Geophysical Res., vol. 113, D17307, 2008, doi:10.1029/2007JD009688

van der Zee, S.C., Dijkema, M.B.A., van der Laan, J., Hoek, G., The impact of inland ships and recreational boats on measured NO_X and ultrafine particle concentrations along the waterways, Atmospheric Environment, vol. 55, 368–376, 2012, doi: 10.1016/j.atmosenv. 2012.03.055.

Van Dingenen, R., Putaud, J.-P., Martins-Dos Santos, S., and Raes, F., Physical aerosol properties and their relation to air mass origin at Monte Cimone (Italy) during the first MINATROC campaign, Atmos. Chem. Phys., 5, 2203–2226, 2005, http,//www.atmos-chem-phys.net/5/2203/2005/.

Venzac, H., Sellegri, K., and Laj, P., Nucleation events detected at the high altitude site of the Puy de Dôme Research station, France, Boreal Environ. Res., 12, 345–359, 2007.

Venzac, H., Sellegri, K., Laj, P., Villani, P., Bonasoni, P., Marinoni, A., Cristofanelli, P., Calzolari, F., Fuzzi, S., Decesari, S., Facchini, M. C., Vuillermoz, E., and Verza, G. P., High frequency new particle formation in the Himalayas, P. Natl. Acad. Sci. USA, 105(41), 15666–15671, 2008.

Venzac, H., Sellegri, K., Villani, P., Picard, D., and Laj, P., Seasonal variation of aerosol size distributions in the free troposphere and residual layer at the Puy de Dôme station, France, Atmos. Chem. Phys., 9, 1465–1478, 2009.

Viana, M., Amato, F., Alastuey, A., Querol, X., Moreno, T., García do Santos, S., Herce, M.D., Fernández-Partier, R., Chemical tracers of particulate emissions from commercial shipping, Environmental Science and Technology 43, 2009.

Viana, M., Querol, X., Alastuey, A., Cuevas, E., Rodríguez, S., Influence of African dust on the levels of atmospheric particulates in the Canary Islands air quality network, Atmospheric Environment, 36, 5861–5875, 2002.

Virkkula, A., Ahlquist, N. C., Covert, D. S., Arnott,W. P., Sheridan, P. J., Quinn, P. K., and Coffmann, D. J., Modification, calibration and a field test of an instrument for measuring light absorption by particles, Aerosol Science and Technology, 39, 68–83, 2005.

Virkkula, A., Correction of the Calibration of the 3-wavelength Particle Soot Absorption Photometer (3λ PSAP), Aerosol Science and Technology, 44, 706–712, 2010Virkkula, A., Mäkelä, T., Yli-Tuomi, T., Hirsikko, A., Koponen, I. K., Hämeri, K., and Hillamo, R., A simple procedure for correcting loading effects of aethalometer data, J. Air Waste Manage., 57, 1214–1222, 2007, doi:10.3155/1047-3289.57.10.1214

Wang, T., Wong, H.L.A., Tang, J., Ding, A., Wu, W.S., and Zhang, X.C., On the origin of surface ozone and reactive nitrogen observed at a remote mountain site in the northeastern Qinghai-Tibetan Plateau, western China, J. Geophys. Res., 111, 2006, D08303, doi:10.1029/2005JD006527

Weber, R. J. and Mc Murry, P. H., Fine particle size distribution at the Mauna Loa Observatory, Hawaii, J. Geophys. Res., 101, 14767–14775, 1996.

Weber, R. J., Marti, J. J., Mc Murry, P. H., Eisele, F. L., Tanner, D. J., and Jefferson, A., Measurements of new particle formation and ultra fine particle growth at a clean continental site, J. Geophys. Res., 102, 4375–4385, 1997.

Wehner, B., Birmili, W., Gnauk, T., and Wiedensohler, A., Particle number size distributions in a street canyon and their transformation into the urban-air background: measurements and a simple model study, Atmospheric Environment, 36, 2215–2223, 2002.

Wehner, B., Wiedensohler, A., Long term measurements of submicrometer urban aerosols: statistical analysis for correlations with meteorological conditions and trace gases. Atmospheric Chemistry and Physcis 3, 867-879, 2003.

Weingartner, E., Nyeki, S., and Baltensperger, U., Seasonal and diurnal variation of aerosol size distributions (10<D<750 nm) at a high-alpine site (Jungfraujoch 3580ma.s.l.), J. Geophys. Res., 104, D21, 26809–26820, 1999.

Weingartner, E., Saathoff, H., Schnaiter, M., Streit, N., Bitnar, B., and Baltensperger, U., Absorption of light by soot particles, 2003. Determination of the absorption by means of aethalometers, Journal of Aerosol Science, 34, 1445–1463, 2003.

Whitby, K.T., The physical characteristics of sulfur aerosols, atmospheric environment, 12:135-59, 1978.

Wichmann, H.E. and Peters, A., Epidemiological evidence of the effects of ultrafine particle exposure, Philosophical Transactions of the Royal Society of London, Series A. Mathematical, Physical and Engineering Sciences, 358, 2751-2769, 2000.

Wiedensohler, A., Hansson, H. C. ,Orsini, D. , Wendisch, M., Wagner, F., Bower, K. N., Choularton, T. W., Wells,M., Parkin, M., Acker, A., Wieprecht, W., Fachini, M. C.,Lind, J. A., Fuzzi, S.,Arends, B. G., and Kulmala, M., Nighttime formation and occurrence of new particles associated with orographic clouds, Atmos. Environ., 31, 2545–2559, 1997.

Willeke, Klaus, and Baron, Paul A., Aerosol Measurement, Principles Techniques and applications, Van Nostrand Reinhold, New York, Library of Congress Catalog card Number 92-11371, ISBN 0-442-00486-9.

Woo K.S., Chen, D.R., Pui, D. Y.H., and Mc Murry, P.H., Measurement of Atlanta aerosol size distributions: observation of ultrafine particle events, Aerosol Science and Technology, 34, 75–87, 2001.

Yu, F., Diurnal and Seasonal Variations of Ultrafine Particle Formation in Anthropogenic SO_2 Plumes, Environ. Sci. Technol. 2010, 44, 2011–2015

Zhang K.M., Wexler A.S., Evolution of particle number distribution near roadways – Part I: Analysis of aerosol dynamics and its implications for engine emission measurement, Atmos. Environ., 38, 6643-6653, 2004.

Dissemination of results

Publications in peer-reviewed journals included in the Science Citation Index

Publications directly resulted from this study

Rodríguez, S., Cuevas, E., **González, Y.**, Ramos, R., Romero, P.M., Querol, X. and Alastuey, A., *Influence of sea breeze circulation and road traffic emissions on the relationship between particle number, black-carbon, PM_{1}, $PM_{2.5}$ and $PM_{2.5-10}$ concentrations in a coastal city*, Atmos. Environ., 42, 6523-6534, 2008. DOI: 10.1016/j.atmosenv.2008.04.022

Rodríguez, S., **González, Y.**, Cuevas, E., Ramos, R., Romero, P.M., Abreu-Afonso, J., and Redondas, A. *Atmospheric nanoparticle observations in the low free troposphere during upward orographic flows at Izaña Mountain Observatory*, Atmos. Chem. Phys., 9, 6319–6335, 2009, www.atmos-chem-phys.net/9/6319/2009/.

González, Y., Rodríguez, S., Guerra, J.-C., Trujillo, J.-L., and García, R., *Ultrafine particles pollution in urban coastal air due to ship emissions*, Atmospheric Environment, 45, 4907-4914, 2011

González, Y., and Rodríguez, S., *Source apportionment of ultrafine particles in a city affected by vehicle exhaust, a crude oil refinery and ship emissions*, Atmos. Res., Submitted.

Publications in which this study has contributed

Domínguez-Rodríguez, A., Abreu-Afonso, J., Rodríguez, S., Juarez-Prera, R.A., Arroyo-Ucar, E., Jiménez-Sosa, A., **González, Y**., Abreu-González, P., Avanzas, P., C*omparative study of ambient air particles in patients hospitalized for heart failure and acute coronary syndrome*, Revista Española de Cardiología, 64, 8, 661–666, 2011

Reche, C., Querol, X., Alastuey, A., Viana, M., Pey, J., Moreno,T., Rodríguez, S., **González, Y.**, Fernández-Camacho, R., Sánchez de la Campa, A.M., de la Rosa, J., Dall'Osto, M., Prévôt, A.S.H., Hueglin, C., Harrison, R.M., Quincey, P., *Variability of levels of PM, black carbon and particle number concentration in selected European cities*, Atmos. Chem. Phys., 11, 6207–6227, 2011. DOI: 10.5194/acp-11-6207-2011

Domínguez-Rodríguez, A., Abreu-Afonso, J., González, Y., Rodríguez, S., Juarez-Prera, R.A., Arroyo-Ucar, E., Jiménez-Sosa, A., Abreu-González, P., Avanzas, P., Relationship between short-term exposure to atmospheric sulfur dioxide and obstructive lesions in acute coronary sindrome, Medicina Clínica, Submitted.

Scientific Meetings

González, Y., Cuevas, E. Ramos, R. García, J.J., Guerra, J.C., Intercomparación de la tecnología de absorción óptica diferencial, UV-vis DOAS, y técnicas in situ para la medida de gases atmosféricos. V Seminario de calidad del aire. Santander. October, 2006.

Milford, C., Marrero, C., Martin, C., **González, Y.**, Rodríguez, S., Querol, X., Cuevas, E., Air Quality Assessment in Santa Cruz de Tenerife (Canary Islands) 2000-2007, "7th International Conference on Air Quality – Science and Application", Istanbul, March 24-27, 2009.

González, Y., Rodríguez, S., Cuevas, E., Ramos, R., Abreu-Afonso, J., Baldasano, J.M., Assessing the impact of the forthcoming decrease in diesel exhaust particulate matter emissions on air quality: implications for black carbon concentrations in ambient air, European Geosciences Union, General Assembly 2009, Vienna, Austria, April 19 – 24, 2009.

Rodríguez, S., **Gonzalez, Y.**, Cuevas, E., Ramos, R. Abreu-Afonso, J., Romero, P.-M., Redondas, A., New Particle Formation In The Low Free Troposphere Upward Flows Observed At Izaña Mount (2367 m a.s.l.) on Tenerife Island, 18th International Conference on Nucleation & Atmospheric Aerosols, August 10 – 14, 2009, Prague, Czech Republic.

González, Y., Rodríguez, S., Cuevas, E., Ramos, R., Guerra, J.C., Baldasano, J.M., A Brief Review of Reactive Gases Observations at Izaña Atmospheric Observatory (2006-2009), Symposium on Atmospheric Chemistry and Physics at Mountain Sites, June 8-10, 2010, Interlaken, Switzerland.

González, Y., Cuevas, E., Alonso, S., Rodríguez, S., Rodríguez, J., Guerra, J.C., Ramos, R., Baldasano, J.M., Long Term Ozone Observations at Izaña Atmospheric Observatory (1988-2009),Simposium on Atmospheric Chemistry and Physics at Mountain Sites, June 8-10, 2010, Interlaken, Switzerland, Oral Presentation.

Reche, C., Querol, X., Viana, M.¸ Moreno, T.¸ Pey, J., Dall'Osto, M., Alastuey, A., Rodríguez, S.¸ **González, Y.**, Fernández-Camacho, R., de la Rosa, J., Prevot, A.S.H., , Hueglin, C., Harrison, R.M., Quincey, P¸ Variability of levels of PM, black carbon and particle number concentration in selected European cities, Geophysical Research Abstracts, Vol. 13, EGU2011-12304-2, 2011, EGU General Assembly.

González, Y., Rodríguez, S., Guerra, J.C., Trujillo, J.L., García, R., Influence of ship emissions in the ultrafine particles pollution in an urban coastal air, V Reunión de la Asociación Española de Ciencia y Tecnología de Aerosoles, RECTA, June 27 – 29, 2011, Poster.

Juarez Prera, R., Domínguez Rodríguez, A., **González, Y.**, Abreu Afonso, J., Arroyo Ucar, E., Rodríguez, S., Avanzas, P., Abreu González, P., Comparative study of short-term exposure to ultrafine particles in patients hospitalized for heart failure and acute coronary syndrome, European Society of Cardiology, August 27th -31st 2011, Paris, France, Poster.

Gómez-Pelaez, A.J., Ramos, R., Gómez-Trueba, V., **González, Y.**, Campo-Hernández, R., and Novelli, P., In-situ CO measurements at Izaña global GAW station: GC-RGA system, data processing, and 2008-2011 time series, 16th WMO/IAEA Meeting on Carbon Dioxide, Other Greenhouse Gases, and Related Measurement Techniques Wellington, New Zealand 25th–28th October 2011, Oral Presentation.

List of Figures

List of Tables